Investigating Thermal and Mechanical Inputs for Rigid Pavement Design in North Carolina

NCDOT Project 2022-07
FHWA/NC/2022-07
June 2024

Gauhar Sabih, Ph.D., et al.
Kimmel School of Construction Management
Western Carolina University

Tara Cavalline, Ph.D., P.E., et al.
William States Lee College of Engineering
University of North Carolina at Charlotte University

RESEARCH & DEVELOPMENT

Technical Report Documentation Page

1. Report No. FHWA/NC/2022-07	2. Government Accession No.	3. Recipient's Catalog No.
4. Title and Subtitle Investigating Thermal and Mechanical Inputs for Rigid Pavement Design in North Carolina		5. Report Date June 2024 6. Performing Organization Code
7. Author(s) Gauhar Sabih, PhD., Tara L. Cavalline, Ph.D., P.E., Brett Q. Tempest, Ph.D., P.E., Clarke Summers, Megan McIntosh, Tasfia Tafannum, and Matthew T. Sheffield		8. Performing Organization Report No.
9. Performing Organization Name and Address Department of Engineering Technology and Construction Management Department of Civil and Environmental Engineering University of North Carolina at Charlotte 9201 University City Boulevard Charlotte, NC 28223-0001		10. Work Unit No. (TRAIS) 11. Contract or Grant No.
12. Sponsoring Agency Name and Address North Carolina Department of Transportation Research and Analysis Group 1 South Wilmington Street Raleigh, North Carolina 27601		13. Type of Report and Period Covered Final Report August 1, 2021 – April 30, 2024 14. Sponsoring Agency Code RP2020-07
Supplementary Notes:		

16. Abstract

The Mechanistic-Empirical Pavement Design Guide (MEPDG) is a tool developed by NCHRP used to aid engineers in pavement design and performance analysis. MEPDG is currently incorporated into the software program AASHTOWare Pavement ME Design. In order for the software to perform at the highest level of accuracy, AASHTO recommends a local calibration of inputs to be performed. The purpose of this research study was to provide additional material inputs for Portland cement concrete to the proposed catalog of inputs developed based on research performed as part of a previous NCDOT research project, RP 2015-03 and evaluate the impact of these inputs on the predicted performance of North Carolina rigid pavements. To accomplish this, concrete mixtures with varying materials and proportions were batched and tested for mechanical properties, thermal properties, and durability performance. A range of findings related to the impact of fly ash content and aggregate types/sources on mechanical/thermal properties and durability performance along with information on the time-dependent change of selected properties and durability prediction measurements is presented. An expanded catalog of input values was prepared for NCDOT's consideration for use in future pavement design. Pavement ME Design (PMED) software is the latest tool for design and performance analysis of rigid pavements. Simulations were conducted using PMED software to evaluate the effects of concrete material inputs, climate, and input levels on the performance and design slab thickness of jointed plain concrete pavements (JPCP) and unbonded concrete overlays. The simulation results were analyzed, and the detailed findings are presented in this report. It was found that the coefficient of thermal expansion (CTE) is the most significant material input affecting the JPCP design and performance. The other thermal properties including heat capacity and thermal conductivity also significantly affect the design and performance of rigid pavements and using PMED default values for these inputs may result in under designed pavement systems. It was also found that the strength gain for concrete paving mixtures that include fly ash takes longer to gain full strength. Level 3 material inputs restrict an accurate representation of fly ash's strength gain properties with only the 28-day compressive strength value while Level 1 material inputs simulate a better depiction of how fly ash properties are included in JPCP pavements. The findings of this report will help the pavement engineers towards improved design of rigid pavement systems.

17. Key Words PMED; CTE; Cracking; Faulting; Concrete; Rigid	18. Distribution Statement		
19. Security Classif. (of this report) Unclassified	20. Security Classif. (of this page) Unclassified	21. No. of Pages 161	22. Price

Form DOT F 1700.7 (8-72) **Reproduction of completed page authorized**

DISCLAIMER

The contents of this report reflect the views of the author(s) and not necessarily the views of the University. The author(s) are responsible for the facts and the accuracy of the data presented herein. The contents do not necessarily reflect the official views or policies of either the North Carolina Department of Transportation or the Federal Highway Administration at the time of publication. This report does not constitute a standard, specification, or regulation.

ACKNOWLEDGMENTS

This research project was sponsored by the North Carolina Department of Transportation (NCDOT) and their continued support is greatly appreciated. The research team would like to express their appreciation to the following:

- The NCDOT personnel serving on the Steering and Implementation Committee for this research study. In particular, we would like to thank Clark Morrison and Shihai Zhang, Chair of the Steering and Implementation Committee for their insight, assistance, and support. Feedback received from all members of the Steering and Implementation Committee (Joshua Law, Brian Hunter, Andrew Wargo, Neil Mastin, Josh Holland, Wiley Jones, Todd Whittington, and Jim Phillips) during the course of this project was greatly appreciated.

- NCDOT Research and Development personnel, particularly Mustan Kadibhai.

- Material suppliers for their generous donations of aggregates, cementitious materials, and admixtures supporting this research.

- UNC Charlotte Research Operations Managers Wesley Maxwell and Douglas Eshenbaugh.

- UNC Charlotte Graduate Research Assistants Samantha Doughty, Isaac Oyawoye, and Rohan Reddy Jonna.

- UNC Charlotte Undergraduate Research Assistants Brandon Ellis, Alec Strickland, Logan Fitzgerald, Kyle Stewart, Jackson Rizzolo, and Kenny Dillon.

- UNC Charlotte Department of Earth, Environmental, and Geographical Sciences Professor Emeritus Dr. John Diemer, Dr. Valerie Reynolds, and Undergraduate Research Assistant Liam Rogers.

EXECUTIVE SUMMARY

The Pavement Mechanistic Empirical Design (PMED) was developed by AASHTO as the standard for rigid pavement design and performance analysis, and as the most advanced tool, it has transformed the pavement design process. Pavement performance analysis and design can now be performed using the PMED software. The PMED software is based on mechanistic-empirical concepts. The design procedure calculates pavement responses such as stresses, strains, and deflections under axle loads and climatic conditions and then accumulates the damage over the design analysis period. The procedure then empirically relates calculated damage over time to pavement distresses and smoothness based on the performance of actual projects throughout the U.S.

PMED incorporates concrete material properties in the design process and research has shown that compressive strength, elastic modulus, modulus of rupture (MOR), and coefficient of thermal expansion (CTE) are the most important inputs. Predicted pavement characteristics including thickness, design life, serviceability, joint faulting, and cracking performance depend on these material input factors. Accurate determination of material properties was not a part of the design process until the advent of PMED. With further research, it was found that accurate determination of these concrete material inputs as part of local calibration of PMED is the key to design of rigid pavements which can reliably last for the designed service life.

Many state DOTs are in the process of implementing PMED into their pavement design processes and are characterizing local concrete materials in this process. NCDOT is also planning to incorporate PMED into the design process for rigid pavements. The NCDOT conducted a research project completed in 2016 as an initial step to conduct the characterization of concrete materials (FHWA Report No. NC/2015-03, Cavalline et al., 2018) which provided a database of concrete material inputs incorporating Piedmont, Coastal, and Mountain coarse aggregates along with a manufactured sand and a natural sand. Although this project provided a range of useful inputs, it is understood that there are differences in aggregates from other areas of North Carolina, including areas where rigid pavements are anticipated to be constructed. So there was a need to characterize the concrete paving mixtures prepared with these coarse aggregates and potentially other variables to obtain a more detailed catalog of PMED inputs for rigid pavement design, and subsequently, to evaluate the effects of the obtained material inputs on the design and performance analysis of rigid pavements.

The need for this work is amplified as NCDOT is undertaking new rigid pavement projects including re-construction/widening of I-26 (costing $531 million) and I-540 expressway project (costing $2.2 billion) and many more rigid pavement projects to come in the future. With an accurately established material database to support PMED inputs, the pavement designers will have the opportunity to understand the predicted performance of rigid pavement designs and potentially select the best suited materials and/or mixture characteristics for a specific project.

The purpose of this study was to provide additional material inputs for Portland cement concrete (PCC) to the proposed catalog of inputs developed based on research performed as part of a previous NCDOT research project, RP 2015-03. To accomplish this, concrete mixtures containing varying amounts of fly ash and aggregates from sources different than those used in RP 2015-03 were batched and tested for mechanical properties, thermal properties, and durability performance. The influence of the aforementioned PCC materials and mixture proportions on the time-dependent change was also studied.

Twenty-four concrete mixtures were produced using varying amounts of fly ash, four different coarse aggregate, and two different natural sands with proportions similar to what would be used in rigid pavement application across the state of North Carolina. Tests included compressive strength, modulus of elasticity (MOE), Poisson's ratio, modulus of rupture (MOR), coefficient of thermal expansion (CTE), thermal conductivity, heat capacity, surface resistivity, and unrestrained shrinkage. It was determined that as expected, the amount of fly ash used in the PCC mixture had the most significant influence on the mechanical properties, thermal properties, and surface resistivity of the concrete. The coarse aggregate used in the mixture had a significant influence on all three thermal properties, CTE, heat capacity, and thermal conductivity. Time-dependent behavior of the PCC was also affected primarily by fly ash content. However, the coarse aggregate source did appear to be linked to some differences in time-dependent behavior observed in several tests, including compressive strength, modulus of elasticity, Poisson's ratio, CTE, thermal conductivity, and heat capacity. Also notable was the finding that region of North Carolina from which the coarse aggregate was sourced also has an influence on the rate of change of surface resistivity.

This proposed research project has resulted in an enhanced database/catalog of Level 1 mechanical and thermal inputs for PMED design process. This catalog amends the catalog prepared as part of NCDOT 2015-03. It should be noted that some PCC inputs such as MOE, Poisson's ratio, heat capacity, and thermal conductivity were measured to be lower than previously recommended inputs, especially for mixtures containing fly ash.

Analysis was conducted to evaluate the impact of concrete material inputs on pavement design, performance, and slab thickness using PMED simulations and it was found that CTE of concrete is the prime contributor in producing pavement distresses and impact the performance of the JPCP and it is the most significant factor affecting the JPCP performance. It became evident that Level 1 material inputs provide the most accurate design out of all three input levels

and using Level 3 inputs for JPCP design will result in a thicker concrete slab, and using Level 1 inputs will produce a more accurate and economical JPCP design. The strength gain for concrete paving mixtures that include fly ash takes longer to gain full strength, and Level 3 material inputs restrict an accurate representation of fly ash's strength gain properties with only the 28-day compressive strength value while Level 1 material inputs simulate a better depiction of how fly ash properties are included in JPCP pavements. Alternatively, later-age strength values of fly ash concrete mixtures could be used in lieu of 28-day values which likely misrepresent later age performance. It was also found that there is significant impact of heat capacity of paving concrete on IRI and cracking of JPCP systems and using the software default values of heat capacity will result in under designed JPCP system which might fail prematurely without completing the design service life. The use of default thermal conductivity values will result in lower transverse cracking predictions and the difference in cracking performance between default thermal conductivity and laboratory obtained thermal conductivity values is up to 26%. Using the default values of thermal conductivity will result in an under-designed JPCP system.

The products of this research are directly implementable by pavement designers, allowing greater confidence in the design and predicted performance of rigid pavements designed using PMED software. The evaluation of various design variables including material inputs, climate, traffic, and geometric properties with regards to the design thickness and predicted performance of rigid pavements have provided a knowledge base to the pavement designers about the impact of these parameters on the rigid pavement design. This will improve the reliability of rigid pavements to provide long lasting service lives with low maintenance.

TABLE OF CONTENTS

LIST OF TABLES

LIST OF FIGURES

LIST OF ABBREVIATIONS

AADT	Annual Average Daily Traffic
AASHTO	American Association of State Highway and Transportation Officials
AASHTOWare	Software that follows AASHTO standards
ACI	American Concrete Institute
ASCE	American Society of Civil Engineers
ASTM	American Society for Testing and Material
cf	cubic feet
cwt	hundred weight of cement
cy	cubic yard
CTE	Coefficient of Thermal Expansion
DOT	Department of Transportation
FDOT	Florida Department of Transportation
FHWA	Federal Highway Administration
ft	foot
g	gram
gal	gallon
hr	hour
ID	identification
in	inch
IRI	International Roughness Index
JPCP	Jointed Plain Concrete Pavement
kg	kilogram
lb	pound
m	meter
M-E	Mechanistic-Empirical
MEPDG	Mechanistic-Empirical Pavement Design Guide
mi.	Mile
Mixture ID	Mixture Identification
με	microstrain
μm	micometer
mL	milliliter
mm	millimeter
MOE	modulus of elasticity
MOR	modulus of rupture
NC	North Carolina
NCC	National Concrete Consortium
NCDOT	North Carolina Department of Transportation
NCHRP	National Cooperative Highway Research Program
NCHRP Project 1-37A	The project that produced a guide for M-E design and analysis
OPC	ordinary portland cement
oz	ounce
Pavement-ME	Simulation Software used in this study that has AASHTOWare
PMED	Pavement Mechanistic-Emperical Design
PCA	Portland Cement Association
PCC	portland cement concrete
pcf	pounds per cubic foot
pcy	pounds per cubic yard
psi	pounds per square inch
RP	Research Project
SCM	supplementary cementitious material
SG	specific gravity
SHA	state highway agency
SHRP	Strategic Highway Research Program

TRB	Transportation Research Board
US	United States
w/cm	water to cementitious materials ratio
WRA	water-reducing admixture
yd	yard
°F	degrees Fahrenheit

1.0 INTRODUCTION AND RESEARCH OBJECTIVES

1.1 Introduction

State highway agencies in the United States have predominantly used the American Association of State Highway Transportation Officials (AASHTO) Guides for Design of Pavement Structures (AASHTO, 1993). These design methodologies, which are empirical in nature, were developed based on field performance data obtained from the AASHO Road Tests. Although the 1993 AASHTO design guide contains state-of-the-practice refinements in material input parameters and design procedures, an update was warranted to incorporate the principles of engineering mechanics in pavement design. NCDOT is currently using a version of the 1993 AASHTO design guide procedure with local adjustment factors.

To implement an improved design guide for new and rehabilitated pavements, a new mechanistic-empirical pavement design guide (MEPDG) and corresponding software were developed through the National Cooperative Highway Research Program (NCHRP) 1-37A project. The MEPDG software currently recognized as Pavement Mechanistic-Empirical Design (PMED) considers relevant input parameters, such as traffic, climate, and pavement material properties, and utilizes the theories of mechanics to assess pavement performance. The mechanistic portion of the PMED refers to application of the theory of engineering mechanics to estimate pavement stress and strain responses based on design inputs and then uses those responses to compute incremental damage over time. Cumulative damage is then converted to typical pavement distresses via transfer functions embedded in the software. These transfer functions are empirically calibrated with pavement distress measurements of in-service sections.

The design and performance analysis of rigid pavements with PMED is based on various input factors including material properties, traffic loads, climatic factors, and road-bed soil characteristics. Among the concrete material factors, elastic modulus (MOE), modulus of rupture (MOR) and coefficient of thermal expansion (CTE) are the most important inputs to the analysis. Predicted pavement characteristics including thickness, design life, serviceability, and cracking performance depend on these input factors. Accurate determination of these material properties was not a part of the design process until the advent of PMED. With further research, it was found that these three concrete material inputs (MOE, MOR, and CTE) can affect pavement performance quite significantly and accurate determination of these concrete material inputs is the key to reliable design of rigid pavements which can last for the desired service life.

Concrete is a composite material comprised of aggregates, water, cement, and supplementary cementitious materials (SCMs), where cement/SCMs and water comprise the cement paste. Thus, concrete CTE is dependent on the CTE of hardened cement paste and on the CTE of the aggregates. The CTE of hardened cement paste is affected by internal re-distribution of water between capillary pores and gel pores (Helmuth, 1961; Bazant, 1970; Sellevold, 2006). The volume of these pores varies with age due to the hydration process (Mindess, 2002; Neville, 2011) thus it can be assumed that CTE varies with concrete age. The rising temperature causes immediate expansion due to increased pore water pressure in gel pores followed by a gradual flow of water out of the gel pores causing contraction. The immediate expansion of gel pores causes thermal expansion of concrete. Since the volume of gel pores increases with the concrete age/hydration process, the CTE of concrete increases with concrete age. The hydration process in concrete is a slow process which can be assumed to be almost completed at 360 days; thus it is viable to assume that CTE values may increase up to 360 days of concrete age. It can also be reasonably assumed that the age-dependent CTE of concrete mixtures will be impacted by use of SCMs which influence the rate of hydration and pozzolanic reactions. Several researchers have studied the effects of different variables including concrete age on CTE values of concrete mixtures but found contradicting conclusions. Some researchers opine that the CTE remains statically constant with concrete age, but others found that age has a considerable effect on CTE of concrete (Alungbe et al. 1992; Tran et al. 2009; Havel et al. 2015; Jeong et al. 2011; Shin et al. 2011; Kim et al. 2015).

1.2 Research Need

NCDOT is planning to incorporate PMED into the design process for rigid pavements and use of appropriate concrete mechanical and thermal properties are an essential part of this design process. The NCDOT research project titled "Improved Data for Mechanistic-Empirical Pavement Design for Concrete Pavements" was completed in 2016, as an initial step to conduct the characterization of concrete materials (FHWA Report No. NC/2015-03, Cavalline et al. 2018) and provided a database of concrete material inputs. This project was conducted on paving mixtures prepared using one aggregate source from each of the NC regions (Piedmont, Coastal, and Mountain). These aggregate sources comprised two granite aggregates and one limestone aggregate with the CTE values ranging from 4.2 to 4.6 με/°F. Mixtures included in this study primarily included a manufactured sand, although several mixtures used a natural sand. In addition to changes in concrete thermal properties attributed to the coarse aggregate type, this study noted changes thermal properties due to fine aggregate type.

Many rigid pavements are being constructed (or are planned for construction) in North Carolina in areas with quarries not included in the RP 2015-03 project. These include rigid pavement projects in the Charlotte area, the Greensboro/Winston-Salem area, the Boone/Blowing Rock area, and the Morganton/Lenoir area which can be potential candidates for inclusion of local materials in an enhanced PMED database. Based on the NC geologic map, there may be some geologic differences that translate into thermal performance changes between these aggregates and the aggregates which were tested in the earlier project. So there is a need to incorporate these coarse aggregate sources and other variables to obtain a more detailed database and to evaluate the effects of the obtained material inputs on the design and performance analysis of rigid pavements. Additionally, contractors are increasingly using concrete mixtures that include blends of natural and manufactured sand, which provide cost savings from the manufactured sand while remaining more workable than manufactured sand-only mixtures. Sand blends were not included in the RP 2015-03 study, which focused primarily on mixtures with manufactured sand. Recent trends have shown a return towards use of natural sand in rigid pavement mixtures submitted to NCDOT, but this trend could change in the future.

This need also amplifies as NCDOT is undertaking new rigid pavement projects including re-construction/widening of I-26 (costing $531 million) and I-540 expressway project (costing $2.2 billion) and many more rigid pavement projects to come in the future. With an expanded, locally calibrated material database, the pavement designers will have the opportunity to select the most suitable concrete inputs for use in a design for a specific project and may be able to target aggregate sources when certain performance characteristics are desirable. When PMED is utilized to conduct the design and performance analysis of the rigid pavement system, predictions of rigid pavement performance will be more accurate and reliable.

Prior research established that concrete CTE has a direct impact on the design and performance of rigid pavements and overlays. CTE regulates the magnitude of curling and related stresses that impact the performance of rigid pavements with regards to cracking, faulting and pavement roughness. Several researchers investigated the effects of concrete age on CTE but found different conclusions. While some researchers opined that the CTE decreases with age, some concluded that CTE increases with age, and some said that CTE remains constant (Alungbe et al. 1992; Tran et al. 2009; Jeong et al. 2011;). Several of the previous studies had some limitations, i.e. use of old test methods, short term CTE testing, and inputs obtained using methods not following the AASHTO T 336 test protocol. The latest studies showed a significant effect of age progression on CTE value of paving concrete with CTE increasing with a percent increase of 6.4% to 12.6% between 28 days and 360 days (Sabih and Tarefder 2019). This variation in CTE with age progression has a significant impact on all the performance parameters of rigid pavements and use of the 28-day CTE may give a non-optimal design and/or inaccurate performance predictions (Sabih and Tarefder 2019). With this in mind, there is a need to conduct long-term testing of concrete paving mixtures being used in North Carolina to evaluate the changes in CTE values of these mixtures with age progression. This will be a step forward towards improved rigid pavement design and constructing pavements that can perform well throughout the designed service life.

1.3 Research Objectives

The objectives of this proposed research project are as follows:

- Batching concrete mixtures according to NCDOT specifications for rigid pavements using aggregates from various sources selected by the Steering and Implementation Committee (StIC) and the research team. Targeted sources included quarries in the Charlotte area, the Greensboro/Winston-Salem area, the Boone/Blowing Rock area, and the Morganton/Lenoir area. Fine aggregates selected for this study were natural sands, expanding the data available to support PMED beyond the primarily manufactured sand mixtures used in RP 2015-03. The mixtures also included a Type I/II cement and a Class F fly ash typically used in North Carolina will be utilized. Other variables including water-to-cement ratio, cementitious materials content, and aggregate contents were incorporated into the experimental matrix.
- Laboratory testing was conducted to determine time series data of concrete mechanical and thermal properties including compressive strength, elastic modulus, MOR, CTE, thermal conductivity, and heat capacity. This will generate a data base of Level 1 inputs to facilitate the design of rigid pavements using PMED. Data to support an improved understanding the potential durability performance of the mixtures was also obtained via surface resistivity and volumetric shrinkage tests. Using the results of laboratory testing, prepare a catalog of Level 1 concrete inputs to be used with PMED software.
- Sensitivity analysis was conducted to evaluate the impact of concrete mechanical and thermal properties on the predicted distress levels of JPCP using PMED simulations and incorporating the time series input data.
- The changes in CTE of concrete paving mixtures with age progression was evaluated by conducting long-term CTE testing up to the age of 360 days and the effects of these changes was evaluated with regards to rigid pavement design using PMED.

- Guidance was prepared to ensure the findings of this study are directly implementable by NCDOT and other stakeholders using the PMED software for design and performance analysis of North Carolina rigid pavements.

2.0 LITERATURE REVIEW - OVERVIEW

To present a concise report, the literature review is included Appendix A. The literature review performed to support this project focused on three key areas, listed below.

- Characterization of concrete materials for implementation of PMED for rigid pavement design
- Effects of mechanical and thermal properties of paving concrete on the pavement performance analysis and pavement design using PMED
- Effects of concrete age on coefficient of thermal expansion of paving concrete
- Performance prediction models incorporated in Pavement ME Design software

3.0 DEVELOPMENT OF CONCRETE MIXTURE DESIGN MATRIX

3.1 Concrete Mixtures

The concrete mixture matrix developed for this project included concrete mixtures typical of those used in interstate and other types of rigid pavement in North Carolina. The mixture matrix leveraged data obtained from RP 2015-03 and focused more on the use of Type I/II cement, two levels of Class F fly ash (20% and 30% replacement rates at 1:1 by weight, per 2018 Specifications) and natural sand. The previous MEPDG project RP 2015-03 only included fly ash at a replacement rate of 20% at 1 lb cement to 1.2 pounds fly ash substitution, per 2012 Specifications. The concrete mixture matrix for RP 2022-07 is shown in Figure 3.1. The notations used in this matrix are as follows:

- Coarse aggregates: 4 coarse aggregates designated as C1 to C4
- Fine aggregates: 2 fine aggregate sources (natural sand) designated as N1 and N2
- Cement type: OPC designated as O
- Fly Ash: fly ash replacement of 20%, and 30% designated as F20 and F30

A sample mixture designation is C1N1OF20 based on Coarse aggregate-1, Natural sand-1, OPC, and 20% Fly Ash.

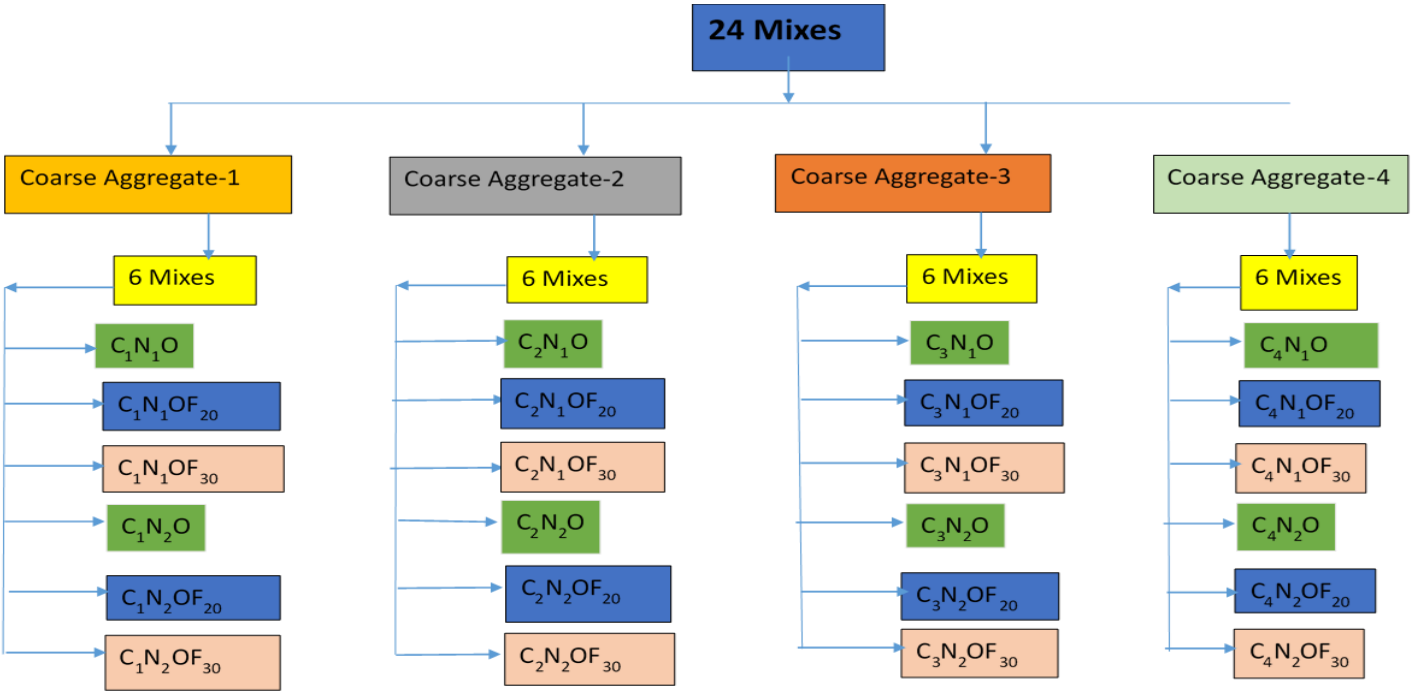

Figure 3.1: Mixtures included in RP 2022-07

Sources of these materials were selected by NCDOT and project personnel based on past and future NCDOT concrete pavement projects. Various options were considered for the selection of coarse aggregate and fine aggregate sources, and

efforts were made to include aggregates being used at I-26 and I-540 projects. Cement and fly ash sources were selected to be consistent with NCDOT RP 2015-03. Table 3.1 provides a list of materials selected for use in this project. A cement mill certificate and fly ash chemical test report are provided in Appendix B, Figures B.1 and B.2, respectively.

Table 3.1: Materials selected for RP 2022-07

Material / Region Represented	Source	Rationale for selection or Project using material
Cement	Holly Hill, SC plant, Type I/II	Consistent with NCDOT RP 2015-03
Fly Ash	Belews Creek	Consistent with NCDOT RP 2015-03
Coarse Aggregate / Piedmont	Statesville Quarry, Statesville, NC	I-40
	Knightdale Quarry, Knightdale, NC	I-540
Coarse Aggregate / Mountain	Hendersonville Quarry, Hendersonville, NC	I-26 / Contractor A
	Black Mountain Quarry, Black Mountain, NC	I-26 / Contractor B
Fine Aggregate	Emery Pit, Jackson Springs, NC	Commonly used in NCDOT projects, material properties "typical" of other NC natural sands
	Buckleberry Mine, Princeton, NC	

Concrete Mixtures Specifications

The research team developed mixture proportions for each of the 24 mixtures included in the project. Mixtures were developed using the following parameters:

- Total cementitious materials content: 573 pcy, consistent with that used in RP 2015-03
- Fly ash replacement rates: 20% and 30% at 1:1 by weight, per 2018 specifications
- w/cm ratio: 0.42. This is lower than that used in RP 2015-03 (0.48), but that project focused on manufactured sand and required a high w/cm to achieve workability. A w/cm of 0.42 corresponds to a moderate w/cm used in the two previous Performance Engineered Mixtures (PEM) projects, RP 2018-14 (Cavalline et al., 2020), and RP 2020-13 (Cavalline et al., 2023).
- Coarse aggregate volume: 11 cf per cy of concrete, consistent with that used in RP 2015-03, and with the approach used in developing adequately stiff paving mixtures by local producers
- Coarse aggregate parameters: Meeting AASHTO #67 gradation; specific gravity, dry rodded unit weight, absorption typical of coarse aggregates of the region supplying NCDOT projects
- Fine aggregate parameters: Meeting ASTM C33; specific gravity, fineness modulus, and absorption typical of the fine aggregates of the region often supplying NCDOT projects

Table 3.2 provides the specific gravity and absorption of aggregates, with additional supporting information on the aggregate minerology provided in Appendix B, Tables B.1 and B.2. Table 33 provides the mixture proportions for the 24 mixtures included in this study. Note that aggregate weights are provided as oven dry, and moisture corrections were made to account for aggregate moisture state at the time of batching. Two commercially available admixtures, a high-range water-reducing admixture and an air entraining admixture, were used throughout the batching process at dosages within manufacturers' recommendations. The target air content for all mixtures kept for testing was kept between 5 to 6%, consistent with previous work by the UNC Charlotte research team and allowing air content to minimally impact measurements of concrete properties and durability performance. Although the aggregate system was designed to meet sufficiently stiff mixtures typically slip-form paved, the target slump was increased using water reducing admixtures to between 4 to 5 inches. However, the w/cm was maintained regardless of slump achieved with a given water content and water-reducing admixture dosage used.

Table 3.2: Specific gravity and absorption values for aggregates included in RP 2022-07

Type of Aggregate	Aggregate Source (Mixture ID code number)	SG	Absorption (%)	Fineness Modulus
Coarse Aggregate	Statesville Quarry (1)	2.879	0.54	N/A
	Knightdale Quarry (2)	2.602	0.60	
	Black Mountain Quarry (3)	2.720	0.50	
	Henderson Quarry (4)	2.644	0.90	
Fine Aggregate	Emery Pit Sand (1)	2.618	1.54	2.70
	Buckleberry Mine Sand (2)	2.639	0.42	2.60

Table 3.3: Mixture proportions for concrete mixtures included in RP 2022-07

Mixture ID	**Coarse Aggregate**	**Fine Aggregate**	**Mixture Proportions, pcy**				
			Cement	**Fly ash**	**Coarse aggregate**	**Fine aggregate**	**Water**
C_1N_1O	Statesville Quarry	Emery Pit	573.0	0	1976.2	1266.7	240.0
$C_1N_1OF_{20}$			458.4	114.6	1976.2	1231.5	240.0
$C_1N_1OF_{30}$			401.1	171.9	1976.2	1213.8	240.0
C_1N_2O		Buckleberry Mine	573.0	0	1976.2	1254.6	240.0
$C_1N_2OF_{20}$			458.4	114.6	1976.2	1219.7	240.0
$C_1N_2OF_{30}$			401.1	171.9	1976.2	1202.3	240.0
C_2N_1O	Knightdale Quarry	Emery Pit	573.0	0	1786.0	1266.7	240.0
$C_2N_1OF_{20}$			458.4	114.6	1786.0	1231.5	240.0
$C_2N_1OF_{30}$			401.1	171.9	1786.0	1213.8	240.0
C_2N_2O		Buckleberry Mine	573.0	0	1786.0	1254.6	240.0
$C_2N_2OF_{20}$			458.4	114.6	1786.0	1219.7	240.0
$C_2N_2OF_{30}$			401.1	171.9	1786.0	1202.3	240.0
C_3N_1O	Hendersonville Quarry	Emery Pit	573.0	0	1867.0	1266.7	240.0
$C_3N_1OF_{20}$			458.4	114.6	1867.0	1231.5	240.0
$C_3N_1OF_{30}$			401.1	171.9	1867.0	1213.8	240.0
C_3N_2O		Buckleberry Mine	573.0	0	1867.0	1254.6	240.0
$C_3N_2OF_{20}$			458.4	114.6	1867.0	1219.7	240.0
$C_3N_2OF_{30}$			401.1	171.9	1867.0	1202.3	240.0
C_4N_1O	Black Mountain Quarry	Emery Pit	573.0	0	1814.8	1266.7	240.0
$C_4N_1OF_{20}$			458.4	114.6	1814.8	1231.5	240.0
$C_4N_1OF_{30}$			401.1	171.9	1814.8	1213.8	240.0
C_4N_2O		Buckleberry Mine	573.0	0	1814.8	1254.6	240.0
$C_4N_2OF_{20}$			458.4	114.6	1814.8	1219.7	240.0
$C_4N_2OF_{30}$			401.1	171.9	1814.8	1202.3	240.0

4.0 LABORATORY TESTING PROGRAM, RESULTS, AND ANALYSIS

4.1. Laboratory Testing Program

The laboratory testing program for this project is shown in Table 4.1.

Table 4.1: Testing program for NCDOT RP 2022-07

	Test	Test Protocol	Age (Days)
Fresh Concrete properties	Slump	ASTM C143, "Standard Test Method for Slump of Hydraulic Cement Concrete."	Fresh Concrete
	Air content	ASTM C231, "Standard Test Method for Air Content of Freshly Mixed Concrete by the Pressure Method."	
	Fresh Density (Unit Weight)	ASTM C138, "Standard Test Method for Density (Unit Weight), Yield, and Air content (Gravimetric) of Concrete."	
	Temperature	AASHTO T 309, "Temperature of Freshly Mixed Hydraulic Cement Concrete."	
Mechanical Properties of Hardened Concrete	Compressive Strength	ASTM C39, "Standard Test Method for Compressive Strength of Cylindrical Concrete Specimens."	3, 7, 28, 90, 180, 270, 360
	Modulus of rupture	ASTM C78, "Standard Test Method for Flexural Strength of Concrete (Using Simple Beam with Third-Point Loading)."	28
	Modulus of Elasticity*	ASTM C469, "Standard Test Method for Static Modulus of Elasticity and Poisson's Ratio of Concrete in Compression."	3, 7, 28, 90, 180, 270, 360
Thermal Properties of Hardened Concrete	Coefficient of Thermal Expansion	AASHTO T 336, "Coefficient of Thermal Expansion of Hydraulic Cement Concrete."	14, 28, 90, 180, 270, 360
	Thermal Conductivity	ASTM E1952 "Standard Test Method for Thermal Conductivity and Thermal Diffusivity by Modulated Temperature Differential Scanning Calorimetry," or alternative method	56, 90
	Heat Capacity	ASTM D2766, "Standard Test Method for Specific Heat of Liquids and Solids," or alternative method	56, 90
Durability	Surface Resistivity	AASHTO T 358, "Standard Method for Surface Resistivity Indication of Concrete's Ability to Resist Chloride Ion Penetration."	3, 7, 28, 90, 180, 270, 360
	Unrestrained Shrinkage	ASTM C157, "Standard Test Method for Length Change of Hardened Hydraulic-Cement Mortar and Concrete."	Per Standard

4.2 Batching and Mixing Procedure

In order to cast enough specimens to satisfy the testing program outlined in Table 4.1, a substantial amount of concrete was required. However, due to size constraints of laboratory equipment and to ensure uniform and consistent mixing, the total amount of concrete required for each mixture was broken into two batches, each 2 cubic feet (cf) in size. Each batch was mixed in compliance with ASTM C685, "Standard Specification for Concrete Made by Volumetric Batching and Continuous Mixing" (ASTM, 2018). Batch 1 of each mixture was used to prepare 21 4 in x 8 in cylinders used for 3, 7, 28, 90, 180, 270, and 360 day surface resistivity, modulus of elasticity, Poisson 's ratio, and compressive strength, three 4 in x 8 in cylinders for thermal conductivity and heat capacity. Batch 2 was utilized to make two 6 in x 6 in x 18 in beams for modulus of rupture and three 4 in x 4 in x 12 in beams for unrestrained shrinkage.

To ensure uniformity and consistency between all batches of concrete, fresh property tests were performed. These tests include slump, air content, fresh density, and temperature. Specimens were prepared in accordance with ASTM C192 "Standard Practice for Making and Curing Concrete Test Specimens in the Laboratory" (ASTM, 2020). Multiple individuals assisted in the batching and preparation of test specimens. When possible, each team member was responsible for the preparation of the same type of specimens (e.g. cylinders, beams) or running fresh tests to minimize variability. Specimens were demolded after 24 hours per ASTM C192 and placed into a curing room in accordance with ASTM C511 "Standard Specification for Mixing Rooms, Moist Cabinets, Moist Rooms, and Water Storage Tanks Used in the Testing of Hydraulic Cements and Concretes" (ASTM, 2021).

4.3 Fresh Concrete Test Results

Results from the fresh concrete tests are shown in Appendix B, Table B.3. Some findings of note include:

- As could be expected, mixtures containing fly ash had greater workability and required less water reducing admixture to achieve the target slump.
- Mixtures containing fine aggregate sourced from Emery Pit were more workable and required less water reducing admixture to achieve the target slump. The fineness modulus of each fine aggregate was similar (Emery Pit - 2.7, Buckleberry Mine - 2.6). However, on a visual inspection, sand sourced from Buckleberry Mine generally appeared to be more angular compared to sand sourced from the Emery Pit.
- Of the mixtures containing coarse aggregate sourced from the Piedmont region, mixtures containing Statesville aggregate had the highest unit weight on average, approximately 148.3 pcf. compared to mixtures containing Knightdale coarse aggregate which had an average unit weight of 142.9 pcf.
- Concrete mixtures containing coarse aggregate sourced from the Mountains generally had similar unit weights to mixtures containing coarse aggregates sourced from the Piedmont. Mixtures containing aggregate sourced from Black Mountain on average had a unit weight of approximately 145.9 pcf. In comparison, mixtures comprised of coarse aggregate sourced from Hendersonville had an average unit weight of 141.7 pcf. These results were to be expected due to the higher specific gravity of the coarse aggregate from Statesville and Black Mountain compared to Knightdale and Hendersonville. The location the fine aggregate was sourced from does not appear to have a significant impact on the unit weight of fresh concrete. Mixtures containing sand sourced from the Emery Pit had an average unit weight of 144.5 pcf, while mixtures containing sand from Buckleberry Mine had an average unit weight of 144.9 pcf.
- Cavalline et al. (2018) found similar results in RP 2015-03 with concrete mixtures containing coarse aggregate sourced from the Piedmont and Mountain regions having a fresh unit weight between 141 and 145 pcf in RP 2015-03. Of note, AASHTOWare Pavement ME Design software uses a default unit weight of 150 pcf for concrete paving mixtures (Geary, 2021).

4.4 Hardened Concrete Test Results

4.4.1 *Rationale and Supplemental Information on Test Methods*

Test of hardened concrete was performed to gain mechanical, thermal, durability properties to be used as inputs for AASHTOWare Pavement ME. Another goal of this study was to identify how certain properties change over an extended period of time. Therefore, later-age testing was performed to a sample age of 360 days for several key tests. The mechanical properties tested in this study include compressive strength, MOE, MOR, and Poisson's ratio, each tested using the standard test method provided in Table 4.1.

The thermal properties include CTE, thermal conductivity, and heat capacity. CTE was tested in accordance with AASHTO T 336 using Pine Instruments AFCT machine. For each mixture design, three 4 in x 8 in cylinders were cut to a length of 7 inches. These samples were allowed to cure in a saturated lime water solution for the entire duration of testing. CTE testing was performed at 14, 28, 90, 180, 270, and 360 days in accordance with AASHTO T 336. Due to the limited size of laboratory equipment and the day-long test duration, testing to determine a CTE value at each age was divided into three testing days. The results for each test were then averaged to get a representative CTE value for the mixture. For example, for 14-day testing, one sample was tested on 13-day, another sample was tested on 14-day, and finally the last sample was tested on 15-day, with the results averaged to determine the 14-day value. The specimens were rotated between each frame of the machine over the three days, helping to reduce error or bias in the measurements.

Heat capacity tests were performed on concrete specimens at 56, 90, and 360 days using the Fox50 Heat Flow Meter Instrument by Laser comp. The Fox50 was used for this study for its ability to test bulk specimens. Tests to measure the heat capacity were performed in accordance with ASTM D2766. Three specimens were tested for each mixture. Specimens

were sourced from the one-inch excess material from the 4 in by 8 in cylinders cut to 7 in length for CTE testing. Specimens were cut into rectangular prisms 1.5 in x 1.5 in x 1 in thick seven days before testing. During sawcutting, care was taken to ensure the test specimen accurately represented the mixture composition and did not contain any large air voids. To ensure a consistent moisture content in each test specimen, after sawcutting, samples were stored in an environmental chamber set at 72°F and 50% relative humidity for seven days prior to testing. Rubber pads and parchment paper were placed on the top and bottom of the specimen to ensure uniform contact between the Fox50 thermal plates and the surface of the specimen. The heat capacity and thickness of the rubber pads and parchment paper were measured and accounted for in the calculations to obtain a corrected heat capacity value.

Thermal conductivity tests were also performed on 56, 90, and 360 days using the Fox50 Heat Flow Meter Instrument by Laser comp. The same specimens used to test heat capacity were also used for thermal conductivity testing. Preparation, conditioning, and testing of specimens are outlined above. Tests to measure thermal conductivity were done in accordance with ASTM E1952. Surface resistivity and unrestrained shrinkage tests were performed to evaluate the durability of each concrete mixture per the standard test methods provided in Table 4.1.

4.4.2 *Mechanical Property Test Results*

4.4.2.1 Compressive Strength

Compressive strength test results are provided in Appendix B, Table B.4. A graph of compressive strength test results with mixtures sorted by fly ash content is provided in Figure 4.1. Similar plots of compressive strength results with mixtures sorted by aggregate type and source are provided in Appendix B, Figures B.3 and B.4. NCDOT 2018 specifications concrete mixtures used in pavement applications must achieve a 28-day compressive strength of 4,500 psi (NCDOT, 2018). All mixtures containing no fly ash met or exceeded the 4,500 psi compressive strength requirement by 28 days. On average, mixtures containing no fly ash had a 28-day compressive strength of approximately 5,343 psi. Mixtures with 20% and 30% fly ash replacement did not achieve NCDOT 28-day strength requirements, exhibiting an average strength of approximately 4,329 psi and 3,662 psi by 28 days, respectively. The lower average 28-day strength not meeting NCDOT specification is likely caused by the delayed hydration of fly ash and the w/cm ratio and cement content being held constant between all mixtures. It should be noted, however, that mixtures with 20% and 30% fly ash replacement did achieve NCDOT specifications by 90 days of age.

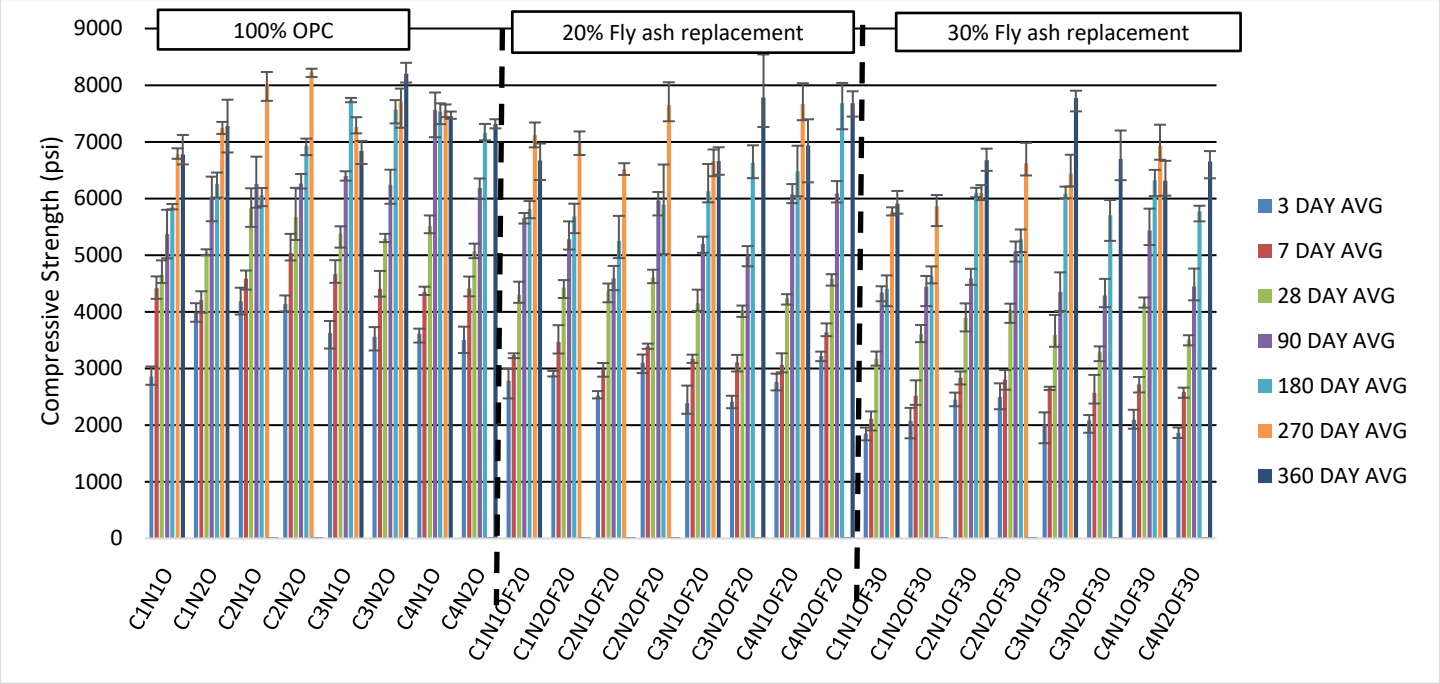

Figure 4.1: Average compressive strength test results with mixtures grouped by fly ash content

On average, the region of North Carolina the aggregate was sourced from – the Piedmont and the Mountain regions – did not significantly influence the compressive strength, as exhibited by an average difference in 28-day compressive strength of less than 100 psi. Additionally, of the four coarse aggregates, mixtures containing aggregate sourced from Knightdale and Black Mountain had the highest compressive strength on average between 28 and 180 days of age. General trends

suggest the source of fine aggregate did not impact the compressive strength, with an average difference in 28-day compressive strength of approximately 45 psi. This analysis is shown in Appendix B, Table B.5.

Graphs of compressive strength gain over time with mixtures grouped by aggregate type and source are shown in Appendix B, Figures B.5 through B.8. As expected, concrete mixtures containing fly ash had lower early age compressive strength compared to mixtures without any fly ash. However, at later ages, mixtures containing fly ash continued to increase in strength. On average, after 90-days of age, mixtures containing coarse aggregate sourced from the Mountain region began to outperform mixtures containing coarse aggregate sourced from the Piedmont. Mixtures produced using the Black Mountain and Statesville coarse aggregate displayed the most disparate behavior, despite being of similar geologic description. On average, the source of the location of fine aggregate does appear to appreciably not impact the compressive strength over time.

The compressive strength test results from this research study were compared to the compressive strength test results compiled from RP 2015-03. Concrete mixtures containing no fly ash produced in the research study RP 2015-03 had similar 28-day compressive strength to those in this project (approximately 5,140 psi). However, concrete mixtures batched in the previous study with mixtures consisting of a 20% fly ash replacement had lower 28-day compressive strength compared to the results found in this study. This is potentially due to the fact that concrete mixtures batched in the previous study conformed to NCDOT 2012 standards and specifications, where fly ash was to be substituted at a rate of 1.2 pounds of fly ash for each pound of cement replaced, up to a maximum of 20% fly ash replacement (NCDOT, 2012). For this study, the concrete mixtures were produced to conform with 2018 NCDOT standards and specifications where fly ash may be substituted at a rate of one pound of fly ash to each pound of cement to be replaced; up to a 30% fly ash replacement (NCDOT, 2018). Therefore, more fly ash is present in the 20% replacement mixtures produced in the previous study, which could be an explanation for the lower compressive strength. Other contributing factors to the difference in average strengths could be a slightly different chemical composition or fineness of the Class F fly ashes used in the two studies.

PMED suggests a default input value of 5,275.3 psi, which is similar to the 28-day average compressive strength of mixtures without fly ash. Many, if not most, North Carolina rigid pavements have recently been constructed using mixtures containing fly ash, and the default input may not accurately represent the 28-day strength of these mixtures.

4.4.2.2 Modulus of Elasticity

Modulus of elasticity test results are provided in Appendix B, Table B.6. A graph of MOE test results with mixtures sorted by fly ash content is provided in Figure 4.2. Similar plots of MOE results with mixtures sorted by aggregate type and source are provided in Appendix B, Figures B.9 and B.10. Similar to compressive strength test results, mixtures containing fly ash had lower 28-day MOE compared to mixtures containing no fly ash. On average, mixtures produced without fly ash substitution had an average 28-day MOE of approximately 2,510,000 psi. Mixtures comprised of a 20% and 30% fly ash replacement had an average 28-day MOE of 2,350,000 and 2,240,000 psi respectively. This difference could be expected due to the later age hydration reactions associated with fly ash mixtures.

Data summarizing the average MOE by aggregate, source, and fly ash content at 28 days is shown in Table B.7. Mixtures containing coarse aggregate sourced from the Piedmont region of North Carolina had an average 28-day MOE of approximately 2,560,000 psi, whereas mixtures comprised of coarse aggregate sourced from the Mountain region had an approximate 28-day MOE of 2,170,000 psi. The difference in these values fall in between the standard deviation of the averages. This may indicate that the region that aggregates are sourced from is not a major factor influencing differences in the MOE. The fine aggregates used appear to also have little influence on the MOE. Mixtures that included fine aggregate from the Emery Pit had an approximate average 28-day MOE of 2,420,000 psi, while mixtures containing fine aggregate sourced from Buckleberry Mine had an average 28-day MOE of approximately 2,310,000 psi.

All 28-day MOE results compiled in this research study were lower than the 28-day MOE results obtained from RP 2015-03 as well as lower than the recommended MEPDG input from the same study. Cavalline et al. (2018) recommended using 3,300,000 psi as a 28-day MOE input for PMED software for concrete paving mixtures containing natural sand, coarse aggregate sourced from the Piedmont region of North Carolina, and no fly ash. PMED software uses a default MOE value of 4,200,000 psi, significantly higher than the recommended value from RP 2015-03 and the values measured during this study.

Figures B.11 through B.14 show the increase in average MOE over time with concrete mixtures grouped by fly ash content, coarse aggregate source, region from which coarse aggregate was sourced, and location from which fine aggregate was sourced, respectively. As expected, due to the delayed hydration of fly ash, mixtures containing fly ash had lower MOE at all ages compared to mixtures not containing fly ash. At later ages, on average, the difference in MOE between mixtures with and without fly ash was reduced. MOE test results were significantly less than the PMED default value and Level 2 equation estimates. Mixtures containing coarse aggregate sourced from the Piedmont on average had higher MOE at early ages (3 to 28-days). After 28-days of age, the difference in test result averages is likely due to natural variation in specimen

preparation or testing. Mixtures produced using the Black Mountain and Statesville coarse aggregate (similar geologic description) displayed different behavior at early ages, but became more similar at later ages. The fine aggregate used does not appear to have a significant impact on the MOE over time.

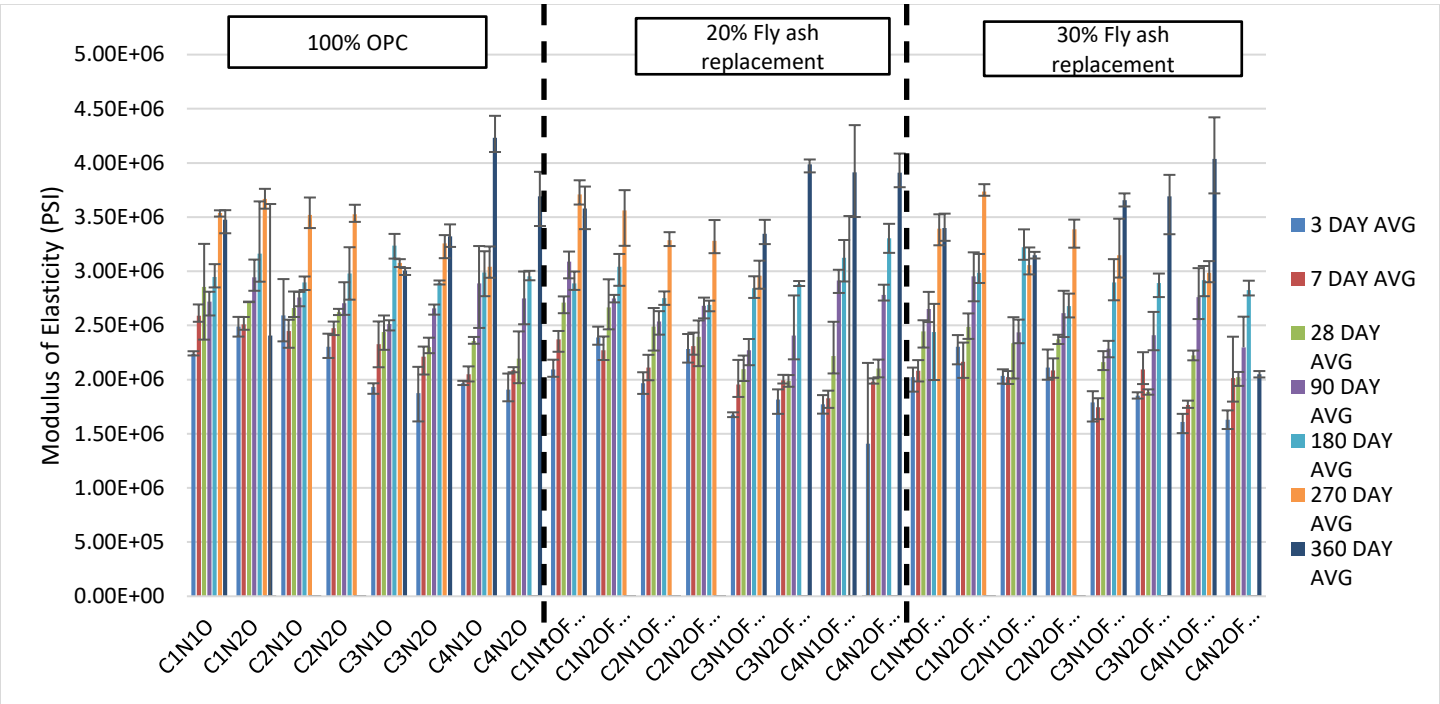

Figure 4.2: Average MOE test results with mixtures grouped by fly ash content

4.4.2.3 Poisson's Ratio

Poisson's ratio test results are provided in Appendix B, Table B.8. A graph of Poisson's ratio test results with mixtures sorted by fly ash content is provided in Figure 4.3. Similar plots of Poisson's ratio test results with mixtures sorted by aggregate type and source are provided in Appendix B, Figures B.15 and B.16. These results are summarized by region of North Carolina coarse aggregate from which coarse aggregate was sourced, location from which the coarse aggregate was sourced, location from which the fine aggregate was sourced, and the percent fly ash replacement.

Table B.9 shows the average 28-day Poisson's ratio of mixtures summarized by region of North Carolina coarse aggregate from which coarse aggregate was sourced, location from which the coarse aggregate was sourced, location from which the fine aggregate was sourced, and the percent fly ash replacement. General trends indicate neither the substitution of coarse aggregate, fine aggregate, nor varying amounts of fly ash in a concrete mixture significantly influence Poisson's ratio at 28-days of age. Figures B.17 through B.20 show Poisson's ratio test results between 0 and 180 days of age, with mixtures grouped by fly ash content, coarse aggregate location, fine aggregate location, and fly ash content, respectively.

RP 2015-03 recommended using a 28-Poisson's ratio 0.16 for concrete mixtures composed of coarse aggregate sourced from the Piedmont and using natural sand. This value is generally greater than the averages found in this study. However, it should be noted RP 2015-03 only tested three concrete mixtures containing natural sand compared to this study, which tested 24 concrete mixtures that included natural sand.

The AASHTOWare Pavement ME Design software default value for Poisson's ratio for newly constructed PCC slabs is 0.20 - higher than what was measured throughout this study with the exception of one specimen. A specimen from mixture C1N2O at 180-days of age was measured to have a Poisson's ratio of 0.224. Figure B.17 shows Poisson's ratio over time grouped by fly ash content. Similar to other mechanical property test results, mixtures containing fly ash had a lower Poisson's ratios at early ages compared to mixtures containing no fly ash until 28-days of age. The coarse and fine aggregate sources do not appear to significantly impact the rate at which Poisson's ratio changes over time, as seen in Figures B.18 through B.20.

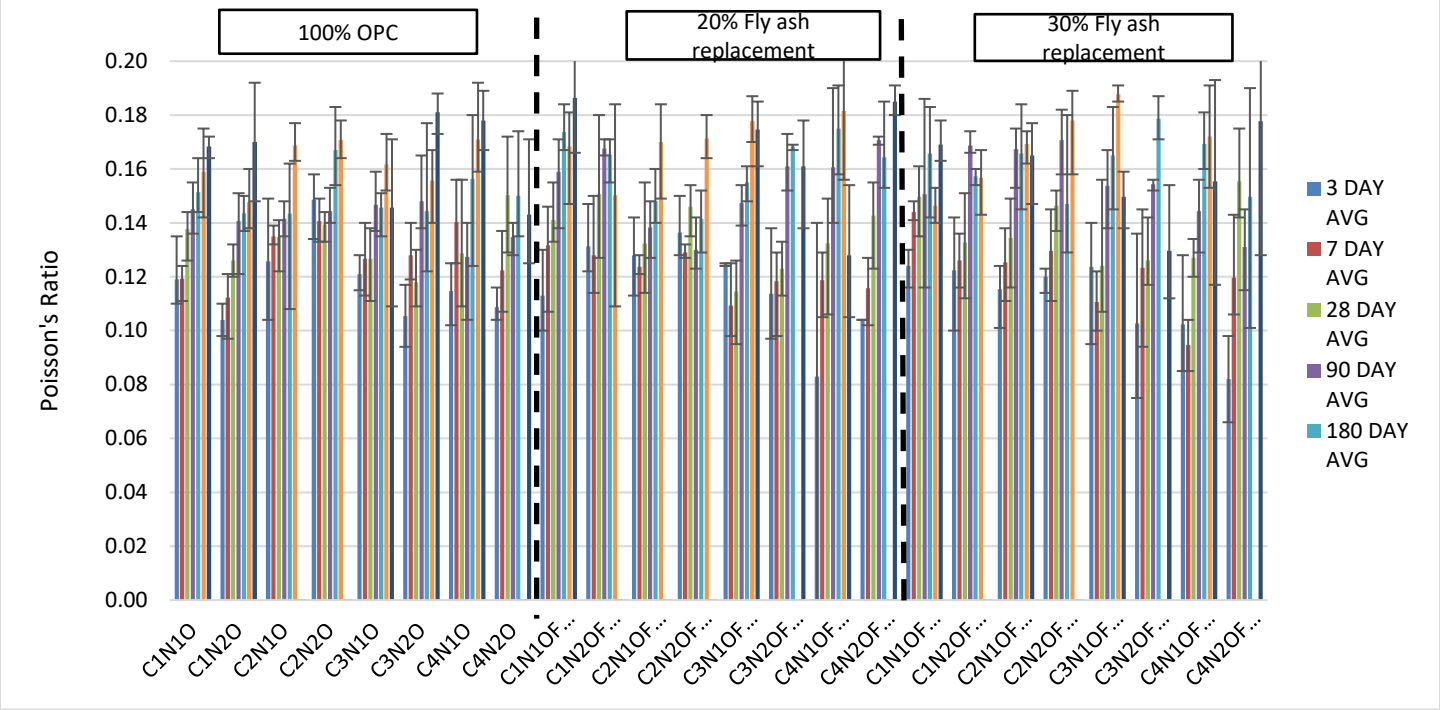

Figure 4.3: Average Poisson's ratio test results with mixtures grouped by fly ash content

4.4.2.4 Flexural Strength

The 28-day MOR test results are shown in B.10, while Table B.11 provides results summarized by aggregate source, region, and fly ash replacement. Figure 4.4 shows 28-day MOR test results with mixtures grouped by fly ash content, while Figures B.21 and B.22 show 28-day MOR with mixtures grouped by coarse aggregate and fine aggregate source, respectively.

According to NCDOT 2018 specifications, concrete mixtures used in pavement applications must achieve a 28-day modulus of rupture of 650 psi (red line on Figure 4.4). On average mixtures containing no fly ash achieved the required modulus of rupture with an average value of approximately 662 psi. Mixtures containing 20% and 30% fly ash replacement, on average, did not achieve the required modulus of rupture by 28 days. Results from RP 2015-03 were similar to the results found in this study. Mixtures containing fly ash failed to meet the requirement or barely met the NCDOT specification of 650 psi at 28 days (Cavalline et al. 2018). AASHTOWare Pavement ME Design software suggests a 28-day MOR default value of 690 psi; higher than all of the mixtures tested in this study, with the exception of two mixtures (C1N1O and C4N1O).

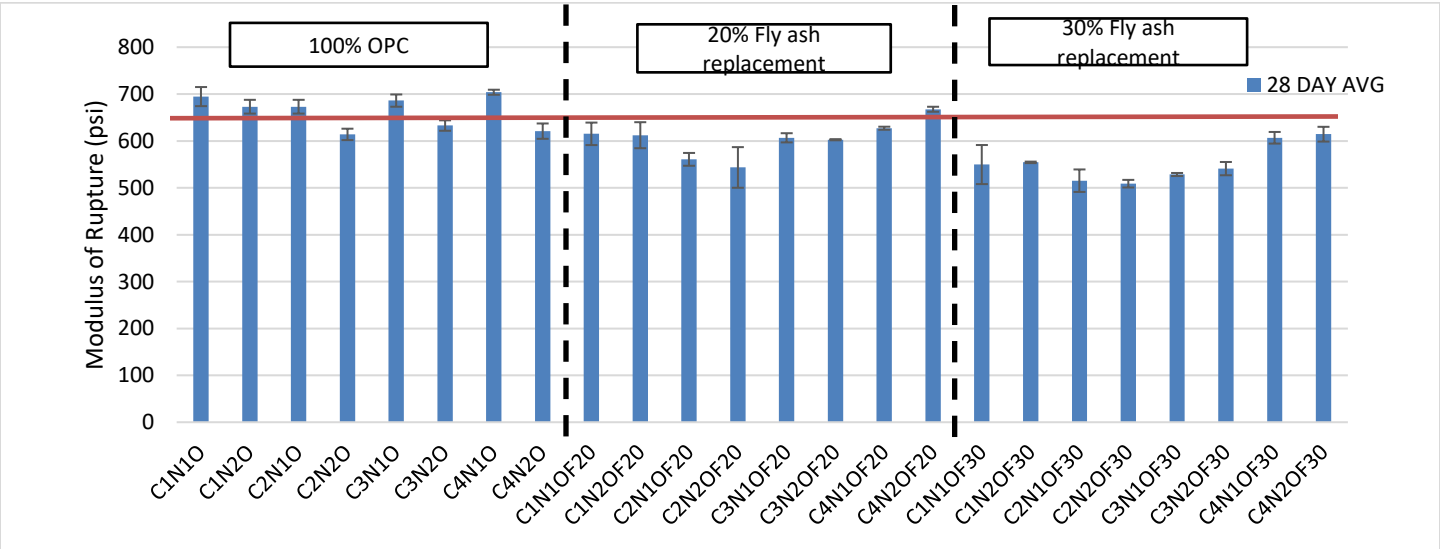

Figure 4.4: 28-day MOR test results with mixtures grouped by fly ash content

4.4.3 *Thermal Property Test Results*

4.4.3.1 Coefficient of Thermal Expansion

Coefficient of thermal expansion test results are provided in Appendix B, Table B.12. A graph of CTE test results with mixtures sorted by fly ash content is provided in Figure 4.5. Similar plots of CTE test results with mixtures sorted by aggregate type and source are provided in Appendix B, Figures B.23 and B.24. These results are summarized by region of North Carolina coarse aggregate from which coarse aggregate was sourced, location from which the coarse aggregate was sourced, location from which the fine aggregate was sourced, and the percent fly ash replacement.

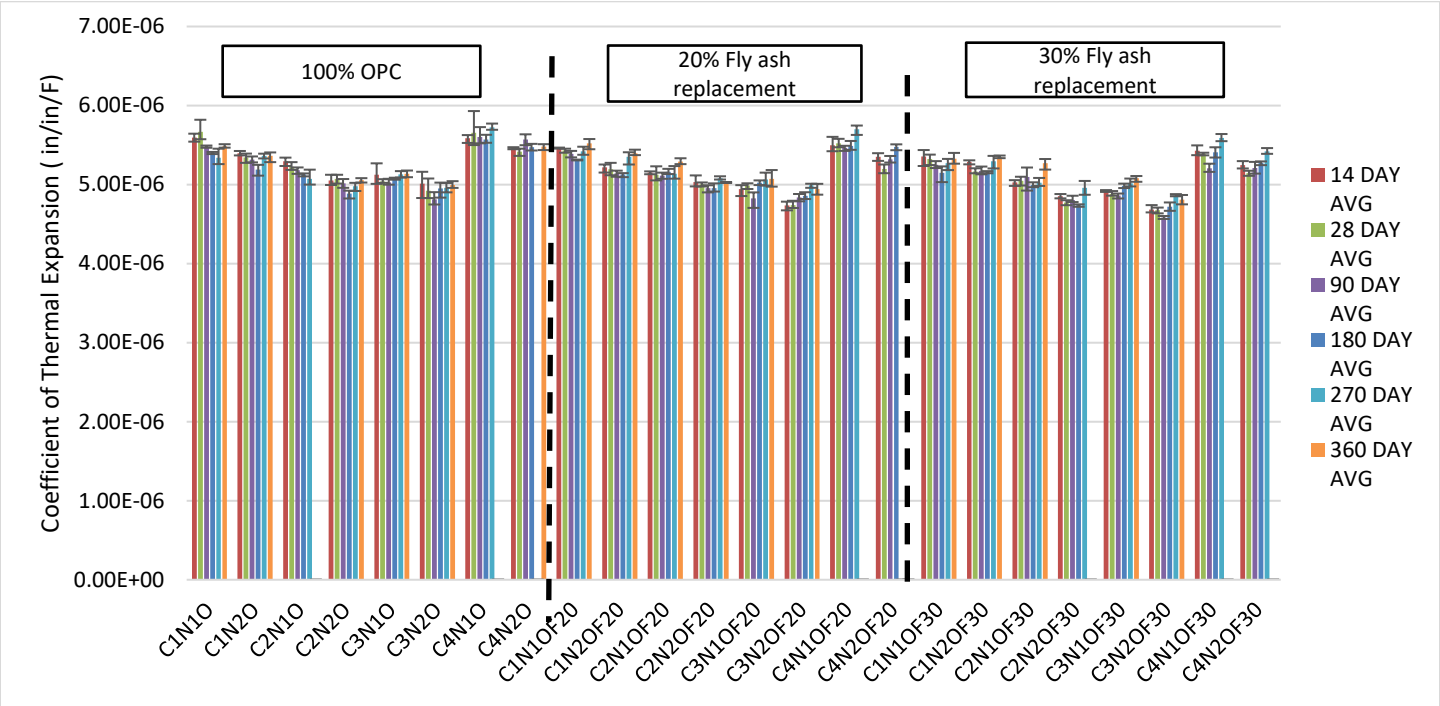

Figure 4.5: 28-day CTE test results with mixtures grouped by fly ash content

Table B.13 shows the average CTE of mixtures summarized by region of North Carolina coarse aggregate from which coarse aggregate was sourced, location from which the coarse aggregate was sourced, location from which the fine aggregate was sourced, and the percent fly ash replacement. Figures B.23 and B.24 show the average CTE of mixtures grouped by coarse aggregate source and fine aggregate source, respectively.

It should be noted that on average as the fly ash content of the mixture increases the CTE decreases, as seen in Figure 4.5. The location from which each coarse aggregate was sourced appears to have had the greatest influence on CTE. Mixtures containing coarse aggregate from Black Mountain and Statesville quarry had the highest measured CTE on average between 5.39 and 5.43×10^{-6} inch per inch per degree Fahrenheit.

Results from RP 2015-03 were similar to the results found in this study. Average 28-day CTE ranged between 5.40 and 4.23×10^{-6} inch per inch per degree Fahrenheit. In RP 2015-03, however, Cavalline et al. (2018) noted the material that with the greatest influence on CTE was the fine aggregate. Concrete mixtures containing manufactured sand had lower CTE ranging between 4.23 and 4.57×10^{-6} inch per inch per degree Fahrenheit whereas concrete mixtures containing natural sand had an average CTE between 5.31 and 5.40×10^{-6} inch per inch per degree Fahrenheit. AASHTOWare Pavement ME Design software suggest 4.9×10^{-6} inch per inch per degree Fahrenheit as a default values (Geary, 2021), similar to the to the average CTE results found for concrete mixtures containing coarse aggregate from the Hendersonville quarry.

Figures B.25 through B.28 show the average CTE test results between 0 and 180 days, with mixtures grouped by fly ash content, coarse aggregates source, region of North Carolina from which the coarse aggregate was sourced, and location from which the fine aggregate was sourced, respectively.

The long-term (360 days) CTE test results show that there is a mixed trend of increase and decrease in CTE values between 28 days and 360 days. Out of the total of 24 concrete mixtures, 13 mixtures showed a % increase of 2.8% to 6.4%, 1 mixture showed a decrease of 3.2%, 8 mixtures showed less than 2% decrease, and 2 mixtures showed less than 2%

decrease. This change in long-term CTE values may have a significant impact on the pavement performance and further investigation will be conducted and will be published over the Summer 2024.

Per the AASHTO T 336 standard (2022) it is expected for results from two properly conducted tests on specimens from the same batch of concrete performed by a single operator to not vary by more than 0.12 microstrain per degree Fahrenheit. Variations in time series data collected from laboratory testing showed that 10 mixtures fall within this 0.12 microstrain per degree Fahrenheit range and 14 mixtures fall outside this 0.12 microstrain per degree Fahrenheit range. One trend that was observed is that as the fly ash content increases the 28 days CTE values tended to decrease for all the 24 mixtures being tested.

4.4.3.2 Thermal Conductivity

Table B.14 provides the results of 56 and 90-day thermal conductivity testing, with Table B.15 showing the average results with mixtures grouped by aggregate source and fly ash content. Figure 4.6 shows the average thermal conductivity test results with mixtures grouped by fly ash content. Similar plots of thermal conductivity test results with mixtures sorted by aggregate type and source are provided in Appendix B, Figures B.29 and B.30. Figures B.31 through B.34 show the change in thermal conductivity over time, with mixtures grouped by fly ash content, coarse aggregate source, region of North Carolina from which the coarse aggregate was sourced, and fine aggregate source, respectively.

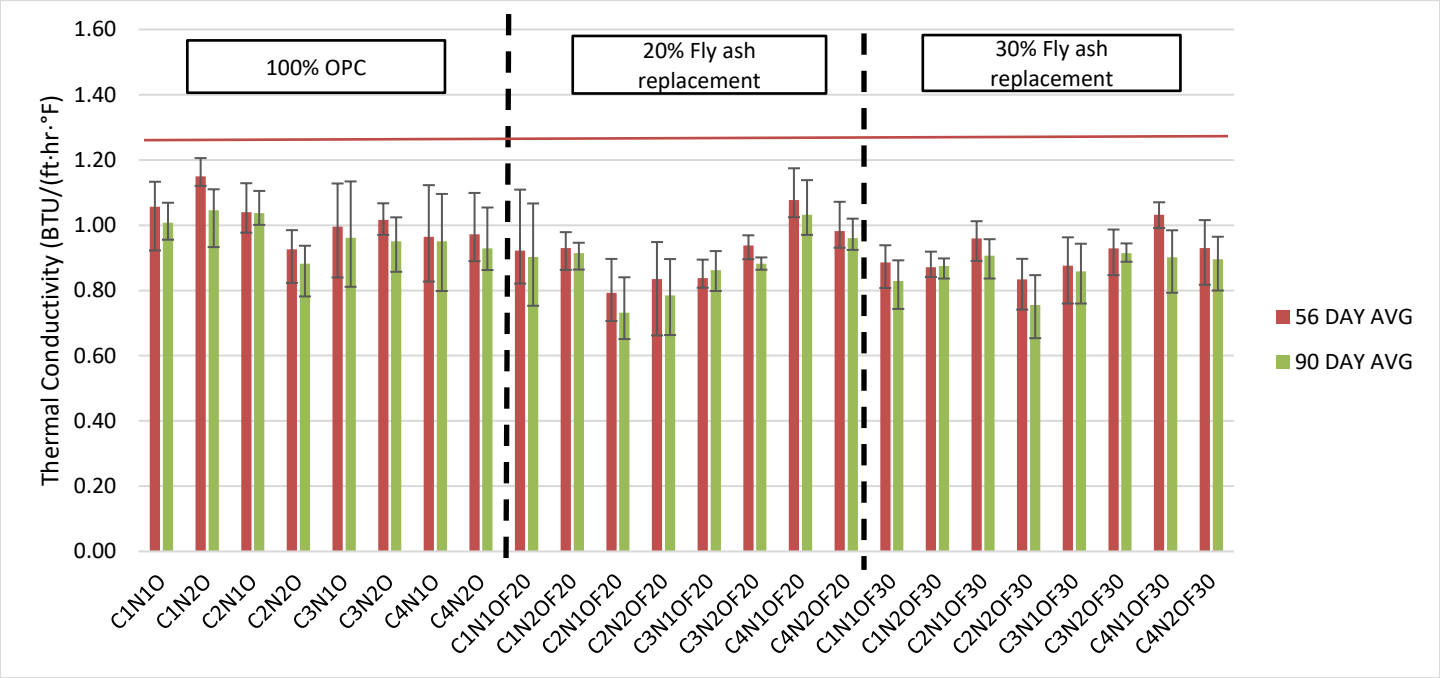

Figure 4.6: Thermal conductivity test results with mixtures grouped by fly ash content

The PMED software suggests a default value of 1.25 Btu/ (ft · hr · °F), shown as a red line on Figure 4.6. According to AASHTO (2008), typical thermal conductivity values for PCC used in paving applications range between 0.44 and 0.81 Btu/ (ft · hr · °F). Cavalline et al. (2018) noted the type of sand – manufactured or natural sand– impacts the thermal conductivity of PCC used in pavement mixtures. Cavalline et al. (2018) recommended using an input value of 1.20 Btu/ (ft · hr · °F) for mixtures comprised of coarse aggregate sourced from the Piedmont region of North Carolina, containing natural sand, and no fly ash. This value is comparable to 56-day averages of mixtures from this study that did not contain fly ash. In this study, it was found that after 56-days, for all mixtures, the recommended 1.20 Btu/ (ft · hr · °F) does not accurately represent the mixtures tested. Mixtures containing fly ash had lower thermal conductivity values compared to mixtures containing no fly ash. On average the mixtures containing fly ash were between 10.5–11% lower in value compared to mixtures not containing fly ash, and the thermal conductivity decreased as the fly ash content increased.

All thermal conductivity results on average ranged between 0.87 and 1.02 Btu/ (ft · hr · °F). General trends show thermal conductivity decreases as specimens age, with an average reduction of 4.7% between 56 and 90 days. The location from which the coarse aggregate was sourced appears to have little impact on the thermal conductivity. Concrete mixtures containing coarse aggregate sourced from the Knightdale quarry had the lowest thermal conductivity compared to mixtures

containing coarse aggregate from the other three quarries. Mixtures produced using the Black Mountain and Statesville coarse aggregate (similar geologic description) displayed similar test results. The location the fine aggregate was sourced from had minimal impact on the thermal conductivity of the specimen as shown in Figure B.30.

4.4.3.3. Heat Capacity

Table B.16 provides the results of 56 and 90-day heat capacity testing, with Table B.17 showing the average results with mixtures grouped by aggregate source and fly ash content. Figure 4.7 shows the average thermal conductivity test results with mixtures grouped by fly ash content. Similar plots of thermal conductivity test results with mixtures sorted by aggregate type and source are provided in Appendix B, Figures B.35 and B.36. Figures B.37 through B.40 show the change in thermal conductivity over time, with mixtures grouped by fly ash content, coarse aggregate source, region of North Carolina from which the coarse aggregate was sourced, and fine aggregate source, respectively.

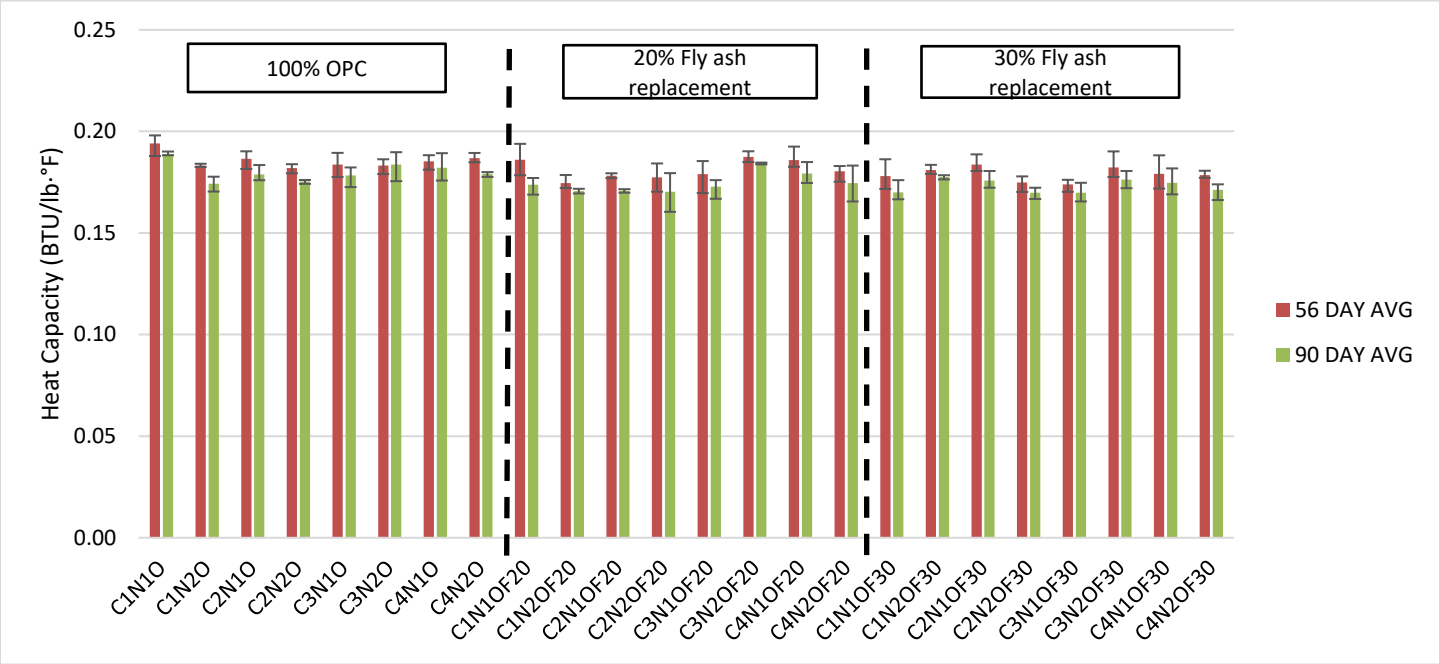

Figure 4.7: Heat capacity test results with mixtures grouped by fly ash content

According to AASHTO, typical heat capacity values for concrete range from 0.22 to 0.40 (Btu/ (lb-°F) and AASHTO recommends use of a default value of 0.28 (Btu/ (lb-°F) in Pavement ME Design (AASHTO, 2015). Cavalline et al. (2018) found that the type of coarse aggregate used had the greatest influence on heat capacity, finding that concrete mixtures including Mountain or Piedmont coarse aggregate had a typical heat capacity of 0.20 (Btu/ (lb-°F). Mixtures containing coarse aggregate sourced from the Coastal region of North Carolina had a heat capacity of 0.22 (Btu/ (lb-°F). Cavalline et al. (2018) recommended using 0.22 (Btu/ (lb-°F) as an input value for heat capacity in AASHTOWare Pavement ME Design software. No mixtures tested during this research study had a heat capacity that fell within AASHTO's typical heat capacity range for PCC. The highest measured heat capacity during this research study was C1N1O, specimen 1 at 56-days of age had a heat capacity of 0.198 (Btu/ (lb-°F).

Similar to other thermal test results, as the fly ash content increased, the heat capacity of the mixture decreased. Additionally, the location and region from which the coarse and fine aggregate were sourced did not have a significant influence on the mixture's heat capacity. On average heat capacity ranged between 0.173 and 0.186 Btu/ (lb-°F). Similar to other thermal property tests, heat capacity decreased over time with an average reduction of 3.4% over a time period of 34 days. Additionally, similar to other thermal property test results, as the fly ash content increased the heat capacity of the concrete decreased. The location of the coarse aggregate used has little impact on the heat capacity over time. As can be observed in Figure B.38, results observed in thermal conductivity tests, concrete mixtures containing coarse aggregate from the Knightdale quarry had slightly lower values on average compared to mixtures containing coarse aggregate sourced from the other three locations. The location from which the fine aggregate was sourced, on average, had little impact on the heat capacity of the test specimens (shown in Figure B.40).

4.4.4 *Durability Performance Test Results*

Durability performance tests included in this work are not currently used as PMED inputs. However, NCDOT is sponsoring ongoing research to support implementation of performance engineered mixtures (Cavalline et al., 2020, Cavalline et al. 2023). Additional details are provided in a thesis supporting this work by Summers (2023).

4.4.1 Surface Resistivity

Results of surface resistivity testing are shown in Table B.18, with Table B.19 providing a summary of test results grouped by fly ash content and aggregate source. Figure 4.8 shows the average surface resistivity test results with mixtures grouped by fly ash content. Similar plots of surface resistivity test results with mixtures sorted by aggregate type and source are provided in Appendix B, Figures B.41 and B.42. Figures B.43 through B.46 show the change in thermal conductivity over time, with mixtures grouped by fly ash content, coarse aggregate source, region of North Carolina from which the coarse aggregate was sourced, and fine aggregate source, respectively. As can be observed, a very notable increase in surface resistivity (indicating improved durability) at later ages can be linked to higher replacement levels of fly ash.

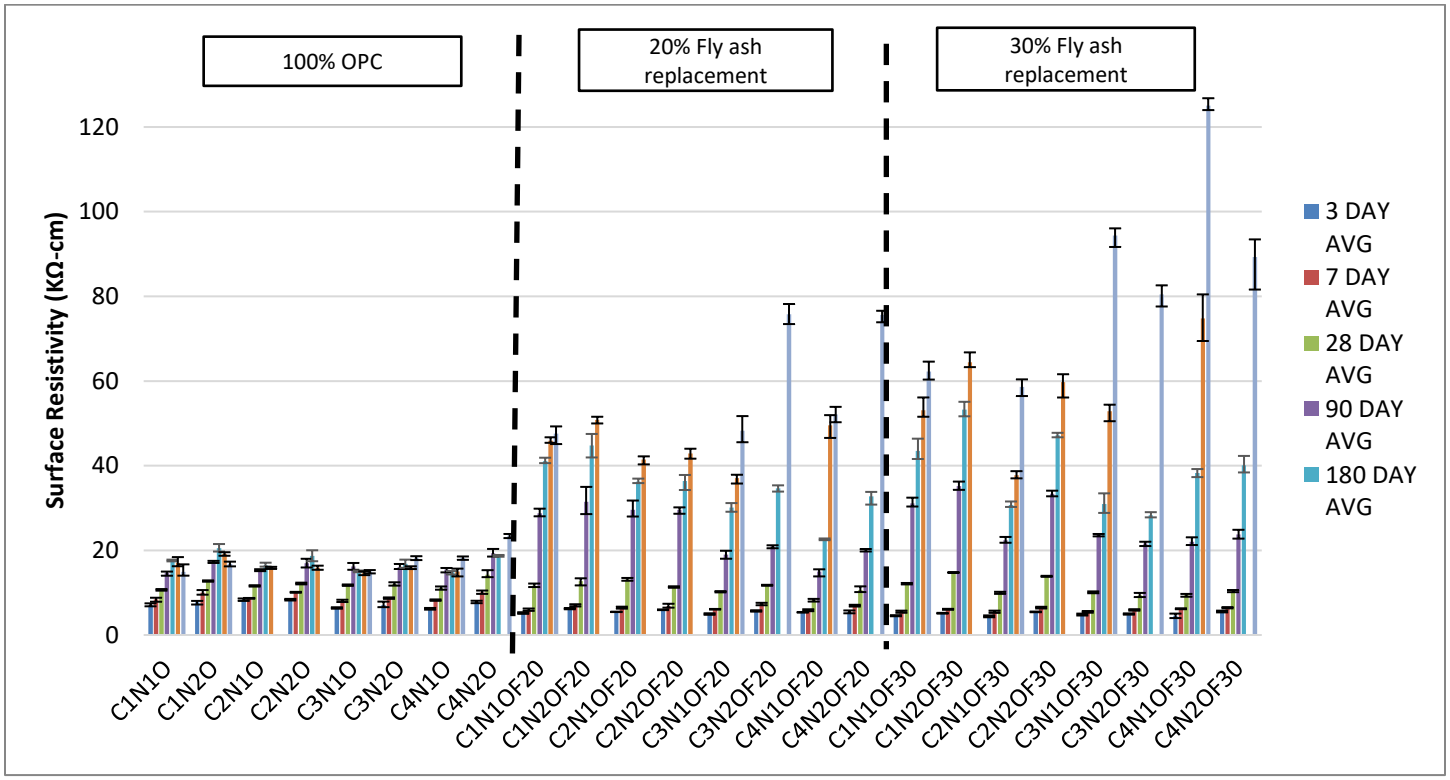

Figure 4.8: Surface resistivity test results with mixtures grouped by fly ash content

The region of North Carolina from which the coarse aggregate was sourced from appears to have the most significant influence on surface resistivity. Mixtures that included coarse aggregate sourced from the Piedmont, on average, outperformed (showed higher surface resistivity) mixtures containing aggregate from the Mountain region (Figure B.45). Figure 4.9 shows the impact of fly ash replacement and coarse aggregate source region on surface resistivity measurements over time. Similar to the coarse aggregate, on average mixtures containing fine aggregate sourced from Buckleberry Mine outperformed similar mixtures containing sand sourced from the Emery Pit (Figure B.46).

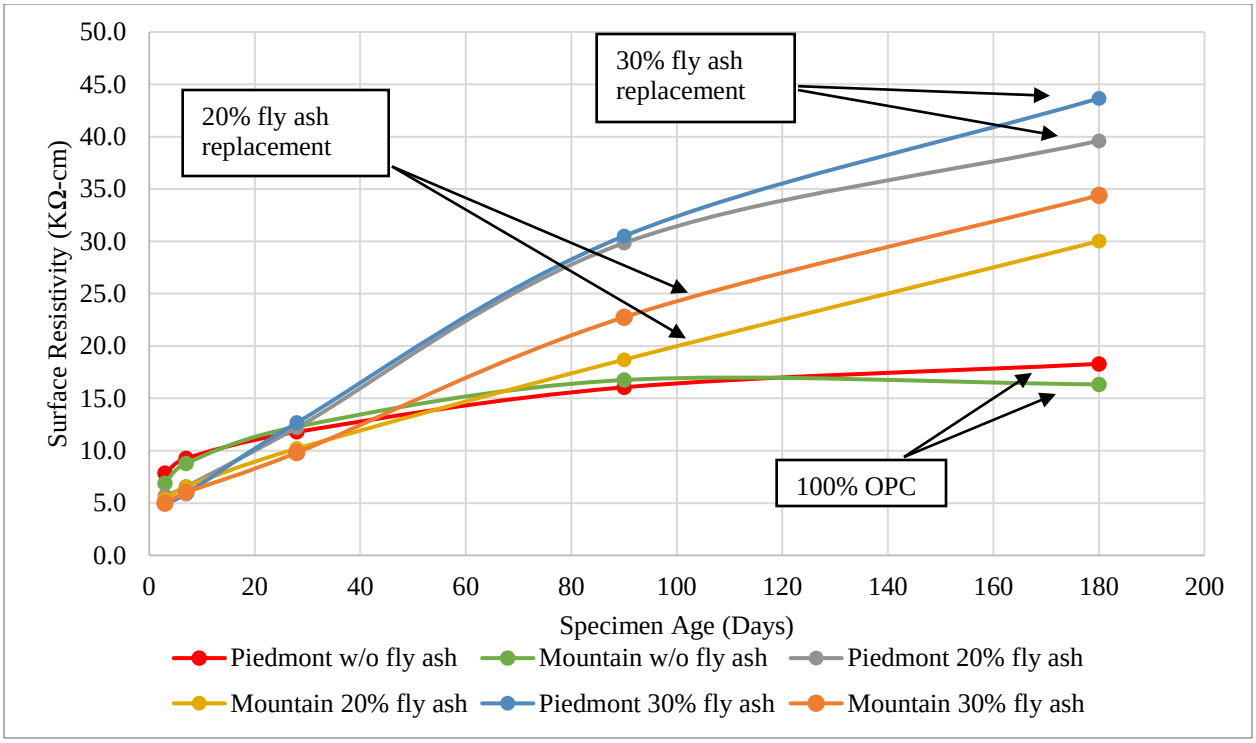

Figure 4.9: Average surface resistivity with concrete mixtures grouped by region of North Carolina from which coarse aggregate was sourced and fly ash content

4.4.2 Volumetric Shrinkage

Results of volumetric shrinkage testing are shown in Table B.20, with Table B.21 providing a summary of test results grouped by fly ash content and aggregate source. Figure 4.11 shows the average volumetric shrinkage test results with mixtures grouped by fly ash content. Plots of 28-day volumetric shrinkage test results with mixtures sorted by aggregate type and source are provided in Appendix B, Figures B.47 and B.48. Figures B.49 through B.52 show the change in thermal conductivity over time, with mixtures grouped by fly ash content, coarse aggregate source, region of North Carolina from which the coarse aggregate was sourced, and fine aggregate source, respectively.

After 28-days in air storage, all test specimens shrank less than 420 microstrains, conforming to the AASHTO R 101 recommendations for a 28-day shrinkage performance target (red line in Figure 4.11). The location from which the coarse aggregate was sourced appears to have the largest influence at 28-days (Figure B.50), with concrete mixtures containing coarse aggregate from the Knightdale quarry exhibiting the largest change in length of approximately 296 microstrains on average. Concrete mixtures containing coarse aggregate from the Statesville quarry experienced the smallest change in length of approximately 223 microstains on average. Concrete mixtures composed of coarse aggregate sourced from the Mountain region – Hendersonville and Black Mountain— on average had similar changes in length to one another and variation in results is most likely due to variation in specimens and testing. The location of the fine aggregate used in the concrete mixtures appears to have minimal influence on volumetric shrinkage (Figure B.52).

Throughout testing the amount of fly ash used in the concrete mixtures appears to have had little impact on the specimens' shrinkage. Paste content has been found to heavily influence PCC shrinkage (Weiss, 2022). In this research study varying amounts of fly ash were used to replace OPC, however, the paste content was held constant for all concrete mixtures, thus explaining the little variation in unrestrained shrinkage results grouped by fly ash.

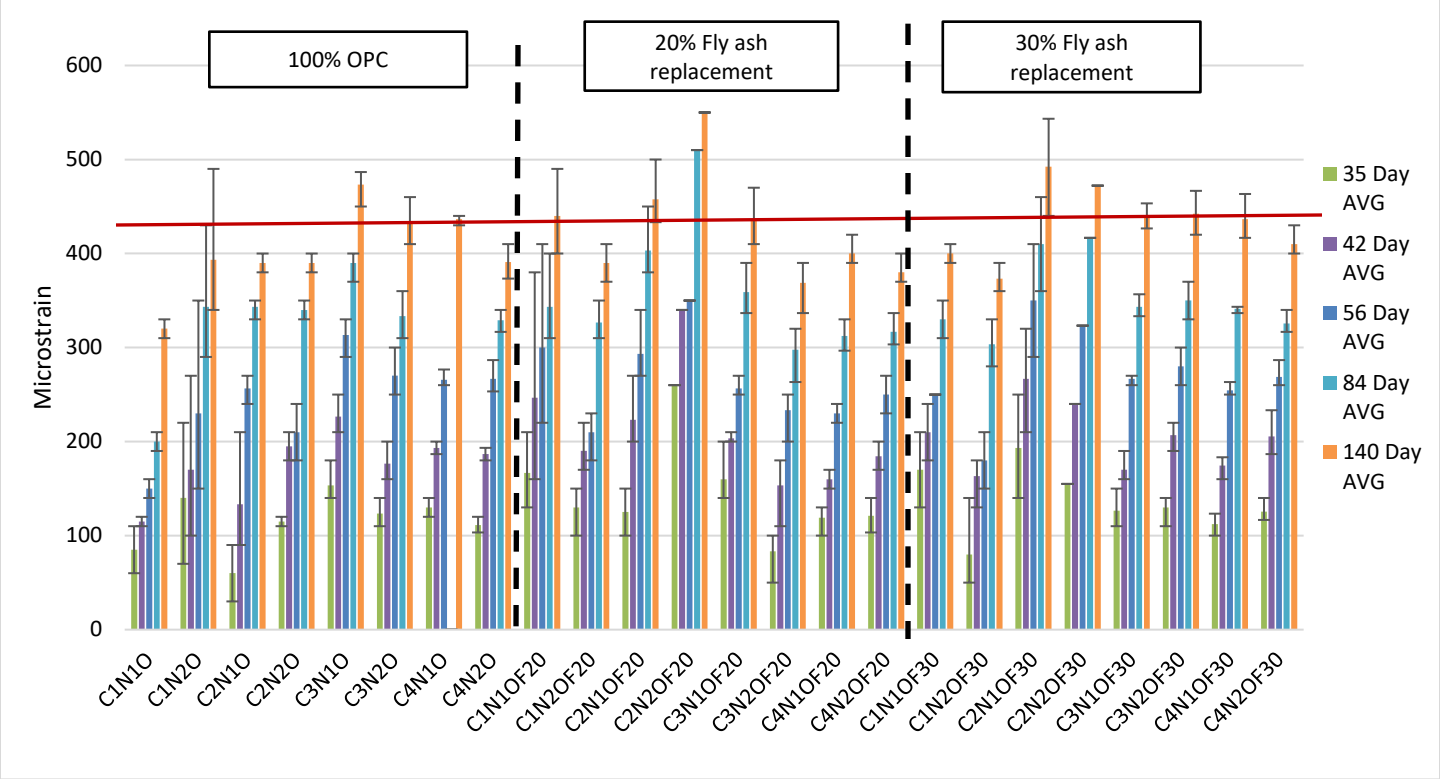

Figure 4.10: Volumetric shrinkage with mixtures grouped by fly ash content

4.5 Catalog of PMED Inputs for Design of Concrete Pavements in North Carolina

Tables 4.2, 4.3, and 4.4 provide a catalog of mechanical properties, thermal properties, and durability performances inputs respectively, to be use for the PMED software for rigid pavements. Proposed inputs are based upon average 28-day laboratory results for mechanical properties, durability performance, and CTE. Heat capacity and thermal conductivity inputs are based on 56-day laboratory test results. The proposed catalog is broken into fly ash content, region, coarse aggregate, and fine aggregate.

Table 4.2: Proposed catalog of PMED PCC mechanical property inputs for North Carolina

Material				Mechanical			
Fly ash content	Region	Coarse Aggregate	Fine Aggregate	MOE (psi)	Poisson's ratio	MOR (psi)	Compressive strength (psi)
100% OPC	Piedmont	Statesville	Emery Pit	2,550,000	0.14	660	5,300
			Buckleberry Mine				
		Knightdale	Emery Pit				
			Buckleberry Mine				
	Mountain	Hendersonville	Emery Pit	2,170,000			
			Buckleberry Mine				
		Black Mountain	Emery Pit				
			Buckleberry Mine				
20%	Piedmont	Statesville	Emery Pit	2,550,000		600	4,300
			Buckleberry Mine				
		Knightdale	Emery Pit				
			Buckleberry Mine				
	Mountain	Hendersonville	Emery Pit	2,170,000			
			Buckleberry Mine				
		Black Mountain	Emery Pit				
			Buckleberry Mine				
30%	Piedmont	Statesville	Emery Pit	2,550,000		550	3,650
			Buckleberry Mine				
		Knightdale	Emery Pit				
			Buckleberry Mine				
	Mountain	Hendersonville	Emery Pit	2,170,000			
			Buckleberry Mine				
		Black Mountain	Emery Pit				
			Buckleberry Mine				
AASHTOWare Pavement ME Design Default values				4,200,000	0.20	690	5,275.3

Table 4.3: Proposed catalog of PMED PCC thermal property inputs for North Carolina

Material				Thermal		
Fly ash content	Region	Coarse Aggregate	Fine Aggregate	CTE ($\times 10^{-6}$ in/in-F)	Heat Capacity (BTU/lb-F)	Thermal conductivity BTU/ft-hr-F
100% OPC	Piedmont	Statesville	Emery Pit	5.67	0.19	1.00
			Buckleberry Mine	5.34	0.18	
		Knightdale	Emery Pit	5.23		
			Buckleberry Mine	5.07		
	Mountain	Hendersonville	Emery Pit	5.04		
			Buckleberry Mine	4.92		
		Black Mountain	Emery Pit	5.66		
			Buckleberry Mine	5.42		
20%	Piedmont	Statesville	Emery Pit	5.43	0.19	0.91
			Buckleberry Mine	5.19	0.18	
		Knightdale	Emery Pit	5.12		
			Buckleberry Mine	5.00		
	Mountain	Hendersonville	Emery Pit	4.99		
			Buckleberry Mine	4.74		
		Black Mountain	Emery Pit	5.52		
			Buckleberry Mine	5.20		
30%	Piedmont	Statesville	Emery Pit	5.32	0.19	
			Buckleberry Mine	5.16	0.18	
		Knightdale	Emery Pit	5.05		
			Buckleberry Mine	4.77		
	Mountain	Hendersonville	Emery Pit	4.88		
			Buckleberry Mine	4.67		
		Black Mountain	Emery Pit	5.39		
			Buckleberry Mine	5.14		
AASHTOWare Pavement ME Design Default values				4.90	0.28	1.25

Table 4.4: Proposed catalog of typical durability performance test values for North Carolina

Material				Durability	
Fly ash content	Region	Coarse Aggregate	Fine Aggregate	28-day Surface Resistivity (KΩ-cm)	28-day Volumetric shrinkage (microstrain)
100% OPC	Piedmont	Statesville	Emery Pit	12.0	225
			Buckleberry Mine		
		Knightdale	Emery Pit		300
			Buckleberry Mine		
	Mountain	Hendersonville	Emery Pit		270
			Buckleberry Mine		
		Black Mountain	Emery Pit		255
			Buckleberry Mine		
20%	Piedmont	Statesville	Emery Pit	11.2	225
			Buckleberry Mine		
		Knightdale	Emery Pit		300
			Buckleberry Mine		
	Mountain	Hendersonville	Emery Pit		270
			Buckleberry Mine		
		Black Mountain	Emery Pit		255
			Buckleberry Mine		
30%	Piedmont	Statesville	Emery Pit		225
			Buckleberry Mine		
		Knightdale	Emery Pit		300
			Buckleberry Mine		
	Mountain	Hendersonville	Emery Pit		270
			Buckleberry Mine		
		Black Mountain	Emery Pit		255
			Buckleberry Mine		

5.0 PAVEMENT DESIGN, PERFORMANCE, AND SLAB THICKNESS ANALYSIS USING PAVEMENT ME DESIGN SIMULATIONS

5.1 Sensitivity Analysis of JPCP Using PMED Simulations

The main purpose of this section is to analyze the effects of JPCP inputs on performance indicators. Analysis of JPCP inputs will help identify the inputs of most sensitivity. Identification of inputs of most sensitivity on performance indicators will enable better design and better efficiency during the JPCP pavement selection process.

5.1.1 *Methodology*

Inputs used and considered for the pavement design process of JPCP were first categorized into different groups. The four groups of categorizations are pavement structural design, pavement materials, traffic, and climate. Each of these factors are the contributing factors to JPCP pavement design and performance analysis. Once the inputs were noted, ranges and a baseline model were generated for each input factor. The ranges in this sensitivity analysis were based on historical data in North Carolina and previous analyses. Factor ranges reflect PMED recommended ranges as well. The factors that are assessed in this sensitivity analysis are AADTT, climate, CTE of paving concrete, PCC slab thickness, PCC slab length, dowel diameter, friction loss, PCC heat capacity, PCC shortwave absorptivity, thermal conductivity, and PCC slab width. Different climate stations were selected across the state of North Carolina. The climate stations selected were based on representation of the coastal, plain, and mountainous regions of North Carolina. Using all three climate types across North Carolina was deemed necessary to simulate the effect of different climates on JPCP. The stations selected were Asheville (AH), Charlotte (CH), Elizabeth City (EC), Fayetteville (FA), Hickory (HI), Morehead City (MC), Rocky Mount (RM), Greensboro (GR), and Winston Salem (WS). Abbreviations for climate stations used in this study are given to each city, respectively.

Each JPCP factor was analyzed based on the baseline model shown in Table 5.1. The bold font in Table 5.1 shows the baseline model. The baseline model follows the NCDOT 2015-03 study. The range of values for each factor were simulated to show the predicted values of terminal IRI, joint faulting, and transverse cracking. Data from each simulation was gathered and categorized into each of the three factors in the sensitivity analysis. The largest and smallest values for each predicted performance produced a numerical range which became the basis of the sensitivity analysis. The data produced from the simulations was also used to create bar charts to graphically show the ranges of data. The data from factors stated above were compared to each other based on Terminal IRI, Joint Faulting, and Transverse Cracking. The results are based on the comparison of performance indicator ranges. The largest ranges are deemed most sensitive, while the smallest ranges are least sensitive. The red line in the analysis shows the baseline model results for Terminal IRI, Joint Faulting, and Transverse Cracking.

Table 5.1: Sensitivity analysis inputs and baseline model

Input Category	Variable
PCC Thickness	7, **8**, 9, 10, 11
AADTT	**6000**, 7000, 8000, 9000, 10000, 11000, 12000
Climate	Asheville, Charlotte, Elizabeth City, Fayetteville, Hickory, Morehead City, Rocky Mount, **Greensboro**, Winston Salem
CTE	4, **5**, 6, 7
Slab Length	**15**, 16, 17, 18, 19
Dowel Diameter	1, **1.25**, 1.5, 1.75
Friction Loss	120 Months, **240 Months**, No Friction
PCC Shortwave Absorptivity	0.65, 0.75, **0.85**, 0.95
PCC Heat Capacity	0.2, 0.22, 0.24, 0.26, **0.28**
Slab Width	**12**, 13, 14
PCC Thermal Conductivity	1, 1.05, 1.1, 1.15, 1.2, **1.25**, 1.3, 1.35, 1.4, 1.45, 1.5

**Bolded variables represent baselined model

The default inputs (kept constant for this analysis) were determined from the NCDOT 2015-03 study and the details from this the NCDOT 2015-03 regarding performance criteria, traffic data, JPCP design properties remained constant (Cavalline et al. 2018a and 2018b). There are four pavement layers that include the PCC layer, a lime stabilized base course layer, a crushed gravel base course layer, and a subgrade layer. The first layer used in the pavement structure is a Portland Cement Concrete (PCC). In this layer, the cementitious material content was 550 lb/cy, water/cement ratio was 0.48. Layer 2 is a lime stabilized layer with a thickness of 8 inches, elastic modulus is 450000 psi, thermal conductivity is 1.25 BTU/hr-ft-◦F, and heat capacity is 0.28 BTU/lb-◦F. Layer 3 is the crushed gravel, A-1-a layer with a thickness of 10 inches. The Poisson's ratio for the gravel layer is 0.35 and the elastic modulus is 25000 psi. Layer 4 is a semi-infinite subgrade layer. The elastic modulus for the fourth layer is 14000 psi. A schematic showing the pavement structural layers is in Figure 5.1. Level 1 inputs were used in this study and Table 5.2 shows the respective Level 1 inputs.

Table 5.2: Level 1 PCC layer inputs

Concrete Age	Modulus of Rupture (psi)	Modulus of Elasticity (psi)
7 days	817	4360000
14 days	846	4560000
28 days	913	5420000
90 days	917	6250000
Strength gain factor 28 days/20 years	1.22	1.22

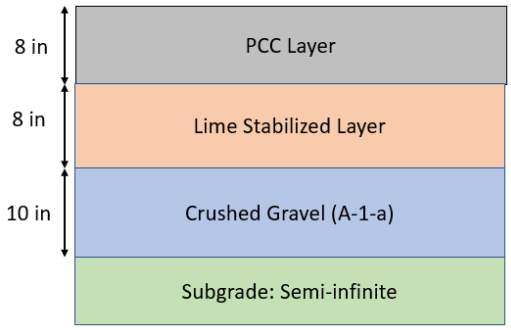

Figure 5.1: JPCP pavement layers

5.1.2 *Results and Analysis*

5.1.2.1 Effects on Terminal IRI

The factors of most impact on terminal IRI are CTE, PCC Thickness, and climate. CTE is the variable of most impact, holding a range of 104.29 in/mile. PCC Thickness has a range of 74.56 in/mile, which is the second variable of most impact on Terminal IRI. Climate is the third most influential variable, having a range of 67.01 in/mile. These three factors hold the largest range over the other variables assessed in Terminal IRI, as shown in Figure 5.2.

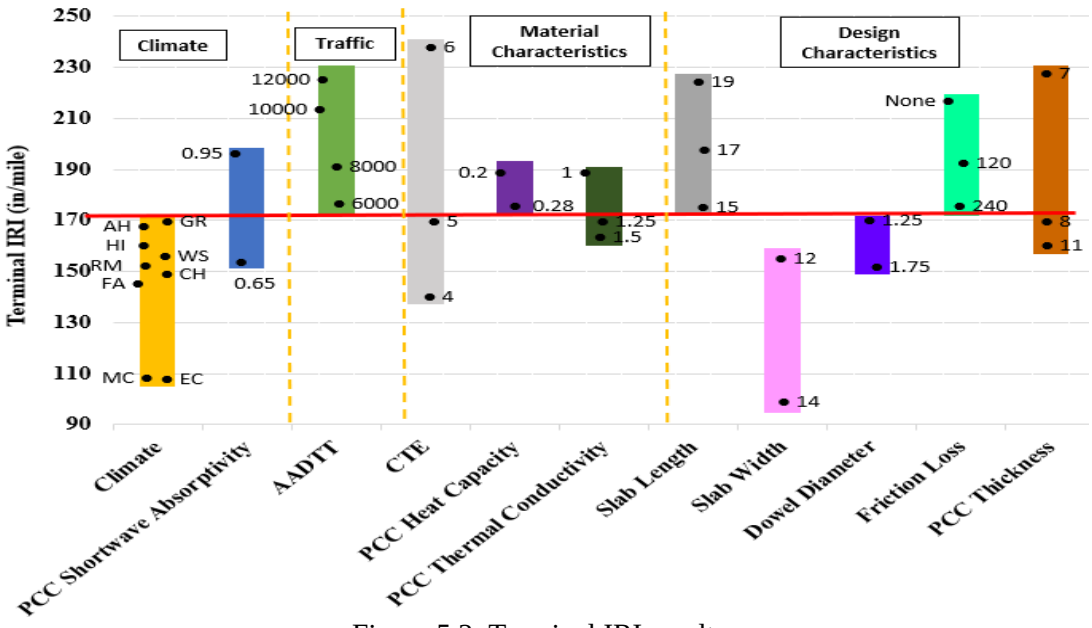

Figure 5.2: Terminal IRI results

5.1.2.2 Effects on Joint Faulting

The simulation results show that CTE, slab width, and climate hold the highest impact out of all of the design variables with a range of 0.09 in. For the purpose of maintaining good quality data, 1-inch diameter dowels were excluded from the dowel diameter data set. The range for this data set if 1-inch dowels were included would be 0.38 in. 1-inch diameter dowels were excluded to prevent skewing of data. Friction loss, and PCC heat capacity are not shown on the figure below because it was shown that these factors do not hold effect on joint faulting. Results of mean joint faulting are presented in Figure 5.3.

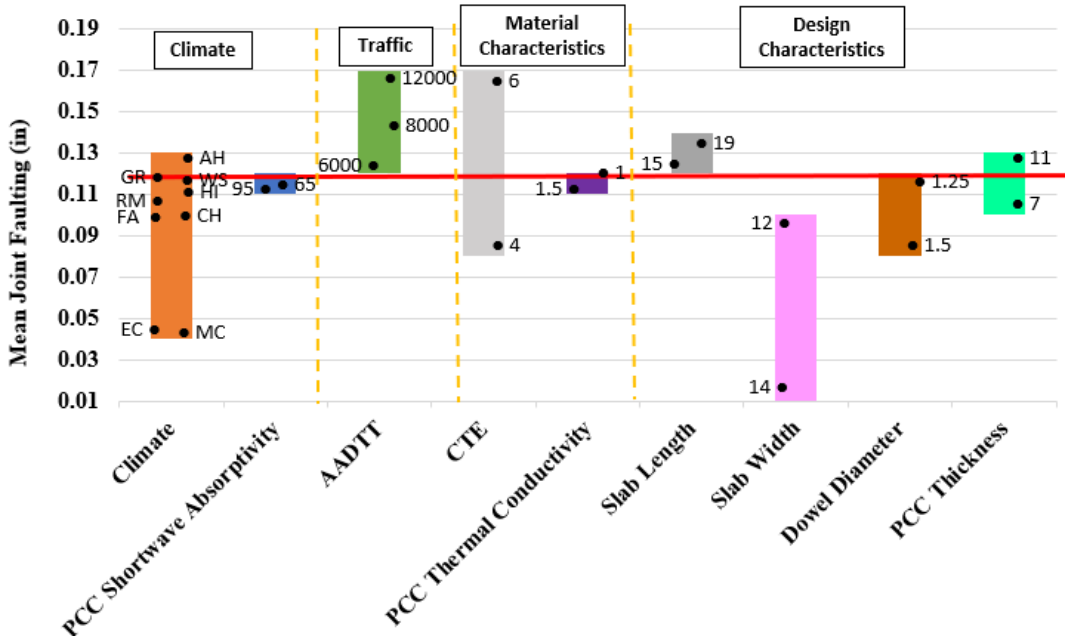

Figure 5.3: Joint faulting results

5.1.2.3 Effects on Transverse Cracking

Analysis of the transverse cracking indicator shows the three most influential factors to be slab length, CTE, and friction loss. Slab length is shown to have the largest impact with a range of 61.94 %. CTE is shown to have the second largest impact with values having a range from 72.16% to 12.99%, with a 59.17% range. Friction loss is the third most influential variable, with a range of 52.95%. It is important to note that 7 inches PCC thickness was excluded from the transverse cracking analysis. Using the data of 7 inches skewed the data for transverse cracking because 7 inches produced 100% cracking in the sensitivity analysis. Using 7 inches for PCC thickness would have given the analysis a range of nearly

100%, skewing the results from the table. Omitting 7 inches is considered necessary to produce a meaningful analysis. Results of transverse cracking are shown in Figure 5.4.

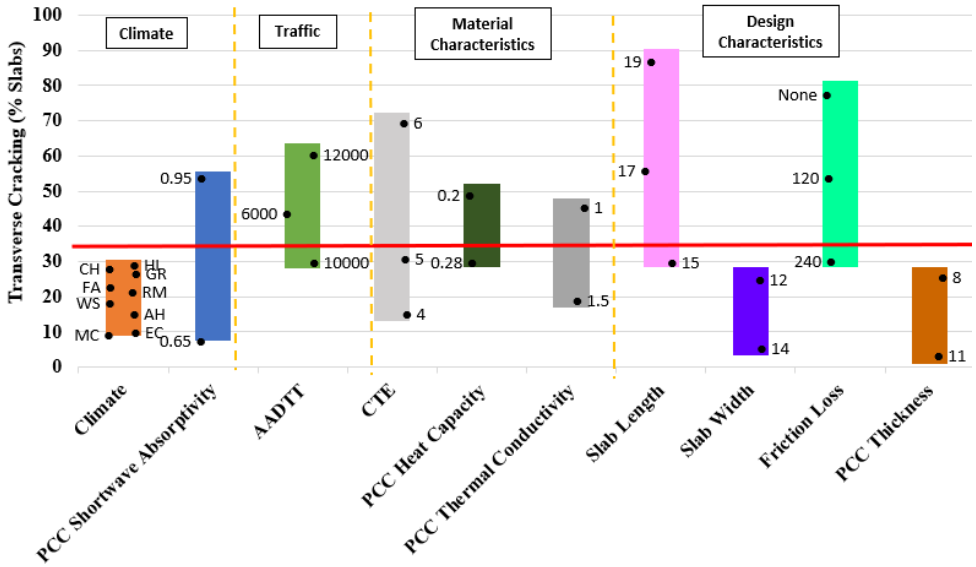

Figure 5.4: Transverse cracking results

5.1.3 *Percentage Change in Performance Indicators*

The comparison of design variables was conducted with regards to the performance indicators of JPCP system by determining the percentage change to assess the variables of most impact. The findings show a clear comparison between the design variables and the performance indicators. Variables with the highest impact on performance indicators have larger percentage change values.

Figure 5.5 shows the percentage change in terminal IRI for the variation in the design factors being simulated. The factor with the greatest percentage change is CTE, followed by slab width, and PCC Thickness. It is shown that CTE has a 76% change indicator value, the greatest value changes out of all indicators on terminal IRI. Slab width has the second highest indicator value change, with a percentage change of 69%. PCC thickness holds an impact of 48% change on terminal IRI indicator values.

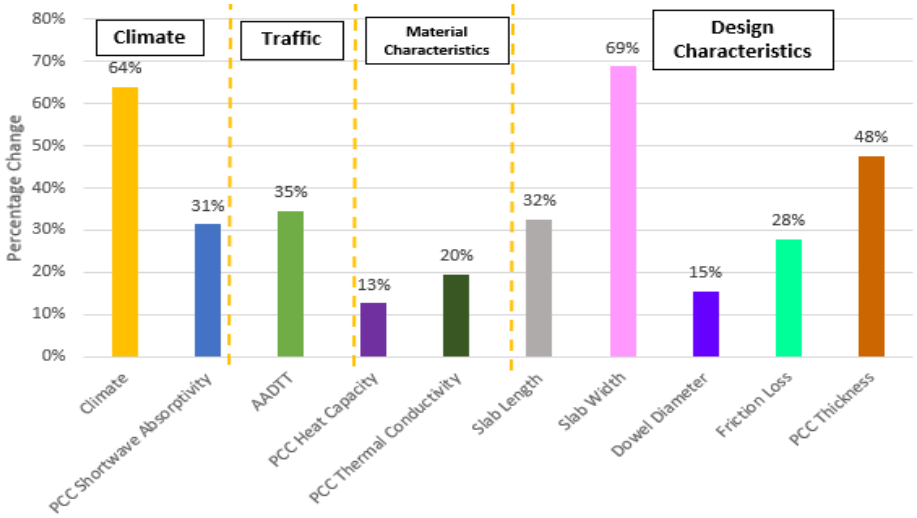

Figure 5.5: Percentage change in terminal IRI

Joint faulting percentage change analysis in Figure 5.6 shows CTE as the highest percentage change design factor, with a change in values of 113%. Friction loss and PCC heat capacity hold no effect on mean joint faulting. In Figure 5.6, it is shown that these two indicators have a zero percent change in indicator values, representing that there is no impact. In the overall scenario, CTE of paving concrete is the most significant factor affecting the joint faulting of JPCP system.

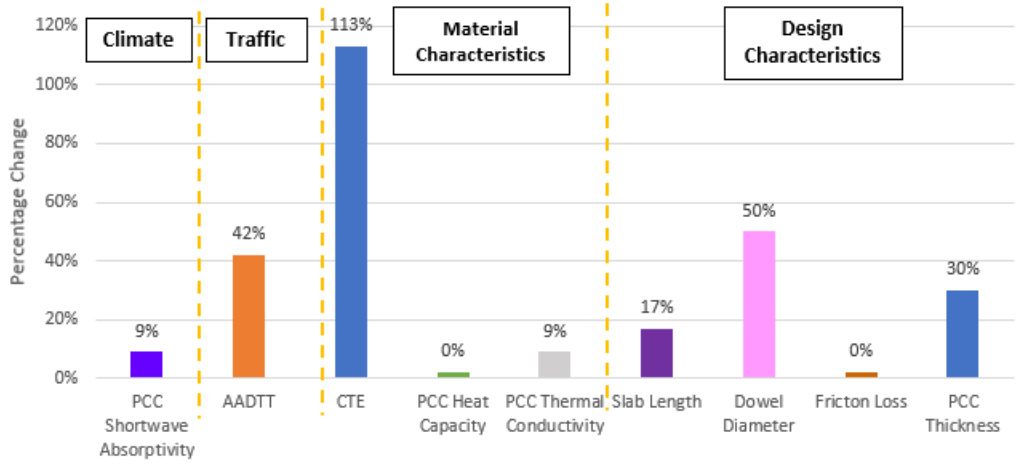

Figure 5.6: Percentage change in joint faulting

The analysis was also done for percentage change in transverse cracking and is shown in Figure 5.7. The variable of the most impact is slab length, with a 61% change in values. CTE and friction loss are the next two factors of most impact. CTE is shown to have a 59% change in values for the cracking indicator, and friction loss has a 52% impact. Figure 5.7 presents clear findings on the variables of most to least impact on cracking in JPCP.

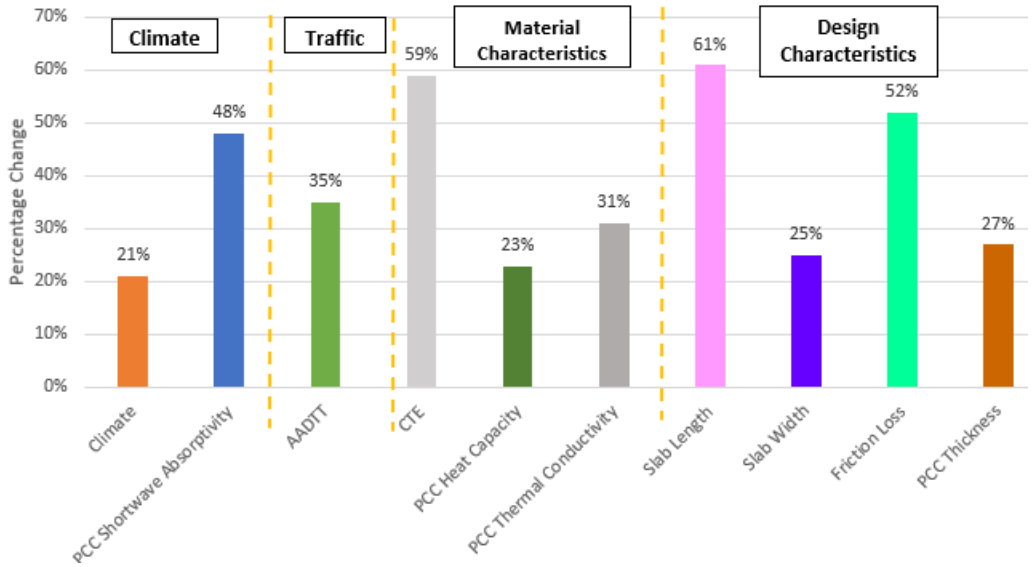

Figure 5.7: Percentage change in transverse cracking

5.1.4 *Findings from Sensitivity Analysis*

The sensitivity analysis covered inputs that affect terminal IRI, joint faulting, and transverse cracking. The analysis provided data leading to the understanding of most influential variables to least influential variables for the pavement and service characteristics used. The bar charts generated from the numerical simulation results show a comparison between the design factors and service conditions including AADTT, climate, CTE, PCC slab length, PCC thickness, dowel diameter, friction loss, heat capacity, PCC shortwave absorptivity, thermal conductivity, and PCC slab width. The analysis of the results provided a list of most influential variables to least influential variables as given below in the order of higher to lower sensitivity. The hierarchical list of variables is in Table 5.3 as follows:

Table 5.3: Sensitivity analysis analyzation results

	Terminal IRI	Joint Faulting	Transverse Cracking
Lower ← → Higher Sensitivity	CTE	CTE	Slab Length
	PCC Thickness	Climate	CTE
	Climate	Slab Width	Friction Loss
	Slab Width	AADTT	PCC Shortwave Absorptivity
	AADTT	Dowel Diameter	AADTT
	Slab Length	PCC Thickness	PCC Thermal Conductivity
	PCC Shortwave Absorptivity	Slab Length	PCC Thickness
	PCC Thermal Conductivity	PCC Shortwave Absorptivity	Slab Width
	Dowel Diameter	PCC Thermal Conductivity	PCC Heat Capacity
	PCC Heat Capacity		Climate

Analysis of the hierarchical list above shows that CTE of paving concrete is the most significant factor affecting IRI and joint faulting and the second most significant factor affecting transverse cracking. This finding aligns with the prior research and the published literature. CTE of concrete is the prime contributor to upward and downward curling of pavement slabs and also controls the resulting curling stresses which are the major factors producing pavement distresses. These distresses impact the performance of the JPCP and so the CTE becomes the most significant factor affecting the JPCP performance.

5.2 Analysis of Material Input Levels on JPCP Design, Slab Thickness, and Performance

There are three levels of concrete material inputs within the framework of the PMED software. Each input level is determined based on testing data available and assumptions when using the PMED software. This data is used to generate design simulations. Level 1 inputs require the most testing data. Level 1 requires modulus of rupture (MOR) and elastic modulus data for 7 days, 14 days, 28 days, and 90 days. Level 1 also requires lab tested coefficient of CTE values. Level 2 requires compressive strength test data for 7 days, 14 days, 28 days, 90 days and the PMED default value for CTE. Level 3 requires the 28-day compressive strength value and the PMED default CTE value. Using the most accurate input level when designing pavements is necessary, as this generates the most accurate pavement analysis/design. The analysis of the effects of different material input levels (Level 1, 2, and 3) for NCDOT paving mixtures is necessary for a better understanding of the differences in the performance indicator values with regards to different input levels. The analysis of input levels will also establish the most accurate input level.

5.2.1 *Methodology*

The mixtures C1N1OF20, C1N1OF30, C1N20, C1N2OF20, C1N2OF30, C2N10, and C2N1OF20 were analyzed to determine the change in performance indicator predictions among Level 1, 2, and 3. In the PMED software, 7-day values, 14-day values, 28-day values, and 90-day values are required to run Level 1 and Level 2 simulations. In the original testing data, 14-day compressive strength data was not available. To generate the 14-day compressive strength data, compressive strength values were interpolated from the lab tested data. Interpolation models were created for each paving mixture to interpolate the 14-day compressive strength value. In addition, 14-day data was not available for modulus of rupture (MOR) or elastic modulus. Interconversion models were created for each mixture to obtain the 14-day elastic modulus values and the MOR values for all the paving mixtures. The finalized data for compressive strength, elastic modulus, and MOR are in the respective tables below. Table 6.1 shows compressive strength testing data. Table 5.4 and Table 5.5 show testing data for elastic modulus and MOR, respectively.

Table 5.4: CTE and compressive strength data

		Compressive Strength (psi)			
Mixture ID	CTE @ 28 Days	7 Days	14 Days	28 Days	90 Days
C1N1OF20	5.43E-06	2785	3236	4303	5656
C1N1OF30	5.33E-06	1855	2113	3176	4339
C1N20	5.36E-06	3988	4208	5051	6034
C1N2OF20	5.20E-06	2894	3469	4425	5279
C1N2OF30	5.16E-06	1674	2516	3610	4440
C2N10	5.23E-06	4186	4586	5829	6255
C2N10F20	5.12E-06	2517	2971	4361	4594

Table 5.5: Elastic modulus and modulus of rupture data

Mixture ID	7 Day EM (psi)	7 Day MOR (psi)	14 Day EM (psi)	14 Day MOR (psi)	28 Day EM (psi)	28 Day MOR (psi)	90 Day EM (psi)	90 Day MOR (psi)
C1N1OF20	2.10E+06	525	2.370E+06	533	2.710E+06	615	3.090E+06	660
C1N1OF30	2.02E+06	441	2.08E+06	456	2.45E+06	550	2.65E+06	592
C1N2O	2.49E+06	585	2.51E+06	594	2.72E+06	673	2.94E+06	678
C1N2OF20	2.39E+06	540	2.27E+06	543	2.67E+06	612	2.75E+06	642
C1N2OF30	2.30E+06	473	2.17E+06	508	2.49E+06	554	2.95E+06	598
C2N1O	2.59E+06	606	2.45E+06	616	2.66E+06	673	2.76E+06	689
C2N1OF20	1.97E+06	507	2.11E+06	518	2.49E+06	561	2.54E+06	606

The default inputs (kept constant for this analysis) were determined from the NCDOT 2015-03 study and the details are given in Appendix C, Table C.1. There are four pavement layers that include the PCC layer, a lime stabilized base course layer, a crushed gravel base course layer, and a subgrade layer.

5.2.2 *Level 1, 2, and 3 Analyses and Results*

Level 1, 2, and 3 input levels were simulated for mixtures C1N1OF20, C1N1OF30, C1N20, C1N2OF20, C1N2OF30, C2N10, AND C2N1OF20. Based on the simulation results for each paving mixture, Level 1, 2, and 3 performance indicators were assessed to see the difference in performance predictions. There is shown to be a significant change in performance indicator predictions of IRI, faulting, and cracking. Each performance indicator, IRI, faulting, and cracking, is assessed individually and the results are as follows.

5.2.2.1 Level 1 Results

As previously described, Level 1 is known to be the most accurate input level, providing project-specific or mixture-specific data. Inputs for 7-, 14-, 28-, and 90-day EM and MOR values, along with the 28-day CTE value, are required to run the design simulations. Each simulation performed was based on the laboratory test results for that specific mixture. The performance indicator results for each individual mixture of the simulation for the Level 1 inputs are shown in Appendix, Figures C.1, C.2, and C.3. The IRI indicator showed a significant change between the mixtures that were assessed. The highest value for the simulations performed on the mixtures was 175, and the lowest value was 141. There was a 24 percent difference in the values for the Level 1 IRI indicator.

The faulting indicator also showed a significant fluctuation. In Figure C.2, the highest value for faulting is 0.11, and the lowest value for faulting is 0.09. There is a 22 percent difference between the highest and lowest values for the Level 1 faulting indicator.

The cracking indicator showed an upward trend as each assessed mixture included more fly ash, as shown in Figure C.3. The lowest value for cracking was 4 percent, and the highest value was 37 percent. This is a 33 percent difference in the highest and lowest values within the Level 1 cracking indicator, which is the most significant one.

5.2.2.2 Level 2 Results

Level 2 simulations were performed for each individual mixture. Level 2 simulations are known to not be as accurate as Level 1 simulations since the inputs are often regional or historically used values. Level 2 simulations require 7-day, 14-day, 28-day, and 90-day compressive strength values. Each simulation performed for Level 2 is based on each individual mixture's laboratory test results for the 7-day, 14-day, 28-day, and 90-day compressive strength values. For Level 2, the CTE default value was used. This value was identified as 10.44 (5.8) (cm/cm)/°C, ((in./in.)/°F) for the granites. Based on these inputs, Level 2 simulations were performed. The results for the Level 2 simulations are shown in Appendix C, Figures C.4, C.5, and C.6. The IRI indicator for Level 2 had a high value of 282 and a low value of 225. The difference in the Level 2 IRI values was 25 percent. The Level 2 IRI indicator followed the same trend as the Level 1 IRI indicator but with more fluctuations in the indicator value. Figure C.4 shows a higher visual difference in indicator value compared to Figure C.1.

The high value for the Level 2 faulting indicator was 0.17, and the low value was 0.15, as shown in Figure C.5. The difference in values for the faulting indicator was 13 percent. The Level 2 faulting indicator showed a decreasing trend in faulting as fly ash was added to the mixture. The Level 2 faulting indicator followed the same trend as the Level 1 faulting indicator. In the Level 2 faulting indicator, there were more fluctuations in the indicator value than in the Level 1 faulting indicator value.

Figure C.6 presents the Level 2 cracking indicator results. The high value for the Level 2 cracking indicator was 100 percent, and the lowest value for the Level 2 cracking indicator was 58 percent. The percentage difference in the Level 2 cracking indicator was 42 percent. Compared to the Level 1 cracking indicator, the Level 2 cracking indicator had higher cracking values for every mixture. The Level 2 cracking indicator showed almost every mixture as 100 percent cracking, which is a significant change in the predictor value for Level 1.

5.2.2.3 Level 3 Results

The Level 3 input level is known to not be as accurate as the Level 1 or two input levels since the Level 3 values are the default values. The requirement for the Level 3 input level is the 28-day compressive strength value. The CTE value used for the Level 3 input level was the CTE default value of 10.44 (5.8) (m/m)/°C, ((in./in.)/°F). Based on these inputs, the simulations were performed, and the indicator results were produced for the IRI, faulting, and cracking. The results for the IRI, faulting, and cracking indicators for Level 3 are shown in Figures C.7, C.8, and C.9. The Level 3 IRI indicator had a high value of 280 and a low value of 222. The percentage difference in the Level 3 IRI indicator value was 26 percent. The Level 3 IRI indicator, compared to the Level 1 IRI indicator, had higher values. The Level 3 IRI indicator followed a similar trend in the prediction of indicator values between the different mixtures. The Level 2 IRI indica-tor predicted very similar values to the Level 3 IRI indicator. The Level 3 IRI indica-tor had slightly lower values compared to the Level 2 IRI indicator.

The high value for the Level 3 faulting indicator was 0.17, and the low value was 0.15, as shown in Figure C.8. The percentage difference in the Level 3 faulting indicator values was 13 percent. Compared to the Level 1 faulting indicator, the Level 3 faulting indicator followed a similar trend in mixture prediction. The Level 3 faulting indicator predicted the performance indicator to be a higher value than the Level 1 faulting indicator. The Level 3 faulting indicator compared to the Level 2 faulting indicator was nearly identical.

In Figure C.9, the high value for the Level 3 cracking indicator was 100 percent, and the lowest value for the Level 3 cracking indicator was 54 percent. The percentage difference in the Level 3 cracking indicator was 46 percent. The Level 3 cracking indicator, compared to the Level 1 cracking indicator, showed significantly higher values. The Level 3 cracking indicator showed a similar trend in the prediction of indicator values between the different mixtures and showed similar cracking values to the Level 2 cracking indicator predictions. The Level 2 cracking indicator, compared to the Level 3 cracking indicator, had a higher value of prediction for the C1N2OF20 mixture. The rest of the mixtures assessed between the Level 2 and Level 3 cracking indicators were the same.

5.2.3 *Level 1, Two, and Three Indicator Comparisons*

Levels one, two, and three are known to have differences in performance indicator values. Analysis of the differences between the Level 1, two, and three indicators is necessary to understand the use of these input levels while designing new JPCP systems. Based on the data from the Level 1, two, and three simulations, the analysis of the difference in each performance indicator was conducted. Through the analysis of the IRI, faulting, and cracking indicators, there will be a greater understanding of the percentage difference in the pavement performance between each input level. To show a clear comparison of each input level and indicator results, the IRI indicator, faulting indicator, and cracking indicator were separately assessed.

5.2.3.1 IRI Indicator Analysis

Figure 5.8 shows the comparison of the Level 1 through to the Level 3 indicator results for the IRIs. The Level 1 IRI indicator had much lower values than both the Level 2 and Level 3 IRI indicators for each mixture. Figure 5.9 shows the percentage change in the performance indicator between the Level 1 and Level 3 simulations. The highest percentage difference between the Level 1 through to the Level 3 inputs was 78 percent, and the lowest difference between the Level 1 through to Level 3 inputs was 57 percent. There is a clear difference in the IRI indicator values between Level 1 through to the Level 3 inputs.

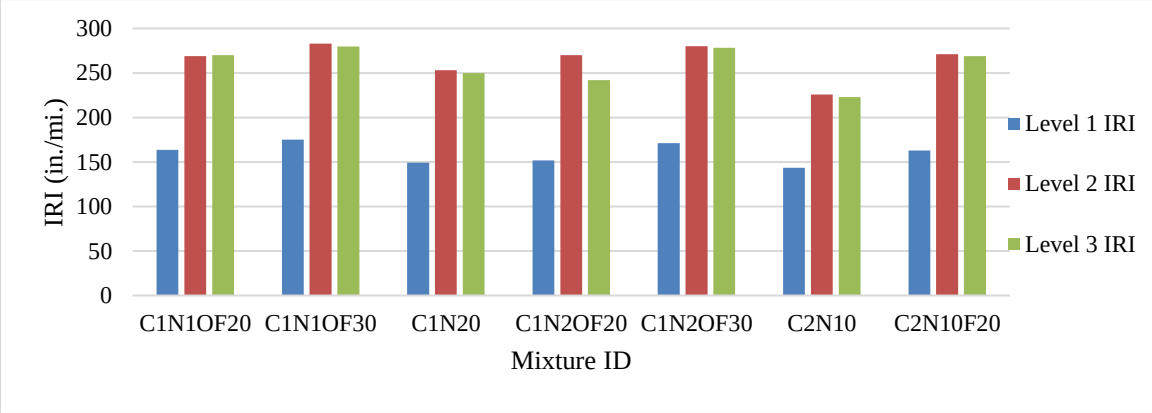

Figure 5.8: Level 1, Level 2, and Level 3 IRI indicator comparison

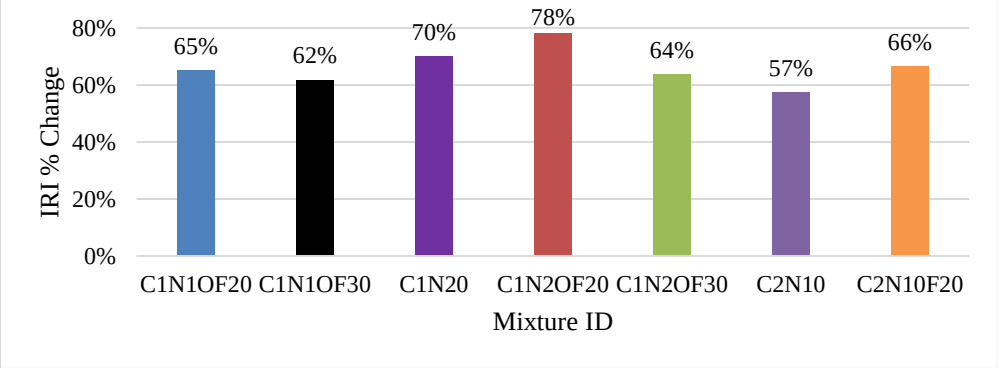

Figure 5.9: Percentage change in IRI between Level 1 and Level 3

The IRI indicators for Level 2 and Level 3 were almost similar for every paving mixture being simulated using this set of design parameters. However, there was a significant difference between the Level 2/Level 3 results and the Level 1 results (as explained earlier). The reason behind the difference in values could be tied to the use of more material data points for the Level 1 analysis. With more laboratory test results being used for the Level 1 analysis for each individual mixture, the results were more accurate than those of the Level 2/Level 3 analysis. This necessitates the use of Level 1 lab-tested inputs for any JPCP system to be designed through PMED.

5.2.3.2 Faulting Indicator Analysis

The faulting indicator results for levels one, two, and three showed that there was a significant difference between Level 1 and the other two input levels. The comparative analysis is shown in Figure 5.10. The Level 1 faulting indicator was significantly lower than the Level 2 and Level 3 faulting indicators. For each individual mixture, the faulting indicator was nearly doubled for levels two and three when compared to Level 1. The results for Level 2 and Level 3 had almost similar indicator values.

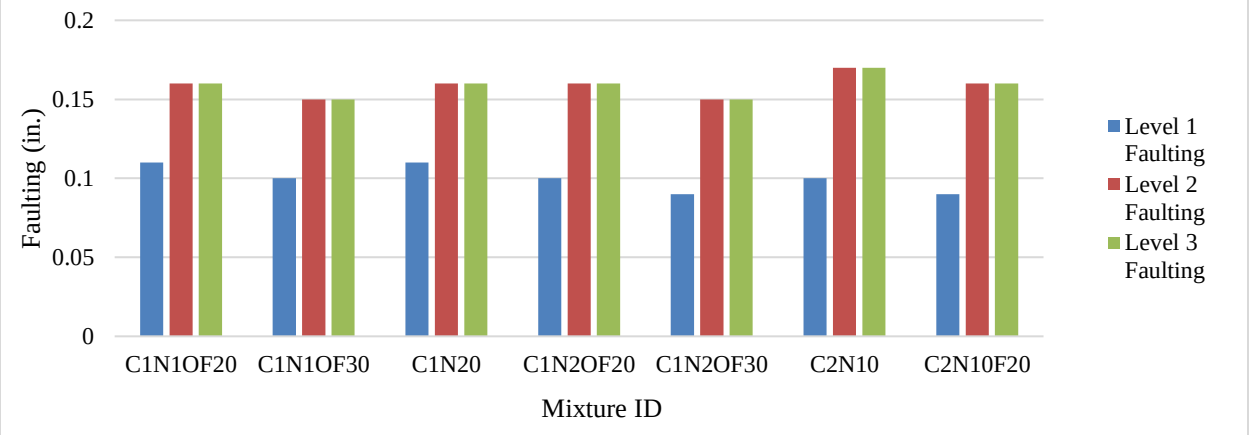

Figure 5.10: Level 1, Level 2, and Level 3 faulting indicator comparison

In Figure 5.11, the percentage difference between the Level 1 indicator value and the Level 3 indicator value is compared. The highest percentage change between the indicator values was 78 percent, which is present in the C2N1OF20 mixture. Additionally, the lowest change in the indicator values was in the C2N1O mixture, at 45 percent. The highest faulting indicator value was for Level 2 or Level 3. The Level 2 and Level 3 inputs were very similar to each other, with little difference in values. The Level 2 and Level 3 values for faulting were significantly higher than the Level 1 inputs.

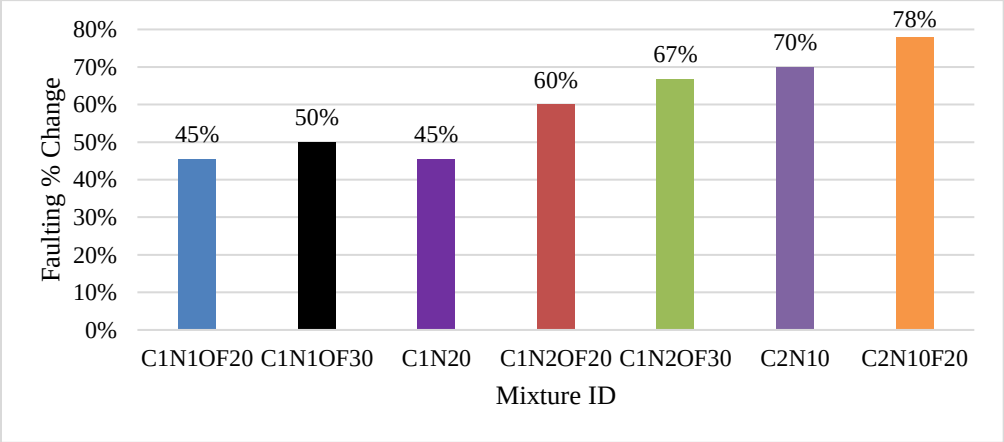

Figure 5.11: Percentage change in faulting between Level 1 and Level 3

With the above in view, using Level 2 or Level 3 inputs may result in inaccurate JPCP design and Level 1 inputs are recommended to be incorporated for the design of any JPCP system. Using Level 2/Level 3 inputs may result in an overdesigned pavement, resulting in the overspending of material and financial resources. These findings should be useful for pavement designers in understanding the potential relative impact of investment in and use of Level 1 inputs.

5.2.3.3 Cracking Indicator Analysis

The cracking indicator analysis between levels one, two, and three showed that there was a significant difference in the results. The comparative analysis is shown in Figure 5.12. The Level 1 cracking indicator values were significantly lower than those of levels two and three. The Level 1 indicator values were the most precise values based on the highest number of laboratory test results used for the Level 1 simulation. The Level 2 and Level 3 results for the cracking indicator were almost similar for most of the paving mixtures.

The percentage change between Level 1 and the highest indicator values of Level 2 or Level 3 showed that there was a significant percentage change. The percentage change in the cracking indicator values is shown in Figure 5.13. The highest percentage change occurred in the C1N2OF20 mixture, with a percentage change of 87 percent. The lowest percentage change in the cracking indicator values was the C2N1O mixture at 53 percent.

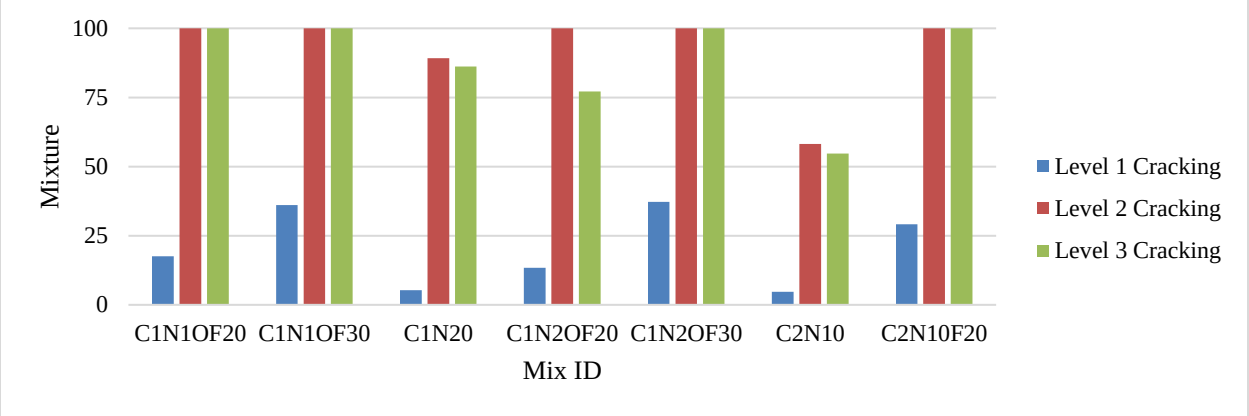

Figure 5.12: Level 1, Level 2, and Level 3 cracking indicator comparison

The simulation results shown in Figures 5.12 and 5.13 confirm that there was a very large difference between Level 1 and the other input levels. Prior research has already shown that Level 1 inputs are the most accurate, and these simulation results indicate that use of Level 2 or Level 3 inputs may result in overdesigned pavement systems. Thus, efforts should be considered to incorporate Level 1 concrete material inputs in the design process if resources and time are available.

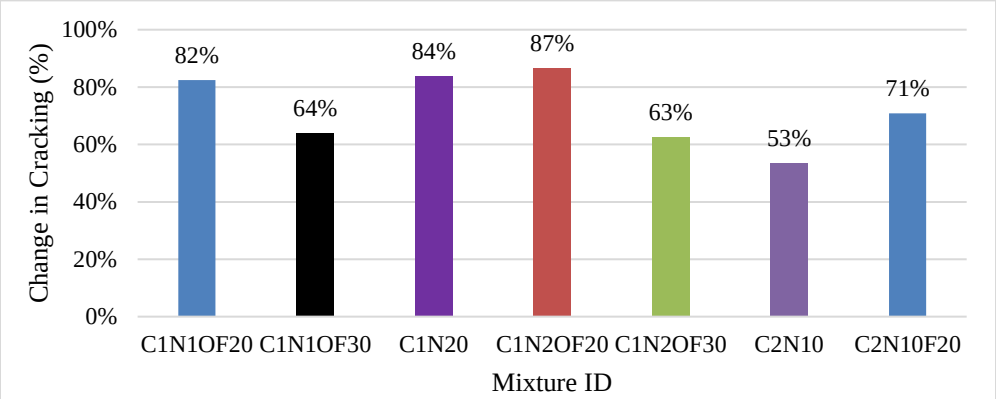

Figure 5.13: Percentage change in cracking between Level 1 and Level 3

The Level 1 inputs are the most accurate out of all three input levels, as supported by the findings from the literature and testing simulations. This is as expected, and the analysis of the simulation results supports the findings that there is a significant increase in the IRI, faulting, and cracking indicators as the concrete material inputs are changed from Level 1 to Level 2/Level 3. As described above, this work helps to quantify the differences in the performance indicators, providing knowledge to those hoping to understand the potential value of Level 1 inputs or aiming to justify investments for obtaining them. The IRI indicator showed a percentage increase in the performance indicator value up to 78 percent when the input level was changed from Level 1 to Level 3. The faulting indicator showed a percentage change of up to 78 percent when changed from Level 1, and the cracking indicator showed a percentage change of up to 87 percent when changed from Level 1 to Level 3. Using the most accurate input level – Level 1 – significantly influences the performance indicator analysis and should be taken into consideration when designing JPCP systems.

5.2.4 *Effects of the Input Levels on Design Slab Thickness of JPCPs*

Concrete slab thickness is one of the most important parameters in JPCP design and also substantially contributes to the initial cost of the pavement's construction. The concrete slab is the strongest structural layer in the JPCP system, and it supports the major portion of stresses, strains, and deflections occurring due to traffic and temperature loading. Variations in concrete slab thickness impact the lifetime performance of JPCP systems. The adjustment of the Level 3 slab thickness parameter to match the Level 1 cracking performance indicator demonstrated a difference in the Level 1 and Level 3 design slab thicknesses.

The performance indicator results for the C1N1OF20, C1N1OF30, C1N2O, C1N2OF20, C1N2OF30, C2N1O, and C2N1OF20 mixtures were compiled for the Level 1 and Level 3 results at the baseline model of an 8-inch PCC slab thickness. The only performance indicator used was the cracking performance indicator. The performance indicator results for 8 inches are shown in Table 5.6. Simulations were performed through PMED software, adjusting the slab thickness at the Level 3 input design for each individual mixture. The slab thickness was changed during the simulations to match the

Level 3 performance indicators to the Level 1 indicators. The performance indicators at the Level 3 design level were not an exact match to the Level 1 performance indicators, but all the indicators fell within a reasonable range of equivalency. Each individual mixture reacted differently to the change in the Level 3 PCC thickness.

Table 5.6: Level 1 and Level 3 cracking indicator results for the baseline model.

Mixture ID	Level 1 (Percentage of Cracked Slabs)	Level 3 (Percentage of Cracked Slabs)
C1N1OF20	17.51	100
C1N1OF30	36.13	100
C1N2O	5.35	86.16
C1N2OF20	13.38	77.14
C1N2OF30	37.29	100
C2N1O	4.69	54.66
C2N1OF20	29.11	100

5.2.4.1 Slab Thickness Results

Changes in the PCC slab thickness in the JPCP system within the Level 3 framework to match the Level 1 cracking indicator results are shown in Table 5.7. Each mixture produced unique performance indicator results, causing each mixture to result in a different slab thickness when the Level 3 cracking indicator matched the Level 1 cracking indicator. The change in slab thickness is shown in Figure 5.14. The highest change is shown as a 2-inch difference in the concrete slab thickness between the baseline model of 8 inches simulated with the Level 1 inputs and the new adjusted slab thickness for the Level 3 input simulations. The percentage change in the PCC thickness values between the Level 1 and Level 3 design is shown in Figure 5.15, and it is evident that there was a significant change in concrete slab thickness, with a 25 percent change in the pavements designed using three mixtures, a 19 percent change in the pavements designed using two mixtures, and a 13 percent change in the pavements designed using the remaining two mixtures. These results show a significant increase in the recommended PCC thickness between the two design/analysis approaches and represent a major cost increase (and increase in material use) for the Level 3 input approach.

Table 5.7: Comparison of cracking results for varying slab thicknesses

		Level 1 Cracking (%)	Level 3 Cracking (%)		
	Mixture	8 inches	10 inches	9.5 inches	9 inches
% Slabs	C1N1OF20	17.51	-	15.27	-
	C1N1OF30	36.13	35.65	-	-
	C1N20	5.35	4.8	-	-
	C1N2OF20	13.38	-	-	12.97
	C1N2OF30	37.29	-	36.68	-
	C2N10	4.69	3.21	-	-
	C2N10F20	29.11	-	-	33.36

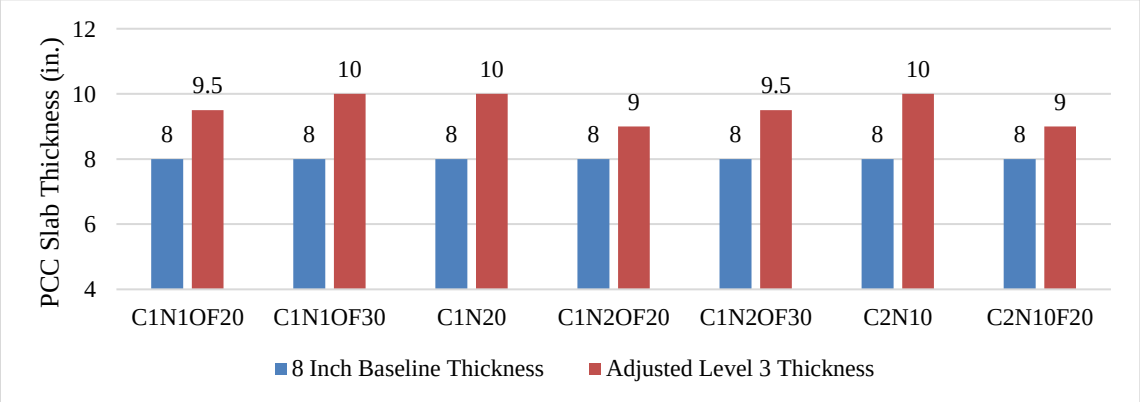

Figure 5.14: Comparison of Level 1 and Level 3 design slab thickness

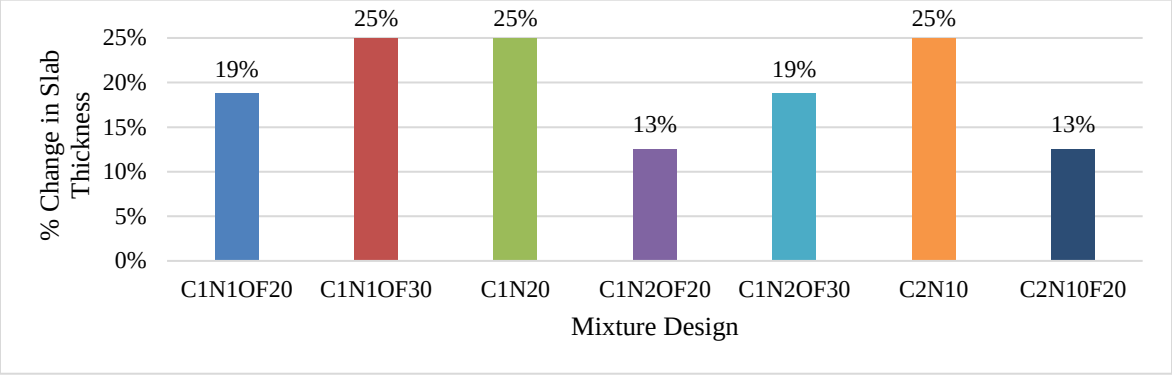

Figure 5.15: Percentage change in slab thickness between Level 1 and Level 3 simulations

5.2.4.2 Performance Indicator Results

Comparison of JPCP Cracking with Level 3 Baseline Models and Readjusted Level 3 Models

The performance indicator results also significantly changed through the readjustment of the Level 3 slab thicknesses. The comparison of the original baseline model for the Level 3 inputs to the newly adjusted Level 3 inputs is shown in Figure 5.16. There was a significant change in the cracking indicator results when the Level 3 PCC slab thickness was changed to reflect the Level 1 cracking indicator results. In Figure 5.17, the percentage change in the cracking indicator values is shown. The percentage change ranged from 84.73 percent to 51.45 percent. It is evident that with the increase in slab thickness, the cracking performance indicator significantly decreased.

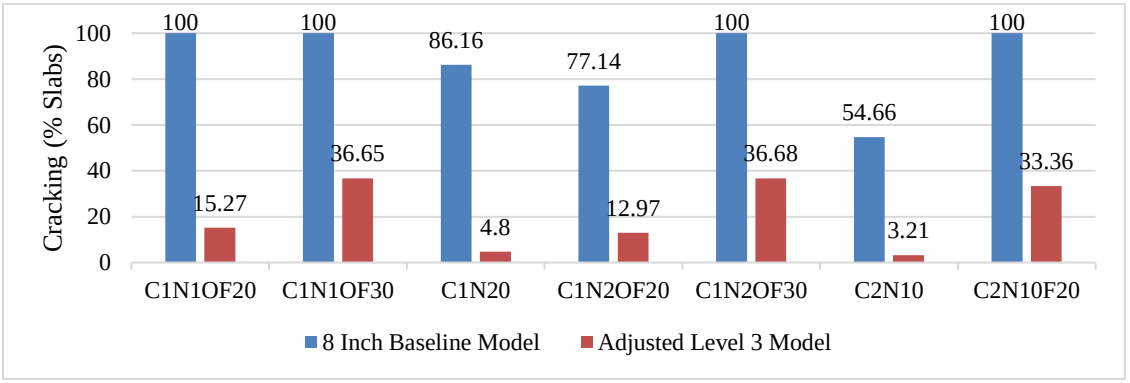

Figure 5.16: Comparison of Level 3 baseline models and adjusted Level 3 models

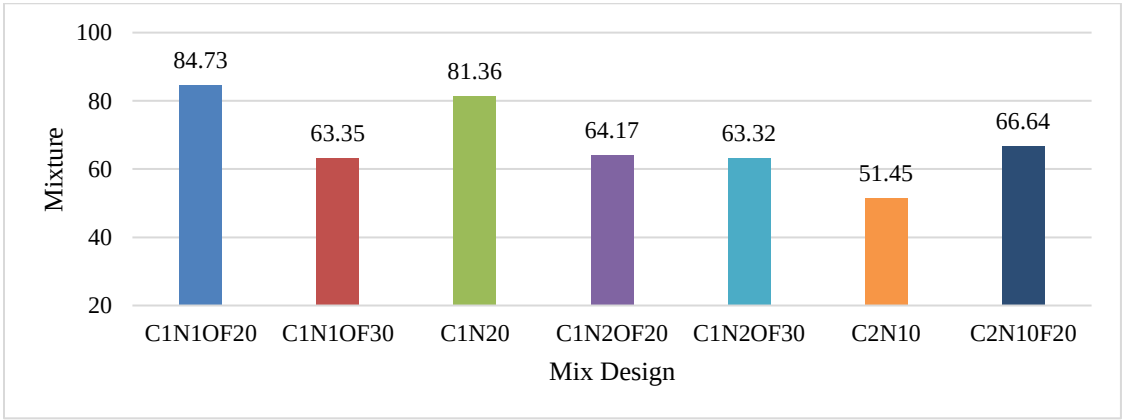

Figure 5.17: Percentage change in cracking indicator between Level 3 baseline model and adjusted Level 3 model

Comparison of JPCP Cracking with Level 1 Baseline Models and Readjusted Level 3 Models

The comparison of the JPCP cracking indicator between the Level 1 baseline models and the readjusted Level 3 models was conducted, as shown in Figure 5.18. All the simulations for the Level 1 baseline models had a constant concrete slab thickness of 8 inches. The slab thickness for each individual mixture varied for the re-adjusted Level 3 simulations, and the details are shown in Abbreviations section. There was still some variation in the cracking performance indicator

results between the Level 1 and readjusted Level 3 values even after slab thickness adjustments were conducted. However, the difference in the cracking indicator values was very small, and these scenarios could be considered equivalent for comparative and analytical purposes.

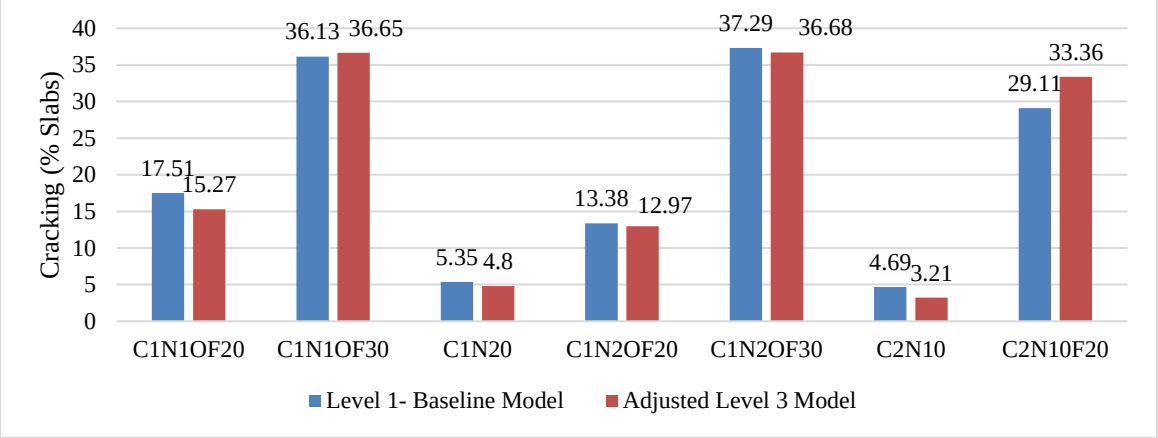

Figure 5.18: Level 1 baseline model vs. adjusted Level 3 model

5.2.5 Inference

As expected, Level 1 material inputs provide the most accurate simulation results out of all three input levels, and there is a significant increase in the IRI, faulting, and cracking indicators as the concrete material inputs are changed from Level 1 to Level 2/Level 3. The IRI indicator showed a percentage increase in performance indicator value up to 78 percent when the input level was changed from Level 1 to Level 3. The faulting indicator showed a percentage change of up to 78 percent when changed from Level 1, and the cracking indicator showed a percentage change of up to 87 percent when changed from Level 1 to level. Using the most accurate input level – Level 1 – significantly influences the performance indicator analysis and should be taken into consideration when designing JPCP systems.

This should result in the design of pavements that provide the sustainability benefits of a lower initial cost, lower environmental impact (due to less material use), and more predictable service lives and maintenance/rehabilitation activities.

The increase in PCC slab thickness for the readjusted Level 3 simulations resulted in improved JPCP performance within the transverse cracking indicator. Increasing the slab thickness caused the Level 3 cracking indicator to align with the Level 1 (baseline) cracking indicator. Each paving mixture behaved differently within the framework of readjusted Level 3 models because of their specific mechanical and thermal properties. The overall difference in PCC slab thickness between the Level 1 and Level 3 designs was from 1 to 2 inches. This represents a significant material and monetary cost difference, with the Level 1 thickness being more optimal for a variety of economic and sustainability reasons.

It is evident from this analysis that using Level 3 inputs for JPCP design will result in a thicker concrete slab, and using Level 1 inputs will produce a more accurate and economical JPCP design. Future research into the life cycle cost differences between pavements designed with Level 1 inputs versus Level 3 inputs would provide a more holistic perspective of the benefits of investing in Level 1 inputs for the design/analysis of a pavement project. Case studies on the service life performance of pavements designed using Level 1 inputs compared to those designed using Level 2 or Level 3 inputs would provide additional insight into both the accuracy of the local pavement-ME calibration as well as provide additional data to support project-specific inputs and the local calibration of the models in the software. Although this work was performed using the materials and characteristics local to one location in the United States, both the approach and the findings could be useful for pavement designers internationally.

5.3 Impact of Material Input Levels on CRCP Performance and Design Slab Thickness

The simulations were conducted in pavement ME design for mixture designs C1N1OF20, C1N1OF30, C1N20, C1N2OF20, C1N2OF30, C2N10, and C2N1OF20 to contrast the impact of Level 1 and level-3 inputs on CRCP design and performance. The lab tested data for concrete mechanical properties including MOR and elastic modulus and CTE were used for level-1 design simulations while, for level-3 design, default CTE value and 28 days compressive strength input were used. CRCP thickness was 10 in and other design parameters were kept constant (as per Table 5.8) to compare the effects of input levels. The comparative results are tabulated in Table 5.9.

Table 5.8: CRCP design parameters for simulation work

Parameter	Value
Design Life	40 years
Design Thickness	10 in.
Shoulders	Tied PCC Shoulders
Steel Reinforcement (%)	0.60
Steel Bar Diameter	0.63 in.
Steel Depth	4 in.
Initial IRI	63 in/mile
Threshold IRI	172 in/mile
Threshold Punch-outs	10 per mile
Reliability	90%
Modulus of Rupture of Concrete	As per Mixture ID
Elastic Modulus of Concrete (28 days)	As per Mixture ID
Poisson's Ratio	0.2
Climate Station	Albuquerque, New Mexico
AADTT	5000
Traffic ESALS	$54x10^6$
Cement Stabilized Base Course Thickness	10 in.
Non-Stabilized Base Course Thickness	10 in.

Table 5.9: Simulation results of impact of input levels on CRCP performance

	IRI	IRI	Punch outs	Punch outs
Mixture ID	Level-1	Level-3	Level-1	Level-3
C1N1OF20	97.1	332.1	7.8	125.2
C1N1OF30	91.4	347.5	4.1	132.8
C1N20	88.1	312.9	0.7	115.6
C1N2OF20	88.7	329.5	1.3	123.9
C1N2OF30	89.3	343.4	2.2	130.7
C2N10	88.1	266.7	0.6	92.9
C2N1OF20	90.5	266.7	3.3	92.7

5.3.1 *Analysis of Simulation Results*

The analysis of simulation results was conducted to quantify the effects of input levels variation on pavement performance indicators.

5.3.1.1 Effects on Pavement Roughness/IRI

The comparison for terminal values of IRI for all the simulated mixtures (C1N1OF20, C1N1OF30, C1N20, C1N2OF20, C1N2OF30, C2N10, and C2N1OF20) is presented in Figure 5.19, which shows that there is a significant variation in IRI values between the results of Level 1 and Level 3 inputs for all the paving mixtures. The variation in IRI with input levels ranges from 176 to 256 in/mile which is highly significant. With these results, it is evident that the CRCP must be designed with the accurately tested Level 1 inputs for the paving mixture to be used on a specific CRCP project so that the designed pavement can last for the entire service life. The PMED default CTE data and Level 3 inputs will not produce an accurate design for NCDOT paving mixtures.

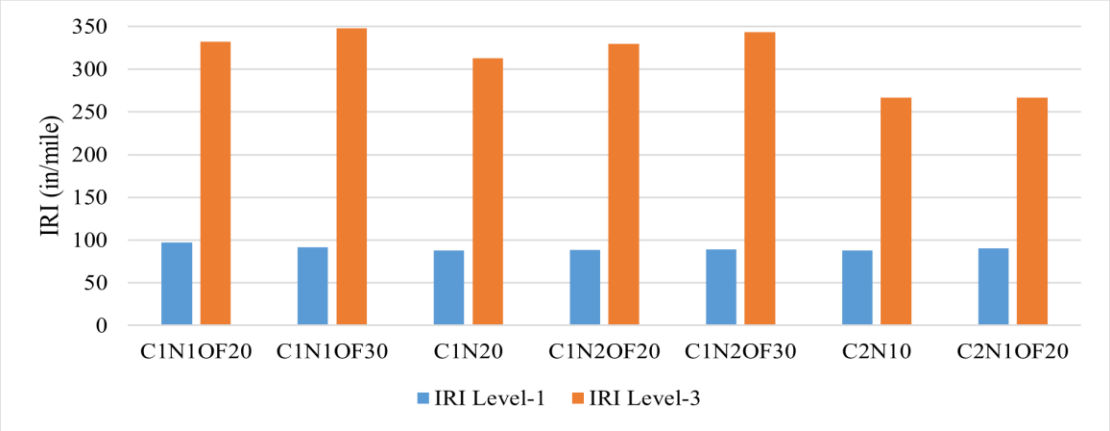

Figure 5.19: Impact of input levels on IRI

5.3.1.2 Effects on Punch Outs

The comparative summary for CRCP punch outs for the impact of material input levels for all the simulated mixtures (C1N1OF20, C1N1OF30, C1N20, C1N2OF20, C1N2OF30, C2N10, and C2N1OF20) is presented in Figure 5.20. It is evident that there is a significant impact on CRCP punch outs between the two material input levels. The difference in terminal punch out values ranges between 89 to 128 per mile. This shows the importance of using accurate concrete material inputs to be used for CRCP design.

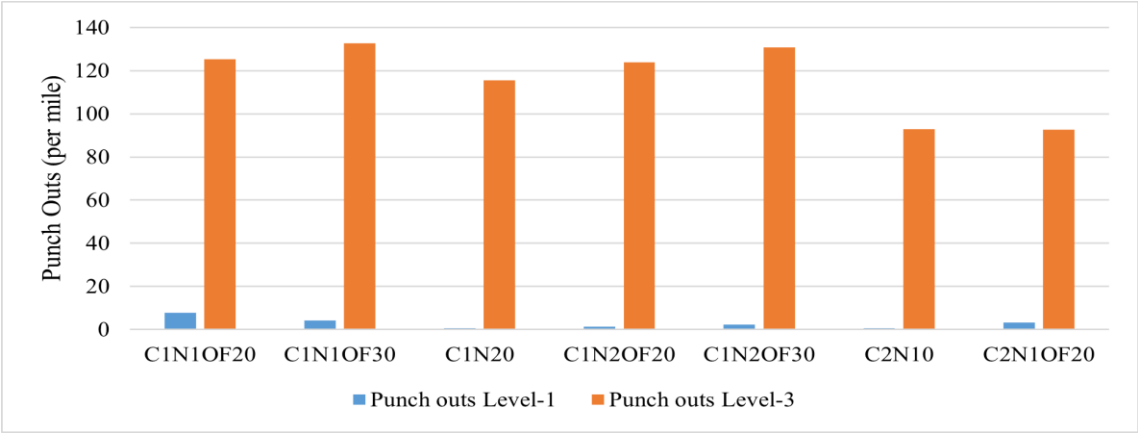

Figure 5.20: Impact of input levels on CRCP punch outs

5.3.2 *Effects of Input Levels on Design Slab Thickness Of CRCP*

Performance indicator results for mixture designs C1N1OF20, C1N1OF30, C1N20, C1N2OF20, C1N2OF30, C2N10, and C2N1OF20 were compiled for Level 1 and Level 3 simulations within the framework of the baseline model of 10-inch CRCP slab thickness as tabulated earlier in Table 5.9. The performance indicators used for the re-adjusted CRCP slab thickness were punch puts and IRI. Simulations were performed through PMED software with the revised slab thickness at the Level 3 input design for each individual mixture. Slab thickness was changed during the simulations to match Level 3 performance indicators to Level 1 performance indicators. The simulation results for the Level 1 baseline model (10 inch slab thickness) and the re-adjusted Level 3 models (12 inch slab thickness) are tabulated in Table 5.10 and it is evident that the performance indicators at the re-adjusted Level 3 designs are not an exact match to Level 1 performance indicators, but all the indicators fall within a reasonable range of equivalency. These results are also presented in Figures 5.21 and 5.22. The difference in punch outs between the two scenarios is in the range of 0.6 to 3.2 per mile whereas the difference in IRI between the two scenarios is in the range of 0.4 to 4.9 inch/mile. This variance is extremely low as compared to the original base line models with similar slab thickness and the re-adjusted scenarios can be considered equivalent in terms of CRCP design.

Table 5.10: Comparison of CRCP performance with re-adjusted CRCP slab thickness

	IRI	IRI	Punch outs	Punch outs
Mixture ID	Level-1 (10 inch Slab Thickness)	Level-3 (12 inch Slab Thickness)	Level-1 (10 inch Slab Thickness)	Level-3 (12 inch Slab Thickness)
C1N1OF20	97.1	94.6	7.8	6.1
C1N1OF30	91.4	96.3	4.1	7.3
C1N20	88.1	88.5	0.7	1.3
C1N2OF20	88.7	89.3	1.3	2.2
C1N2OF30	89.3	92.1	2.2	4.5
C2N10	88.1	88.1	0.6	0.5
C2N1OF20	90.5	88.1	3.3	0.4

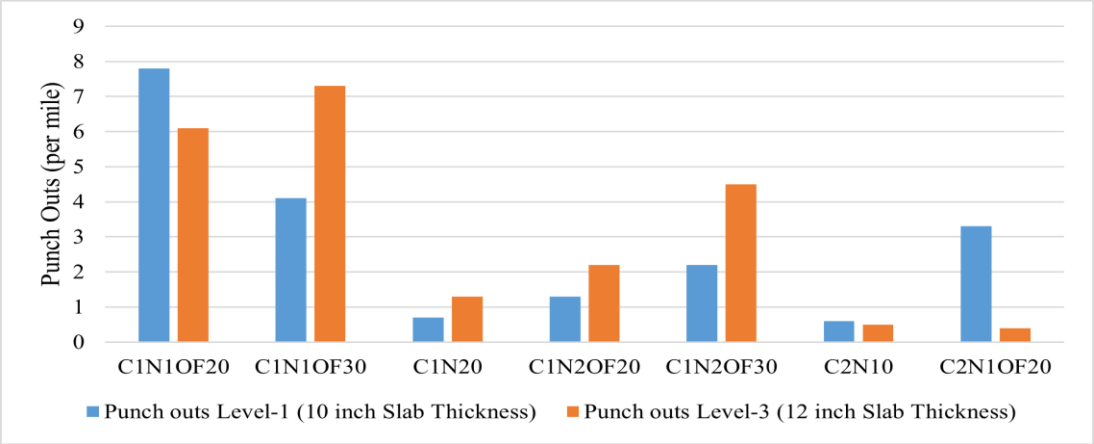

Figure 5.21: Comparison of punch outs in Level 1 baseline models and re-adjusted Level 3 models

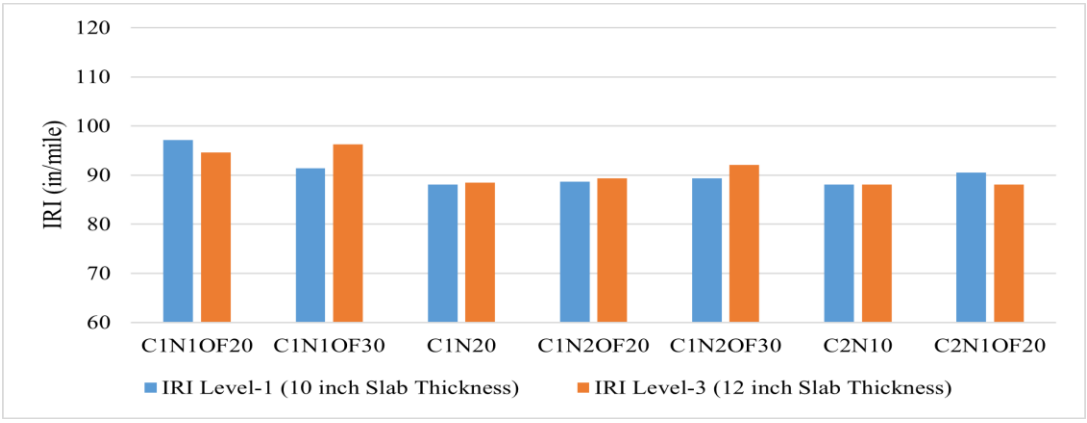

Figure 5.22: Comparison of IRI in Level 1 baseline models and re-adjusted Level 3 models

5.3.4 Inference

These results show that the increase in CRCP slab thickness results in significantly improved CRCP performance with respect to IRI and punch outs. The performance indicator values of re-adjusted Level 3 simulations (with CRCP slab thickness of 12 inch) align well with the performance indicator values of Level 1 design simulations. There is a difference of 2 inches in pavement slab thickness between the two input level scenarios and it is evident from this analysis that using Level 3 material inputs will result in an over-designed pavement with a huge loss of financial, material, and labor resources. It can be concluded that any CRCP project should be designed with accurately determined Level 1 material inputs for an effective pavement design.

5.4 Effects of Fly Ash on the Performance and Design Slab Thickness of JPCP

5.4.1 *Effects of Fly Ash on the Performance of JPCP*

Fly ash is a supplementary cementitious material (SCM) used in paving concrete. Fly ash poses potential benefits from sustainability and cost point of view. To determine the effects of fly ash on concrete, thorough analysis should be performed. Fly ash as a material substitute for cement causes changes in the material content of the paving concrete. Analysis of the effects of fly ash on JPCP performance and its impact on the slab thickness is presented in this section.

5.4.2 *Methodology*

To analyze the effects that fly ash has on JPCP pavements, simulations in Pavement ME Design were performed and IRI, faulting, and cracking indicators were compared. In Pavement ME, Level 3 analysis was used in phase-1 and Level 1 analysis was conducted in phase-2. For each individual mixture, coefficient of thermal expansion (CTE) and compressive strength were selected for Level 3 analysis and time series data of elastic modulus and modulus of rupture were used for Level 1 analysis. The JPCP slab thickness was kept constant at 9 inches for this analysis. The baseline model used for simulations is found in Appendix C, Table C.2. The 28-day data used for coefficient of thermal expansion (CTE) and compressive strength is found in Appendix C, Table C.3. After conducting the simulations, analysis of the effects of fly ash on each of the three performance indicators for JPCP was performed. For the analysis purposes, the paving mixtures were placed into groups. The groups were made based on percentage of fly ash for a base mixture. Base mixtures are C1N20, C2N10, C2N20, C3N10, C3N20, and C4N10. For example, of a mixture group, C1N20, C1N2OF20, and C1N2OF30 are designated as a mixture group. The change in each indicator group is between 0% fly ash and 30% fly ash. After analyzation of the change in JPCP performance indicators, effects of fly ash on pavement thickness were analyzed with additional simulation work. The results of Level 3 analysis are presented first, and Level 1 analysis are presented later in the following section.

5.4.3 *Analysis of Level-3 Simulation Results*

5.4.3.1 Effects of Fly Ash on IRI Indicator

The IRI Indicator was analyzed between 0% Fly ash and 30% Fly ash. The results of the IRI Indicator are as follows. Figure C.10 presents the comparison of IRI results for all mixture groups including 0%, 20%, and 30% fly ash and it shows that 0% fly ash produces a lower IRI indicator than 30% fly ash for all of the paving mixture groups. The trend from Figure C.10 shows that adding fly ash to JPCP will cause the IRI indicator to increase. The change in the IRI indicator between 0% and 30% fly ash mixtures is shown in Figure C.11 and it is evident that the IRI indicator is affected by adding fly ash to the paving mixtures. This is likely an artifact of the lower 28-day strength values for fly ash mixtures. As discussed previously, fly ash mixtures gain strength at a slower rate than non-fly ash mixtures, and the 28-day strength values do not represent the later-age and long term strength of these mixtures.

In this analysis, the IRI indicator has the largest change of 20.95 in/mile for mixture group C3N20. Figure C.12 shows the change in the IRI indicator when 30% fly ash is added to base mixtures. In Figure 5.23, it is shown that adding fly ash to a base mixture causes an increase in the IRI for all the mixtures being simulated and the % change in IRI is in the range of 0.3% to 13.1%. An observation of the material input data indicates that the 30% fly ash mixtures produce lower 28 day compressive strength and lower CTE when compared with the base mixtures and these changed properties affect the performance of JPCP resulting in a higher IRI/decreased performance. The lower CTE should produce better performance in the form of reduced IRI but the lower compressive strength of the fly ash mixtures is counteractive and the results in increased IRI. All of the paving mixture groups show a significant increase in the IRI indicator when 30% fly ash is added and performance is compared with their counterparts with no fly ash content.

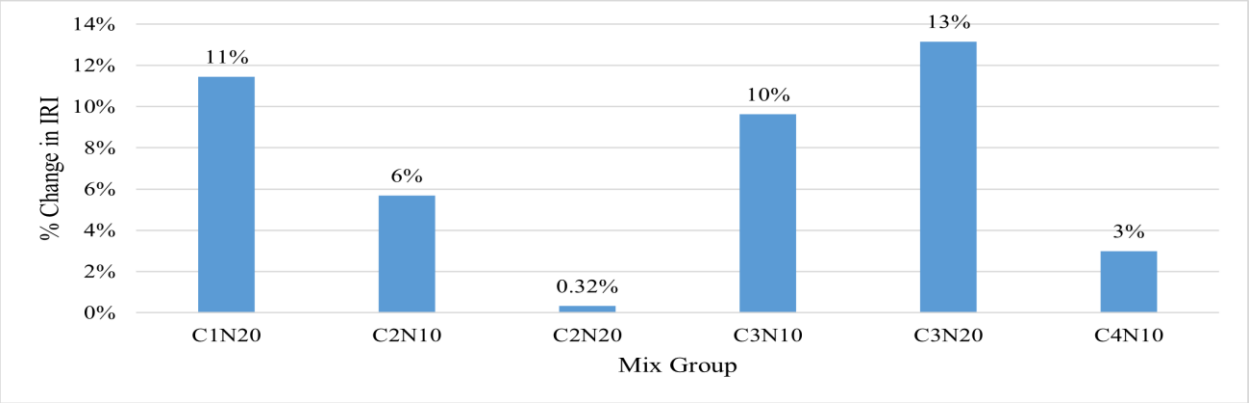

Figure 5.23: % Change in IRI indicator between 0% and 30% fly ash mixtures

5.4.3.2 Effects of Fly Ash on Faulting Indicator

The simulation results on joint faulting were analyzed and the faulting indicator for each mixture group is presented in Figure C.13. It is evident that the faulting indicator decreases for each mixture group between 0% and 30% fly ash mixtures. The change in the faulting indicator between 0% and 30% fly ash mixtures is shown in Figure C.14 and the largest change for the faulting indicator is 0.02 inch. The percentage change in the faulting indicator is shown in Figure C.14. The largest change for the faulting indicator is 18 percent with an overall range of 8% to 18% but most of the mixtures are at 8%. Fly ash is shown to give a decreasing effect on the faulting indicator in all the paving mixtures being simulated but looking at the simulation data it can be assumed that it is not a very significant change in faulting and most of the mixtures show less than 10% change in joint faulting with the addition of 30% fly ash.

5.4.3.3 Effects of Fly Ash on Cracking Indicator

The simulation results on transverse cracking are analyzed and the comparison of cracking indicator data is shown in Figure 5.24. In Figure 5.24, the cracking indicator is shown to increase when fly ash is added to the paving mixture. It is evident that all the paving mixture group's cracking indicator increases as fly ash is added. An observation of the material input data indicates that the 30% fly ash mixtures produce lower 28-day compressive strength and lower CTE when compared with the base mixtures and these changed properties affect the performance of JPCP resulting in a higher transverse cracking/decreased performance. The lower CTE should produce better performance in the form of reduced cracking, but the lower compressive strength of the fly ash mixtures is counteractive, and this results in increased transverse cracking. Figure 5.25 shows the percentage change of the cracking indicator between 0% and 30% fly ash mixtures. The largest change in the cracking indicator is 32.1%, for the mixture group C3N20. Each mixture group increases by at least 10 percent and the overall % change in cracking is in the range of 10.7% to 32.1% when 30% fly ash is added to the mixture. This is a very significant increase in transverse cracking and adding fly ash will result in decreased predicted performance of the JPCP system. In many cases, this is contrary to what has been observed in field performance. As discussed previously, the 28-day value is not representative of the later-age strength of fly ash mixtures, exhibiting a limitation of PMED for fly ash mixtures. It may be recommended to use a 56-day or 90-day strength input for fly ash mixtures to mitigate this effect on PMED prediction.

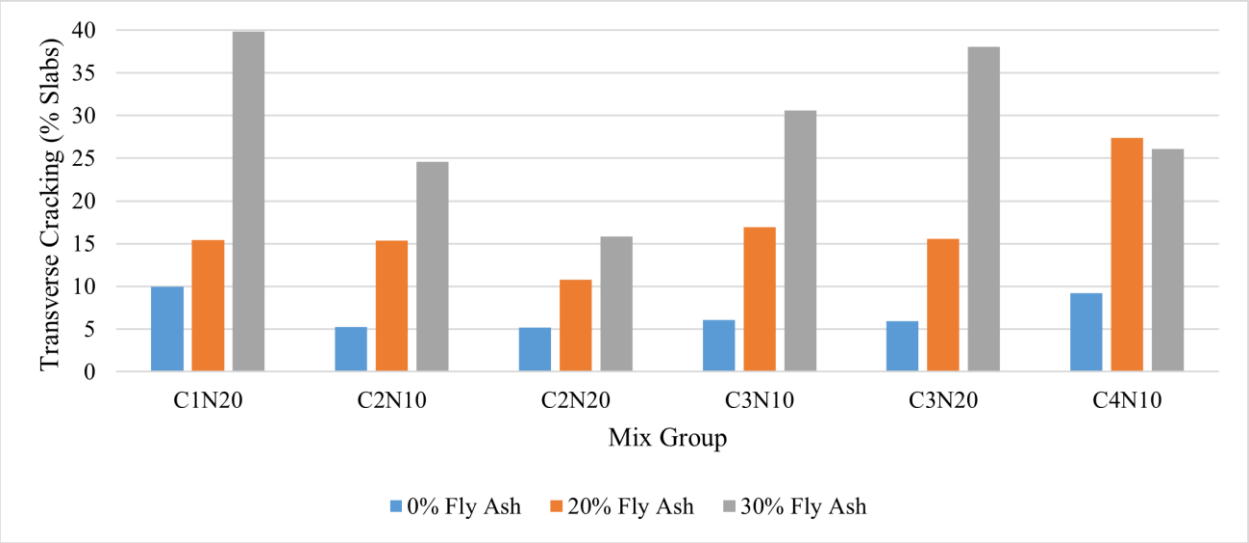

Figure 5.24: Cracking indicator results

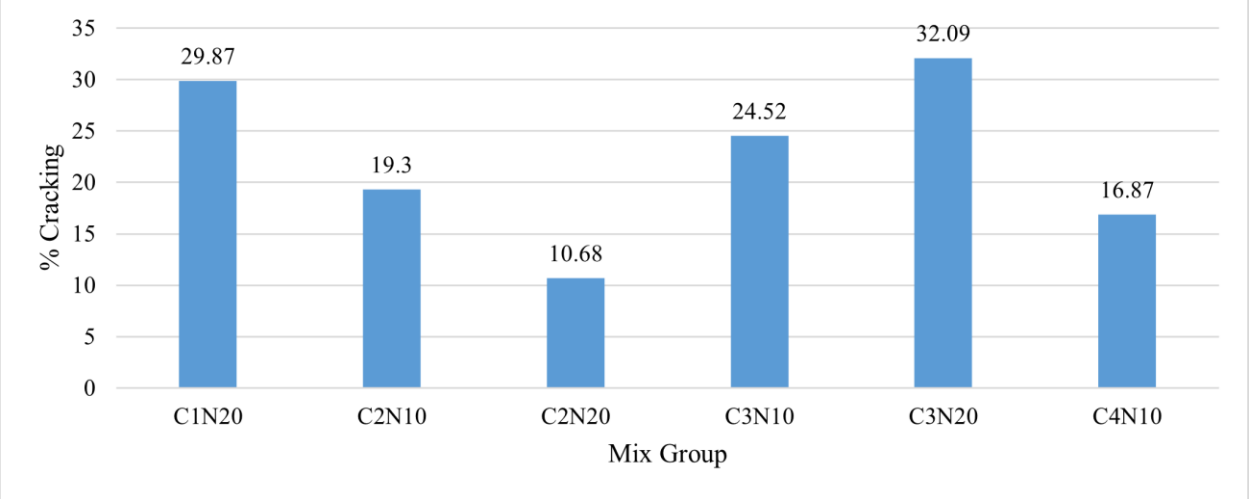

Figure 5.25: % Change in cracking indicator between 0% and 30% fly ash mixtures

5.4.4 *Inference from the Level-3 JPCP Simulation Results*

Averages were taken between the JPCP performance indicator results. The percentage change in zero percent fly ash and thirty percent fly ash were used for Figure 5.26. As shown in Figure 5.26, each of the performance indicators increased by at least 10 percent when 30 percent fly ash was added. The cracking indicator experienced the greatest percentage change, having a 28% average change in the simulated paving mixtures. Joint faulting shows a 12 percent decrease in performance indicator values and IRI has an average change of 10 percent. As shown from Figure 5.26, adding fly ash to concrete paving mixtures will cause performance indicator values to increase significantly for IRI and cracking and a careful consideration is needed when designing the JPCP systems with the fly ash concrete mixtures. One recommendation is to use later-age strength values as inputs in lieu of 28-day strengths.

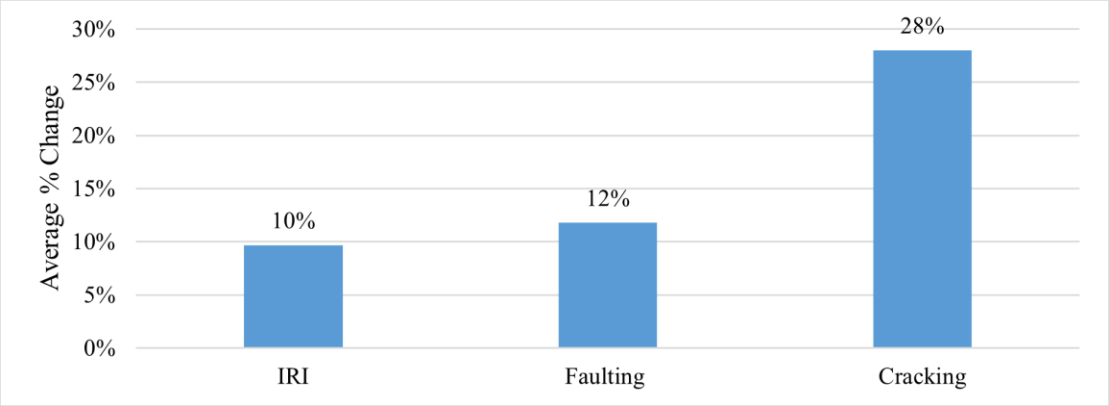

Figure 5.26: Performance indicator comparison

5.4.5 *Effects of Fly Ash on the Design Slab Thickness of JPCP with Level-3 Analysis*

Addition of fly ash as SCM to the concrete paving mixture causes JPCP performance to decrease with an increase in IRI, joint faulting, and transverse cracking. Increasing the PCC slab thickness can help improve the pavement performance. Analysis was conducted to quantify the impact of fly ash on the slab thickness of JPCP system. Additional simulations were conducted in Pavement ME Design with the increased PCC slab thickness to match the cracking indicator values of the thirty percent fly ash mixture to the zero percent fly ash mixture. The cracking indicator was selected for this matching analysis because the cracking performance indicator has the most severity in the % change among all three performance indicators. To analyze the change in the PCC slab thickness, the 30% fly ash mixture for each mixture group was selected for simulations. Adjustment of the PCC slab thickness on the 30% fly ash mixture was performed to generate cracking indicator results that were similar to the 0% fly ash mixture. The cracking indicator comparison for 0% fly ash mixtures and for 30% fly ash mixtures is tabulated in Table 5.11. The 0% fly ash mixtures have a PCC slab thickness of 9 inches and after running the simulations in Pavement ME Design for 30% fly ash mixtures, a PCC slab thickness of 10 inches shows similar cracking indicator results. It is evident that an increase of one inch in the PCC slab thickness matches cracking values for 0% fly ash and 30% fly ash. When using 30% fly ash mixtures for JPCP projects, the PCC layer may be increased by one inch to accommodate the pavement performance.

Table 5.11: Comparison of baseline model with 30% fly ash re-designed model

MIXTURE ID 0% Fly Ash	Cracking Indicator	MIXTURE ID 30% Fly Ash	Cracking Indicator
9 inch Slab Thickness		10 inch Slab Thickness	
C1N20	9.98	C1N20F30	7.67
C2N10	5.26	C2N10F30	5.22
C2N20	5.19	C2N20F30	3.79
C3N10	6.09	C3N10F30	5.87
C3N20	5.95	C3N20F30	6.79
C4N10	9.24	C4N10F30	3.29

5.4.6 *Analysis of Level-1 Simulation Results*

Simulations were performed for JPCP in the PMED software using Level 1 input values. The 28-days to 20-year ratio used for simulation is 1.22. All other input values are the same input values used in Level 3 JPCP simulations. Input values kept constant can be found in previous section. Results for simulations for JPCP simulations are as follows.

5.4.6.1 Effects of Fly Ash on IRI Indicator

Simulation Results for the IRI indicator are presented in Figures C.15, C.16, and 5.27. Figure 1 highlights the different mixture groups and their individual group change when fly ash is added to the mixture. Each mixture group shown in Figure C.15, excluding C2N20 and C4N10 groups, shows that the 30 percent fly ash mixture has a higher IRI value and the zero percent mixture. The difference in value between zero percent fly ash and 30 percent fly ash is presented in Figure C.16. Note that mixture groups C2N20 and C4N10 difference is shown as a positive value but are negative. The

highest change in value for the IRI indicator is in mixture group C1N20, with a 17-point change between zero and thirty percent fly ash. Mixture group C1N10 has the second-highest IRI change with a 14-point difference. Figure 5.27 presents the percentage change between zero and thirty percent fly ash. Mixture groups C1N10 and C1N20 have the highest percentage change in value with an eight and nine percent difference, respectively. Each other mixture group underwent a change in value between zero and thirty percent fly ash, averaging around four percent.

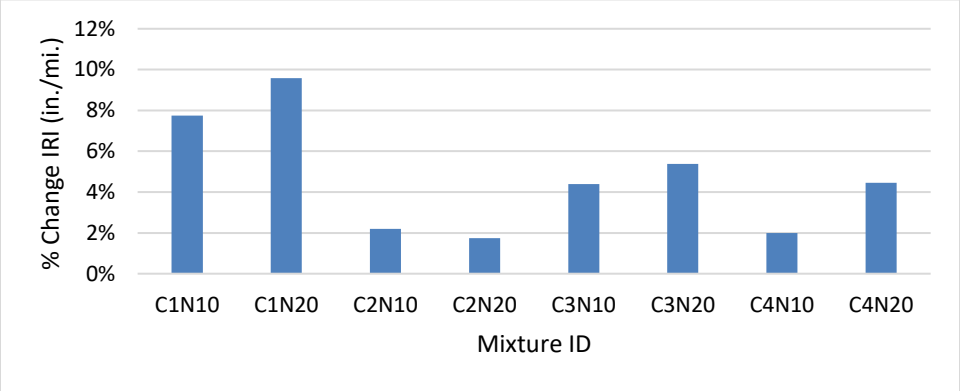

Figure 5.27: Percent change in IRI for 0% and 30% fly ash mixtures (Level 1)

5.4.6.2 Effects of Fly Ash on Joint Faulting Indicator

Faulting simulation results and analyzation are in Figures C.17, C.18, and 5.28. Figure C.17 presents the faulting simulation results at Level 1. For each mixture group, the faulting indicator decreases as fly ash is added from zero percent to thirty percent. Figure C.18 shows the difference in the faulting indicator values for each mixture group. Mixture groups C1N10, C1N20, C2N10, C3N10, and C3N20 all changed an average of 0.01. Mixture groups C4N10 and C4N20 changed by 0.02. Figure 5.28 shows the percentage change when fly ash is added to thirty percent. Please note the percentage change values are shown to be high, but the difference in value is 0.01 or 0.02. The largest percentage change is 13 percent in mixture group C4N20. Mixture group C4N10 has a percentage change of 12 percent, which is the second largest. Each other mixture group has an average percentage change of seven percent.

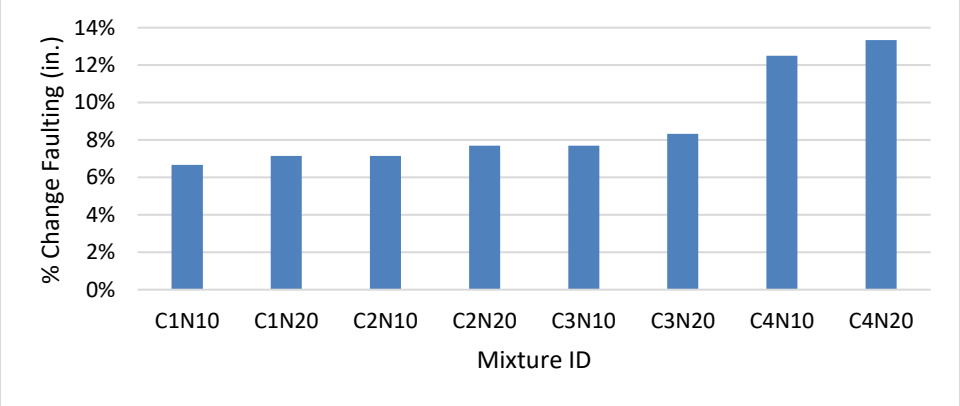

Figure 5.28: Percent change in faulting for 0% and 30% fly ash mixtures (Level 1)

5.4.6.3 Effects of Fly Ash on Transverse Cracking Indicator

The cracking indicator simulation results are presented in Figures 5.29 and 5.30. Figure 5.29 shows as fly ash is added from zero to thirty percent to each mixture group, the cracking indicator increases in value. Mixture group C1N10 has the most severe change in the cracking indicator, as shown in Figure 5.29. Each mixture group has a substantial change in the indicator value as fly ash is added to the mixture groups. The change in the cracking indicator between zero percent fly ash and thirty percent fly ash is in Figure 5.30. Mixture groups C1N10, C4N20, and C3N20 have the highest change in the cracking indicator. C1N10 has a 24 percent difference in value. The lowest change in the cracking indicator value is in mixture group C2N20, with a change of five percent. It is evident that the addition of fly ash into the mixtures will decrease pavement performance. The limitations of excluding values after 90 days for MOR and EM will produce a lower

pavement performance for transverse cracking. The lower CTE should produce better performance in the form of reduced cracking, but the lower 28-day compressive strength of the fly ash mixtures is counteractive, and this results in increased predicted transverse cracking.

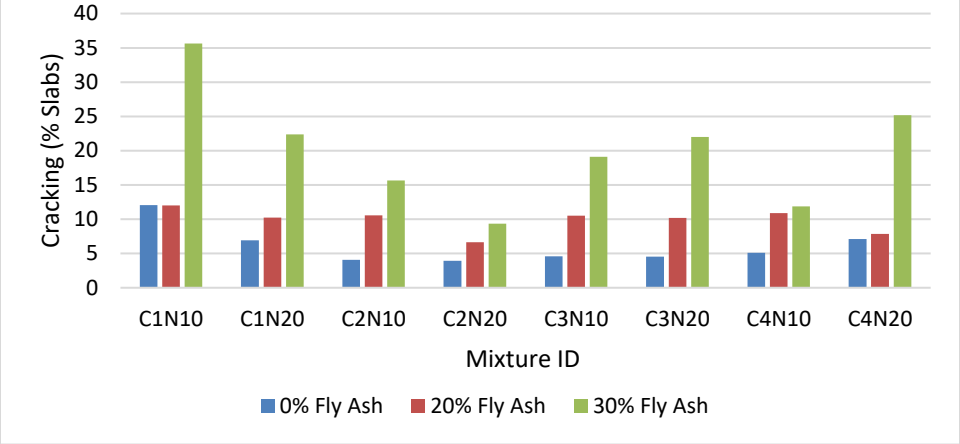

Figure 5.29: Comparison of cracking simulation results (Level 1)

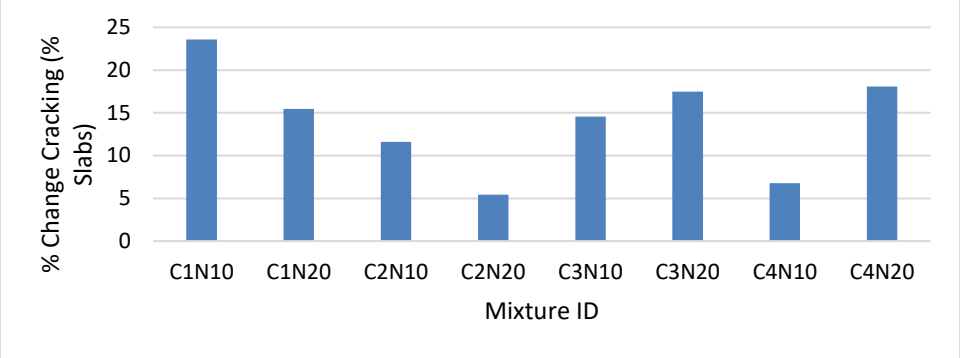

Figure 5.30: Percent change in cracking for 0% and 30% fly ash mixtures (Level 1)

5.4.7 Inference from Level 1 JPCP Simulation Results

A summary of the IRI indicator, faulting indicator, and cracking indicator is shown in Figure 5.31. An average of the percentage change for each indicator between zero and thirty percent fly ash was produced. IRI has an average percentage change of 5%. The faulting indicator has an average percentage change of 9%, and cracking has an average percentage change of 14%. The faulting indicator has a decrease in value as fly ash is added, but the percentage change is shown as positive. The IRI and cracking indicators have a significant average change when zero percent and thirty percent fly ash simulation results are produced at the Level 1 input level. The cracking indicator has the highest change in indicator value, with an average change of 14%. There is a significant difference in pavement performance for IRI and cracking indicators and careful consideration should take place when performing Level 1 simulations with fly ash.

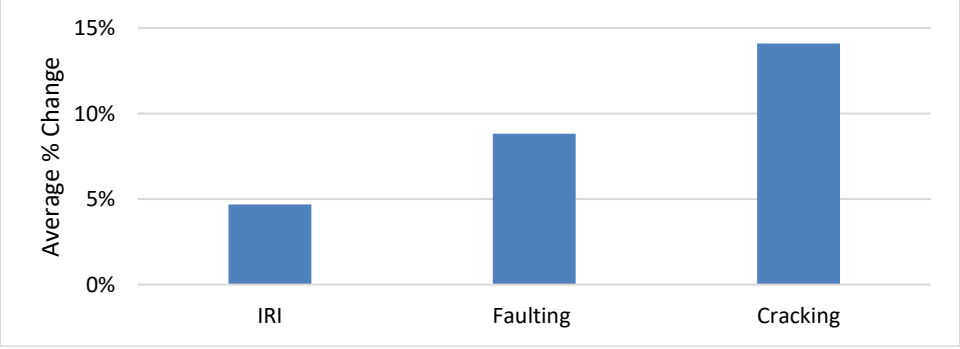

Figure 5.31: Performance indicator comparison between 0% and 30% fly ash mixtures

5.4.8 Comparison of Cracking Indicator between Level 1 and Level 3 Simulations

There is a known difference between Level 1 and Level 3 input level simulations. The difference in simulation results can be attributed to the input values necessary to perform each set of simulations. Level 1 requires 7-, 14-, 28-, and 90-day values for EM and MOR. Level 3 simulations require a 28-day compressive strength value. Level 1 simulations gather a larger picture of strength gain in the PCC layer, while Level 3 simulations are restricted to only one value. Strength gain for cementitious mixtures that include fly ash takes longer to gain full strength. Level 3 simulations restrict an accurate representation of fly ash's strength gain properties with only the 28-day compressive strength value. Level 1 input level simulates a better depiction of how fly ash properties are included in JPCP pavements. Figure 5.32 shows the difference in the cracking indicator for Level 1 and Level 3 simulations when fly ash is increased from 0% to 30%. As shown in Figure 10, Level 3 simulations predict significantly higher values for every mixture group. Even with a more accurate depiction of how mixtures that include fly ash gain strength over time, the Level 1 input level still restricts the full picture strength gain of fly ash. The inability to include a tested value past 90 days does not allow for any strength gain representation that does occur. Mixtures that include fly ash still gain strength past the 90-day mark. The limitations of fly ash mixtures in PMED software should be noted. Investigation into a more fly ash-friendly component to the PMED software would enable a better depiction of pavement performance for pavement that includes fly ash as an SCM.

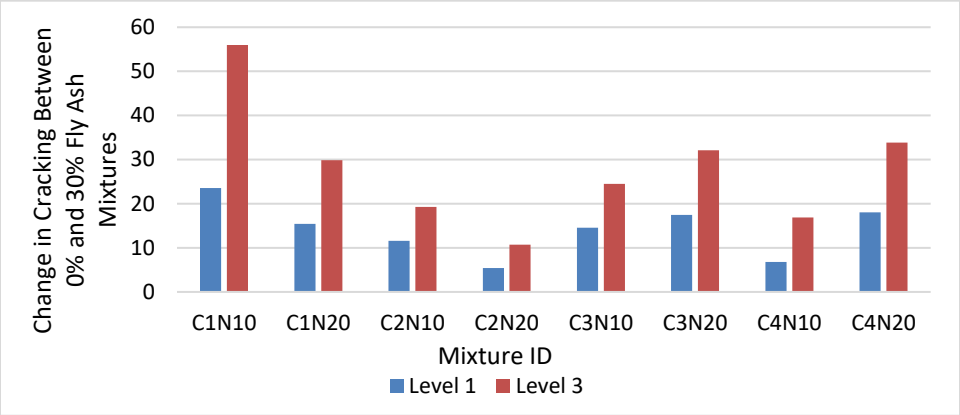

Figure 5.32: Change in cracking between 0% and 30% fly ash mixtures between Level 1 and Level 3 input levels

5.5 Effects of Fly Ash on Unbonded Concrete Overlay Performance and Design Slab Thickness

5.5.1 *Effects of Fly Ash on the Performance of Unbonded Concrete Overlay*

Unbounded concrete overlay (UBCO) is a cost/time effective rehabilitation technique to restore an existing cracked/unservicable JPCP system. A new JPCP slab is placed over an existing JPCP system. The placement of a new JPCP layer over an existing JPCP system occurs at the end of the lifespan of the orignal JPCP system. The layer structure of a unbounded concrete overlay pavement is shown in Figure 5.33. In Figure 5.33, the existing JPCP pavement's PCC layer is shown as the bottom layer. Cracking is shown in the bottom layer to represent wear over time of a JPCP pavement. A hot mix asphalt (HMA) layer is placed over the existing JPCP layer. This HMA layer is known as an interlayer and the purpose of this interlayer is to prevent distresses, such as cracking, in the existing JPCP pavement reflecting to the new JPCP layer placed as an overlay.

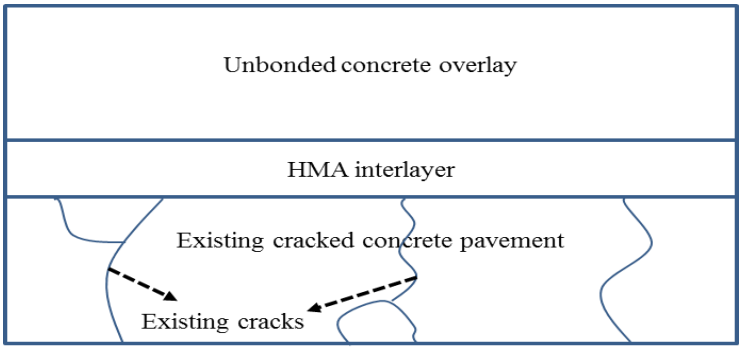

Figure 5.33: Schematic of unbonded concrete overlay

In the unbounded concrete overlay layer, fly ash can be incorporated into the concrete paving mixture as SCM. The assessment of the affects of fly ash on the unbounded concrete overlay layer is necessary to determine potential affects on performance indicators. Performance indicators for JPCP unbounded concrete overlay are the same as a new JPCP system including IRI, joint fautling, and transverse cracking.

5.5.2 *Methodology*

To assess the affects of fly ash on JPCP unbounded concrete overlay, simualations were performed in Pavement ME Design. Level 3 simulations were performed and 28-day compressive strenght values for each individual mixture were used. Coefficient of thermal expansion (CTE) 28-day values were used for each individual mixture. Nine inches was used for simulations to generate quality data. Groups were assigned for each mixture with the 0% fly ash mixture being the group name. Groups are made of a baseline mixture with 0% fly ash and 2 other mixtures with 20% and 30% fly ash contents. For example, Group C1N20 contains mixtures C1N20, C1N20F20, and C1N20F30. The software requires various inputs including design life, traffic volume, overlay structure, concrete thermal and strength properties, properties of sub-layers, and condition of existing JPCP. To evaluate the impact of fly ash, all the design inputs were considered constant for entire simulation work except the CTE and compressive strength of overlay concrete. Primary design inputs are shown in Table 5.12. After simulations were performed and groups were assigned, analysis of performance indicators data was conducted. Results of performance indicator analysis are discussed in the following section.

Level 1 and Level 3 simulations were performed. Level 3 simulations were performed first, and input data and analysis are provided in the first section. Level 1 simulations were performed second, and input data and analysis are provided in the following section. Table 5.12 design input values were used for both simulation input levels.

Table 5.12: Design inputs for simulations

Parameter	Value
Design Life	30 years
JPCP Overlay Thickness	9 in
Dowel Diameter	1 in
Joint Spacing	15 ft
Traffic (AADTT)	4000
Traffic (ESALS)	29×10^6
Initial IRI	63 in/mile
IRI Threshold	172 in/mile
Transverse Cracking Threshold (% Slabs)	15%
Joint Faulting Threshold	0.12 in.
Reliability	90%
Modulus of Rupture of Overlay Concrete	690 psi
Elastic Modulus of Overlay Concrete	4.2×10^6 psi
Water to Cement Ratio in Overlay Concrete	0.42
HMA (Interlayer) Thickness	2 in
HMA Binder Grade	PG 64-22
Existing JPCP Thickness	8 in
Distressed Elastic Modulus of Existing JPCP	2.44×10^6 psi

5.5.3 *Analysis of Level 3 Simulation Results*

5.5.3.1 Effects of Fly Ash on IRI Indicator of UBCO

The IRI performance indicator results are shown in Figure C.19. As shown in Figure C.19, there is a difference in the IRI indicator between 0% fly ash and 30% fly ash. Mixture group C1N20 shows an increase in the IRI indicator between 0% fly ash and 30% fly ash. All of the other mixture groups show a decrease in IRI performance indicator values. The

change in the IRI performance indicator between 0% fly ash and 30% fly ash mixtures is shown in Figure C.20. The largest change in performance indicator between 0% fly ash and 30% fly ash is 13.37 in/mi and the smallest change in IRI indicator is 2.05 in/mi. The percentage change in the IRI indicator is shown in Figure 5.34. The largest percentage change in the IRI indicator is 7% and the smallest percentage change in the IRI performance indicator is 1%. In Figures C.20 and 5.34, the IRI performance indicator is shown as a positive change for mixture groups C2N20, C3N10, C3N20, and C4N10 when the change is negative.

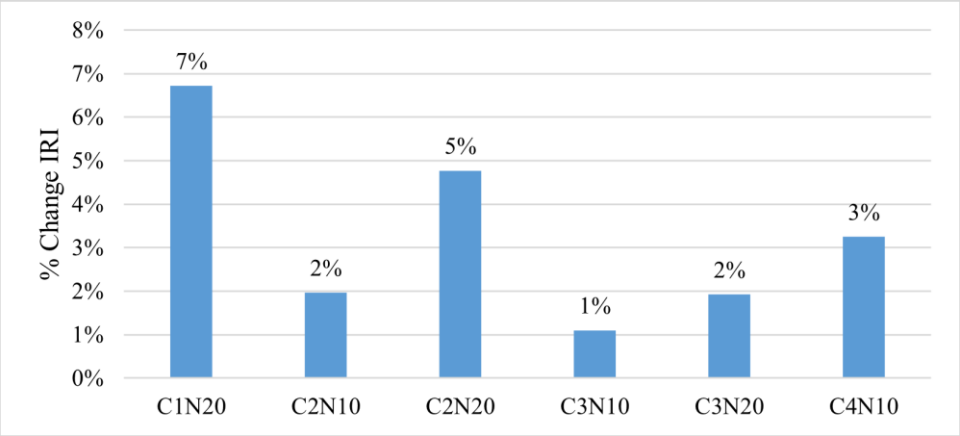

Figure 5.34: IRI performance indicator percentage change (Level 3)

5.5.3.2 Effects of Fly Ash on Joint Faulting Indicator of UBCO

Results of the simulations for the faulting indicator are presented in Figure C.21. In Figure C.21, the faulting indicator shows a decreasing trend among all mixture groups between 0% fly ash and 30% fly ash. In Figure C.22, the largest change in the faulting indicator is 0.02 and the smallest change in the faulting indicator in the mixture groups is 0.01, which is mixture group C1N20. The percentage change between 0% fly ash and 30% fly ash in each mixture group is shown in Figure 5.35. The largest percentage change in the mixture groups for the faulting indicator is 13% and the smallest percentage change for the faulting indicator is 6%. In Figures C.22 and 5.35, the data is shown positive where as the actual values are negative as faulting is decreasing with increase in fly ash content.

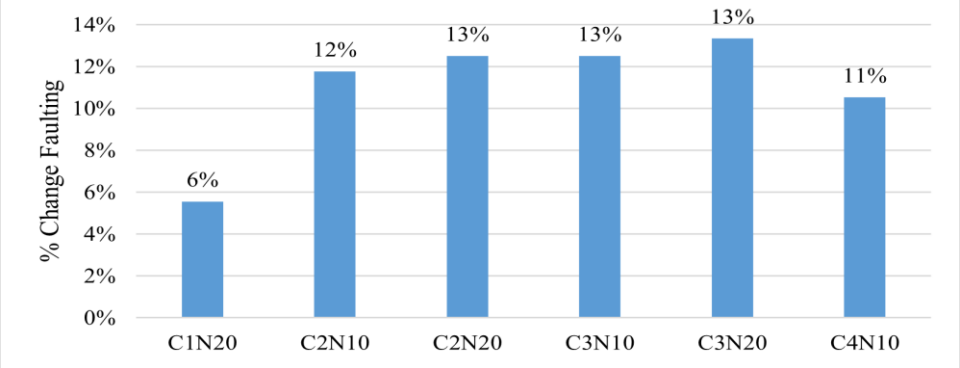

Figure 5.35: % change in fualting indicator between 0% fly ash and 30% fly ash mixtures (Level 3)

5.5.3.3 Effects of Fly Ash on Transverse Cracking Indicator of UBCO

The results for the transverse cracking indicator is shown in Figure 5.36. Each mixture group shows an increase in the cracking indicator when fly ash is added. The percentage change in the cracking indicator between 0% fly ash and 30% fly ash mixtures is shown in Figure 5.37. The largest percentage change in the cracking indicator is 21%, which is in group C1N20. When 30% fly ash was added to mixture group C1N20, the cracking indicator increased by 21%. The other mixture groups had an increase in transverse cracking in the range of 3% to 7%. An insight into the material inputs indicate that the 30% fly ash mixtures results in lower 28 day compressive strength and lower CTE when compared with the base mixtures and these changed properties affect the performance of UBCO resulting in a higher transverse cracking. The lower CTE should produce better performance in the form of reduced cracking, but the lower compressive strength of the fly ash mixtures is counteractive, and this results in overall effect of increased transverse cracking of the overlay pavement.

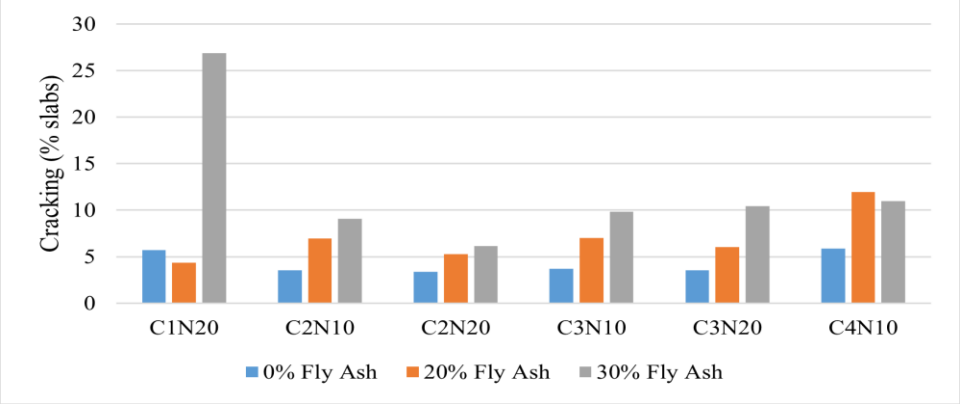

Figure 5.36: Cracking indicator results (Level 3)

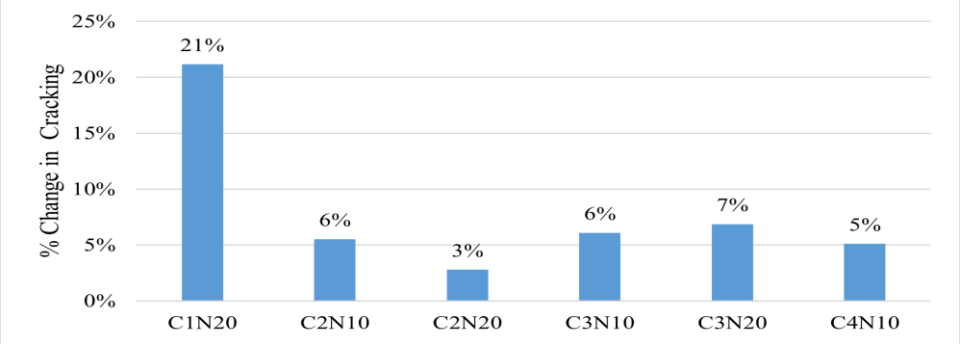

Figure 5.37: % change in cracking indicator between 0% fly ash and 30% fly ash mixtures (Level 3)

5.5.4 Summary of the Analysis

There is significant change in each performance indicator when fly ash is added to a mixture. The average percentage change in each performance indicator between between 0% fly ash and 30% fly ash mixrures is presented in Figure 5.38. The faulting indicator has the greatest percentage change in performance indicator when fly ash is added, followed by cracking, and IRI. Although faulting holds the smallest indicator change, it holds the greatest percentage change. The faulting indicator is shown positive in Figure 5.38, but is negative as when fly ash is added, the faulting indicator decreases. The cracking indicator changes on average of 8% and it is a significant increase in cracking and this is also significant when performing life cycle assessments of unbounded concrete overlay pavement with incorporation of fly ash. To accommodate the percentage change in the cracking indicator, change in the PCC slab thickness was performed to analyze the impact of fly ash on the design slab thickness.

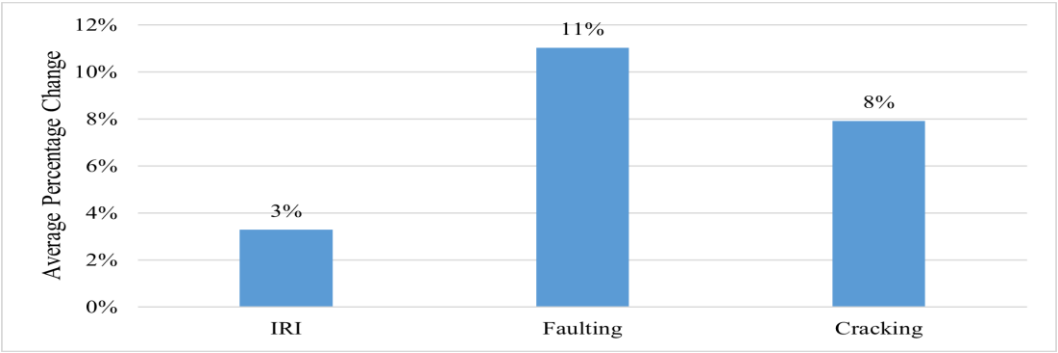

Figure 5.38: Average % change in performance indicators between 0% and 30% fly ash mixtures

5.5.5 Impact of Fly Ash on the Design Slab Thickness of Unbonded Overlay

To analyze the thickness that the PCC overlay slab should be at if 30% fly ash was incorporated into the baseline mixtures, simulations were performed in Pavement ME Design. For each mixture group, analyzation of the cracking indicator change occurred. The 0% fly ash mixture for each group was selected as the baseline model. The comparative data of simulation results is presented in Table 5.13. Simulations were performed on the thirty percent fly ash mixtures to generate similar cracking indicator results as the 0% fly ash mixtures. After simulations were performed, 10 inches was

selected as the PCC overlay slab thickness and it matches the cracking indicator with 0% fly ash with 9 inches. In the overall scenario predicts that if 30% fly ash is to be used on UBCO project then a higher overlay slab thickness is needed as compared to the overlay designed with 0% fly ash. However, it is anticipated that these results are an artifact of use of the 28-day strength value for fly ash mixtures, which is unrepresentative of later-age strengths.

Table 5.13: Comparison of 0% baseline model with 30% fly ash re-designed model

MIXTURE ID 0% Fly Ash	Cracking Indicator	MIXTURE ID 30% Fly Ash	Cracking Indicator
9 inch Slab Thickness		10 inch Slab Thickness	
C1N20	5.69	C1N20F30	7.84
C2N10	3.56	C2N10F30	3.36
C2N20	3.36	C2N20F30	2.52
C3N10	3.73	C3N10F30	3.62
C3N20	3.56	C3N20F30	3.79
C4N10	5.87	C4N10F30	3.95

5.5.6 *Analysis of Level 1 Simulation Results*

5.5.6.1 Effects of Fly Ash on IRI Indicator of UBCO

Simulation results for the IRI indicator at the Level 1 input level are in Figures C.23, C.24, and 5.39. Figure C.23 shows as fly ash is increased in mixture groups the IRI indicator decreases. The mixture group C1N20 does not follow this pattern. The difference in value between 0% and 30% fly ash in mixture groups is in Figure C.24. Figure C.24 shows C4N10 as the highest change in value between 0% and 30% fly ash, with a value of 9. All other mixture groups decreased in value when fly ash was added, with an average value of four in difference. Percentage change of the IRI indicator when fly ash was increased from 0% to 30% is in Figure 5.39. Mixture group C4N10 changed about 4.5% when fly ash was added. Mixture group C2N20 changed by 3.5 percent when fly ash was increased to 30%. Figures C.24 and 5.39 are shown as positive, but the change is negative.

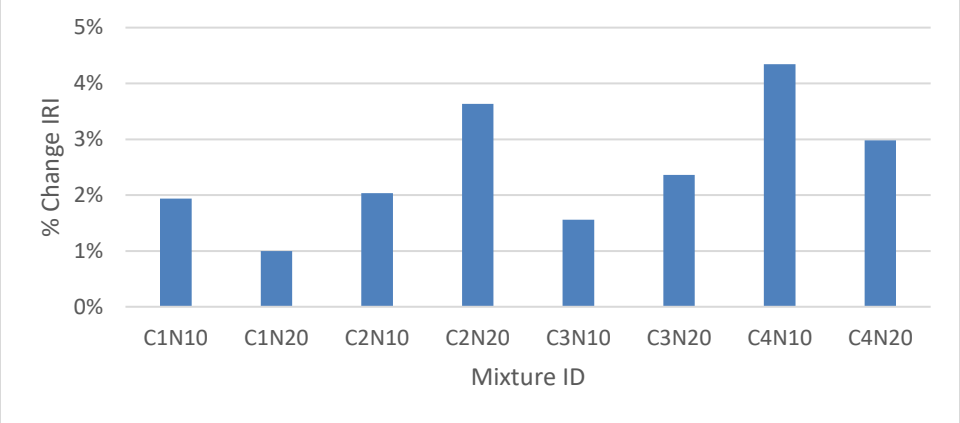

Figure 5.39: Percentage Change in IRI performance indicator between 0% fly ash and 30% fly ash (Level 1)

5.5.6.2 Effects of Fly Ash on Faulting Indicator of UBCO

Simulation results for the faulting indicator are in Figures C.25, C.26, and 5.40. The faulting indicator decreases in value as fly ash in increased from 0% to 30%, as shown in Figure C.25. The difference in the faulting indicator between 0% fly ash and 30% fly ash is in Figure C.26. Figure C.26 shows mixture group C1N10, C3N20, C4N10, and C4N20 all changed by 0.02 when fly ash was increased from 0% to 30%. The values in Figure C.26 are shown as positive but are negative. Mixture groups C1N20, C2N10, C2N20, and C3N10 changed by 0.01. The percentage difference in the faulting indicator is in Figure 5.40. C3N20 has the highest value change for the faulting indicator, with a percentage difference of almost 14%. The percentage change for the faulting indicator is a large number, but it should be noted that the real difference in performance is small. Figure 5.40 values are also shown as positive percentage change but are actually

negative percentage values. Absolute values were used for the presentation of data. It is shown that fly ash improves pavement performance for UBCO in Level 1 input simulations.

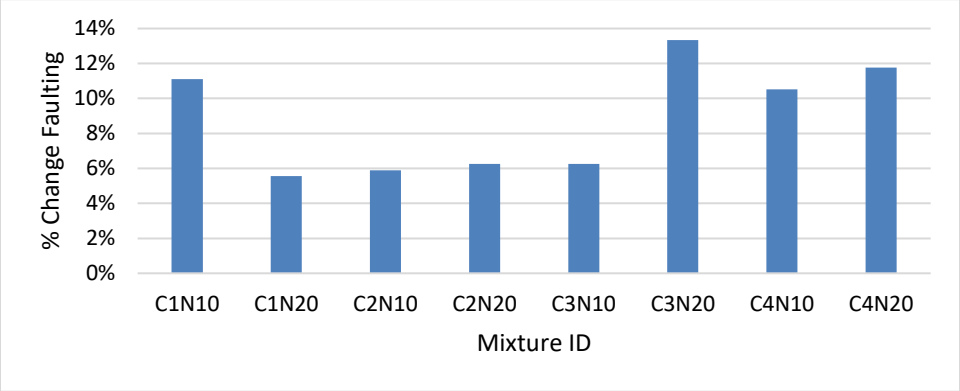

Figure 5.40: Percentage change in faulting performance indicator between 0% fly ash and 30% fly ash (Level 1)

5.5.6.3 Effects of Fly Ash on Cracking Indicator of UBCO

Transverse Cracking indicator results for UBCO Level 1 simulations are in Figures 5.41 and 5.42. Each of the mixture groups show that increasing the percentage of fly ash into the PCC layer will decrease the performance of the cracking indicator. Figure 5.41 shows that no inclusion of fly ash has a lower cracking indicator than including 20% or 30% fly ash into the mixture. Figure 5.42 shows the percentage difference between 0% and 30% fly ash in each mixture. It should be noted that C4N20 was compared between 0% and 30% fly ash content for maintaining consisent data comparison. The 20% fly ash composition for C4N20 has a higher cracking indicator than 30%, but was not selected for use in the data comparison. The percentage change for mixtures C1N10 and C1N20 have the highest cracking percentage change value of 4.5% and 5% between 0% and 30% fly ash content. Each of the other mixture groups have an average percentage change value for the cracking indicator of 2%.

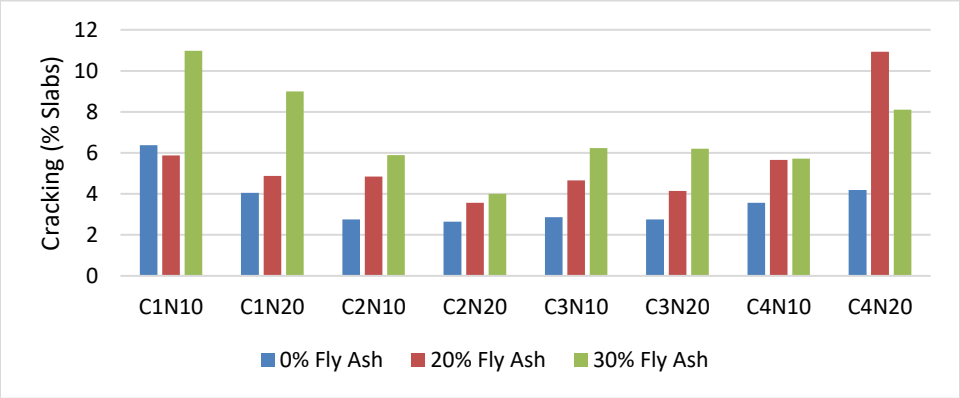

Figure 5.41: Cracking performance indicator comparison (Level 1)

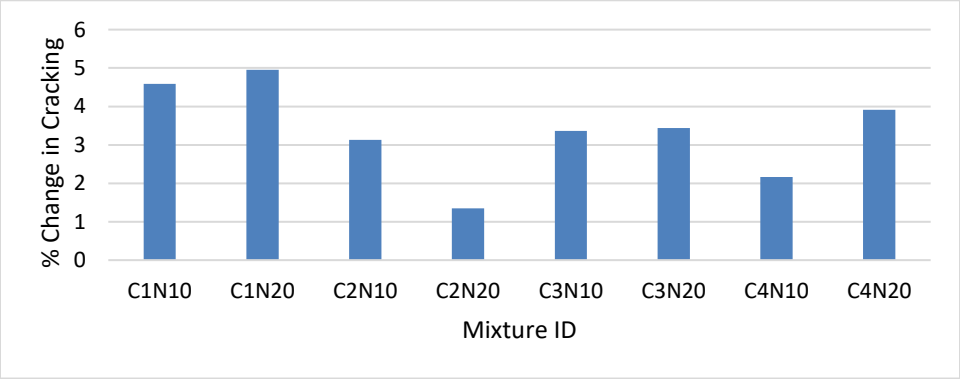

Figure 5.42: Percentage change in cracking performance indicator between 0% fly ash and 30% fly ash (Level 1)

5.5.7 Summary of the Analysis

Each of the three performance indicators experienced change in performance when fly ash was increased from 0% to 30%. A summary of the average percentage change for the UBCO performance indicators in in Figure 5.43. The faulting indicator and IRI indicator should be noted to be negative but are shown as positive. The faulting indicator experienced the greatest average change of 9%. It should be noted that the faulting indicator difference in value is small with a difference of 0.01 or 0.02. The cracking indicator has the second largest change in performance, with an average percentage change of 3%. IRI has an average percentage change of 2%. IRI and faulting indicator performance appears to improve as fly ash in increased from 0% to 30%. The cracking indicator performance decreased as fly as composition increased from 0% to 30%, but this is likely an artifact of use of the 28-day strength value for fly ash mixtures as an input. Later-age strength values may provide performance predictions that are more representative of field performance.

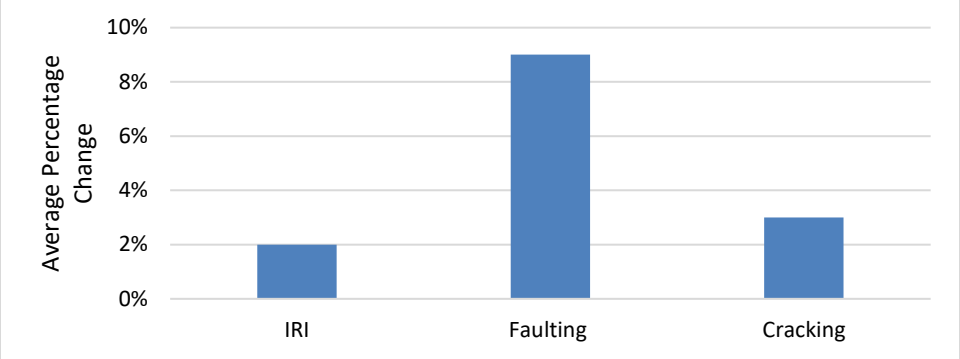

Figure 5.43: Summary of UBCO Level 1 average percentage change between 0% fly ash and 30% fly ash

5.5.8 Input Level 1 versus Input Level 3 Cracking Indicator Comparison

Level 1 and Level 3 simulations are known to have differences in pavement performance prediction. The difference in simulation results can be attributed to the input values necessary to perform each set of simulations. Level 1 is known to be more accurate than Level 3. Level 1 UBCO simulations require 7-, 14-, 28-, and 90-day values for EM and MOR and the 28-day Split Tensile Strength value. Level 3 simulations require a 28-day compressive strength (CS) value. Level 1 simulations gather a larger picture of strength gain in the PCC layer, while Level 3 simulations are restricted in strength gain picture because only one value is in consideration for pavement performance. Level 3 simulations restrict an accurate representation of fly ash's strength gain properties, with only the 28-day compressive strength value being used for performance prediction. Fly ash is known to have a longer strength gain cycle, and Level 3 simulations restrict the capability for a more accurate picture. Level 1 input level simulates a better depiction of how fly ash properties are included in the PCC layer of pavements and depicts a better prediction picture. Figure 5.44 shows the difference in the cracking indicator for Level 1 and Level 3 simulations when fly ash is increased from 0% to 30%. As shown in Figure 5.44, Level 3 simulations predict significantly higher values for every mixture group. Mixture groups C1N10 and C1N20 have the most significant change, with the Level 3 prediction value almost tripling or quadrupling performance predictions. Level 1 does provide a more accurate depiction of how mixtures that include fly ash gain strength over time, but the Level 1 input level still restricts the full picture strength gain of fly ash. The inability to include a tested value past 90 days does not allow for any strength gain representation that does occur. Mixtures that include fly ash still gain strength past the 90-day mark. The limitations of fly ash mixtures in PMED software should be noted. Investigation into a more fly ash-friendly component to the PMED software would enable a better depiction of pavement performance.

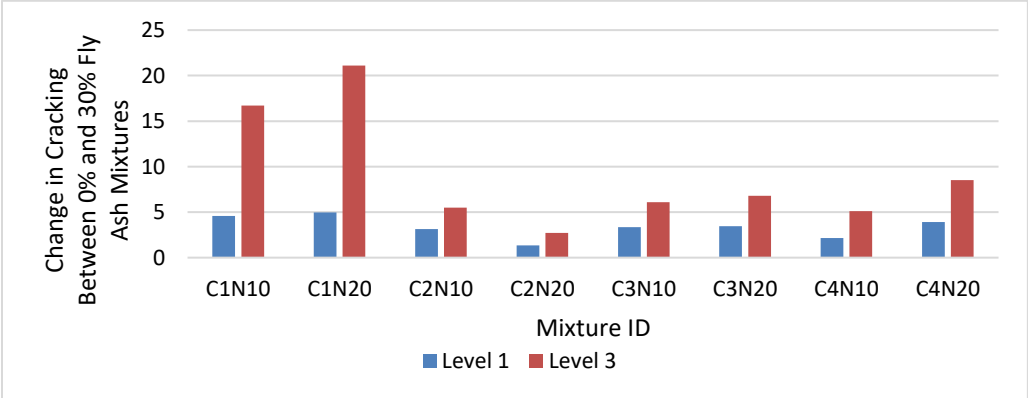

Figure 5.44: Change in cracking between 0% and 30% fly ash mixtures between Level 1 and Level 3 input levels

5.6 Effects of Heat Capacity on Jointed Plain Concrete Pavement's Performance and Design Slab Thickness

5.6.1 *Effects of Heat Capacity on Jointed Plain Concrete Pavement's Performance*

Heat capacity is an important thermal property of paving concrete, but it has not gained much significance in the past with the empirical design methods in place. With the advent of MEPDG and PMED, the importance of mechanical and thermal properties came to the forefront, but the focus of research revolved around the mechanical properties including compressive strength, elastic modulus, and modulus of rupture MOR and thermal properties including coefficient of thermal expansion (CTE) (Sabih 2016; Vandenbossche 2011; Ceylan 2013). There is a model proposed to predict the heat capacity of fly-ash concrete (Pongsak et al. 2009) and another work that examines the effect of heating rates on high performance concrete mixtures (John et al. 2010). Also, there are a few works on the analysis of the effect of thermal stress and coefficient of thermal expansion on concrete pavements (Kodide 2010; Mackiewicz 2014; Shin 2011). Not much research is available on the effects of heat capacity on the performance of the jointed plain concrete pavement (JPCP) system (Cavalline et al. 2018).

The focus of this part of the study is to analyze and quantify the impact of heat capacity of paving concrete on the JPCP performance and how it affects the design slab thickness. JPCP is a commonly used concrete pavement, which uses contraction/transverse joints to control cracking, and there is no reinforcing steel. For the purpose of this study, simulations were conducted in PMED software, and the sensitivity analysis was carried out to analyze the impact of the heat capacity of paving concrete mixture on the terminal pavement performance parameters and the performance over the design life of JPCP. The impact of using laboratory measured heat capacity values were also evaluated in comparison to using the PMED default heat capacity values by employing PMED simulations on different paving concrete mixtures. The effects of using default heat capacity values in comparison to the laboratory measured heat capacity values was analyzed on the JPCP slab thickness.

5.6.2 *Methodology*

To analyze the effects of heat capacity on JPCP pavements, several design simulations were performed in PMED and IRI, faulting, and cracking indicators were compared. In PMED, Level 3 analysis was used and for each individual mixture, CTE and compressive strength were selected for Level 3 analysis. The JPCP slab thickness was kept constant at 10 inches for the baseline model for this analysis. The details of the baseline model used for simulations is found in Table C.4. The laboratory measured material inputs used for this study are given in Table 5.14.

The range of heat capacity values for paving mixtures as per PMED is 0.1 to 0.5 Btu/ (lb-°F) with a default value of 0.28 Btu/ (lb-°F). In the first phase, the effects of the typical range of heat capacity values were analyzed on the performance of JPCP with PMED simulations and keeping other design variables as constant. After conducting the simulations, analysis of the effects of heat capacity on each of the three performance indicators for JPCP was performed. In the second phase, the effects of using the default value of heat capacity were compared to using the laboratory measured value of heat capacity. In the third phase of the analysis, the impact of heat capacity on the design slab thickness was analyzed using PMED simulations.

Table 5.14: Laboratory measured material inputs

Mixture ID	28 Day CTE	28 Day Compressive Strength	56 Days Heat Capacity Values
C1N10	5.66	4656	0.194
C1N1OF20	5.433	4303	0.186
C1N1OF30	5.325	3176	0.178
C1N20	5.358	5051	0.183
C1N2OF20	5.195	4425	0.175
C1N2OF30	5.164	3610	0.181

5.6.3 *Effects of Heat Capacity on JPCP Performance Indicators of Baseline JPCP Model*

5.6.3.1 Impact of Heat Capacity on IRI

The analysis of simulation results indicates that when heat capacity is at its lowest simulated value of 0.2 Btu/ (lb-°F), the IRI reaches 133.19 in/mi, indicating a relatively rough pavement surface. However, as heat capacity value increases, the IRI consistently decreases. When heat capacity increases to 0.24 Btu/ (lb-°F), 0.28 Btu/ (lb-°F), and beyond,

the IRI continues to decline, reaching its lowest point of 113.29 in/mi at a heat capacity of 0.5 Btu/ (lb-°F). This trend suggests that higher heat capacity values are associated with improved pavement performance. Higher heat capacity paving concrete has better thermal properties, which can help the pavement resist temperature-induced stresses, reducing cracking and roughness. Consequently, smoother road surfaces are achieved, leading to a lower IRI.

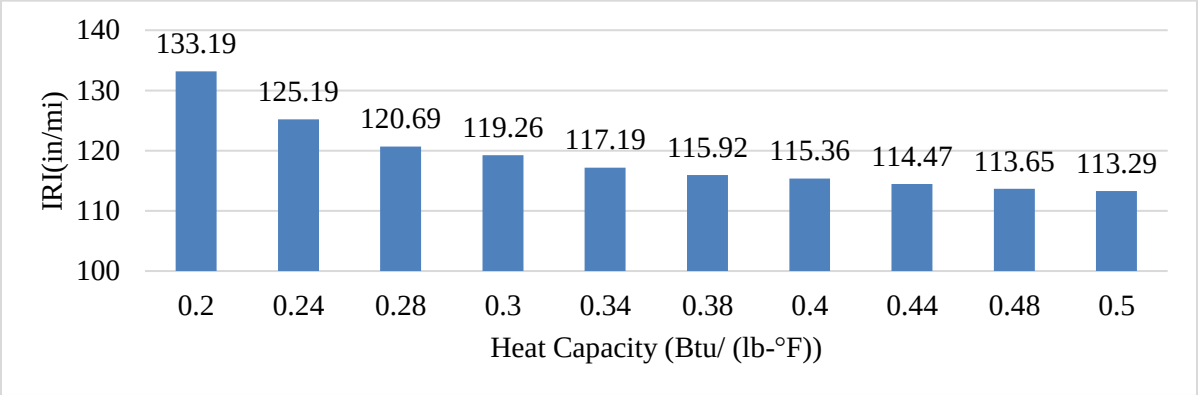

Figure 5.45: IRI indicator comparison

5.6.3.1 Impact of Heat Capacity on Joint Faulting

The analysis of simulation data indicates that the variation in heat capacity has a slight impact on faulting at the lower range of heat capacity values. When heat capacity is at its lowest simulated value of 0.2 Btu/ (lb-°F), faulting is at 0.07 in. As heat capacity gradually increases to 0.28 Btu/ (lb-°F), faulting remains relatively stable at 0.06 in. and there is no effect on faulting when the heat capacity is increased from 0.28 Btu/ (lb-°F) to 0.5 Btu/ (lb-°F). This indicates that within this range, there may not be a significant impact on joint faulting with a change in heat capacity values. So, it is inferred that there is some influence of heat capacity on faulting in JPCP, the effect is relatively minor within the range studied.

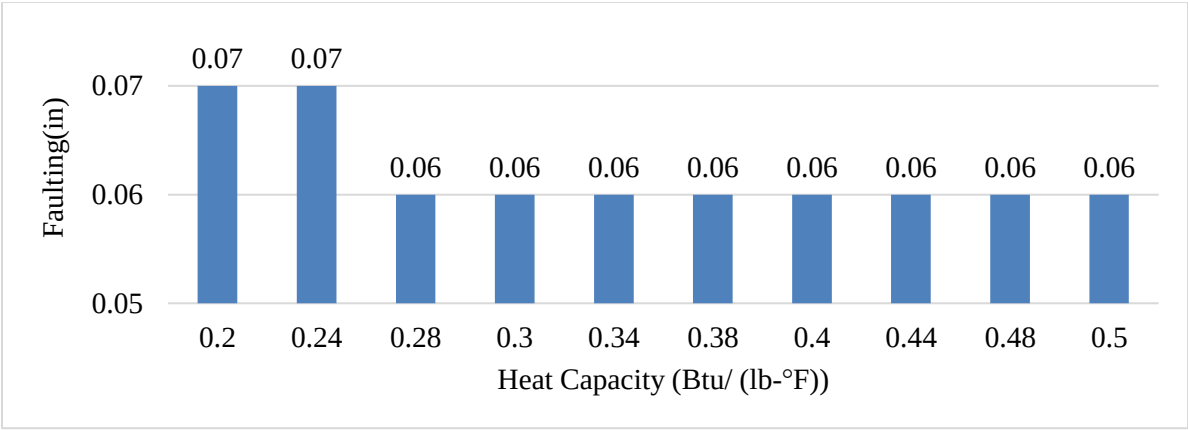

Figure 5.46: Faulting indicator comparison

5.6.3.2 Impact of Heat Capacity on Transverse Cracking

As heat capacity increases from 0.2 Btu/ (lb-°F)to 0.5 Btu/ (lb-°F), there is a noticeable and consistent trend of decreasing cracking. When heat capacity is at its lowest point (0.2 Btu/ (lb-°F)), cracking is the highest at 25.08%. This indicates that lower heat capacity allows for greater temperature fluctuations within the concrete pavement, leading to higher thermal stresses and, consequently, more extensive cracking. As heat capacity gradually increases to 0.24 Btu/ (lb-°F), 0.28 Btu/ (lb-°F), and 0.3 Btu/ (lb-°F), cracking decreases significantly to 16.15%, 10.85%, and 9.1%, respectively. This demonstrates that higher heat capacity helps mitigate thermal stresses, reducing the likelihood of cracking. The trend continues as heat capacity rises further, with cracking levels decreasing as heat capacity increases. When heat capacity reaches 0.5 Btu/ (lb-°F), cracking is at its lowest point, measuring 3.36%. This pattern suggests that higher heat capacity provides better thermal stability to the JPCP, minimizing the temperature-induced stresses that lead to cracking. Therefore, selecting concrete mixtures with higher heat capacity can be an effective strategy to reduce the occurrence of cracking in JPCP systems.

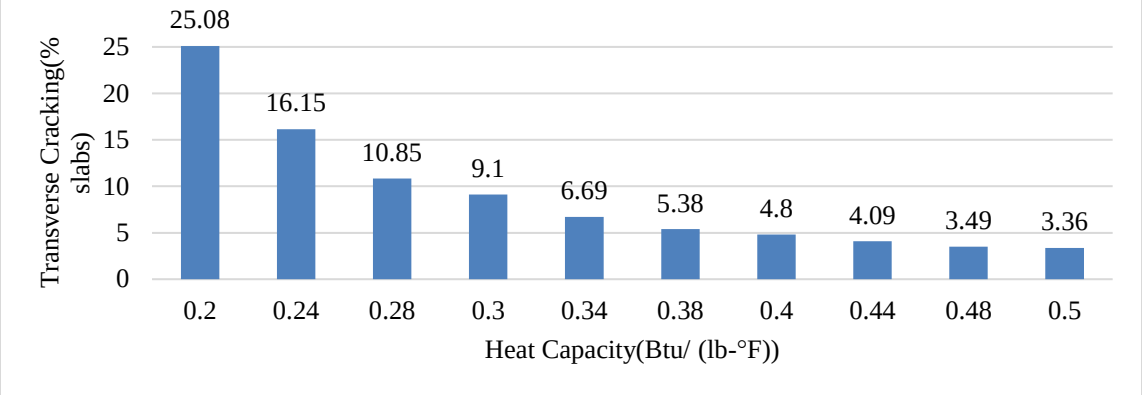

Figure 5.47: Cracking indicator results

5.6.4 *Summarized Comparison of Heat Capacity Impact On IRI, Faulting, and Cracking Of JPCP*

Increasing heat capacity is associated with a reduction in IRI. When heat capacity increases from 0.2 Btu/ (lb-°F)to 0.5 Btu/ (lb-°F), the IRI decreases significantly, indicating that higher heat capacity promotes a smoother pavement surface. This is likely because materials with higher heat capacity can better resist temperature-induced stresses, resulting in a smoother ride for vehicles. The data shows that heat capacity has a relatively minor impact on faulting. Regardless of the heat capacity value within the provided range (0.2 Btu/ (lb-°F)to 0.5 Btu/ (lb-°F)), faulting remains consistently low at 0.06 in to 0.07 in. This suggests that other factors, such as other concrete properties, construction quality and traffic loads, may have a more significant influence on faulting in JPCP than the heat capacity. Heat capacity also has a significant influence on cracking. Increasing heat capacity from 0.2 Btu/ (lb-°F)to 0.5 Btu/ (lb-°F)leads to a significant reduction in cracking. This suggests that higher heat capacity concrete is more effective at mitigating temperature-related stresses, resulting in fewer cracks in the concrete pavements.

In summary, heat capacity has a significant impact on IRI and cracking in JPCP, with higher heat capacity values associated with smoother surfaces and reduced cracking. However, its effect on faulting appears to be minimal within the specified heat capacity range. It's essential to consider a comprehensive approach to pavement design and maintenance, considering various design factors, to optimize JPCP performance.

5.6.5 *Effects of Heat Capacity PMED Default Value vs Lab Obtained Values on JPCP Performance*

5.6.5.1 Impact on IRI

In this scenario, the laboratory measured heat capacity data was used for each of the simulated paving mixtures (C1N1O, C1N1OF20, C1N1OF30, C1N2O, C1N2OF20, C1N2OF30) and their corresponding IRI values were compared with the simulation results of the PMED default heat capacity (base) values. The IRI indicator comparison for laboratory measured vs base heat capacity is presented in Figure 5.48.

It is evident from the simulation results that there is a significant difference in IRI indicators between the laboratory data-based simulations and the default/base data simulations of heat capacity values. The difference in IRI indicator ranges between 26.2 to 66.3 in/mi which is a significant increase in IRI between the simulated scenarios for each of the paving mixtures. These findings highlight the importance of accurately characterizing material properties, like heat capacity, to predict and manage pavement performance effectively. The default/baseline heat capacity results in a lower IRI for all the simulated paving mixtures in comparison to the laboratory measured heat capacity values so the JPCP systems designed with the default heat capacity value will always be under-designed and may fail before the design service life.

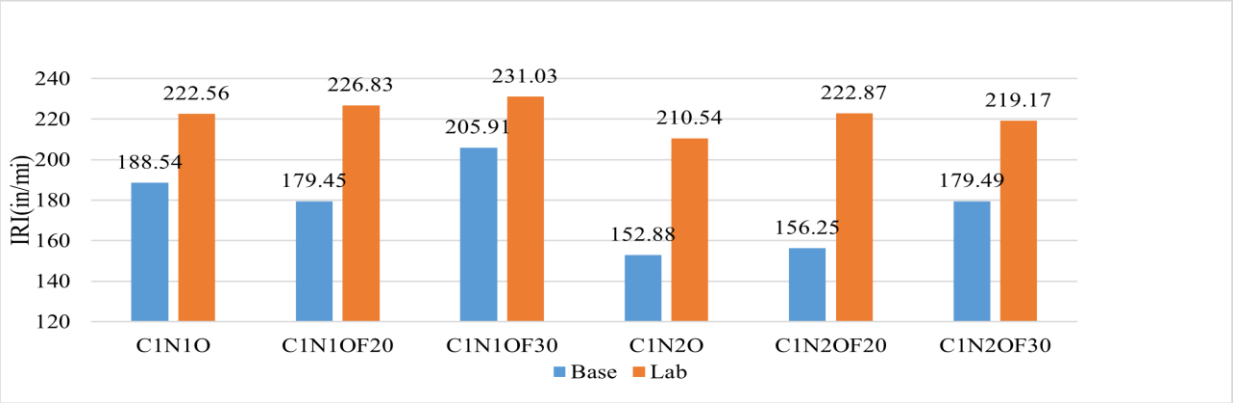

Figure 5.48: Comparison of IRI indicator (lab vs baseline heat capacity)

5.6.5.1 Impact of Baseline vs Lab Measured Heat Capacity on Joint Faulting

The analysis of joint faulting in JPCP for different mixtures reveals that heat capacity has minimal influence on this pavement distress parameter, as the values for both baseline and laboratory. Measured heat capacity data remain consistent for all the simulated mixtures.

In summary, the data suggests that heat capacity does not exert a discernible influence on faulting for the simulated paving mixtures. Other factors, such as other concrete properties, joint design, construction quality, and traffic loads, may play more substantial roles in affecting the faulting levels in concrete pavements.

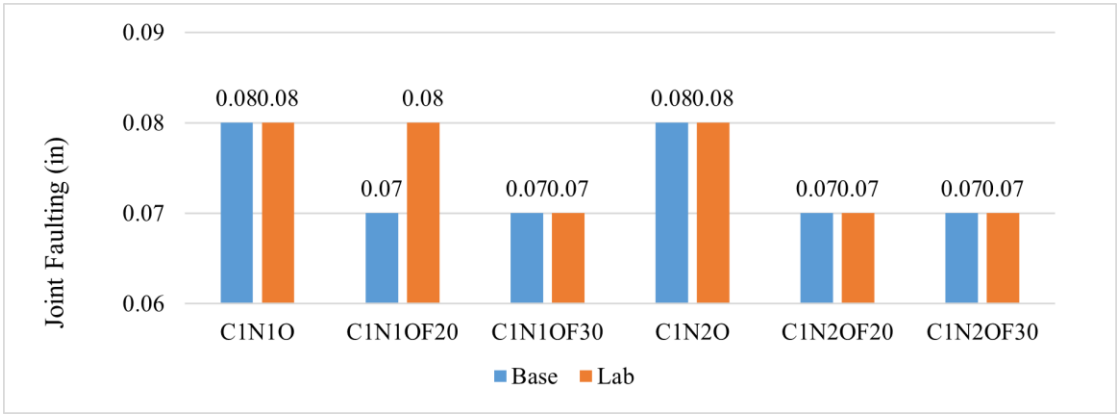

Figure 5.49: Comparison of faulting indicator (lab vs baseline heat capacity)

5.6.5.2 Impact of Baseline vs Lab Measured Heat Capacity on Transverse Cracking

The effects of heat capacity on transverse cracking in Jointed Plain Concrete Pavement for the simulated mixtures is evident from the simulation results shown in Figure 5.50. The results indicate significant variations in transverse cracking levels between baseline and laboratory measured heat capacity data for each simulated mixture. The variation between the two simulated scenarios for all the paving mixtures ranges between 5.1% to 41.9% which is a very significant difference. The use of laboratory measured heat capacity data consistently results in higher cracking compared to the baseline/default heat capacity scenario and this phenomenon was found in all the simulated mixtures. Accurate characterization of material properties including the heat capacity is crucial for predicting and managing pavement cracking effectively. Using the baseline/default values of heat capacity in the JPCP design process may result in an under designed JPCP system.

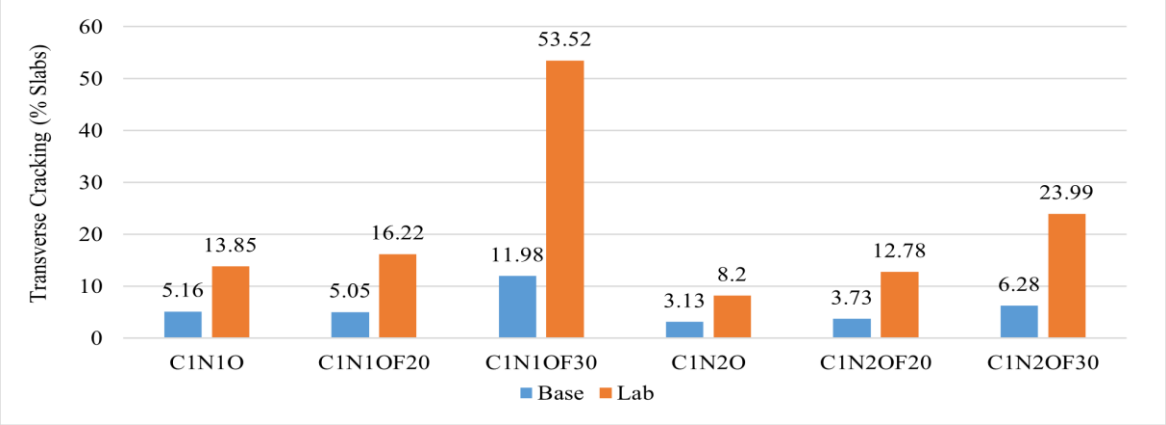

Figure 5.50: Comparison of cracking indicator (lab vs baseline heat capacity)

5.6.6 *Summary of Baseline/Default vs Lab Tested Heat Capacity Values on JPCP Performance*

Across all the simulated mixtures, using laboratory measured heat capacity data consistently results in significantly higher IRI values compared to the baseline heat capacity data. Heat capacity has little to no influence on joint faulting levels in JPCP for all the simulated paving mixtures. Both baseline and laboratory measured heat capacity data result in similar faulting values, suggesting that other factors are more dominant in impacting the joint faulting indicator. Heat capacity has a very significant impact on transverse cracking. Laboratory measured heat capacity data consistently leads to higher cracking indicator values compared to baseline heat capacity data for all the simulated mixtures. In summary, heat capacity primarily affects IRI and cracking in JPCP, with lab data consistently showing higher distress levels, while faulting remains relatively unaffected by heat capacity variations. Pavement designers must consider these effects when interpreting data and making decisions related to JPCP design.

5.6.7 *Effects of Heat Capacity Values on JPCP Design Slab Thickness*

The use of default/baseline heat capacity values of the concrete paving mixture results in in-accurate performance indicator values in comparison to the scenarios where laboratory measured heat capacity values are used for the simulations. Increasing the PCC slab thickness can help reduce the difference between the two simulated scenarios. Analysis was conducted to quantify the impact of baseline heat capacity vs laboratory measured heat capacity on the slab thickness of the JPCP system. Additional simulations were conducted in Pavement ME Design with the increased PCC slab thickness to match the cracking indicator values of the laboratory measured cases to the baseline cases for all the mixtures. The cracking indicator was selected for this matching analysis because the cracking performance indicator has the most severity among all three performance indicators. To analyze the change in the PCC slab thickness, the laboratory measured heat capacity simulations were selected for each mixture and adjustment of the PCC slab thickness was performed to generate cracking indicator results that were similar to the baseline heat capacity simulations. The summary of the analysis is given in Table 5.15. The baseline heat capacity simulations have a PCC slab thickness of 10 inches and after running the simulations in Pavement ME Design for the laboratory measured heat capacity models for all the paving mixtures, a PCC slab thickness of 11 inches shows similar cracking indicator results. It is evident that an increase of one inch in the PCC slab thickness matches cracking values for both the simulated scenarios for all the paving mixtures.

It is evident from this analysis that using the default/baseline values of heat capacity will result in an under-designed JPCP system which might fail prematurely without completing the design service life. The difference between using the laboratory measured heat capacity and the PMED default/baseline heat capacity is 1 inch of PCC slab thickness which has numerous financial, sustainability, and environmental implications. It is highly recommended that JPCP design should be conducted according to the laboratory measured concrete properties including heat capacity values.

Table 5.15: Comparison of baseline model with lab measured heat capacity model with increased slab thickness

Mixture ID	Baseline Model	Lab Tested Heat Capacity Model
	10 inch Slab Thickness	11 inch Slab Thickness
C1N1O	5.16	3.49
C1N1OF20	5.05	4
C1N1OF30	11.98	11.56
C1N2O	3.13	2.76
C1N2OF20	3.73	3.49
C1N2OF30	6.28	5.6

5.6.8 *Findings*

The analysis conducted in this study showed that there is significant impact of heat capacity of paving concrete on IRI and cracking of JPCP systems and using the default/baseline values of heat capacity will result in under designed JPCP system which might fail prematurely without completing the design service life. The difference between using the laboratory measured heat capacity and the PMED default/baseline heat capacity is up to 1 inch of PCC slab thickness which has numerous financial, sustainability, and environmental implications. These implications may become more pronounced in the future due to the temperature-related effects of climate change. It is highly recommended that JPCP design should be conducted according to the laboratory measured concrete properties including heat capacity values. To provide additional confidence and support local calibration of PMED, these findings should also be confirmed through field observations and measurements.

5.7 Effects of North Carolina Climatic Regions on JPCP Performance

JPCP performance indicators react differently depending on the climate. The PCC layer is known to perform differently depending on the climatic condition where the pavement is built. In North Carolina, there are three distinct climatic zones which are the western mountains, the piedmont, and the coastal plain. Each climatic zone has different climatic conditions. AASHTO PMED software uses The North American Regional Reanalysis (NARR) model to simulate climate station weather conditions. Within the PMED software, the four main criterion from NARR used are mean annual air temperature (˚ F), mean annual precipitation (in.), freezing index (˚ F-days), and average annual number of freeze/thaw cycles. Each of these criterion causes distress on the PCC layer of the JPCP system, impacting the performance. Generally speaking, the more severe the climate station data, the more potential there is for deteriorated performance.

5.7.1 *Methodology*

Eight climate stations within North Carolina were selected for the analysis. The eight stations were chosen based on location within the three climatic zones of North Carolina. The eight climate stations chosen are Greensboro, Asheville, Charlotte, Raleigh, Fayetteville, Wilmington, Elizabeth City, and Cape Hatteras. The climate stations chosen are shown in Figure 5.51. The red triangles represent the Western Mountain climate stations. The blue triangles represent the Piedmont climate stations, and the yellow triangles represent the Coastal Plain climate stations. Only one climate station was chosen in the Western Mountains as there was only one available within the PMED software.

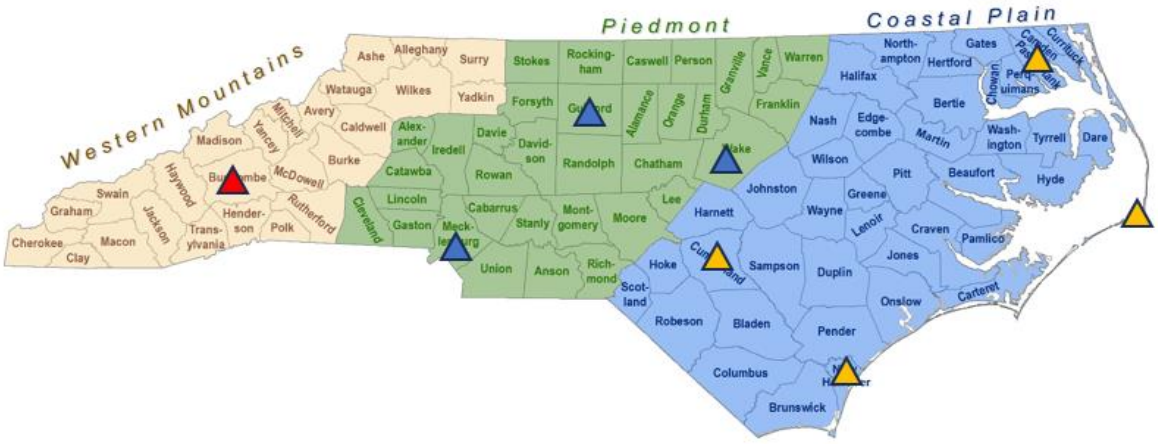

Figure 5.51: North Carolina climate stations

The data provided by NARR used within the AASHTO PMED Software is in Table 5.16. Figure C.27 shows a visual of the difference in the individual climate station data. As shown in Figure C.27, Asheville is shown to have the highest freezing index. Asheville also has the lowest mean annual air temperature. Cape Hatteras has the lowest freezing index and lowest number of freeze thaw cycles. Cape Hatteras also has the highest mean annual air temperature. Greensboro has the second highest freezing index. Wilmington has the second lowest freezing index and number of freeze thaw cycles.

Table 5.16: North Carolina climate station data

Climate Station	Mean Annual Air Temperature (˚ F)	Mean Annual Precipitation (in.)	Freezing Index (˚ F-days)	Average Annual Number of Freeze/Thaw Cycles
Asheville	55.78	49.46	124.99	45.64
Cape Hatteras	66.33	29.48	0.75	0.78
Charlotte	61.11	41.95	46.73	42.19
Elizabeth City	61.90	44.79	49.51	39.08
Fayetteville	62.20	44.32	38.76	45.33
Greensboro	58.83	42.39	93.45	52.42
Raleigh	60.55	42.63	66.41	47.48
Wilmington	64.37	49.47	17.83	23.85

Simulations were performed in the PMED software to determine the performance of JPCP pavements among the different climate stations in North Carolina. One mixture was selected for performing simulations. The mixture used for simulations was mixture ID C1N20. Level 3 simulations were performed. The test data for mixture C1N20 for Level 3 simulations is in Table C.5. The baseline model used for simulations is in Table C.6. The PCC layer for simulation baseline model is 9 inches. Analyzation of the difference in IRI, faulting, and cracking between the different climates was performed.

5.7.2 *Analysis of Simulation Results*

Effects of Climate on IRI Indicator

The simulation results for the IRI indicator are shown in Figure 5.52. The colors in Figure 5.52 coordinate with the colors of the climate station map in Figure 5.51. The red color represents the Western Mountains, the blue color represents the Piedmont, and the orange color represents the Coastal Plains. Cape Hatteras has the lowest IRI simulation result of 129.7. The highest IRI indicator result is in Asheville, which is 217.96. There is a significant difference in the performance of the IRI indicator between the climate station furthest West in NC to the climate station furthest East in

NC. Wilmington has the second lowest IRI indicator at 179.93. There is a significant change in the IRI indicator between Cape Hatteras and Wilmington, the two lowest IRI indicators. This could be attributed to where Cape Hatteras is located geographically and the freezing index and freeze thaw cycles being significantly lower than the other climate stations. As you move from West to East in North Carolina, the IRI indicator decreases in value. This is shown in the downward trend in IRI indicator value as shown in Figure 5.52.

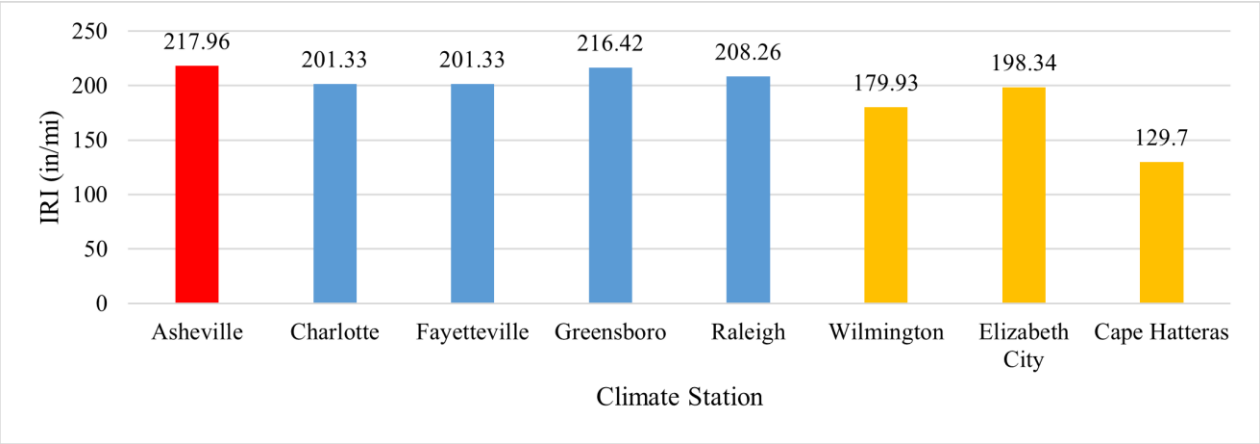

Figure 5.52: IRI indicator results

Effects of Climate on Faulting Indicator

The faulting indicator results are in Figure 5.53. The colors in Figure 5.53 coordinate with the colors of the climate station map in Figure 5.51. The red color represents the Western Mountains, the blue color represents the Piedmont, and the orange color represents the Coastal Plains. The lowest faulting indicator value of 0.09 occurs at Cape Hatteras. The highest faulting indicator is at Asheville being a value of 0.21. There is a significant difference in the faulting indicator between the furthest West climate station and the furthest East climate station. The furthest West and East climate stations in North Carolina have the highest and lowest values for the faulting indicator. As you move from West to East in North Carolina, the faulting indicator decreases in value. The downward trend in the faulting indicator is shown in Figure 5.53, as the values of the faulting indicator decreases as you move to the right, East.

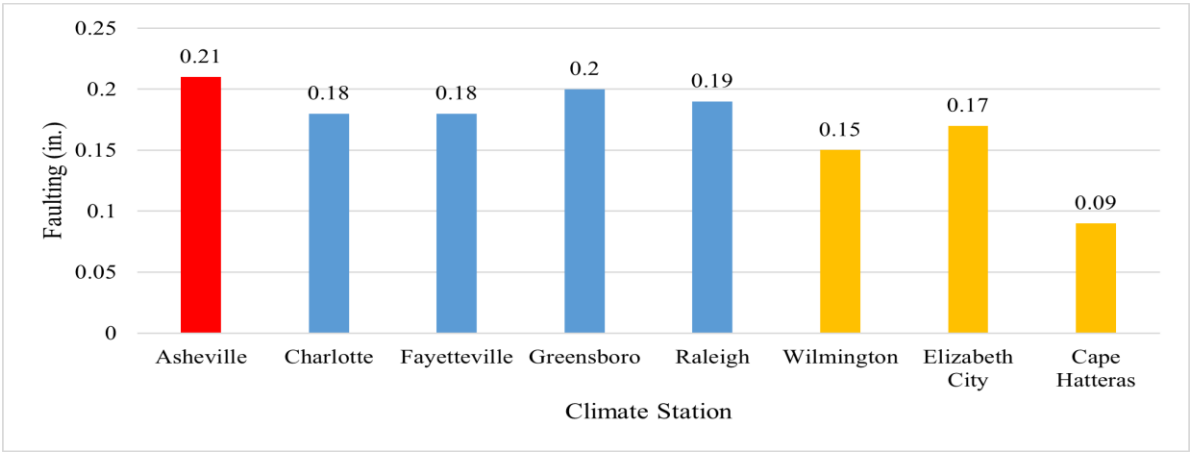

Figure 5.53: Faulting indicator results

Effects of Climate on Transverse Cracking Indicator

The transverse cracking indicator results are shown in Figure 5.54. The highest cracking value occurs at Charlotte and Fayetteville, with a value of 23.71. The lowest cracking value occurs at Cape Hatteras with a value of 6.01. Elizabeth City has the second highest cracking value of 23.62. The cracking indicator is unique because the highest cracking value occurs in the Piedmont and in the northern part of the Coastal Plain. The cracking indicator does not follow the trend of the IRI and faulting indicators. Asheville's cracking indicator is lower than all of the Piedmont and Coastal Plain cracking indicators, excluding Cape Hatteras. The cracking indicator trend could be attributed to any of the four climate data inputs. Mean annual air temperature, mean annual precipitation, freezing index, and number of freeze-thaw cycles all impact pavement performance. Each climate station has unique values for each of the four climate data inputs. More

investigation of how the four climate data inputs impact JPCP pavement performance will need to be done in the future. The scope of this study does not include this component. It is assumed that the climate data impacts the cracking indicator performance. As shown in Figure 5.54, the trend for the cracking indicator shows a higher cracking trend value as you move away from the Western Mountains. The Piedmont shows the area of highest cracking. It can be concluded that as one moves towards the central part of NC, a higher value for cracking is predicted.

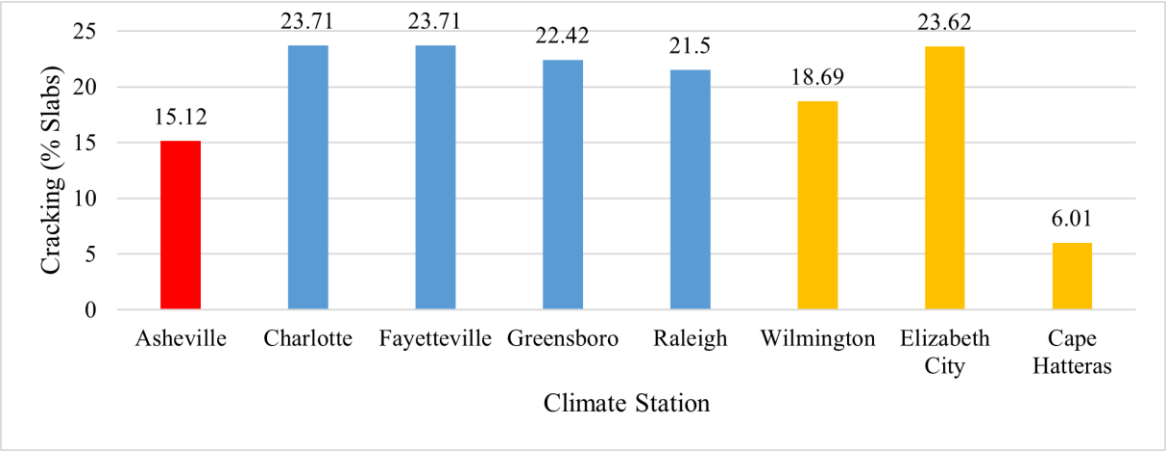

Figure 5.54: Cracking indicator results

5.7.3 *Summary of the Simulation Results*

Each of the three performance indicators were significantly affected by the change of climate station. In Figure 5.55, the percentage change in the indicator value between the highest and lowest values is shown. The faulting indicator is shown to have the greatest level of impact when changing climate station in North Carolina, with a percentage change of 133 percent. The highest value for the faulting indicator occurred in Asheville with a value of 0.21. The lowest value for the faulting indicator is Cape Hatteras, with a value of 0.09. The change in the faulting indicator is shown to be the most extreme out of all three performance indicators. The extreme percentage change value could be attributed to the smaller values the faulting indicator presents. There is a 12-point difference in the highest and lowest value for the faulting indicator.

The point change for the cracking and IRI indicators have more magnitude than the faulting indicator but cannot be shown because the faulting indicator has smaller values. The IRI indicator percentage change between the highest and lowest value is 68 percent and the cracking indicator percentage change is 18 percent. The highest value for the IRI indicator is 217.96 in Asheville and the lowest IRI indicator value is 129.7 in Cape Hatteras. The cracking indicator has the highest value in Charlotte and Fayetteville, both with values of 23.71. The lowest value for cracking is in Cape Hatteras with a cracking indicator value of 6.01. Cape Hatteras holds the lowest extreme value for each of the three performance indicators of IRI, faulting, and cracking. Cape Hatteras also holds an extreme value for each of the climate station data criterion of air temperature, freezing index, precipitation, and number of freeze/thaw cycles. The climate station criterion values for Cape Hatteras hold the highest value for air temperature of 66.33. Cape Hatteras holds the lowest value for freezing index, precipitation, and number of freeze thaw cycles, which are 0.75, 29.48, and 0.78. The extreme values for Cape Hatteras's climate station criterion can be attributed to Cape Hatteras's extreme values in the performance indicators.

Asheville holds the highest performance indicator results for the IRI and faulting indicators. Asheville's climate station criterion holds the highest value for the freezing index criterion and precipitation criterion, which are 124.99 and 49.46, respectively. Asheville has the lowest value for air temperature which is 55.78. The number of freeze thaw cycles for Asheville is high but does not hold the highest value. Asheville's climate station criterion holding an extreme value can be attributed to Asheville holding the highest performance indicator value for IRI and faulting. Charlotte and Fayetteville both hold the highest value for cracking. Neither climate stations hold any extreme values for any of the climate station criterion. For each of the climate station criterion, Charlotte and Fayetteville hold values in the "middle" of the data sets. The combination of the four-climate station criterion not holding an extreme value could be attributed to Charlotte and Fayetteville holding the highest cracking values. More investigation will need to be conducted.

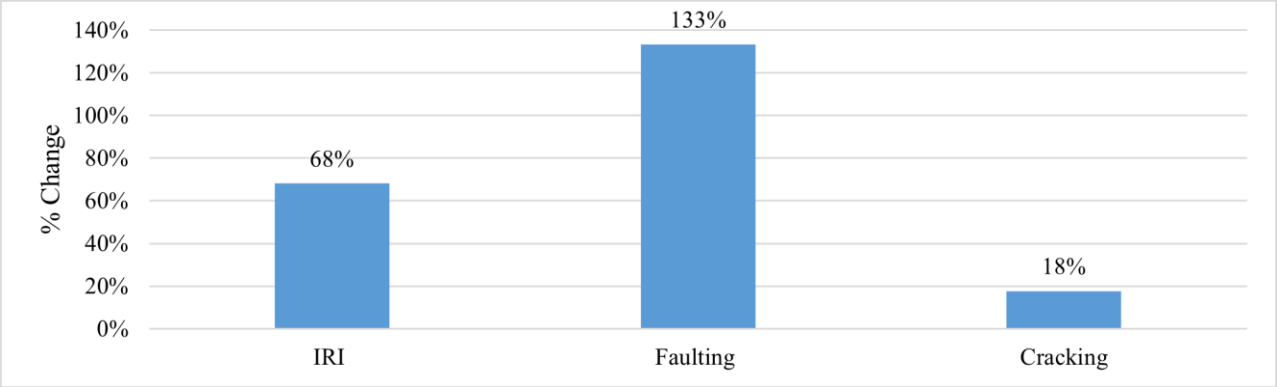

Figure 5.55: Percentage change in indicator values between climate stations

5.7.4 *JPCP Thickness Recommendation*

The cracking indicator values for the simulations performed exceeded the 15 percent cracking threshold. To improve pavement performance across NC for the cracking indicator, simulations were performed at 10 inches. Simulation values for each of the climate stations are shown in Figure 5.56. Table 5.17 shows the climate station with the cracking indicator value at 9 inches and cracking indicator value at 10 inches. An increase in the PCC layer by one inch significantly decreases the cracking indicator value. The use of a 10-inch PCC layer on JPCP pavement for all climate stations meets the criterion for JPCP cracking performance. The highest percentage change in JPCP pavement system from increasing the PCC layer by one inch is 18.36 percent in Charlotte. The increase to ten inches caused Charlotte's cracking indicator to decrease from 23.71 to 5.35 percent cracking. The lowest percentage change in the cracking indicator occurred at Cape Hatteras. The cracking indicator changed by 3.83 percent and caused the cracking indicator for Cape Hatteras to decrease from 6.01 to 2.18 percent. The increase of the PCC layer by one inch improves the durability of the PCC layer and reduces the percentage cracking.

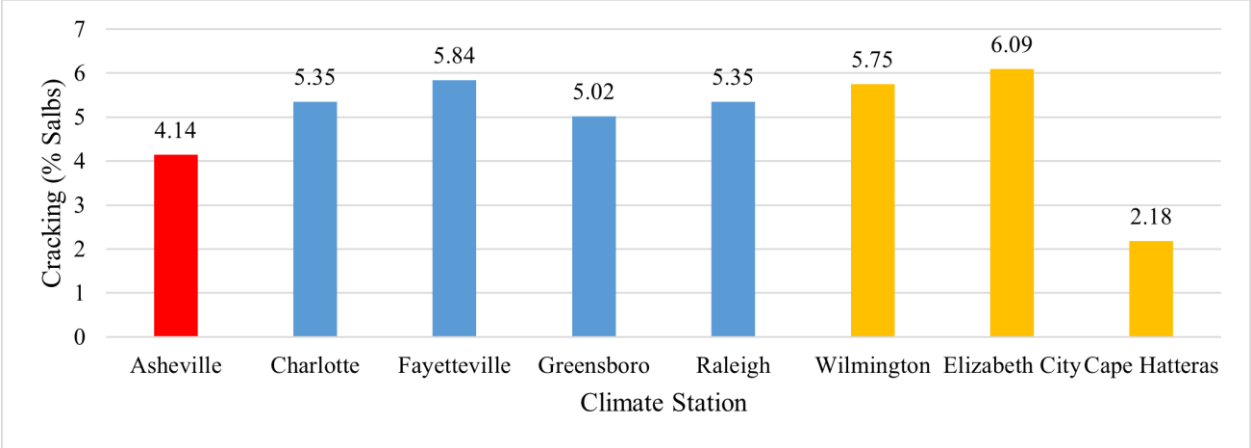

Figure 5.56: Cracking indicator values at 10 inches

Table 5.17: Cracking indicator comparison 9 inches vs. 10 inches

	Cracking Indicator Value		
Climate Station	9 inches	10 inches	Percentage Change
Asheville	15.12	4.14	10.98 %
Charlotte	23.71	5.35	18.36 %
Fayetteville	23.71	5.84	17.87 %
Greensboro	22.42	5.02	17.40 %
Raleigh	21.5	5.35	16.15 %
Wilmington	18.69	5.75	12.94 %
Elizabeth City	23.62	6.09	17.53 %
Cape Hatteras	6.01	2.18	3.83 %

5.8 Effects of North Carolina Climatic Regions on Unbonded Concrete Overlay (UBCO) Performance

5.8.1 *Methodology*

Simulations were performed for unbonded concrete overlay (UBCO) under the same parameters as the JPCP, previously mentioned in this section. The same climate stations of Asheville, Charlotte, Fayetteville, Greensboro, Raleigh, Wilmington, Elizabeth City, and Cape Hatteras were selected for simulations. The climate station data can be found previously in Figures 5.51 and C.27, and Table 5.16. Level 3 simulations were selected as well for concrete overlay comparison. The mixture C1N20 is kept the same for the concrete overlay simulations. Input data for Level 3 simulations for C1N20 are located previously in Table C.5. The pavement structure of Concrete Overlay has two PCC layer thicknesses. One layer is the existing PCC layer, and the second layer is the new PCC overlay layer. The thickness for simulations for both the existing and new layers is selected as nine inches. Simulations were performed and the results are as follows.

5.8.2 *Analysis of Simulation Results*

Effects of Climate on IRI Indicator of UBCO

The IRI indicator results are shown in Figure 5.57. The highest value for the IRI indicator for concrete overlay is 265.04 in Greensboro and the lowest value for the concrete overlay simulations is 224.12 in Wilmington. The second highest value for the IRI indicator is 255.87 in Asheville and the second lowest value is 246.17 in Cape Hatteras. The IRI indicator shows as you move from the Western Mountains to Costal Plains, the IRI indicator decreases. The red bar shows the Western Mountains, blue bars show Piedmont, and the orange bars show the Coastal Plains.

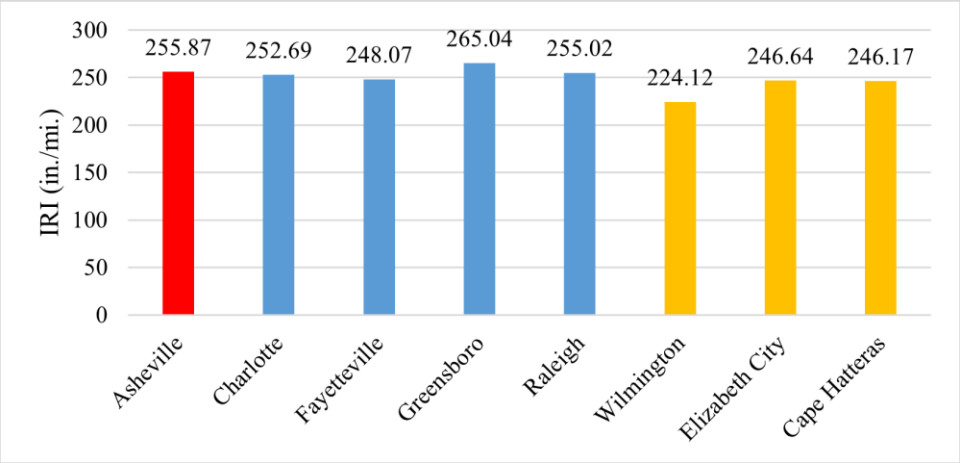

Figure 5.57: Concrete overlay IRI indicator results

Effects of Climate on Faulting Indicator of UBCO

The faulting indicator results are shown in Figure 5.58. The highest value for the faulting indicator is in Asheville, with a value of 0.27. The two next highest values for faulting are in Greensboro and Raleigh, with a value of 0.26. The lowest faulting indicator value is 0.22 in Wilmington. The trendline for the faulting indicator shows as you move from West to East in North Carolina, the faulting indicator decreases in value. In the overall scenario the faulting indicator remains comparatively constant and there is not much difference observed between different climate stations.

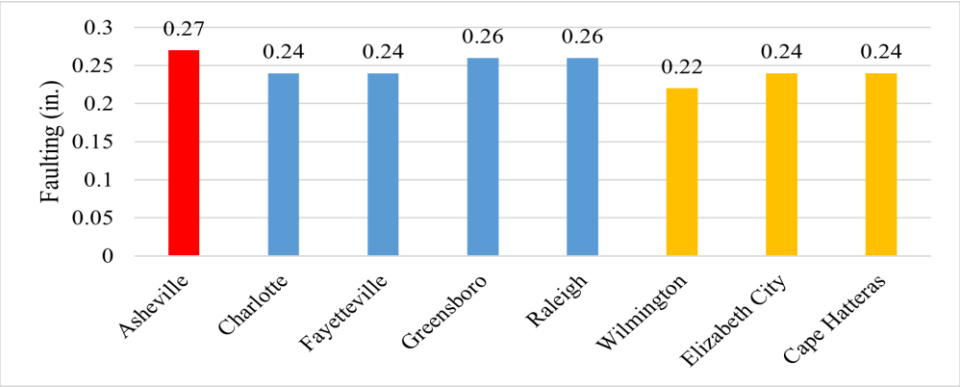

Figure 5.58: Concrete overlay faulting indicator results

Effects of Climate on Transverse Cracking Indicator of UBCO

Cracking indicator results are shown in Figure 5.59. The highest value for the cracking indicator is 38.44 in Charlotte. The lowest value for the cracking indicator is 20.19. Both the Piedmont and Coastal Plain regions have similar average cracking results for concrete overlay simulations. The Western Mountains show a significant drop in the cracking indicator results as compared to both the Piedmont and Western Mountains. The Western Mountains having a lower cracking indicator than the Piedmont and Western Mountains follows the same trend as a new JPCP pavement. Asheville has higher climate station data for the freezing index, precipitation, and number of freeze/thaw cycles, as well as the lowest climate station data for air temperature. The combination of holding an extreme value for each climate station data criterion could be attributed to the way the concrete overlay pavement reacts to cracking.

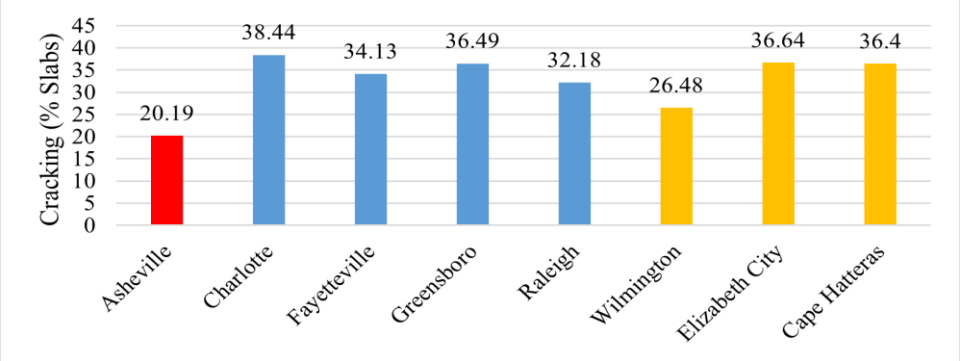

Figure 5.59: Concrete overlay cracking indicator results

5.8.3 *Summary of the Simulation Results*

There are differences in each of the performance indicators of IRI, faulting, and cracking between climate stations in North Carolina. Figure 5.60 shows the percentage change in each of the performance indicators for concrete overlay. The faulting indicator holds the largest percentage change of 23 percent. Although the faulting indicator holds the largest percentage change, the differences in the values of faulting are very small. The highest value for the faulting indicator is 0.27 in Asheville and the lowest value is 0.22 in Wilmington. This is a small difference between the highest and lowest values for the faulting indicator. Cracking and IRI both hold an 18 percent change in values. The values for both the IRI and cracking indicators hold a higher difference in point value, compared to the faulting indicator. The highest IRI value is 265.04 in Asheville and the lowest IRI value is 224.12 in Wilmington. The cracking indicator has a high value of 38.44 in Charlotte and a low value of 20.19 in Asheville. For all three of the performance indicators, Asheville holds an extreme value. Asheville holds the highest value for the performance indicators of faulting and IRI, and the lowest value for the performance indicator of cracking. Asheville holding these extreme values is attributable to the climate station data criterion. Asheville holds the highest value for freezing index, precipitation, and number of freeze/thaw cycles and the lowest value for the mean air temperature criterion. Wilmington holds an extreme value for the faulting indicator and the IRI indicator. Wilmington holding these extreme values is also attributable to climate station data criterion. Wilmington holds a very low number for the freezing index and number of freeze/thaw cycles criterion. Wilmington holds one of the highest values for air temperature and precipitation. Charlotte has the highest number for the cracking indicator. The climate station data criterion for Charlotte does not hold the max or low values for each category. The values for Charlotte's climate station data criterion for air temperature, freezing index, precipitation, and number of freeze/thaw cycles are towards the average of all values. Charlotte holding the highest value for cracking could possibly be attributed to the combination of the climate values mentioned. More investigation into the way the concrete overlay pavement reacts to cracking will have to be investigated further.

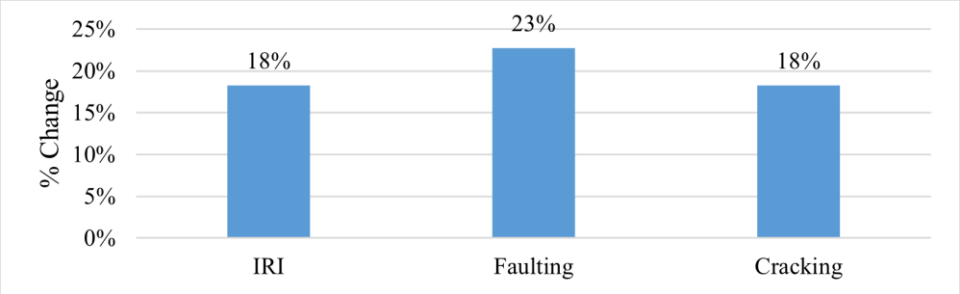

Figure 5.60: Concrete overlay indicator percentage change

5.8.4 *UBCO Slab Thickness Recommendation*

The cracking indicator values for the simulations performed exceeded the 15 percent cracking threshold. To improve pavement performance across NC for the cracking indicator, simulations were performed at 10 inches. Simulation values for each of the climate stations are shown in Figure 5.61. Table 5.18 shows the climate station with the cracking indicator value at 9 inches and cracking indicator value at 10 inches. An increase in the PCC layer by one inch significantly decreases the cracking indicator value. The use of a 10-inch PCC layer on UBCO pavement for all climate stations meets the criterion for UBCO cracking performance. An increase of one-inch in UBCO slab thickness has the highest value of percentage change in cracking of 33.88 percent in Cape Hatteras. The change of 33.88 percent brought the Cape Hatteras climate station cracking value from 36.40 to 2.52. The lowest value for percentage change in cracking is 14.24 percent at Asheville. The change in the cracking indicator for Asheville brought the climate station cracking from 20.19 to 5.95.

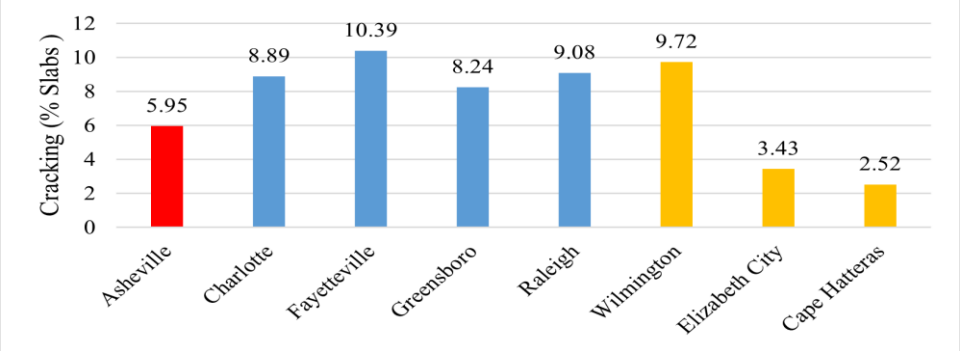

Figure 5.61: Concrete overlay cracking indicator values at 10 inches

Table 5.18: Concrete overlay cracking indicator comparison 9 inches vs. 10 inches

	Cracking Indicator Value (%)		
Climate Station	9 inches	10 inches	Percentage Change
Asheville	20.19	5.95	14.24%
Charlotte	38.44	8.89	29.55%
Fayetteville	34.13	10.39	23.74%
Greensboro	36.49	8.24	28.25%
Raleigh	32.18	9.08	23.10%
Wilmington	26.48	9.72	16.76%
Elizabeth City	36.64	3.43	33.21%
Cape Hatteras	36.40	2.52	33.88%

5.9 Effects of Thermal Conductivity of Concrete on JPCP's Performance and Design Slab Thickness

Thermal conductivity is an important thermal property of paving concrete, but in the past with the empirical design methods in place it did not provide much influence on the design. With the advent of Mechanistic-Empirical Pavement Design Guide (MEPDG) and Pavement ME Design software (PMED), the importance of mechanical and thermal properties came to the forefront, but the focus of most research revolved around the mechanical properties including compressive strength, elastic modulus, and modulus of rupture (MOR) and thermal properties including coefficient of thermal expansion (CTE) (Sabih 2016), (Vandenbossche 2011), (Ceylan 2013). There are a few works on the analysis of the effect of thermal stress and coefficient of thermal expansion on concrete pavements (Mackiewicz 2014), (Shin 2011) but not much research is available on the effects of thermal conductivity (TC) on the performance of the JPCP system (Mirnezami 2023), (Panchmatia 2014), (Kodide 2010), (Cavalline 2018), (Cavalline et al. 2018b). The focus of this study is to analyze and quantify the impact of thermal conductivity on the JPCP performance and how it affects the design slab thickness.

5.9.1 *Methodology*

To analyze the effects of thermal conductivity on JPCP pavements, several design simulations were performed in Pavement ME Design and IRI, Faulting and Cracking indicators were compared. In pavement ME, Level 3 analysis was used for each individual mixture, coefficient of thermal expansion (CTE) and compressive strength were selected for Level 3 analysis. The baseline model found in Table 5.19, used for simulations was kept constant for the entire simulation work which included four pavement layers that include the PCC layer, a lime stabilized base course layer, a crushed gravel base

course layer, and a subgrade layer. The JPCP design life was also kept constant at 30 years while all other design inputs were set at PMED default values. The test data used for thermal conductivity, coefficient of thermal expansion (CTE) and compressive strength is found in Table 5.20.

The concrete mixture designs were based on type of coarse aggregates, fine aggregates, and percentage of fly ash. The mixtures used in this study used the following denotation for the mixture matrix. Coarse aggregates are designated as C1 and C2. Fine aggregates (natural sand) are designated as N1 and N2. Cement type is designated as O, as there is only one type. Fly ash composition is designated as 20% or 30%, which is denoted as F20 and F30. An example of a mixture designation is C1N1OF20 based on Coarse aggregate-1, Natural sand-1, OPC, and 20% Fly Ash.

The range of thermal conductivity values for paving mixtures as per PMED is 0.2 to 2.0 Btu/ (ft · hr · °F) with a default value of 1.25 Btu/ (ft · hr · °F). In the initial phase, the effects of the typical range of thermal conductivity values were analyzed on the performance of JPCP with PMED simulations and keeping other design variables as constant. After conducting the simulations, analysis of the effects of thermal conductivity on each of the three performance indicators for JPCP was performed. In the next phase, the effects of using default value of thermal conductivity were compared to using the lab tested value of thermal conductivity. In the final phase of the analysis, the impact of thermal conductivity on the design slab thickness was analyzed using PMED simulations.

Table 5.19: Sensitivity analysis inputs and baseline model

Input Category	Variable
PCC Thickness	8
AADTT	6000
Climate	Charlotte
Slab Length	15
Dowel Diameter	1.25
Friction Loss	240 Months
PCC Shortwave Absorptivity	0.85
PCC Heat Capacity	0.28
Slab Width	12

Table 5.20: Level 3 simulation input data

Mixture ID	28 Day CTE	28 Day Compressive Strength	56 Days Thermal Conductivity
C1N10	5.66	4656	1.057
C1N1OF20	5.433	4303	0.922
C1N1OF30	5.325	3176	0.886
C1N20	5.358	5051	1.150
C1N2OF20	5.195	4425	0.930
C1N2OF30	5.164	3610	0.871

5.9.2 *Effects of Thermal Conductivity on JPCP Performance Indicators of Baseline JPCP Model*

Impact Of Thermal Conductivity on IRI

The simulation results are shown in Figure C.28, and it is evident that as thermal conductivity increases from 0.7 to 2 Btu/ (ft · hr · °F), there is a consistent trend of decreasing IRI values, indicating that higher thermal conductivity is associated with smoother pavement surfaces. When thermal conductivity is at 0.7 Btu/ (ft · hr · °F) the IRI is highest at 162 in/mi, signifying a rougher pavement surface. As thermal conductivity gradually increases up to 1.2 Btu/ (ft · hr · °F), there is a sharp decreasing trend in IRI. This suggests that materials with higher thermal conductivity tend to result in smoother pavement surfaces. The decreasing trend continues as thermal conductivity rises further, with IRI values consistently decreasing. At thermal conductivity values of 1.5 Btu/ (ft · hr · °F) and 2 Btu/ (ft · hr · °F), the IRI is 116.78 in/mi and 113.43 in/mi, respectively, indicating a significantly smoother pavement surface compared to lower thermal conductivity values. So, the concrete mixture with better thermal conductivity has the advantage of dissipating heat more efficiently, reducing temperature-induced stresses, and contributing to a smoother pavement surface.

Impact Of Thermal Conductivity on Faulting

The analysis of simulation results is shown in Figure C.29. It was found that while thermal conductivity does have some influence on faulting in JPCP, the effect is relatively minor within the range studied. Engineers and pavement designers should consider a holistic approach, considering various factors, to mitigate faulting issues effectively and ensure long-lasting concrete pavement performance.

Impact of Thermal Conductivity on Cracking

As shown in Figure C.30, when thermal conductivity increases from 0.7 to 2, there is a clear trend of decreasing cracking. When thermal conductivity is at its lowest value of 0.7, cracking is at its highest (57%). This suggests that materials with low thermal conductivity do not efficiently dissipate heat, leading to greater temperature differentials within the pavement, and thus, a higher likelihood of cracking. As thermal conductivity gradually increases up to 1.2, a sharply decreasing trend in cracking is visible. This implies that materials with higher thermal conductivity can dissipate heat more effectively, reducing the temperature-induced stresses within the pavement and resulting in fewer cracks. The trend continues as thermal conductivity increases further, with cracking levels decreasing as thermal conductivity rises. When thermal conductivity reaches 2.0, cracking is at its lowest point, measuring 2.76%. This demonstrates that materials with excellent thermal conductivity offer superior thermal stability to the JPCP, minimizing the temperature-related stresses that lead to cracking. In practice, selecting concrete mixtures or materials with higher thermal conductivity can be a valuable strategy to reduce the occurrence of cracking in concrete pavements.

5.9.3 *Summary of Thermal Conductivity Impact on IRI, Faulting, and Cracking Of JPCP*

The summarized comparison is shown in Figure C.31. As thermal conductivity increases from 0.2 to 2, IRI consistently decreases. Higher thermal conductivity values are associated with smoother pavement surfaces, as more efficient heat dissipation minimizes temperature-induced stresses, resulting in a smoother ride quality. TC has little impact on faulting and across the entire thermal conductivity range (0.2 to 2), faulting remains relatively constant at 0.05 to 0.07 inch. Increasing thermal conductivity from 0.2 to 2 substantially reduces cracking. Higher thermal conductivity materials better handle thermal stresses, resulting in fewer cracks. The relationship is nonlinear, with a significant reduction in cracking as thermal conductivity exceeds 0.5. In summary, thermal conductivity significantly affects IRI and cracking, with higher thermal conductivity values correlating with smoother surfaces and fewer cracks. However, thermal conductivity has minimal impact on faulting and it's essential to consider all factors holistically for effective pavement design and maintenance.

5.9.4 *Results of JPCP Performance Indicators (Using thermal conductivity Lab Data and Default Data)*

Impact of Thermal Conductivity on IRI

A comparison of the effects of laboratory obtained thermal conductivity values and the PMED default values with regards to the pavement roughness (IRI) of JPCP is presented in Figure C.32. The effects of thermal conductivity on the IRI in JPCP varies among different concrete mixtures, as evident from the provided data with varying values of IRI obtained for different mixtures. In the overall scenario, 5 of the 6 simulated mixtures show a higher IRI for laboratory obtained thermal conductivity in comparison to the PMED default thermal conductivity. Only one concrete mixture showed a lower IRI value with laboratory obtained thermal conductivity as compared to PMED default thermal conductivity value. It is found that there is a significant difference between the IRI indicators obtained with the laboratory obtained thermal conductivity and the PMED default thermal conductivity values and pavement designers need to take this in to account while designing any new JPCP system.

Impact of Thermal Conductivity on Faulting

The effects of thermal conductivity on faulting in JPCP appear to be minimal across different mixtures, as indicated by the results of the simulations as shown in Figure C.33. The simulations conducted with laboratory obtained thermal conductivity values and the simulations conducted with the PMED default thermal conductivity values show the same faulting indicator values. In summary, the simulation results indicate that thermal conductivity has minimal to no effect on faulting levels in JPCP for the studied mixtures.

Impact of Thermal Conductivity on Transverse Cracking

The impact laboratory obtained thermal conductivity on transverse cracking in JPCP varies across different mixtures, as indicated by the simulation results shown in Figure C.34. In summary, the simulation data indicates that thermal conductivity has varying effects on cracking in JPCP for different mixtures. Laboratory obtained thermal

conductivity values tend to result in higher cracking severity compared to PMED default thermal conductivity values for all of the simulated mixtures. It is evident that accurate characterization of material properties is vital for predicting and managing pavement cracking effectively.

5.9.5 *Summary of Comparison of Laboratory Obtained Thermal Conductivity and Default TC on JPCP Performance*

Thermal conductivity variations have a mixed impact on IRI. In some mixtures, such as C1N1O, lab TC data results in higher IRI values than baseline data, indicating potential differences in material properties. However, for other mixtures like C1N2OF20 and C1N2OF30, thermal conductivity variations have minimal impact on IRI. Thermal conductivity has negligible influence on faulting across different mixtures. Both baseline and lab thermal conductivity data consistently yield similar faulting values, indicating that thermal conductivity variations do not significantly affect faulting levels. Thermal conductivity differences have a more pronounced impact on cracking. In mixtures like C1N1O and C1N2O, lab thermal conductivity data leads to higher cracking severity compared to baseline data. In summary, the effects of thermal conductivity on JPCP performance indicators vary across different mixtures, with lab thermal conductivity data generally showing higher IRI and cracking values for some mixtures, while faulting remains largely unaffected by thermal conductivity variations. Accurate characterization of material properties is crucial for reliable pavement performance predictions and design decisions.

5.9.6 *Effects of Thermal Conductivity Values on Design Slab Thickness*

The use of default thermal conductivity values of the concrete paving mixtures results in in-accurate performance indicator values in comparison to the scenarios where laboratory obtained thermal conductivity values are used for the simulations. Increasing the PCC slab thickness can help reduce the difference between the two simulated scenarios. Analysis was conducted to quantify the impact of baseline thermal conductivity vs laboratory obtained thermal conductivity values on the slab thickness of JPCP system. Additional simulations were conducted in PMED with the increased PCC slab thickness to match the cracking indicator values of the laboratory obtained cases to the baseline cases for all the mixtures. The cracking indicator was selected for this matching analysis because the cracking performance indicator has the most severity among all three performance indicators. The summary of the analysis is given in Table 5.21. The baseline thermal conductivity simulations have a PCC slab thickness of 10 inches and after running the simulations for the laboratory obtained thermal conductivity models for all the paving mixtures, a PCC slab thickness of up to 12 inches shows similar cracking indicator results. It is evident that an increase of up to 2 inch in the PCC slab thickness matches cracking values for both the simulated scenarios for all the paving mixtures.

Table 5.21: Effects of thermal conductivity on design slab thickness

	Default TC Simulations	Slab Thickness for Laboratory Obtained Thermal Conductivity Simulations				
Mixture ID	10 inches	10 inches	10.5 inches	11 inches	11.5 inches	12 inches
C1N1O	5.16	-	5.89	-	-	-
C1N1OF20	5.05	-	-	6.91	-	-
C1N1OF30	11.98	-	-	-	-	11.48
C1N2O	3.13	3.62	-	-	-	-
C1N2OF20	3.73	-	5.45	-	-	-
C1N2OF30	6.28	-	-	-	7.65	-

5.9.7 *Summary of Findings*

It was found that the use of default thermal conductivity values will result in lower transverse cracking predictions and the difference in cracking performance between default thermal conductivity and laboratory obtained thermal conductivity values is up to 26%. It is evident from the analysis that using the default/baseline values of thermal conductivity will result in under designed JPCP system which might fail prematurely without completing the design service life and the difference between using the laboratory obtained thermal conductivity and the PMED default/baseline thermal conductivity is up to 2 inches of PCC slab thickness which has numerous financial, sustainability, and environmental implications. It is highly recommended that JPCP design should be conducted according to the laboratory obtained concrete properties including thermal conductivity values. To provide additional confidence and support local calibration of PMED, these findings should also be confirmed through field observations.

5.10 Concrete Pavement Life Cycle Assessment and Life Cycle Cost Analysis for Improving Pavement Sustainability and Resilience in North Carolina

As an amendment to this study, an analysis using life cycle cost analysis (LCCA) and life cycle assessment (LCA) methods is planned on different design options for rigid pavement sections typically constructed in North Carolina, as well as flexible pavements. This work, which was begun in addition to the initial scope of work, was not completed at the time of submission of this report. However, it will appear in future publications once complete.

During this project timeframe, the pavement design procedure used in North Carolina was used to develop pavement sections of equivalent performance over the desired service life. These pavement design options were modeled and simulated using the PMED software to predict their performance. NCDOT specific design inputs for materials, and traffic spectra for truck traffic were used in the simulation of each of the pavement options.

5.10.1 *Input Data*

This study used two current NCDOT highway projects to create two pavement design scenarios from two highway classifications with different traffic spectra (Table 5.22).

Table 5.22: Summary of traffic inputs

Project	AADT 2025	% Trucks	AADTT 2025	Design ESALs (AASTHO 93-NCDOT Flexible)	Design ESALs (AASTHO 93-NCDOT Rigid)	Cumulative Trucks (AASTHO ME)
R-2530B	17,940	10%	1,794	11,954,616	15,999,411	12,975,800
HE-0011	13,830	10%	1,383	9,895,338	13,360,632	10,010,300

The equivalent single axle loads (ESALs) were computed utilizing the traffic data provided in the project information from the NCDOT. The NCDOT utilizes class 5 for dual axle trucks (duals) and class 9 for tractor trailer semi trucks (TTST) with the default average truck axle load distribution factors (ALDF).

Each design scenario consists of three pavement design options based on AASHTO 1993 empirical design methodology as described in the NCDOT Pavement Design Manual and three pavement design options based on AASHTO mechanistic-empirical (ME) design methodology. The three design options include one flexible pavement with an unbound base, one flexible pavement with a bound base, and one rigid pavement design. Due to plasticity index of the residual soils on these projects the subgrade must be chemically stabilized. During the modeling phase it was determined that the ME software would not allow two stabilized layers. Due to this limitation an alternate rigid design option was developed that utilizes less ABC. The rigid design option 1 for project HE-0011 was determined by using the minimum recommended design thickness as described in the NCDOT Pavement Design Manual, while design option 2 was determined utilizing the rigid pavement design equations as described in the NCDOT Pavement Design Manual. The pavement design options were designed as equivalent sections with the same traffic spectrum and design life (Table 5.23).

Table 5.23: Pavement design options

Project	Original Design	Rigid Design Option 1	Rigid Design Option 2
R-2530B	3 inches of S9.5C 4 inches of I19.0C 3 inches of B25.0C	10 inches of JPCP 6 inches of ABC	10 inches of JPCP 4 inches of ABC
HE-0011	3 inches of S9.5C 4 inches of I19.0C 5 inches of B25.0C	7 inches of JPCP 6 inches of ABC	9.5 inches of JPCP 6 inches of ABC

Each of these pavement sections were designed using equivalent ESALs as described by the NCDOT Pavement Design Manual. These sections were modeled and simulated using the same traffic spectra over a 30-year period to determine a predicted performance for each section.

5.10.2 *Results*

The simulation results for three design scenarios for project R-2530B and HE-0011 are shown below (Figure 5.62 and 5.63).

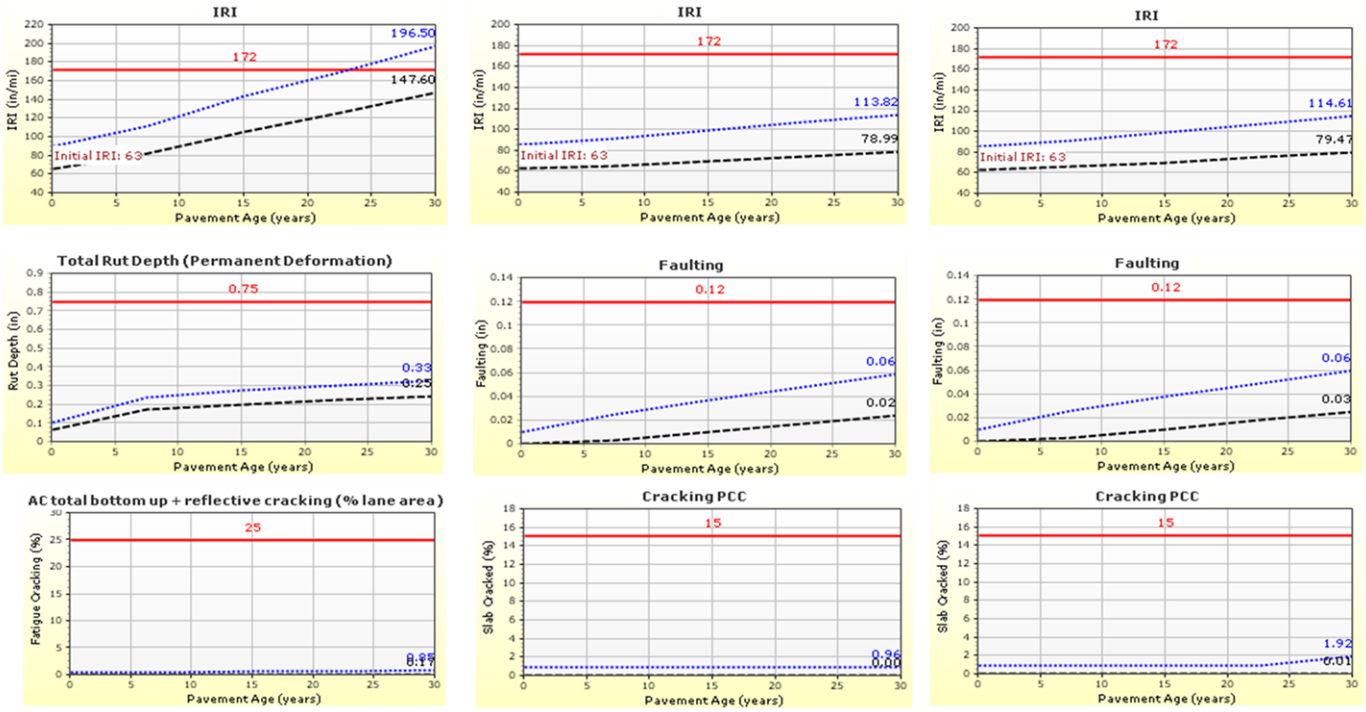

(a): Original Design (b): Rigid Design Option 1 (c): Rigid Design Option 2

Figure 5.62: Predicted Pavement Distresses for R-2503B

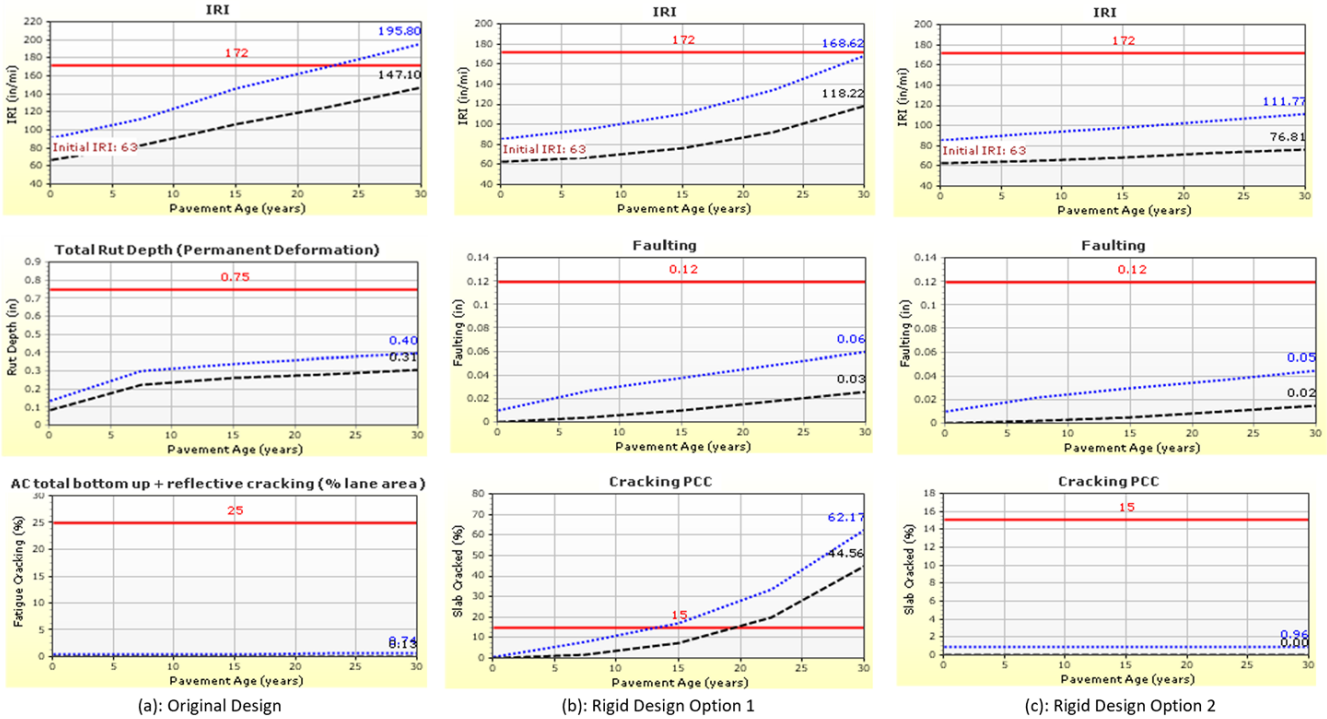

(a): Original Design (b): Rigid Design Option 1 (c): Rigid Design Option 2

Figure 5.63: Predicted Pavement Distresses for HE-0011

The original pavement design for project R-2503B is predicted to have a terminal IRI of 196.5, a total transverse thermal and reflective cracking of 2399.20 ft/mile, 15.48% fatigue cracking and a total rut depth of 0.33 inches. The rigid pavement design option 1 for project R-2503B is predicted to have a terminal IRI of 113.82 , 0.06 inches of faulting, and

0.96% of slabs cracked. The rigid pavement design option 2 for project R-2503B is predicted to have a terminal IRI of114.61, 0.06 inches of faulting, and 1.92% of slabs cracked. These results indicated that both rigid design option for project R-2503B has better predicted performance than the original design. Additionally, the reduced ABC thickness offers a potential cost saving without sacrificing performance.

The original pavement design for project HE-0011 is predicted to have a terminal IRI of 195.80, a 0.74% fatigue cracking, a total transverse thermal and reflective cracking of 2481.40 ft/mile, and a total rut depth of 0.75 inches. The rigid pavement design option 1 for project HE-0011 is predicted to have a terminal IRI of 168.62 , 0.06 inches of faulting, and 62.17% of slabs cracked The rigid pavement design option 2 for project HE-0011 is predicted to have a terminal IRI of 111.72, 0.05 inches of faulting, and 0.96% of slabs cracked. These results indicated that both rigid design option 2 for project HE-0011 has better predicted performance than the original flexible design and the standard rigid design inputs. In this particular scenario the minimum structure depths for a section with an AADT less than 20,000 using rigid pavement did not perform well in terms of cracking. It is important to note that this analysis did not incorporate any maintenance or rehabilitation efforts into the simulated performance of these sections.

LCCA and LCA are being developed and will appear in future publications by Sheffield et al.

6.0 SUMMARY AND CONCLUSIONS

A detailed summary of findings for each of the areas of work was presented at the end of the all the sections of this report. Although the reader is referred to the appropriate chapters/sections for a summary of findings, key conclusions from each of the areas of work are provided below.

6.1 Laboratory Testing Program, Results, and Analysis (Chapter 4)

Fresh Properties

- Concrete mixtures containing fine aggregate from the Emery Pit were more workable and required less water reducing admixtures to achieve the target slump compared to mixtures containing fine aggregate sourced from Buckleberry Mine.

Mechanical Properties

- Compressive strength was most influenced by the fly ash content in the concrete mixture, with increasing amounts of fly ash resulting in slower strength gain. On average, mixtures containing fly ash did not achieve NCDOT's 28-day compressive strength of 4,500 psi, although this strength was readily met at later ages as expected. The AASHTOWare Pavement ME Design default value of 5,275.3 psi for 28-day compressive strength does not accurately represent concrete mixtures containing fly ash.
- At early ages, MOE was influenced by the region of North Carolina and the fly ash content, with mixtures containing coarse aggregate sourced from the Piedmont region outperforming mixtures containing coarse aggregate from the Mountain region. At 28-days, MOE on average ranged between 2,150,000 and 2,640,000 psi, significantly lower than the AASHTOWare Pavement ME Design default input value of 4,200,000 psi.
- Poisson's ratio was not significantly influenced by the substitution of fly ash or varying aggregates used in the concrete mixtures. At 28-days of age, Poisson's ratio averaged between 0.12 and 0.14, significantly lower than the AASHTOWare Pavement ME Design default value of 0.20.
- The fly ash content had the largest influence on MOR. On average, concrete mixtures containing fly ash did not achieve NCDOT's 28-day flexural strength of 650 psi. Based on later-age compressive strength test results, it is expected that mixtures likely reached 650 psi flexural strength at later ages (not tested as part of this study).

Thermal Properties

- General trends suggest that as concrete ages, values for thermal properties decrease. This general trend in decreasing thermal properties was observed for CTE, heat capacity, and thermal conductivity.
- Fly ash had a large influence on the measured concrete thermal properties. As the percent replacement of fly ash increases in the concrete mixture, the value for thermal properties (CTE, heat capacity, and thermal conductivity) decreased.
- The quarry location from which the coarse aggregate was sourced had a significant influence on the CTE, with average values ranging between 4.83 and 5.45 $\times 10^{-6}$ inch per inch per degree Fahrenheit. The rate of change of the concrete CTE was most influenced by the location from which the coarse aggregate was sourced. The CTE values of concrete measured as part of this study are significantly lower than the recommended input value of 4.9 $\times 10^{-6}$ inch per inch per degree Fahrenheit.
- Thermal conductivity was most influenced by the location the coarse aggregate was sourced. The presence of fly ash in the mixture did not significantly influence the rate of change for thermal conductivity and heat capacity between 56 and 90-day testing.
- The measured input values for heat capacity and thermal conductivity were between 0.17 to 0.19 BTU/lb-F and 0.83 to 1.15 BTU/ft-hr-F compared to the recommended input values of 0.28 BTU/lb-F and 1.25 BTU/ft-hr-F, respectively.

Durability Performance

- On average, surface resistivity for concrete mixtures containing coarse aggregate sourced from the Piedmont region of North Carolina outperformed mixtures containing coarse aggregate from the Mountain region.

Recommended PMED Inputs and Related Typical Test Values

Table 4.2 provides a proposed catalog of PMED PCC mechanical property inputs for North Carolina. Table 4.3 provides a Proposed catalog of PMED PCC thermal property inputs for North Carolina. Table 4.4 provides a proposed catalog of typical durability performance test values for North Carolina.

6.2 Pavement Design, Performance, and Slab Thickness Analysis using Pavement ME Design Simulations (Chapter 5)

- CTE of concrete is the prime contributor in producing pavement distresses and impact the performance of the JPCP and it is the most significant factor affecting the JPCP performance.
- Level 1 material inputs provide the most accurate design out of all three input levels and using Level 3 inputs for JPCP design will result in a thicker concrete slab and using Level 1 inputs will produce a more accurate and economical JPCP design.
- The strength gain for concrete paving mixtures that include fly ash takes longer to gain full strength. Level 3 material inputs restrict an accurate representation of fly ash's strength gain properties with only the 28-day compressive strength value while Level 1 material inputs simulate a better depiction of how fly ash properties are included in JPCP pavements. It is recommended to use later-age strength values for fly ash mixtures when using PMED software.
- There is significant impact of heat capacity of paving concrete on IRI and cracking of JPCP systems and using the software default values of heat capacity will result in under designed JPCP system which might fail prematurely without completing the design service life.
- The use of default thermal conductivity values will result in lower transverse cracking predictions and the difference in cracking performance between default thermal conductivity and laboratory obtained thermal conductivity values is up to 26%. Using the default values of thermal conductivity will result in under designed JPCP system which might fail prematurely.

7.0 VALUE OF RESEARCH FINDINGS AND RECOMMENDATIONS

7.1 Value of Research Findings

Research products produced from this work included:

- An enhanced database/catalog of Level 1 mechanical and thermal inputs for PMED design process. This catalog amends the catalog prepared as part of NCDOT 2015-03. It should be noted that some PCC inputs such as MOE, Poisson's ratio, heat capacity, and thermal conductivity were measured to be lower than previously recommended inputs, especially for mixtures containing fly ash. This catalog will help the pavement designers in accurate designing of rigid pavements and implementation of PMED software in the design process.
- The sensitivity analysis confirmed that CTE of paving concrete is the prime contributor in producing pavement distresses and impact the performance of the JPCP and it is the most significant factor affecting the JPCP performance. Laboratory obtained CTE values should be used for any specific rigid pavement design process for an effective pavement design.
- Level 1 concrete material inputs provide the most accurate design out of all three input levels and using Level 3 inputs for JPCP design will result in a thicker concrete slab, and using Level 1 inputs will produce a more accurate and economical JPCP design.
- The strength gain for concrete paving mixtures that include fly ash takes longer to gain full strength and Level 3 material inputs restrict an accurate representation of fly ash's strength gain properties with only the 28-day compressive strength value while Level 1 material inputs simulate a better depiction of how fly ash properties are included in JPCP pavements and unbonded concrete overlays. The faster strength gain trends for the fly ash mixtures continues after 90 days and become close to compatible to the no-fly ash mixtures at 360 days. Incorporating long-term strength data for fly ash mixtures is recommended, as it will result in more accurate performance prediction, and design of thinner pavement slabs resulting in cost savings in the pavement projects along with the durability performance benefits offered by fly ash mixtures.
- There is significant impact of heat capacity of paving concrete on IRI and cracking of JPCP systems and using the PMED default values of heat capacity will result in under designed JPCP system which might fail prematurely without completing the design service life resulting in early rehabilitation of the in-service pavement systems.
- The use of PMED default thermal conductivity values will result in lower transverse cracking predictions and the difference in cracking performance between default thermal conductivity and laboratory measured thermal conductivity values is up to 26%. Using the PMED default values of thermal conductivity will result in under designed JPCP system which has numerous financial, sustainability, and environmental implications. These implications may become more pronounced in the future due to the temperature-related effects of climate change.

7.2 Recommendations

Following are the recommendations pertaining to the findings of this study:

- The catalog of Level 1 mechanical and thermal inputs should be incorporated in the implementation of the PMED in the rigid pavement design process in the state of North Carolina.
- Laboratory measured CTE values of paving concrete should be used in the rigid pavement design process using PMED software. Using PMED default CTE values will result in over designed concrete pavement slab while laboratory measured CTE will result in thinner pavement slabs resulting in cost savings.
- Level 1 material inputs of paving concrete mixture for any specific pavement project should be used in the design process with PMED software which will result in effective rigid pavement design that can last for the designed service life.
- PMED software lacks to incorporate the complete picture of strength gain of fly ash mixtures. This results in PMED predicted performance that very likely does not reflect the true performance of fly ash mixtures in the field, and in design of overly thick PCC sections. Long-term strength gain of fly ash mixtures should be incorporated in the PMED software design process for accurate designing of rigid pavement systems.
- The fly ash mixtures result in lower CTE values and lower early age strength properties as compared to regular mixtures. There is a need to conduct future study on the combined effect of long-term strength properties and CTE values to determine the accurate impact of using fly ash mixtures in rigid pavements.
- Laboratory measured heat capacity and thermal conductivity values of paving concrete mixtures should be incorporated in the rigid pavement design process with PMED software in place of the software default values for effective design of rigid pavements that can perform for the designed service life.

8.0 IMPLEMENTATION AND TECHNOLOGY TRANSFER PLAN

Research Product 1	Catalog of recommended PCC inputs for PMED
Suggested User	Pavement Design and Collection Unit, Materials & Tests Unit
Recommended Use	These inputs can be used by NCDOT to support analysis and design of rigid pavements immediately.
Recommended Training	None recommended at this time.

Research Product 2	Laboratory test data to support an improved understanding of concrete mixtures.
Suggested User	Materials & Tests Unit
Recommended Use	Information contained in this database could serve as reference data for evaluation of concrete mixtures and/or test methods in future work. Data could also be used to supplement additional databases on maintained by the Materials and Tests Unit. It can also be used to support movement towards performance specification provisions as part of NCDOT's PEM efforts.
Recommended Training	None recommended at this time.

Research Product 3	Surface resistivity measurements of a range of North Carolina concrete pavement mixtures.
Suggested User	Materials & Tests Unit
Recommended Use	Surface resistivity tests results have been shown to strongly correlate with long term durable performance of concrete infrastructure. Surface resistivity measurements could be utilized to specify more durable concrete and to evaluate the durability of existing concrete. These values verify the findings of previous PEM studies aimed at developing surface resistivity specifications, and can be used by NCDOT to help justify implementation of resistivity in project special provisions or in future specifications.
Recommended Training	None recommended at this time, beyond use of materials previously prepared to assist NCDOT with training of their personnel in PEM and use of surface resistivity.

Research Product 4	Recommended practices for interpreting PMED predictions and sensitivity
Suggested User	Pavement Design and Collection Unit, Materials & Tests Unit
Recommended Use	Use of fly ash in concrete paving mixtures have shown to take longer to gain full strength and using 28 day compressive strength of fly ash mixtures may result in under/over designed pavement systems. Later-age strength values should be incorporated for fly ash mixtures when using PMED software for resilient designs of pavement systems.
Recommended Training	None recommended at this time.

References

- AASHTO. (2022). "Standard Practice for Developing Performance Engineered Concrete Pavement Mixtures." R 101-22, American Association of State Highway and Transportation Officials, Washington, DC.
- AASHTO. (2022). "Standard Test Method for the Temperature of Freshly Mixed Hydraulic-Cement Concrete." T 309, American Association of State Highway and Transportation Officials, Washington, DC.
- AASHTO. (2019). "Standard Test Method for the Coefficient of Thermal Expansion of Hydraulic Cement Concrete." T 336-19, American Association of State Highway and Transportation Officials, Washington, DC.
- AASHTO. (2017). "Standard Method for Surface Resistivity Indication of Concrete's Ability to Resist Chloride Ion Penetration." T 358, American Association of State Highway and Transportation Officials, Washington, DC.
- AASHTO. (2008). "Mechanistic-Empirical Pavement Design Guide: A Manual of Practice." Washington, DC: American Association of State Highway Transportation Officials.
- AASHTO. (2010). "Guide for the Local Calibration of the Mechanistic-Empirical Pavement Design Guide." Washington, DC: American Association of State Highway Transportation Officials.
- American Society for Testing and Materials (ASTM). (2021). ASTM Standard C39/C39M-21. "Standard Test Method for Compressive Strength of Cylindrical Concrete Specimens." 134 ASTM International, West Conshohocken, PA. DOI: 10.1520/C0039_C0039M-21. www.astm.org
- American Society for Testing and Materials (ASTM). (2022). ASTM Standard C78/C78M-22. "Standard Test Method for Flexural Strength of Concrete." ASTM International, West Conshohocken, PA. DOI: 10.1520/C0078_C0078M-22. www.astm.org
- American Society for Testing and Materials (ASTM). (2017). ASTM Standard C138/C138M-17a. "Standard Test Method for Density (Unit Weight), Yield, and Air Content (Gravimetric) of Concrete." ASTM International, West Conshohocken, PA. DOI: 10.1520/C0138_C0138M-17A. www.astm.org
- American Society for Testing and Materials (ASTM). (2020). ASTM Standard C143. "Standard Test Method for Slump of Hydraulic-Cement Concrete." ASTM International, West Conshohocken, PA. DOI: 10.1520/C0143_C0143M-20. www.astm.org
- American Society for Testing and Materials (ASTM). (2017). ASTM Standard C157/C157M-17. "Standard Test Method for Length Change of Hardened Hydraulic-Cement Mortar and Concrete." ASTM International, West Conshohocken, PA. DOI: 10.1520/C0157_C0157M-17. www.astm.org
- American Society for Testing and Materials (ASTM). (2020). ASTM Standard C192/C192M-19. "Standard Practice for Making and Curing Concrete Test Specimens in the Laboratory." ASTM International, West Conshohocken, PA. DOI: 10.1520/C0192_C0192M-19. www.astm.org
- American Society for Testing and Materials (ASTM). (2022). ASTM Standard C231/C231M-22. "Standard Test Method for Air Content of Freshly Mixed Concrete by the Pressure method." ASTM International, West Conshohocken, PA. DOI: 10.1520/C0231_C0231M-22. www.astm.org
- American Society for Testing and Materials (ASTM). (2022). ASTM Standard C469/C469M-22. "Standard Test Method for Static Modulus of Elasticity and Poisson's Ratio of Concrete in Compression." ASTM International, West Conshohocken, PA. DOI: 10.1520/C0469_C0469M-22. www.astm.org
- American Society for Testing and Materials (ASTM). (2021). ASTM Standard C511-21. "Standard Specification for Mixing Rooms, Moist Cabinets, Moist Rooms, and Water Storage Tanks Used in the Testing of Hydraulic Cements and Concretes" 134 ASTM International, West Conshohocken, PA. DOI: 10.1520/C0511-21. www.astm.org
- American Society for Testing and Materials (ASTM). (2021). ASTM Standard C518-21. "Standard Test Method for Steady-State Thermal Transmission Properties by Means of the Heat Flow Meter Apparatus." ASTM International, West Conshohocken, PA. DOI: 10.1520/C0518-21. www.astm.org
- American Society for Testing and Materials (ASTM). (2018). ASTM Standard C685/C685M-17. "Standard Test Method for Concrete Made by Volumetric Batching and Continuous Mixing." ASTM International, West Conshohocken, PA. DOI: 10.1520/C0685_C0685M-17. www.astm.org
- American Society for Testing and Materials (ASTM). (2017). ASTM Standard D2766-95. "Standard Test Method for Specific Heat of Liquids and Solids." ASTM International, West Conshohocken, PA.. www.astm.org
- American Society for Testing and Materials (ASTM). (2017). ASTM Standard E1952-17. "Standard Test Method for Thermal Conductivity and Thermal Diffusivity by Modulated Temperature Differential Scanning Calorimetry," or alternative method." ASTM International, West Conshohocken, PA. DOI: 10.1520/E1952-17. www.astm.org
- Cavalline, T., Tempest, B., Blanchard, E., Medlin, C., and Chimmula, R. (2018a). "Improved Data for Mechanistic-Empirical Pavement Design for Concrete Pavement." Report FHWA/NC/2015-03. North Carolina Department of Transportation, Raleigh, NC.
- Cavalline, T., Tempest, B., Blanchard, E., Medlin, C., Chimmula, R., and Morrison, C. (2018b). "Impact of Local Calibration Using Sustainable Materials for Rigid Pavement Analysis and Design." Journal of Transportation Engineering, Part B: Pavements, 144(4). https://doi.org/10.1061/JPEODX.0000073

- Cavalline, T.L., Tempest, B.Q., Biggers, R.B., Lukavsky, A.J., McEntyre, M.S., and Newsome, R.A. (2020). "Durable and Sustainable Concrete Through Performance Engineered Concrete Mixtures." Final Report, Project FHWA/NC/2018-14, North Carolina Department of Transportation.
- Cavalline, T.L., Tempest, B.Q., Theilgard, P., Dillworth, D.A., and OCampo, J. (2023). "Continuing Toward Implementation of Performance Engineered Concrete Mixtures for Durable and Sustainable Concrete." Final Report, Project FHWA/NC/2019-22, North Carolina Department of Transportation.
- Geary, G. M., (2021). "Updates to AASHTOWare Pavement ME Design Software Affecting Concrete Pavements: A Synthesis of the Change to the Software Related to Concrete Pavements." InTrans Project 15-532. Iowa State University, Ames, IA.
- North Carolina Department of Environmental Quality (NCDEQ). (2016). "1985 Geologic Map of North Carolina." N.C. Division of Energy, Mineral and Land Resources website: https://ncdenr.maps.arcgis.com/apps/MapSeries/index.html?appid=a8281cbd24b84239b29cd2ca798d4a10. Accessed April 28, 2023.
- North Carolina Department of Transportation. (2012). "Standard Specifications for Roads and Structures." Raleigh, North Carolina.
- North Carolina Department of Transportation. (2018). "Standard Specifications for Roads and Structures." Raleigh, North Carolina.
- Pavement Interactive. (2012). "What is Mechanistic-Empirical Design? – The MEPDG and You." Pavement Interactive website, www.pavementinteractive.org/2012/10/02/what-is-mechanistic-empirical-design-themepdg-and-you/. Accessed May 1, 2023.
- Summers, C. (2023). "Investigating Time Sensitive Thermal and Mechanical Inputs for Rigid Pavements." Masters Thesis. University of North Carolina at Charlotte, Charlotte, NC.
- Weiss, J, (2022) "Guidance to Reduce Shrinkage and Restrained Shrinkage Cracking" InTrans Project 15-532. Washington, DC.

APPENDICES

FOR
FINAL REPORT

North Carolina Department of Transportation
Research Project No. 2022-07

Investigating Thermal and Mechanical Inputs for Rigid Pavement Design in North Carolina

By

Gauhar Sabih, Ph.D.
Assistant Professor

Tara L. Cavalline, Ph.D., P.E.
Professor

Brett Q. Tempest, Ph.D., P.E.
Associate Professor

Clarke Summers
Graduate Research Assistant

Megan McIntosh
Undergraduate Research Assistant

Western Carolina University
1 University Drive
Cullowhee, NC 28723
&
University of North Carolina at Charlotte
9201 University City Boulevard
Charlotte, NC 28223

April 2024

APPENDIX A – LITERATURE REVIEW AND REFERENCES

A.1 Introduction

The Pavement Mechanistic Empirical Design (PMED) was developed by AASHTO as the standard for rigid pavement design and performance analysis, and as the most advanced tool, it has transformed the pavement design process. Pavement performance analysis and design can now be performed using the PMED software. The PMED software is based on mechanistic-empirical concepts. The design procedure calculates pavement responses such as stresses, strains, and deflections under axle loads and climatic conditions and then accumulates the damage over the design analysis period. The procedure then empirically relates calculated damage over time to pavement distresses and smoothness based on the performance of actual projects throughout the U.S.

PMED incorporates concrete material properties in the design process and research has shown that compressive strength, elastic modulus, modulus of rupture (MOR), and coefficient of thermal expansion (CTE) are the most important inputs. Predicted pavement characteristics including thickness, design life, serviceability, joint faulting, and cracking performance depend on these material input factors. Accurate determination of material properties was not a part of the design process until the advent of PMED. With further research, it was found that accurate determination of these concrete material inputs as part of local calibration of PMED is the key to design of rigid pavements which can reliably last for the designed service life.

Many state DOTs are in the process of implementing PMED into their pavement design processes and are characterizing local concrete materials in this process. NCDOT is also planning to incorporate PMED into the design process for rigid pavements. The NCDOT conducted a research project completed in 2016 as an initial step to conduct the characterization of concrete materials (FHWA Report No. NC/2015-03) which provided a database of concrete material inputs incorporating Piedmont, Coastal, and Mountain coarse aggregates along with a manufactured sand and a natural sand. Although this project provided a range of useful inputs, it is understood that there are differences in aggregates from other areas of North Carolina, including areas where rigid pavements are anticipated to be constructed. These areas, including the Charlotte area, the Greensboro/Winston-Salem area, the Boone/Blowing Rock area, and the Morganton/Lenoir area, may have quarries that will be potential candidates for use in future concrete paving mixtures. Based on the NC geologic map, there may be some geologic differences that translate into thermal performance changes between these aggregates and the aggregates which were tested in the earlier project. So, there is a need to characterize the concrete paving mixtures prepared with these coarse aggregates and potentially other variables to obtain a more detailed catalog of PMED inputs for rigid pavement design, and subsequently, to evaluate the effects of the obtained material inputs on the design and performance analysis of rigid pavements.

The need for this work is amplified as NCDOT is undertaking new rigid pavement projects including re-construction/widening of I-26 (costing $531 million) and I-540 expressway project (costing $2.2 billion) and many more rigid pavement projects to come in the future. With an accurately established material database to support PMED inputs, the pavement designers will have the opportunity to understand the predicted performance of rigid pavement designs and potentially select the best suited materials and/or mixture characteristics for a specific project.

This proposed research project will result in an enhanced database/catalog of Level 1 mechanical and thermal inputs for PMED design process. The products of this research will be directly implementable by pavement designers, allowing greater confidence in the design and predicted performance of rigid pavements designed using PMED software. The evaluation of various design variables including material inputs, climate, traffic, and geometric properties with regards to the design thickness and predicted performance of rigid pavements will provide a knowledge base to the pavement designers about the impact of these parameters on the rigid pavement design. This will improve the reliability of rigid pavements to provide long lasting service lives with low maintenance.

Prior research has also shown the changes in CTE of paving concrete with age progression and there is a need to conduct long-term testing of concrete paving mixtures being used in North Carolina to evaluate the changes in CTE values of these mixtures with age progression. This will be a step forward towards improved rigid pavement design and constructing pavements that can perform well throughout the designed service life.

A comprehensive literature review of the current state of practice of rigid pavement design, performance analysis, characterization of concrete materials, and effects of material properties of concrete on pavement design and performance has been conducted. The detailed literature review is appended below:

A.2 Rigid/Concrete Pavements

Rigid pavements (commonly known as concrete pavements) are composed of a Portland Cement Concrete (PCC) surface course. With high elastic modulus (stiffness) of the PCC layer, the concrete slab itself supplies most of a rigid

pavement's structural capacity. Concrete pavements may be either unreinforced (plain) or reinforced depending on how the designer prefers to control the cracking of the pavement. The high modulus of elasticity and rigidity of concrete compared to other road making materials provides a concrete pavement with a reasonable degree of flexural strength. This property leads to externally applied wheel loads being widely distributed and limits the pressures applied to the sub-layers. In totality, the concrete layer alone provides the major portion of the load carrying capacity of concrete pavement.

A.2.1 Types of Concrete Pavements

The different types of concrete pavements, generally used in the United States are Jointed Plain Concrete Pavement (JPCP), Jointed Reinforced Concrete Pavement (JRCP) and Continuously Reinforced Concrete Pavement (CRCP). According to the statistics on new construction pavement types used by the agencies of various states in the United States, JPCP is the most widely used pavement type as being used by 44 states while CRCP is being used by 9 states (NCHRP, 2014). JRCP is not commonly used in the United States.

A.2.1.1 Jointed Plain Concrete Pavement (JPCP)

JPCP is unreinforced concrete pavement with transverse joints and longitudinal joints. Dowel bars are provided at transverse joints and tie bars at the longitudinal joints. Transverse joints are used to control the transverse cracking of pavement slab and the transverse joint spacing ranges between 10 to 20 ft. Dowel bars increases the load transfer efficiency (Caltrans 2015). JPCP can be designed with PMED.

A.2.1.2 Jointed reinforced concrete pavement (JRCP)

Jointed reinforced concrete pavement (JRCP) is constructed with transverse joints and reinforcing steel. The transverse joint spacing ranges between 25 to 50 ft. Reinforcing steel is used to control cracking. Dowel bars help in load transfer across transverse joints. The use of JRCP is lesser as compared to JPCP and CRCP. These pavements cannot be designed using PMED.

A.2.1.3 Continuously reinforced concrete pavement (CRCP)

CRCP is typically used for interstate applications where high traffic loads are expected. Reinforcing steel is placed throughout the slab width and length, providing continuous reinforcement. These steel bars are spaced relatively close together to help provide support for transverse cracks, as well as to effectively limit the width of cracks as they form. CRCP has no transverse joints. CRCP is a durable highway which can provide an effective service life of 40 years or more. CRCP can be designed using PMED software.

A.3 Concrete Materials

Concrete is composed of cementitious materials, coarse aggregate, fine aggregate, water, and admixtures. Most of the concrete properties are materials dependent. The percentage range of the volume of concrete constituents is shown in Figure 1.

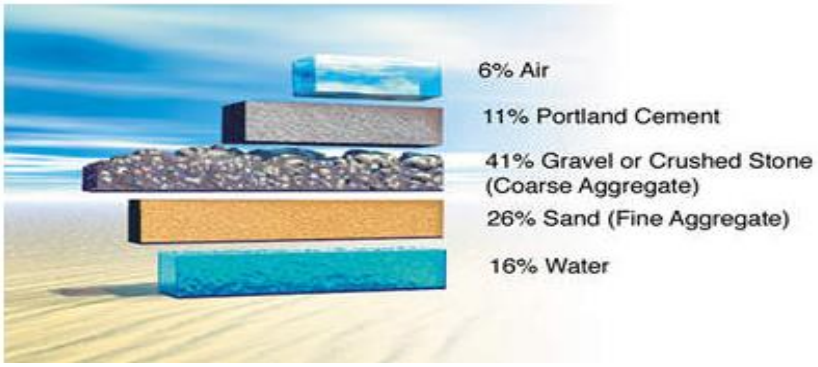

Fig 1: A typical concrete mixture design by volume

A.3.1 Cementitious Materials

Cementitious material comprises Portland cement and supplementary cementitious materials (SCM). Portland cement consists of lime, iron, silica, and alumina. Different types of cement have varying physical and chemical properties. SCMs are used to lower the demand for cement. It also improves workability and durability properties.

A.3.2 Aggregate

Aggregates constitute around 70% of the total volume of concrete thus it has a significant effect on the mechanical and thermal properties of concrete. Coarse aggregates are crushed rock or gravels that are retained by a No. 4 sieve and fine aggregates are usually sand, passing a No. 4 sieve.

A.3.3 Water

Water with no pronounced taste or odor is used for concrete. Water is tested according to AASHTO T-26. Water with a PH value of 6.0 to 8.5 should be used. The water to cementitious ratio (w/c) is an important parameter contributing to the concrete strength.

A.3.4 Admixtures

Different types of admixtures are used in concrete to obtain specific concrete mixture properties. Some chemical admixtures are used to increase workability or strength gain rate. Air-entraining admixtures create a matrix of air bubbles inside concrete so that water in the concrete can expand when frozen or contract when thawed. Chemical admixtures must comply with AASHTO M 194.

A.4 History of Pavement Design

The American Association of State Highway Officials (AASHO) was established in Dec 1914, with the purpose to "study the various materials, methods of construction and maintenance, and other highway problems of the United States for the purpose of conserving the capital invested in highway construction and maintenance by producing the highest possible efficiency". To meet these objectives, a large-scale pavement test was conducted, from 1958 to 1960, known as the AASHO Road Test. These tests consisted of constructing six test loops, where each segment consisted of a four-lane divided highway. A test section containing both flexible and rigid pavements was specified in each of these loops. Each test section had different pavement layers to help analyze the influence of different structural variables on pavement performance. Variables included surface layer thickness, base layer thickness, and subgrade thickness.

The tests were conducted for 2 years with varying vehicle types consisting of different axle configurations and weights. These vehicles were routinely driven on the test loops and a total accumulation of 1,114,000 axle-load applications was obtained.

The pavement sections were continually tested for serviceability and performance as deterioration occurred over the test period. These data became the basis for future design guides produced by AASHO. AASHO was officially renamed to the American Association of State Highway and Transportation Officials (AASHTO) in Nov 1973.

A.4.1 AASHTO Pavement Design Guides

The development of pavement design guides started in 1960s with the release of the AASHO Interim Guide for the Design of Rigid Pavement Structures (1962). With the advent of new test methods, materials and ongoing research, several revised pavement design guides were developed. These revised versions included AASHO Interim Guide for the Design of Pavements (1972); AASHTO Rigid Pavement Design Revisions (1981); AASHTO Guide for Design of Pavement Structures (1986); AASHTO Guide for Design of Pavement Structures (1993); AASHTO Guide for Design of Pavement Structures, Supplement (1998); AASHTO Mechanistic–Empirical Pavement Design Guide; and AASHTOWare Pavement ME Design (PMED) (2011).

A.4.2 Pavement Mechanistic Empirical Design

Pavement ME design, PMED (previously known as MEPDG) is the latest tool for design and performance analysis of all types of pavement systems including JPCP, CRCP, and concrete overlays. It is based on mechanistic-empirical design concepts meaning that the design procedure calculates pavement responses such as stresses, strains, and deflections under axle loads and climatic conditions and then accumulates the damage over the design analysis period. The procedure then empirically relates calculated damage over time to pavement distresses and smoothness based on the performance of actual projects throughout the United States. ME design uses a mix of algorithms and models to characterize new or existing pavement foundation, structure, layer materials, traffic, and climate and simulate stress/strains/deflection due to the interactions between applied traffic load and climate. The resulting damage manifested as different performance parameters over the design life of a pavement is then calculated (Mallela et al. 2014).

The design of rigid pavements using PMED is dependent on various material properties of concrete which affect the pavement performance over the service life. In a recent study of the sensitivity of various factors on rigid pavement performance, the coefficient of thermal expansion (CTE) of concrete was identified as a major factor that had a measurable

impact on the concrete pavement's performance over time (Schwartz et al. 2013). Thus, accurate determination of concrete mechanical and thermal properties is necessitated for accurate design of rigid pavements which can perform effectively through its service life.

A.4.3 Hierarchical Input Levels for Pavement ME

The input levels in PMED are used to categorize the designer's knowledge of the input parameter. Three levels are available to input the concrete material properties (AASHTO 2008).

Level 1 input scheme is the most accurate one and consist of laboratory tested data of the specific concrete mixture to be used for the project. This level has the highest testing and data collection costs.

Level 2 inputs are estimated from correlations or regression equations. These input values are calculated from other site-specific data or parameters that are less costly to measure. These values may represent measured regional values.

Level 3 inputs are based on the best estimated or default values. This input level has the lowest testing and data collection costs, but it may result in inaccurate pavement design.

A.4.4 Performance Indicators for Jointed Plain Concrete Pavements

The performance indicators for JPCP are joint faulting, transverse cracking and IRI. According to PMED, the threshold limit for IRI is 172 in/mile, for mean joint faulting is 0.12 in and for slabs cracked with transverse cracking is 15%.

A.4.4.1 Transverse Joint Faulting

Joint faulting is the differential elevation across the transverse joint. Mean joint faulting of all transverse joints is the parameter predicted by the Pavement ME. The unit of faulting is inches. The major impact of faulting is on ride quality. Faulting is the result of repeated traffic load applications, poor load transfer, moisture beneath pavement slab, erosion of the supporting base/subbase, subgrade material, and upward curling of the slab (Bautista et al. 2008).

Joint Faulting Model

Transverse joint faulting is the differential elevation across the joint measured approximately 0.3 m from the slab edge. Since joint faulting varies significantly from joint to joint, the mean faulting of all transverse joints in a pavement section is the parameter predicted by the ME design software. The unit of faulting is mm or inch. ME design uses an incremental approach method for calculation of mean transverse joint faulting. Based on this method, faulting values for each month is calculated and summed, beginning with the traffic opening date, to determine the faulting value at any time. Transverse joint faulting prediction is calculated from the following set of equations (AASHTO 2008):

$$Fault_m = \sum_{i=1}^{m} \Delta Fault_i \quad (1)$$

$$\Delta Fault_i = C_{34} \cdot (FaultMax_{i-1} - Fault_{i-1})^2 \cdot DE_i \quad (2)$$

$$FaultMax_i = FaultMax_{i-1} + (C_7 / 10^6) \sum_{j=1}^{m} DE_j \cdot \log(1 + C_5 \cdot 5^{Erod})^{C6} \quad (3)$$

$$FaultMax_0 = C_{12} \cdot \delta_{curl} \cdot [\log(1 + C_5 \cdot 5^{Erod}) \cdot \log(\frac{P_{200} \cdot Wetdays}{P_s})]^{C6} \quad (4)$$

where $Fault_m$ = Mean joint faulting at the end of month m; $\Delta FAULT_i$ = Incremental change (monthly) in mean joint faulting during month I; $FaultMax_i$ = Maximum mean transverse joint faulting for month I; $FaultMax_0$ = Initial maximum mean transverse joint faulting; Erod = Base/subbase erodibility factor; DE_i = Differential density of energy of subgrade deformation accumulated for month I; δ_{curl} = Maximum mean monthly slab corner upward deflection in PCC due to temperature curling and moisture warping; Ps = Overburden on subgrade; P_{200} = Percent subgrade material passing #200 sieve; Wet Days = Average annual number of wet days; C1, 2, 3, 4, 5, 6, 7, 12, 34 = Calibration coefficients

A.4.4.2 Transverse Cracking in Concrete Slabs

There are two types of transverse cracking in JPCP namely top-down transverse cracks and bottom-up transverse cracks. When there is a positive temperature gradient in the pavement slab resulting in downward curling of the slab and the truck axles are near midway between the transverse joints, a critical bending stress occurs at the bottom center of the

slab. Repeated loadings in such an arrangement result in fatigue damage, which results in a transverse crack. The factors that affect bottom-up cracking are CTE of concrete, slab thickness, joint spacing and concrete strength (NCHRP 2003).

When the pavement is exposed to a negative temperature gradient it results in upward curling of the pavement slab. During this condition when the axles load opposite ends of the slab, a tensile bending stress occurs at the top of the slab. Such repeated loadings will result in fatigue damage and initiation of top-down crack in the pavement slab.

Transverse Cracking Model

This parameter is calculated as a percent of slabs with transverse cracks and combines the percentage of slabs with top-down transverse cracks and the percentage of slabs with bottom-up transverse cracks. Bottom-up cracking occurs when the truck axles are near the longitudinal edge of the slab, midway between the transverse joints, critical tensile stress occurs at the bottom of the slab under the wheel load. This stress increases greatly when there is a high-positive temperature gradient through the slab (the top of the slab is warmer than the bottom of the slab). Repeated loadings of heavy axles under those conditions result in fatigue damage along the bottom edge of the slab, which eventually results in a transverse crack that propagates to the surface of the pavement.

Top-down cracking is a result of repeated loading by heavy trucks when the pavement is exposed to high negative temperature gradients (the top of the slab cooler than the bottom of the slab). It eventually results in a transverse crack that is initiated on the surface of the pavement. The critical wheel loading condition for top-down cracking involves a combination of axles that loads the opposite ends of a slab simultaneously. In the presence of a high-negative temperature gradient, such load combinations cause high-tensile stress at the top of the slab near the critical pavement edge. Major factors that affect transverse cracking are CTE of PCC, slab thickness, joint spacing, slab widening, and concrete strength (NCHRP 2003).

Transverse slab cracking predictions are calculated from a set of equations as follows (AASHTO 2008):

$$\log(N_{allowable}) = C_1\left(\frac{MOR}{\sigma_{PCC}}\right)C_2 \quad (5)$$

$$Crack = \frac{100}{1 + C_4 * \left(\frac{N_{applied}}{N_{allowable}}\right)^{C_5}} \quad (6)$$

where MOR = Modulus of rupture of the concrete; σ = Critical stress in the slab; $N_{applied}$ =Applied number of load applications; $N_{allowable}$ = Allowable number of load applications; C_1, C_2, C_4, C_5 = Calibration coefficients Total transverse cracking predictions are calculated as follows (AASHTO 2008).

$$T_{crack} = (Crack_{bottom-up} + Crack_{top-down} - Crack_{bottom-up} * Crack_{top-down}) * 100 \quad (7)$$

where T_{crack} = Total transverse cracking (percent); $Crack_{Bottom\text{-}up}$ = Predicted amount of bottom-up transverse cracking (fraction); $Crack_{Top\text{-}down}$ = Predicted amount of top-down transverse cracking (fraction)

There are four calibration coefficients which can be categorized into two groups. C_1 and C_2 are related to the stress ratio (MOR/σ) for fatigue damage estimation and C_4 and C_5 are in the transverse-cracking transfer model to convert fatigue damage estimations into transverse-cracking predictions.

A.4.4.3 International Roughness Index (IRI)

Pavement roughness is an expression of irregularities in the pavement surface which affect the ride quality. Roughness is generally expressed as international roughness index (IRI). IRI is a characteristic of the longitudinal profile of a traveled wheel-track and constitutes a standardized roughness measurement. The recommended units are meters per kilometer (m/km) or inch per mile (in/mile). Pavement ME uses such a performance model to predict IRI. This model considers initial IRI, percentage of slabs with transverse cracking and total joint faulting to predict IRI value (Abd El-Hakim and El-Badawy 2013). Both an initial IRI and terminal IRI must be selected for any design project. The terminal IRI typically selected is similar to that used in pavement management to establish when roadways require rehabilitation (Mallela et al. 2014).

Pavement Roughness Model

Pavement roughness is generally defined as an expression of irregularities in the pavement surface that adversely affect the ride quality of a vehicle. Roughness is an important pavement characteristic because it affects not only ride quality but also vehicle delay costs, fuel consumption, and maintenance costs. Roughness is typically quantified using international roughness index (IRI) and it is used to define a characteristic of the longitudinal profile of a traveled wheel-track and constitutes a standardized roughness measurement. The commonly recommended units are cm/km or in/mile.

The Pavement ME design IRI prediction model for JPCP systems consists of the transverse cracking prediction, the joint faulting prediction, the spalling prediction, and a site factor, along with calibration coefficients. IRI prediction model is as follows:

$$IRI = IRI_{ini} + C_1 \cdot Crack + C_2 \cdot Spall + (C_3 \cdot Fault \cdot 5280 / JSP) + C_4 \cdot SF \quad (8)$$

Where IRI = Predicted IRI; IRI_{ini} = Initial smoothness measured as IRI; $Crack$ = Percent slabs with transverse cracks (all severities); $SPALL$ = Percentage of joints with spalling (medium and high severities); Fault = Total joint faulting cumulated; SF = Site factor; $C_{1, 2, 3, 4}$ = Calibration coefficients; JSP = Transverse joint spacing

A.4.5 Characterization of Portland Cement Concrete Materials for Rigid Pavement Design

Different material properties including elastic modulus, Poisson's ratio, flexural strength, coefficient of thermal expansion, unit weight, air content, thermal conductivity, heat capacity, ultimate shrinkage, etc. are used to characterize PCC materials within the PMED framework for the design of rigid pavements. Key parameters can be determined for each PCC mixture design through laboratory testing. These key parameters are used by the analytical models for critical response calculations, for damage calculations, and for performance predictions. One of the features of the PMED software is its ability to use the default, regional, or site-specific values for materials data inputs. Table 1 shows a summary of the requirement of PCC material properties for Level-1 design process according to AASHTO design guide, 2021. Table 2 outlines the PCC material inputs for Level-2 and Level-3 design criteria.

NCHRP conducted a survey in 2014 regarding the use of default, regional, and site-specific values for various material inputs by various agencies in the United States. According to the results, most agencies were using either the ME default values or regional values. Relatively few agencies indicated the use of site-specific/Level-1 inputs.

Table 1. Level-1 PCC material inputs for rigid pavement design (AASHTO, 2021)

Design Type	Measured Property	Source of Data		Recommended Test Protocol and/or Data Source
		Test	Estimate	
New PCC and PCC overlays and existing PCC when subject to a bonded PCC overlay	Elastic modulus	X		ASTM C469
	Poisson's ratio	X		ASTM C469
	Flexural strength	X		AASHTO T 97
	Indirect tensile strength (CRCP only)	X		AASHTO T 198
	Unit weight	X		AASHTO T 121
	Air content	X		AASHTO T 152 or T 196
	Coefficient of thermal expansion	X		AASHTO T 336
	Surface shortwave absorptivity		X	Use AASHTOWare Pavement ME Design defaults
	Thermal conductivity	X		ASTM E1952 (or use AASHTOWare Pavement ME Design defaults)
	Heat capacity	X		ASTM D2766 (or use AASHTOWare Pavement ME Design defaults)
	PCC zero-stress temperature		X	National test protocol not available. Estimate using agency historical data or select AASHTOWare Pavement ME Design defaults
	Cement type		X	Select based on actual or expected cement source
	Cementitious material content		X	Select based on actual or expected concrete mix design
	Water to cement ratio		X	Select based on actual or expected concrete mix design
	Aggregate type		X	Select based on actual or expected aggregate source
	Curing method		X	Select based on agency recommendations and practices
	Ultimate shrinkage		X	Testing not practical. Estimate using prediction equation in AASHTOWare Pavement ME Design
	Reversible shrinkage		X	Estimate using agency historical data or select AASHTOWare Pavement ME Design defaults
	Time to develop 50 percent of ultimate shrinkage		X	Estimate using agency historical data or select AASHTOWare Pavement ME Design defaults

Table 2. Level-2 & 3 PCC material inputs for rigid pavement design (AASHTO, 2021)

Material Property	**Level-2**	**Level-3**
Compressive Strength	7, 14, 28, 90 days	28 days
Elastic Modulus	Optional	Nil
Modulus of Rupture	Optional	Nil
Poisson's Ratio	Default	Default
Coefficient of Thermal Expansion	Default	Default
Thermal Conductivity	Default	Default
Heat Capacity	Default	Default

A.4.6 Coefficient of Thermal Expansion and Rigid Pavement Design

A.4.6.1 Coefficient of Thermal Expansion (CTE)

CTE is a measure of concrete's expansion or contraction with a change in temperature. It is usually expressed in micro-strains per unit temperature change. The test method to determine the CTE is AASHTO T-336 (Tanesi et al. 2010). The importance of CTE in rigid pavement design came to the forefront after the advent of PMED. The CTE of PCC ranges from about 3.5 to 6.5 micro-strains/°F for the mixtures cast with different coarse aggregates. In the absence of CTE test data, an average value of 5.5 micro-strains/°F is commonly used in the design process.

As aggregates are the main component of concrete thus CTE value of concrete also depends upon the type of coarse aggregate. Concrete containing limestone aggregate has a lower CTE than concrete containing siliceous aggregate. S. Jahangirnejad and his team conducted research on CTE of PCC produced with various types of aggregates. They concluded that the magnitude of the measured CTE of PCC varies with aggregate geology. The CTE of hardened cement paste, which is a function of factors such as water to cement ratio, cement fineness, and cement composition, also affects the CTE of concrete (Jahangirnejad et al. 2009). Hak-Chul Shin and Yoonseok Chung found that the measured CTEs at various ages (3, 5, 7, 14, 28, 60, 90 days) fluctuates within 0.2 micro-strain/°F (0.36 micro-strains/°C) and the age of concrete, statistically have no significant effect on CTE (Shin et al. 2011).

A.4.6.2 Importance of Coefficient of Thermal Expansion in Rigid Pavement Design

CTE of PCC is a very important parameter in concrete pavement design and analysis because the magnitudes of temperature related pavement deformations are directly proportional to this value. These deformations affect the resulting curling stresses in the hardened slab. Accurate values of the CTE are required to predict potential thermally induced movements in a concrete pavement. J. Mallela et al. (2005) found that higher transverse and longitudinal fatigue cracking is caused by higher curling stresses and higher amounts of faulting is caused by loss of slab support due to curling. Huang (2004) indicated that concrete pavement distresses are directly related to the thermal properties of concrete.

The magnitude of curling and respective stresses are dependent on the CTE of concrete. The downward curling of a concrete pavement slab happens with a positive temperature gradient through the thickness of the slab, which means that top surface of the slab is at a higher temperature than the bottom of the slab (usually happens during the daytime). This results in downward curling of the pavement slab and slab lift off from the center that makes the pavement slab unsupported from the center. When wheel load is at the top center of the slab, tensile stress is generated at the bottom center of the slab. These repeated tensile stresses cause bottom-up cracking of the pavement slab.

Similarly, when there is a negative temperature gradient in the pavement slab (usually during night time), the slab curls upward and with wheel loads at the edges results in tensile stresses at the top center of the slab, which causes top-down cracking of pavement slab on repeated applications. The upward curling of the pavement slab due to a negative thermal gradient also results in slab lift-off at the transverse joints and creates void spaces between the slab edges and the sub-layer. The sublayer gets exposed to the ingress of moisture and with repetitive heavy traffic loading, the sublayer starts to erode resulting in joint faulting. Higher CTE means the higher probability of curling causing higher pavement distresses during the design life if other conditions remain the same.

The magnitude of temperature related pavement deformations is directly proportional to the CTE value during early ages as well as during the pavement design life. These deformations, in combination with the restraint offered by the base layer and slab weight, affect the resulting curling stresses in the hardened slab both during the early stages and in the long term. Using an inaccurate value of CTE may, therefore, lead to erroneous assumptions about the pavement's thermal response and possible distress. One of the keys to characterize the effects of thermal properties on a concrete pavement's structure is to account for thermal movements. Accurate values of the CTE are needed to predict potential thermally induced movements in a concrete pavement. J. Mallela et al. found that CTE affects the following aspects of pavement performance (Mallela et al. 2005):

- Early-age or premature cracking, if the excessive longitudinal slab movement (i.e. movement in the direction of traffic) caused by high CTE concrete is resisted by restraint forces (e.g., slab–base friction).
- Higher mid-panel transverse and longitudinal fatigue cracking caused by higher curling stresses.
- Higher amounts of faulting caused by a greater loss of slab support, larger joint openings during adverse seasons, and greater corner deflections from curling.

Tanesi et al. (2008) determined the effect of the variability of the CTE on the predicted pavement performance. They performed a sensitivity analysis by varying the CTE values on JPCP and found that with the increase in CTE value, the percentage of cracked slabs also increases. Hein (2012) described that thermal expansion and contraction of a concrete

pavement can have a significant effect on its performance. Thermal contraction can result in transverse cracking of slabs depending on the joint spacing. Thermal effects also impact slab bending and curling and when joints/edges are curled upwards, they do not have full contact with the base and are subject to cracking under traffic loading. This could be particularly significant for long, thin slabs under heavy, frequent loading. The results of the sensitivity analysis indicate that the selection of the appropriate value for the coefficient of thermal expansion is important in the consideration of rigid concrete pavements. He gave the following conclusions from his analysis:

• The CTE significantly impacts the amount of joint faulting.
• The CTE has a lesser impact on the percentage of cracked slabs. However, the percentage of crack slabs increases as the slab width is reduced and the traffic level is increased.
• Variation in the CTE has a lesser impact on the projected roughness of the pavement.

A.4.7 Factors Affecting the Coefficient of Thermal Expansion (CTE) of Concrete

The CTE of a concrete paving mixture depends significantly on the aggregate type and degree of saturation. Since coarse aggregate makes up the bulk of the volume of concrete, the most influential factor in the CTE of the concrete is the CTE of the coarse aggregate. Quartz has the highest CTE of the coarse aggregate types commonly used in concrete pavement construction, and the CTEs of other commonly used coarse aggregate types depend largely on their quartz content. The coarse aggregate has the most effect on the CTE value, but the fine aggregate is also a factor. Natural sands are typically high in silica (high CTE) and manufactured/crushed limestone fine aggregates are lower in CTE. The range of CTE values for different concretes reflects the variation in the CTE of the concrete's component materials. In general, CTE of cement paste lies between 6.1 to 11.1 micro-strains/°F, which may be twice that of the CTE of aggregate (Meyers 1951). However, the CTE of concrete is dominated by the CTE of aggregate because of the high volume of aggregate in the concrete. Other variables influencing the CTE of concrete are the type of coarse aggregate, the age of the paste, and the distribution of moisture within the pore structure (Sellevold and Bjontegaard 2006).

A.4.7.1 Effect of aggregates

Aggregate mineralogy and volume are major factors that affect concrete CTE. Dettling (1964) found that the concrete with quartzite as coarse aggregate has the highest CTE and the one with limestone has the lowest CTE. Concrete CTE is dependent on the CTE of the aggregate (Mehta and Monteiro 2006). Won (2005) tested the CTE from various aggregate sources. Even the concrete with the same type of aggregates showed different CTE values, which shows the impact of an aggregate's mineralogical composition on CTE. Won (2005) also studied the impact of aggregate volume on the CTE and found that CTE decreases as the volume of coarse aggregate increases because it reduces the volume of the cement paste. As cement paste has higher CTE than aggregate so concrete CTE can be reduced by reducing cement paste volume.

Mindess et al. (2002) found that the CTE of any coarse aggregate depends on its silica content. Higher silica content results in higher CTE like river gravel or quartz whereas lower silica content will give lower CTE such as limestone. McCullough et al. (2000) studied the effect of mineralogical composition on the CTE of aggregate and found that an increase in silicon oxide content results in CTE increase. Neville and Brooks (1987) found that the CTE of concrete decreases when aggregate volume increases.

A.4.7.2 Effect of moisture content and relative humidity

Moisture content and relative humidity have a significant effect on CTE of cement paste and concrete (Chung and Shin 2011). Emanuel and Hulsey (1977) documented the effect of moisture content on the CTE of cement paste. They found that peak CTE occurs at 60 to 70% moisture content. Chung and Shin (2011) found that the peak CTEs for expansion and contraction were obtained at about 65 and 85% relative humidity, respectively. Yeon et al. (2009) found that the maximum CTE of concrete was obtained at 80% relative humidity.

A.4.7.3 Effect of water-to-cement ratio

Different researchers have a different opinion regarding the effect of water to cement ratio on CTE of concrete. Berwanger and Sarkar (1976) found that CTE of concrete decreases with increased water to cement ratio. Alungbe et al. (1992) conducted experimental work and found that there is no effect of water to cement ratio on the CTE of concrete.

A.4.7.4 Effect of concrete paste content and composition

The cement paste has a higher CTE than most of the aggregate types thus CTE of concrete increases when cement paste increases (Bonnell and Harper 1950). Hossain at al. (2006) also confirmed these findings. Bonnell and Harper (1950) also studied the effect of cement type on the CTE of concrete and found that blast-furnace cement has higher CTE in

comparison to high-alumina cement. Emanuel and Hulsey (1977) observed that when the cement fineness increases so CTE also increases.

A.4.7.5 Effects of concrete age on CTE

Many researchers worked on the effects of different variables including concrete age on CTE values of concrete mixtures but found contradicting conclusions. Some researchers opine that the CTE remains statically constant with concrete age but others say that age has a considerable effect on CTE of concrete. A brief description of previous studies is presented in this section.

Alungbe et al. (1992), conducted experimental work on the effects of aggregate type and concrete age on the magnitude of CTE. Three types of aggregate were investigated including porous limestone, dense limestone, and river gravel. Three combinations of water to cement ratio and cement content were studied as well as two curing durations (28 and 90 days). Another variable was the specimen condition with two levels, water-saturated, and oven-dried. A length comparator was used to measure the length changes of specimens. The specimens were square prisms with dimensions of 3 x 3 x 11.25 in. In this study, the concrete samples with porous limestone as coarse aggregate, had a CTE that ranged from 5.42 to 5.80 με/˚F, concrete samples produced from dense limestone had a range of 5.82 to 6.14 με/˚F, and concrete samples made of gravel coarse aggregate had a CTE range of 6.49 to 7.63 με/˚F. A statistical analysis (factorial design) was used to study the effect of different variables on CTE magnitude. Based on statistical analysis, the authors concluded that aggregate type significantly affects the CTE value, but water to cement ratio and cement content have no effect on the CTE. There was no significant difference between samples with different curing durations in water-saturated specimens. However, the CTE values of the 28-day cured specimens were higher than the value of 90-day cured samples in oven-dried specimens.

Won (2005) evaluated the effect of coarse aggregate type on the CTE along with the effect of concrete age, and size of the specimen. The CTE calculation method was different from the TP60 protocol and was based on a regression analysis between temperature and displacement readings. Concrete cylinders were tested over a period of 3 weeks and it was found that the age of concrete had little effect on CTE for up to three weeks. For the effect of aggregate type on the CTE value, it was indicated that concrete specimens fabricated using the limestone aggregate sources had CTE values of about 4.44 με/˚F with a variability of 0.4 με/˚F whereas, concrete specimens fabricated with gravel as coarse aggregate had a CTE range of 4.5 to 7.2 με/˚F. It was concluded that this variability is attributed to the different geological make-up of the gravel sources.

Tran et al. (2008) evaluated the effects of mixture properties on concrete CTE. Twelve concrete mixtures were prepared using four aggregate types including limestone, sandstone, syenite, and gravel. For each mixture, three replicates were fabricated and the samples were tested at 7 and 28 days. The range of the CTE values was approximately 5 to 7 με/˚F. The mixtures made with limestone and syenite had the lowest average CTE of about 5.2 με/˚F while mixtures made with gravels had the highest average CTE value of approximately 6.9 με/˚F. After conducting a multi-factor analysis of variance (ANOVA) on mixture properties, it was reported that the aggregate type had a pronounced effect on the CTE. The fully saturated concrete specimens showed no significant difference in their respective CTE values at 7 and 28 days.

Shin and Chung (2011) investigated the effects of age on CTE, by measuring the CTE at 3, 5, 7, 14, 28, 60, and 90 days for concrete prepared with different aggregates. They concluded that the CTE at different ages of the mixtures fluctuated within 0.2 με/°F and verified by the statistical analysis (ANOVA) that there was no significant difference due to concrete age but this statistical analysis cannot be compared with the effects on pavement performance.

Kim et. al (2013) found with Statistical analyses of the experimental data that the CTEs measured at 120 days are significantly lower than those measured at 28 days. They concluded that the magnitude of the measured CTE is significantly (statistically) influenced by the age of the sample at the time of testing.

Havel et al. (2014) conducted a CTE experimental study on concrete mixtures with three Basaltic coarse aggregates. They performed CTE testing at the age of 28 and 56 days and confirmed that CTE values of paving mixtures vary with age of specimens. Jeong et al. (2012) performed their research on one concrete mixture with sandstone as coarse aggregate. They used one cylindrical sample to observe CTE variation with age and implied that there is no CTE variation after the age of 10 hours up to the age of 180 days. They did not follow the standard test protocol for their testing.As concrete is a composite material comprising aggregates, water and cement. Cement and water make the cement paste. Thus, concrete CTE is dependent on CTE of hardened cement paste and CTE of aggregates. CTE of hardened cement paste is caused by internal re-distribution of water between capillary pores and gel pores (Helmuth 1961; Bazant 1970; Sellevold 2006). Volume of these pores varies with the age/hydration process (Mindess 2002; Neville 2011) thus it can be assumed that CTE varies with concrete age. The rising temperature causes immediate expansion due to increased pore water pressure in gel pores followed by a gradual flow of water out of the gel pores to capillary pores causing contraction. The immediate expansion of gel pores causes thermal expansion of concrete or CTE. Since, the volume of gel pores increases with the concrete age/hydration process thus, CTE of concrete increases with concrete age. The hydration process in concrete is a

slow process which almost culminates at 360 days thus it is viable to assume that CTE values may varies up to 360 days of concrete age.

A.4.8 CTE prediction models

Concrete is a composite mixture of cement, coarse aggregate, fine aggregate, and water. A volumetric schematic of a concrete mixture is shown in Figure 2. CTE of concrete is dependent on its constituents as different constituents have different CTEs. Various prediction models for determination of CTE of concrete have been proposed in the literature. Emanuel and Hulsey (1977) proposed a CTE model based on the volumetric weighted average of the constituents. The model can be described as shown in Eq. 9.

$$\alpha_T = f_T[f_M \cdot f_A \cdot \beta_P \cdot \alpha_S + \beta_{FA} \cdot \alpha_{FA} + \beta_{CA} \cdot \alpha_{CA}] \quad (9)$$

Where, α_T = CTE of concrete

f_T = correction factor for temperature alternations (considered unity for controlled environment)

f_A = correction factor for age based on moisture content (considered unity up to 6 months age)

β_P = proportion by volume of cement paste

α_S = CTE of saturated cement paste

β_{FA} = proportion by volume of fine aggregate

α_{FA} = CTE of fine aggregate

β_{CA} = proportion by volume of coarse aggregate

α_{CA} = CTE of coarse aggregate

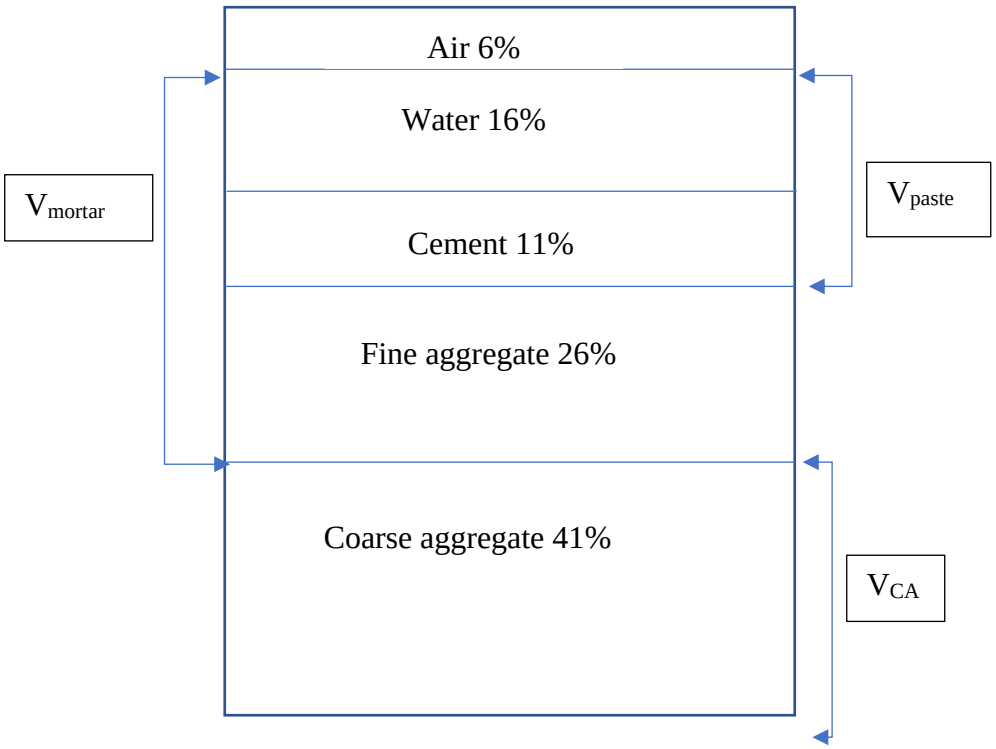

Fig 2: Average percentage of concrete constituents.

Another model was proposed by Neekhra et al. (2004) (based on the concept of Hirsch's composite model) for determination of CTE of concrete. CTE of mortar and coarse aggregate are the two main inputs. The model is shown in Eq. 10.

$$\alpha_T = X(\alpha_m \cdot V_m + \alpha_a \cdot V_a) + (1-X)\frac{\alpha_m \cdot V_m \cdot E_m + \alpha_a \cdot V_a \cdot E_a}{V_m \cdot E_m + V_a \cdot E_a} \quad (10)$$

Where, $\alpha_T, \alpha_m, \alpha_a$ = CTE of concrete, mortar and coarse aggregate respectively

V_m, V_a = volume fraction of mortar and coarse aggregate

E_m, E_a = elastic modulus of mortar and aggregate

X = relative proportions of material conforming with an upper and lower bound solution (considered as 0.5)

Pavement ME design uses a CTE prediction model based on concrete mixture volumetrics as shown in Eq. 11 (AASHTO 2008).

$$\alpha_T = \alpha_{CA} \cdot V_{CA} + \alpha_{paste} \cdot V_{paste} \quad (11)$$

where

$\alpha_T, \alpha_{CA}, \alpha_{paste}$ = CTE of concrete, coarse aggregate and cement paste respectively

V_{CA}, V_{paste} = volume fraction of coarse aggregate and cement paste

It is evident that all of these models do not consider concrete age in the determination of CTE of concrete which has a significant effect on CTE thus there is a need to include concrete age factor in CTE prediction model.

A.4.9 CTE Incorporation in PMED

The stress/strain relation with regards to CTE is generally expressed as follows:

$$\sigma_T = (\alpha_T \cdot \Delta_T) \cdot E_{PCC} \quad (12)$$

$$\varepsilon_T = \alpha_T \cdot \Delta_T \quad (13)$$

Where, α_T = CTE of concrete

σ_T = stress due to thermal gradient

Δ_T = temperature difference between top of the slab and bottom of the slab

E_{PCC} = elastic modulus of concrete

ε_T = strain due to temperature gradient

Pavement ME design uses an extended form of this relation to determine the bending stress at the bottom surface of the pavement slab by combining the stresses due to thermal gradient and the stresses due to traffic loading to quantify the pavement slab distresses with the help of performance prediction models. The bending stress at the bottom surface of the pavement slab is a function of various factors including CTE of concrete as shown in Eq. 14 (NCHRP 2003). This also signifies the importance of CTE in the pavement design and performance prediction process.

$$\sigma_{PCC} = f(\alpha_T, \Delta_T, E_{PCC}, h_{PCC}) \quad (14)$$

Where,

σ_{PCC} = bending stresses at the bottom surface of pavement slab

α_T = CTE of concrete

Δ_T = temperature difference between top of the slab and bottom of the slab

E_{PCC} = elastic modulus of concrete

h_{PCC} = pavement slab thickness

As described earlier, the faulting distress is dependent on upward curling of the pavement slab and the magnitude of curling is a function of various factors including CTE of concrete as shown in Eq. 15 (NCHRP 2003). Higher CTE combined with negative temperature gradient will result in higher upward curling of the overlay slab which will produce a greater amount of joint faulting.

$$\delta_{curl} = f(\alpha_T, \Delta_T, h_{PCC}, JSP, l, k, \mu) \quad (15)$$

where

δ_{curl} = the magnitude of deflection due to curling

α_T = CTE of concrete

Δ_T = temperature difference between top of the slab and bottom of the slab

h_{PCC} = pavement slab thickness

JSP = transverse joint spacing of overlay slab

l = radius of relative stiffness of the concrete

K = modulus of subgrade reaction

u = poisson's ratio of concrete

The effects of CTE on the structural response and performance predictions (including transverse cracking, joint faulting, and international roughness index, (IRI)) can be summarized as shown in Figure 3.

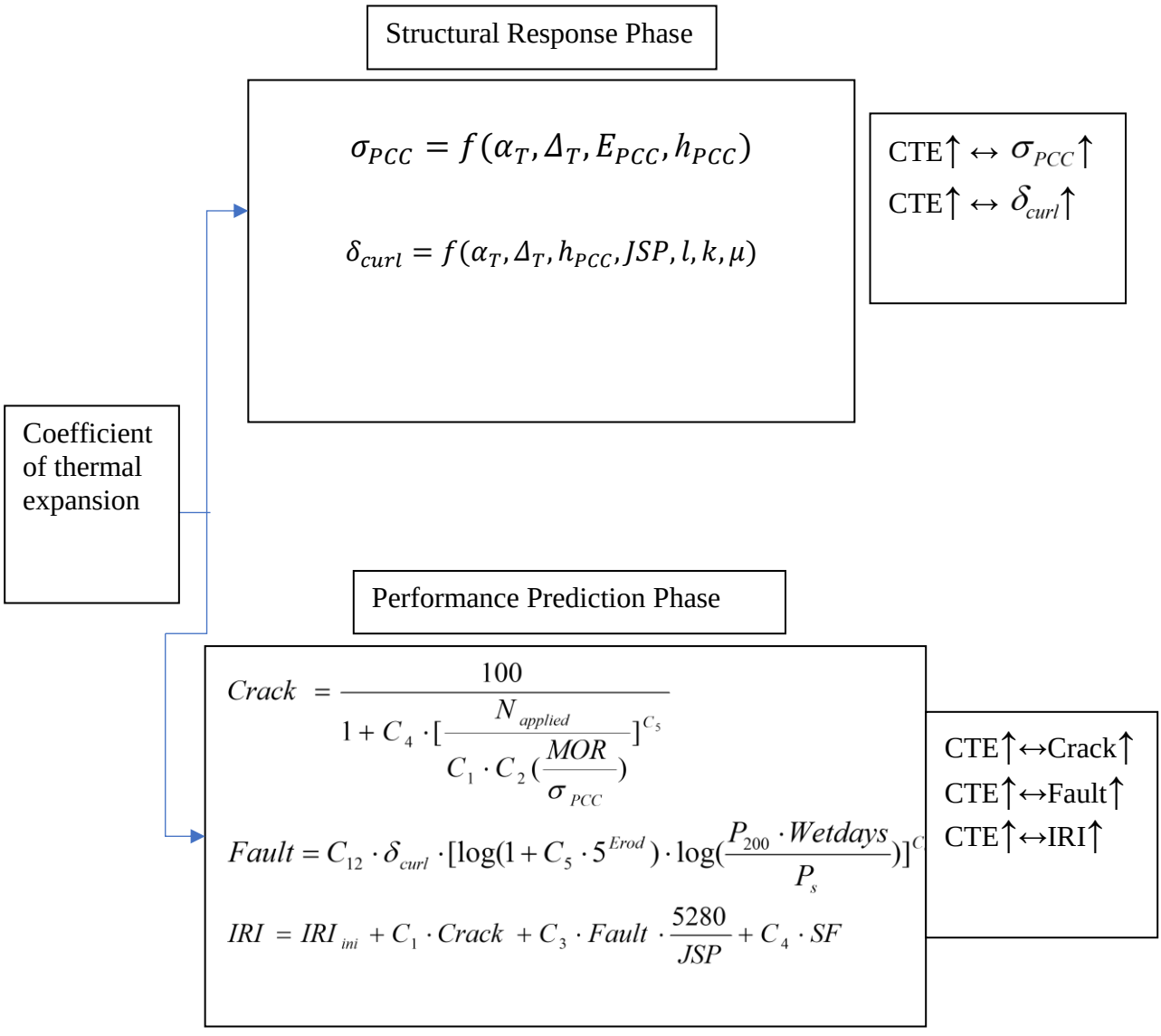

Fig 3: Effects of CTE on rigid pavement response.

A.4.10 Modulus of Elasticity and Rigid Pavement Design

A.4.10.1 Elastic Modulus

Elastic modulus measures material stiffness and is a ratio of the applied stress to measured strain. It is measured according to ASTM C 469 with a concrete cylinder loaded in longitudinal compression at a relatively slow constant rate.

American Concrete Institute (ACI) developed a relation between elastic modulus and compressive strength of concrete (at 28 days), which gives quite satisfactory results for the elastic modulus values of concrete. Typical elastic modulus of normal strength Portland cement plain concrete ranges between 2x106 to 6x106 psi (14 to 41 GPa). In general, the material characteristics affect the elastic modulus in the same manner as the compressive strength. However, the elastic modulus is more sensitive to aggregate characteristics and volumes. The higher the modulus of elasticity of the aggregate, the higher will be the elastic modulus of the concrete. The shape of coarse aggregate particles and their surface characteristics also influence the value of modulus of elasticity of concrete.

A.4.10.2 Importance of Elastic Modulus in JPCP Design

Elastic modulus of concrete is an important variable in pavement design. It controls the overall slab deflections from traffic loading and slab curling stresses. Historically, in pavement applications, this value was not rigorously estimated. The typical value of 4.2x106 psi was assumed during the design of rigid pavement because it was perceived to have little effect. However, newer design methods such as PMED has brought the importance of this parameter to the forefront. As elastic modulus is directly related to concrete strength so concrete with higher elastic modulus behaves in a better way to deal with the curling and loading stresses as compared to the concrete with lower elastic modulus.

A.4.11 Modulus of Rupture and Rigid Pavement Design

A.4.11.1 Modulus of Rupture (MOR)

The flexural strength or MOR of concrete defines the tensile capacity of concrete. Typically, concrete is not tested under direct tension because the test apparatus and the loading mechanism introduce secondary stresses that are not easy to compensate for in test results. MOR can be determined as the maximum tensile strength at rupture at the bottom of a simply supported concrete beam during a flexural test with third point loading, as standardized in ASTM C-78. This test measures the tensile capacity of the concrete in bending or flexure. MOR is influenced by mixture design parameters including water to cement ratio, cement type, cement-content, and aggregate properties.

A.4.11.2 Importance of Modulus of Rupture in Concrete Pavement

Modulus of rupture is the basis for estimating flexural fatigue in concrete. A true estimation of modulus of rupture would improve the accuracy of cracking prediction. Although modulus of rupture is an important parameter in evaluating the design of rigid pavement, it was not given due importance in the past. With the advent of PMED, a lot of emphases has been given to the accurate determination of modulus of rupture and its use in the design of rigid pavement.

A.4.12 Thermal Conductivity and Rigid Pavement Design

Thermal conductivity is the ratio of heat flux to the temperature gradient. Heat transfer in concrete is similar to that of metals due to its porous and heterogeneous nature as a solid material. Multiple factors, including aggregate type, temperature and moisture of local environment, cement paste content, coarse and fine aggregate, porosity, and admixtures affect the thermal conductivity of concrete (Kodide 2010).

The primary influencing factors of concrete thermal conductivity are aggregate type, proportion of coarse aggregate, moisture content, and the use of supplementary cementitious materials (Shin and Kodide 2012). Notably, the size and shape of the mold has no effect on PCC thermal conductivity (Shin and Kodide 2012). The aggregates were determined to play a major role in the thermal conductivity of the concrete mixtures. The mixtures containing the gravel aggregate had a much higher thermal conductivity than the mixtures containing limestone. Moisture is also a crucial factor affecting thermal conductivity in concrete specimens. Kodide (2010) also investigated the relevance of thermal conductivity on a pavement section using an PMED analysis. The study found that while there was little interaction between thermal conductivity and mean joint faulting, thermal conductivity did have an effect on transverse cracking. A higher thermal conductivity value reduced the temperature difference from the top to the bottom of the pavement structure, which caused a reduction in predicted distresses.

Bentz et al. (2011) conducted a study exploring the relationship between density and thermal conductivity in concrete mixtures. Varying amounts of fly ash were substituted for the cement to produce a lower density concrete mixture. The study demonstrated a positive correlation between density and thermal conductivity in the tested specimens. They concluded that a larger fly ash replacement percentage resulted in a lower density, which produced a lower thermal conductivity. The study went on to discover that lower thermal conductivity values result in lower thermal diffusivity. A lower thermal diffusivity allows concrete to serve as a thermal buffer and be less affected by changes in environmental temperature.

A.4.13 Heat Capacity and Rigid Pavement Design

Heat capacity is the ability of a concrete mixture to store its internal energy while being subjected to temperature change and remaining in the same physical state. Therefore, it is the actual amount of heat energy required to change the temperature of a unit mass by a single degree (Chintakunta 2007). For concrete mixtures, the water content, along with porosity also play a role in heat capacity (Kodide 2010). Heat capacity demonstrated an inverse relationship with a linear decrease in heat capacity as the moisture increased.

Fly ash has been proven to have little impact on specific heat capacity test results in concrete mixtures. Bentz et al. (2011) concluded that water content was the key factor affecting the specific heat capacity of concrete. Water's specific heat value of 4.18 J/(g K) is significantly higher than that of other concrete constituent materials and provides an explanation for water playing the largest role in specific heat capacity values for concrete mixtures.

The study performed by Chintakunta (2007) explored the sensitivity of thermal properties of pavement materials using the PMED. The study performed sensitivity analyses to identify the general behavior of the thermal properties in the PMED models and the research outcomes are as follows:

- The transverse cracking in JPCP was proven to be sensitive to both thermal conductivity and CTE, and the faulting model was sensitive to thermal conductivity and CTE. International roughness index exhibited sensitivity with respect to CTE, and thermal conductivity. These analyses proved the obvious correlations between thermal properties and common pavement distresses.
- CTE proved to be the most critical input for IRI and punchouts, while crack spacing, ultimate shrinkage strain, thermal conductivity, and climate also played a role in punchouts for CRCP structures.
- Cracking in JPCP is most affected by thermal conductivity, heat capacity, and CTE.
- Punchouts in CRCP structures are most affected by thermal conductivity, ultimate shrinkage, heat capacity, and CTE.

A.4.14 Concrete Shrinkage and Rigid Pavement Design

Due to varying moisture throughout the concrete slab, differential shrinkage may occur, causing warping, high cracking potential, and faulting. Drying shrinkage is caused by moisture changes within the concrete after it has hardened (Kosmatka and Wilson 2016). The moisture changes that occur are usually a result of humidity changes in the air surrounding the concrete or from the evaporation of water trapped within the concrete during the mixing operation. Within the pavement slab, stresses that are developed because of drying shrinkage leads to tensile cracks. The tensile stresses are due to the pavement being restrained and the tensile stresses will exceed the capacity of the concrete and crack.

The best method to limit drying shrinkage is to control the amount of water per unit concrete. Mixtures with less water have less potential for volume change due to drying shrinkage, as a result of a smaller water volume that must be evaporated. Since drying shrinkage is a paste property, it is possible to reduce the shrinkage by the appropriate selection of aggregate type and quantity, causing an increase in the hardened concrete density (Kosmatka and Wilson 2016).

A.5 References

1. AASHTO T-121. (2012). Standard Method of Test for Density (Unit Weight), Yield and Air Content (Gravimetric) of Concrete.
2. AASHTO T-152. (2013). Standard Method of Test for Air Content of Freshly Mixed Concrete by the Pressure Method.
3. AASHTO. (2008). "Mechanistic-Empirical Pavement Design Guide, A Manual of Practice." American Association of State Highway and Transportation Officials.
4. Abd El-Hakim, R., and S. El-Badawy. (2013). International Roughness Index Prediction for Rigid Pavements: An Artificial Neural Network Application. *Advanced Materials Research*, Vol. 723, pp. 854–860.
5. Alungbe, G. D., M. Tia, and D. G. Bloomquist. (1992). Effects of Aggregate, Water/Cement Ratio, and Curing on the Coefficient of Linear Thermal Expansion of Concrete. Transportation Research Record: Journal of the Transportation Research Board.
6. American Association of State Highway and Transportation Officials. (2009). AASHTO Standard T 336-09. "Standard Test Method for the Coefficient of Thermal Expansion of Hydraulic Cement Concrete." Washington, DC.
7. American Society for Testing and Materials (ASTM). (2010). ASTM Standard C78. "Standard Test Method for Flexural Strength of Concrete." ASTM International, West Conshohocken, PA.

8. American Society for Testing and Materials (ASTM). (2011). ASTM Standard E1592. "Standard Test Method for Thermal Conductivity and Thermal Diffusivity by Modulated Temperature Differential Scanning Calorimetry." ASTM International, West Conshohocken, PA.
9. American Society for Testing and Materials (ASTM). (2014). ASTM Standard C469. "Standard Test Method for Static Modulus of Elasticity and Poisson's Ratio of Concrete in Compression." ASTM International, West Conshohocken, PA.
10. ASTM C 192/192M. (2012). "Standard Practice for Making and Curing Concrete Test Specimens in the Laboratory." ASTM International, 100 Barr Harbor Drive, PO Box C700, West Conshohocken, PA 19428-2959, United States.
11. ASTM C39 / C39M - 12a. (2012). "Standard Test Method for Compressive Strength of Cylindrical Concrete Specimens." ASTM International, 100 Barr Harbor Drive, PO Box C700, West Conshohocken, PA 19428-2959, United States.
12. Bautista, F. E., and I. Basheer. (2008). *Jointed Plain Concrete Pavement (JPCP) Preservation and Rehabilitation Design Guide*.
13. Bentz, D.P., Peltz, M.A., Duran-Herrera, A., Valdez, P., and Juarez, C.A. (2011). "Thermal Properties of High-volume Fly Ash Mortars and Concretes." Journal of Building Physics, 34(3), pp. 263–275.
14. Bonnell, D.G., & Harper, F.C. (1950). The Thermal Expansion of Concrete.
15. Buch, N., and Jahangirnejad, S. (2008). "Quantifying Coefficient of Thermal Expansion Values of Typical Hydraulic Cement Concrete Paving Mixtures."
16. Caltrans. (2015). "Concrete Pavement Guide." Sacramento, CA.
17. Chintakunta, S. (2007). Sensitivity of Thermal Properties of Pavement Materials Using Mechanistic–Empirical Pavement Design Guide. Master's thesis. Iowa State University, Ames, Iowa.
18. Darter, M. I., Titus-Glover, L., Von Quintus, H., Bhattacharya, B. B., & Jagannath, M. (2014). Calibration and Implementation of the AASHTO Mechanistic-Empirical Pavement Design Guide in Arizona. *Arizona Department of Transportation*, *FHWA-AZ-14-606*, 208. https://apps.azdot.gov/ADOTLibrary/publications/project_reports/PDF/AZ606.pdf
19. Emanuel, J. H., and J. L. Hulsey. (1977). Prediction of the Thermal Coefficient of Expansion of Concrete. ACI Journal, Vol. 74, No. 4, pp. 149–155.
20. Havel, S., A. Archilla, and L. Shen. (2015). Coefficient of Thermal Expansion of Concrete Mixes in Hawaii: Determination and Implications for Concrete Pavement Design. Journal of Materials in Civil Engineering, Vol. 27, No. 5.
21. Hein, D. K., and Sullivan, S. (2012). "Concrete Coefficient of Thermal Expansion (CTE) and Its Significance in Mechanistic-Empirical Pavement Design." No. 234.
22. Huang, Y. H. (2004). Pavement Analysis and Design, 2nd Ed., Prentice Hall, Englewood Cliffs, NJ.
23. Jahangirnejad, S., Buch, N., & Kravchenko, A. (2009). "Evaluation of Coefficient of Thermal Expansion Test Protocol and its Impact on Concrete Pavement Performance." *ACI Materials Journal*, *106*(1), 64–71.
24. Jeong, J.-H., D. G. Zollinger, J.-S. Lim, and J.-Y. Park. (2011). Age and Moisture Effects on Thermal Expansion of Concrete Pavement Slabs. Journal of Materials in Civil Engineering, Vol. 24, No. 1.
25. Kim, S. H., J. Yang, B. H. Nam, and J. H. Jeong. (2015). Effect of Materials and Age on the Coefficient of Thermal Expansion of Concrete PavingMixture. Road Materials and Pavement Design, Vol. 16, No. 2.
26. Kodide, U. (2010). Thermal Conductivity and its Effects on the Performance of PCC Pavements in MEPDG. Master's thesis in Civil Engineering, Louisiana State University, Baton Rouge, LA.
27. Kosmatka, S.H. and Wilson, M.L. (2016). Design and Control of Concrete Mixtures. 16th ed., Vol. EB001, Portland Cement Association, Skokie, IL.
28. Mallela, J., Abbas, A., Harman, T., Rao, C., Liu, R., and Darter, M. (2005). "Measurement and Significance of the Coefficient of Thermal Expansion of Concrete in Rigid Pavement Design." *Transportation Research Record*, Vol. 1919, No. 1919, pp. 38–46.
29. Meyers, S. L. (1951). "How Temperature and Moisture Changes May Affect the Durability of Concrete." *Rock Prod.*, 54(8), 153–162.
30. Mindess, S., J. F. Young, and D. Darwin. (2003). Concrete. 2nd ed. Prentice Hall.
31. NCHRP. (2004). Guide for Mechanistic–Empirical Design of New and Rehabilitated Pavement Structures. ARA, Inc., ERES Division, Champaign, IL.
32. NCHRP. (2014). "Implementation of the AASHTO Mechanistic-Empirical Pavement Design Guide and Software."
33. Neekhra, S. (2004). A New Mineralogical Approach to Predict Coefficient of Thermal Expansion of Aggregate and Concrete. Master's Thesis, Texas A&M University.

34. Schwartz, C., Li, R., Kim, S. H., Ceylan, H., and Gopalakrishnan, K. (2013). "Sensitivity Evaluation of MEPDG Performance Prediction." National Cooperative Highway Research Program Research Results Digest, RRD 372, Washington, D.C. National Research Council.
35. Sellevold, E. J., and · Ø Bjøntegaard. (2006). "Coefficient of Thermal Expansion of Cement Paste and Concrete: Mechanisms of Moisture Interaction." *Materials and Structures*, Vol. 39, pp. 809–815.
36. Shin, A.H.C. and Kodide, U. (2012). "Thermal Conductivity of Ternary Mixtures for Concrete Pavements." Cement & Concrete Composites, 34(4), pp. 575–582.
37. Shin, H., Y. Chung, B. Rouge, and F. Report. (2011). Determination of Coefficient of Thermal Expansion Effects on Louisiana's PCC Pavement Design. No. 2.
38. Shin, H.-C., and Chung, Y. (2011). "Determination of Coefficient of Thermal Expansion Effects on Louisiana's PCC Pavement Design."
39. Tanesi, J., Crawford, G. L., Nicolaescu, M., Meininger, R. and Gudimettla, J. M. (2010). "New AASHTO T336-09 Coefficient of Thermal Expansion Test Method How Will It Affect You?" *Transportation Research Record: Journal of the Transportation Research Board*, Vol. 2164, No. 1, pp. 52–57.
40. Tanesi, J., Kutay, M. E., Abbas, A., and Meininger, R. (2008). "Effect of Coefficient of Thermal Expansion Test Variability on Concrete Pavement Performance as Predicted by Mechanistic-Empirical Pavement Design Guide." *Transportation Research Record*, Vol. 2020, pp. 40–44.
41. Tran, N. H., K. D. Hall, and M. James. (2009). Coefficient of Thermal Expansion of Concrete Materials: Characterization to Support Implementation of the Mechanistic- Empirical Pavement Design Guide. Transportation Research Record: Journal of the Transportation Research Board.
42. Won, M. (2005). "Improvements of Testing Procedures for Concrete Coefficient of Thermal Expansion." *Journal of the transportation research board*, pp. 23–28.
43. Yeon, J. H., Choi, S., & Won, M. C. (2009). Effect of Relative Humidity on Coefficient of Thermal Expansion of Hardened Cement Paste and Concrete. *Transportation Research Record*, *2113*(1), 83–91.

APPENDIX B – SUPPORTING MATERIAL FOR LABORATORY TESTING PROGRAM AND RESULTS

[redacted]

Material Certification Report

Material: Portland Cement
Type: I-II (MH)
Test Period: 23-Aug-2021 to 23-Aug-2021
Date Issued: 16-Sep-2021

Certification

This cement meets the specifications of ASTM C150 and AASHTO M85 for Type I-II (MH) cement.

General Information

Supplier: [redacted]
Address:
Contact:

Source Location: [redacted]
Contact:

The following is based on average test data during the test period. The data is typical of product shipped from this source; individual shipments may vary.

Test Data on ASTM Standard Requirements

Chemical			Physical		
Item	**Limit [1]**	**Result**	**Item**	**Limit [1]**	**Result**
SiO_2 (%)	-	20.0	Air Content (%)	12 max	7
Al_2O_3 (%)	6.0 max	5.0	Blaine Fineness (m^2/kg)	260-430	408
Fe_2O_3 (%)	6.0 max	3.5			
CaO (%)	-	63.8	Autoclave Expansion (%) (C151)	0.80 max	-0.01
MgO (%)	6.0 max	1.3	Compressive Strength MPa (psi)		
SO_3 (%) [2]	3.0 max	3.2	3 day	10.0 (1450) min	27.7 (4020)
Loss on Ignition (%) [5]	3.5 max	2.2	7 day	17.0 (2470) min	34.7 (5030)
Insoluble Residue (%)	1.50 max	0.26	28 day (previous month's data)	-	42.7 (6190)
CO_2 (%)	-	0.8			
$CaCO_3$ in Limestone (%)	70 min	88	Initial Vicat (minutes)	45-375	105
Potential Phase Compositions [3]:					
C_3S (%)	-	56	Mortar Bar Expansion (%) (C1038)	0.020 max	0.003
C_2S (%)	-	15			
C_3A (%)	8 max	7			
C_4AF (%)	-	11			
$C_3S + 4.75C_3A$ (%)	100 max	91			

Test Data on ASTM Optional Requirements

Chemical			Physical		
Item	**Limit [1]**	**Result**	**Item**	**Limit [1]**	**Result**
Equivalent Alkalies (%)	-	0.47	Heat of Hydration kJ/kg (cal/g) (ASTM C1702) 3 Days [4]	-	285 (68)

Notes (*1-9)

1 - Dashes in the Limit / Result columns mean Not Applicable.
2 - It is permissible to exceed the specification limit provided that ASTM C1038 Mortar Bar Expansion does not exceed 0.020% at 14 days.
3 - Adjusted per Annex A1.6 of ASTM C150 and AASHTO M85.
4 - Test results represent the most recent value and is provided for information only.
5 - Limit = 3.0 when limestone is not an ingredient in the final cement product
8/23/2021
Grind 234

Additional Data

Item	Limestone	Inorganic Processing Addition	Base Cement Phase Composition	Result
Amount (%)	2.1	-	C_3S (%)	57
SiO_2 (%)	2.2	-	C_2S (%)	15
Al_2O_3 (%)	0.6	-	C_3A (%)	7
Fe_2O_3 (%)	0.6	-	C_4AF (%)	11
CaO (%)	54.4	-		
SO_3 (%)	0.4	-		

Figure B.1: Cement mill test report

Report of Results for Product Testing *June 4, 2020*
Product Name: Roxboro DS 11/23-12/11 (2015)
TEC Services Project #: 20-1612
TEC Laboratory #: 20-461

Table 1 – Results of the Chemical Analysis

Oxides	Results Weight (%)
Silicon Dioxide (SiO_2)	**52.7**
Aluminum Oxide (Al_2O_3)	**26.7**
Iron Oxide (Fe_2O_3)	**11.12**
Sum ($SiO_2 + Al_2O_3 + Fe_2O_3$)	**90.5**
Calcium Oxide (CaO)	**2.1**
Magnesium Oxide (MgO)	**1.1**
Sodium Oxide (Na_2O)	**0.34**
Potassium Oxide (K_2O)	**2.24**
Equivalent Alkalies ($Na_2O+0.658\ K_2O$)	**1.81**
Titanium Dioxide (TiO_2)	**1.42**
Manganic Oxide (Mn_2O_3)	**0.026**
Phosphorus Pentoxide (P_2O_5)	**0.21**
Sulfur Trioxide (SO_3)	**0.75**
Loss on Ignition	**1.9**
Moisture Content	**0.38**

Figure B.2: Fly ash chemical analysis report

Table B.1: Coarse aggregate identification from 1985 geological map of North Carolina (NC Geological Survey, 1985)

Region	**Quarry Location**	**ID**	**Description**
Piedmont	Statesville, NC	CZab	Amphibolite and biotite gneiss- interlayered; minor layers and lenses of hornblende gneiss, metagabbro, mica schist, and granite rock.
Piedmont	Knightdale, NC	PPmg	Foliated to massive granite rock; megacrystic to equigranular. Rolesville suite, wise and lemon springs intrusive.
Mountain	Hendersonville, NC	Chg	Henderson gneiss; monzonitic to granodioritic, inequigranular.
Mountain	Black Mountain, NC	Zatw	Muscovite-biotite gneiss; foliated to massive, locally conglomeratic; interlayered and gradational with mica schist, muscovite-biotite gneiss, and rare graphitic schist

Table B.2: Fine aggregate identification from 1985 geological map of North Carolina (NC Geological Survey, 1985)

Region	Location	ID	Description
Coastal plain	Emery pit, Jackson Springs, NC	Tp/Km	Tp: Sand, medium- to coarse-grained, cross bedding and rhythmic bands of clayey sand common, unconsolidated Km: Sand, sandstone, and mudstone, gray to pale gray with an orange cast, mottled; clay balls and iron-cemented concretions common, beds laterally discontinuous, cross-bedding common
Coastal plain	Buckleberry Mine, Princeton, NC	Kc	Sandstone and sandy mudstone, yellowish gray to bluish gray, mottled red to yellowish orange, indurated, graded and laterally continuous bedding, blocky clay, faint cross-bedding, feldspar and mica common

Table B.3: Fresh concrete test results

Mixture ID	Slump (in)		Air Content (%)		Unit weight (pcf)	
	Batch 1	Batch 2	Batch 1	Batch 2	Batch 1	Batch 2
C1N1O	1.8	0.8	6.0	5.0	146.2	151.7
C1N1OF20	1.3	1.5	5.0	5.0	151.8	147.7
C1N1OF30	1.8	2.0	5.9	6.0	144.2	145.6
C1N2O	2.5	0.5	5.6	5.1	149.1	151.2
C1N2OF20	1.3	0.5	5.2	5.1	149.2	150.3
C1N2OF30	1.5	1.5	5.4	5.7	146.4	146.2
C2N1O	1.1	0.5	5.2	5.5	144.5	142.4
C2N1OF20	1.8	2.0	5.9	5.6	138.9	140.8
C2N1OF30	2.0	1.8	5.3	5.1	140.9	141.4
C2N2O	1.3	0.5	5.1	5.4	146.5	146.1
C2N2OF20	1.5	1.5	5.4	5.7	143.8	144.0
C2N2OF30	0.5	1.3	5.3	5.2	142.3	142.7
C3N1O	1.5	2.3	5.4	5.3	143.6	144.2
C3N1OF20	4.8	4.0	6.0	5.2	139.0	140.5
C3N1OF30	2.3	2.3	5.1	5.3	143.9	143.0
C3N2O	1.3	2.5	5.7	5.3	143.0	143.0
C3N2OF20	3.5	2.0	5.8	5.2	139.8	141.8
C3N2OF30	2.5	3.8	5.4	5.8	140.0	138.8
C4N1O	1.0	0.3	5.1	5.5	145.6	148.3

C4N1OF20	1.2	1.5	5.0	5.4	145.6	145.0
C4N1OF30	0.5	0.8	5.0	5.2	146.8	145.6
C4N2O	2.0	0.5	5.3	5.8	145.4	144.4
C4N2OF20	1.0	1.5	5.2	5.0	146.4	147.2
C4N2OF30	1.0	0.8	5.1	5.2	145.3	145.1

Table 4.3: Average compressive strength test results

Mixture ID	3-day average	7-day average	28-day average	90-day average	180-day average	270-day average	360-day average*
C1N1O	2860	4417	4656	5371	5843	6776	6777
C1N1OF20	2785	3236	4303	5656	5812	7118	6670
C1N1OF30	1855	2113	3176	4339	4407	5766	5906
C1N2O	3988	4208	5051	6034	6260	7245	7278
C1N2OF20	2894	3469	4425	5279	5679	6982	7257 (595)
C1N2OF30	2074	2516	3610	4440	4619	5866	6462 (595)
C2N1O	4186	4586	5829	6255	6062	8025	8450 (579)
C2N1OF20	2517	2971	4361	4594	5254	6517	7076 (572)
C2N1OF30	2451	2835	3897	4588	6098	6094	6674
C2N2O	4141	5036	5676	6266	6928	8226	8203 (588)
C2N2OF20	3098	3397	4603	5964	5890	7648	7670 (588)
C2N2OF30	2499	2803	4037	5068	5278	6621	7595 (579)
C3N1O	3628	4664	5375	6398	7737	7323	6838
C3N1OF20	2388	3168	4149	5199	6126	6662	6661
C3N1OF30	2009	2657	3592	4351	6081	6791	7771
C3N2O	3561	4403	5293	6239	7571	7707	8201
C3N2OF20	2412	3106	4027	4999	6632	---	7781
C3N2OF30	2084	2572	3287	4289	5706	---	6700
C4N1O	3613	4347	5510	7806	7532	7557	7458
C4N1OF20	2764	3063	4239	6069	6480	7669	6938
C4N1OF30	2096	2716	4147	5436	6318	6931	6312
C4N2O	3501	4409	5068	6187	7155	---	7314
C4N2OF20	3221	3635	4585	6088	7684	---	7683
C4N2OF30	1866	2587	3511	4446	5770	---	6655

* due to an issue, several mixtures were tested for late age strength at an age greater than 360 days. The age at which these tests were made is denoted in parentheses next to the average test result.

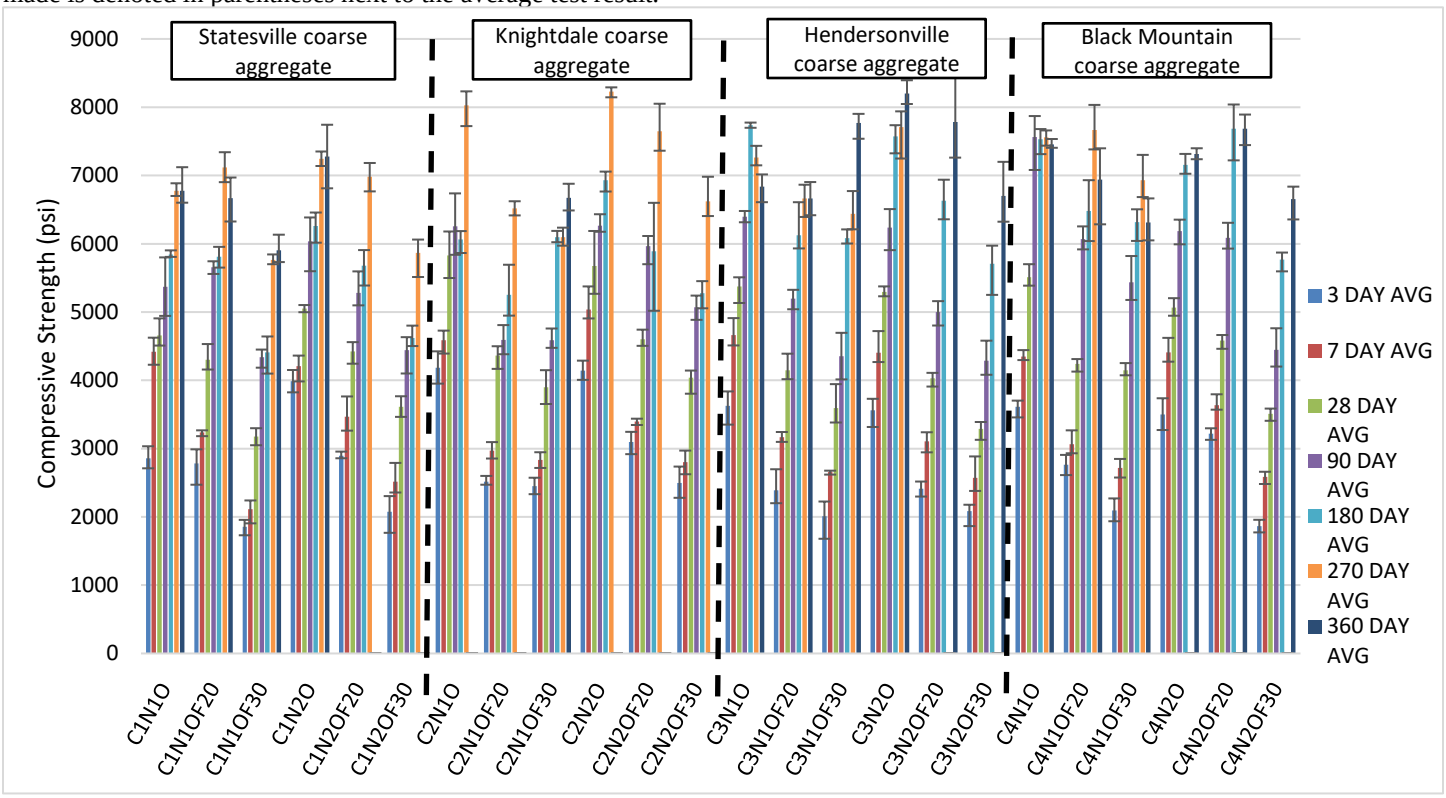

Figure B.3: Average compressive strength test results with mixtures grouped by coarse aggregate source

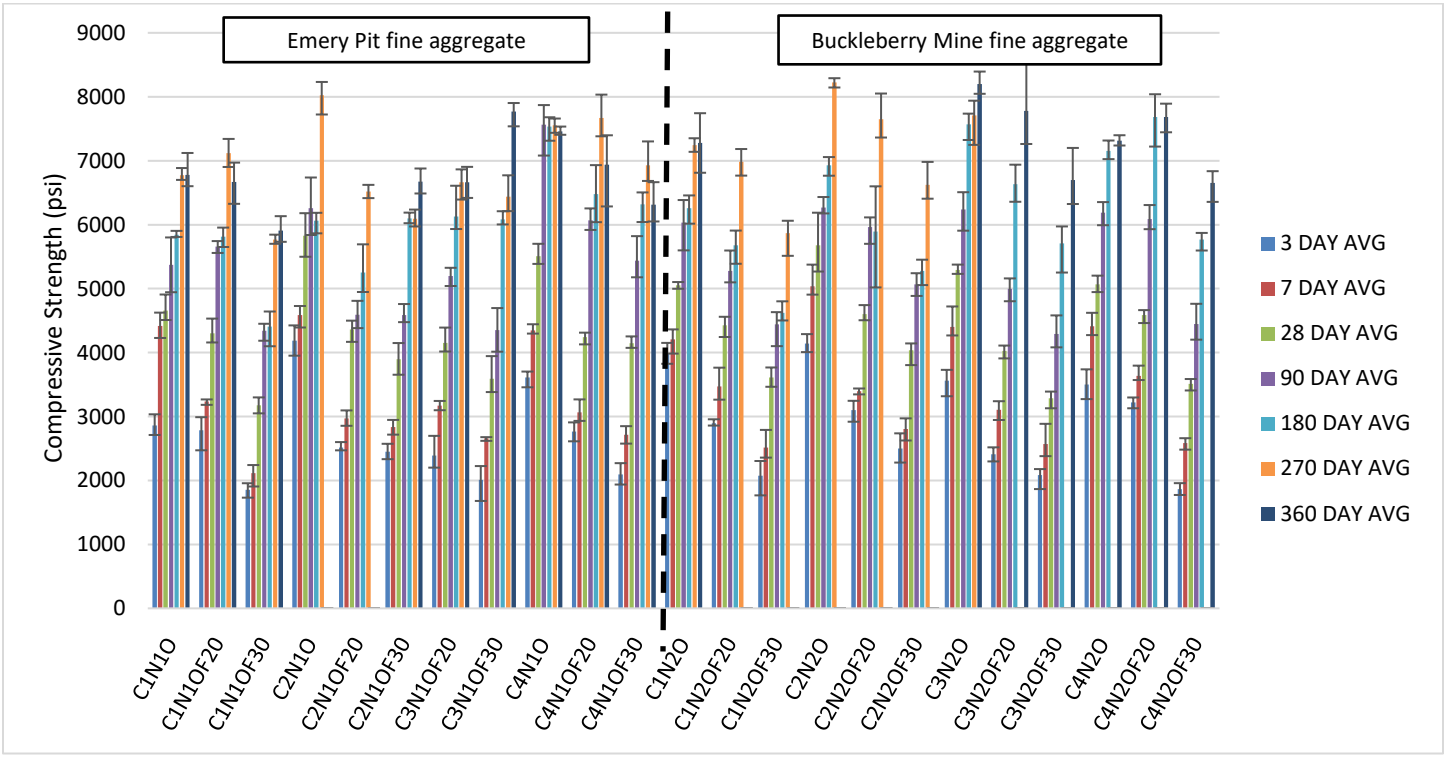

Figure B.4: Average compressive strength with mixtures grouped by fine aggregate source

Table B.4: Average compressive strength summarized by aggregate and fly ash content

Material		Compressive strength (psi)		
		7 Day average	28 Day average	90 Day average
Coarse Aggregate	Statesville	3,323	4,139	5,154
	Knightdale	3,614	4,734	5,513
	Hendersonville	3,448	4,244	5,033
	Black Mountain	3,421	4,524	5,899
	Piedmont	3,472	4,471	5,342
	Mountain	3,430	4,374	5,431
Fine Aggregate	Emery Pit	3,382	4,445	5,295
	Buckleberry Mine	3,521	4,400	5,465
Fly ash Content	100% OPC	4,524	5,343	6,023
	20% Fly ash replacement	3,254	4,329	5,458
	30% Fly ash replacement	2,603	3,662	4,612

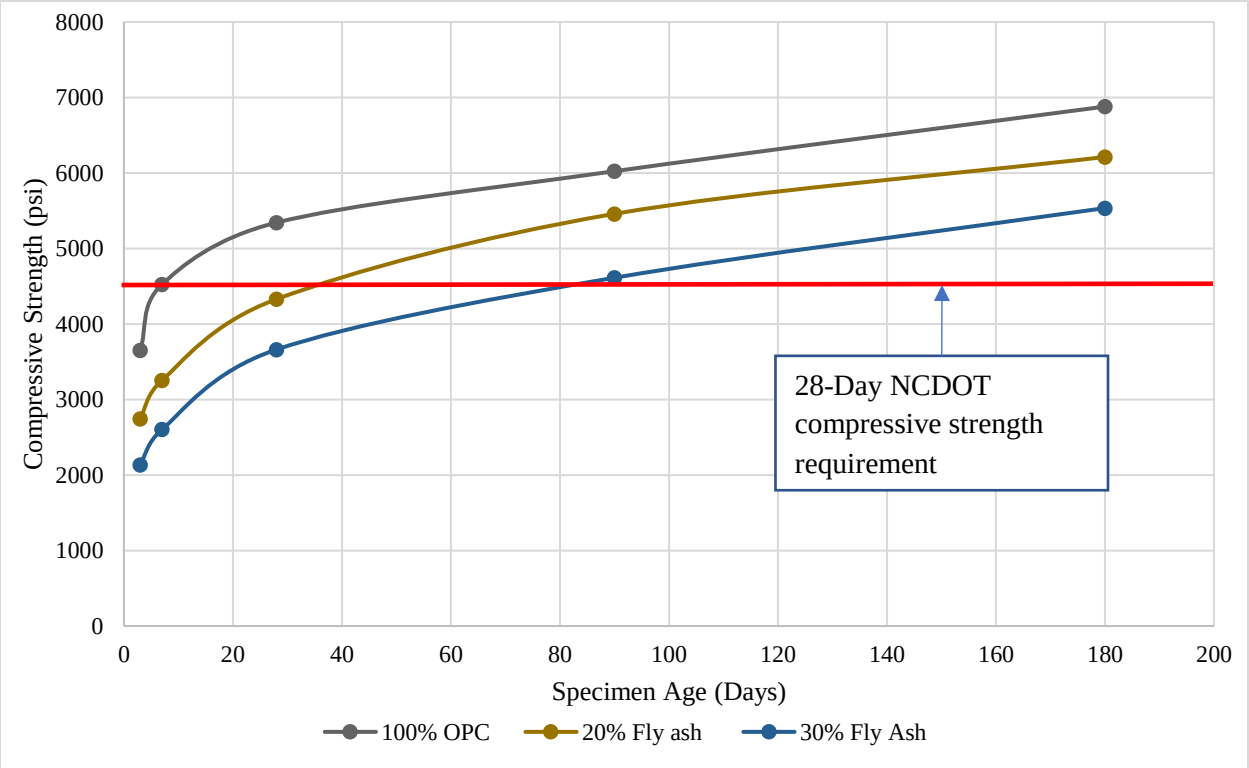

Figure B.5: Average compressive strength with mixtures grouped by fly ash content

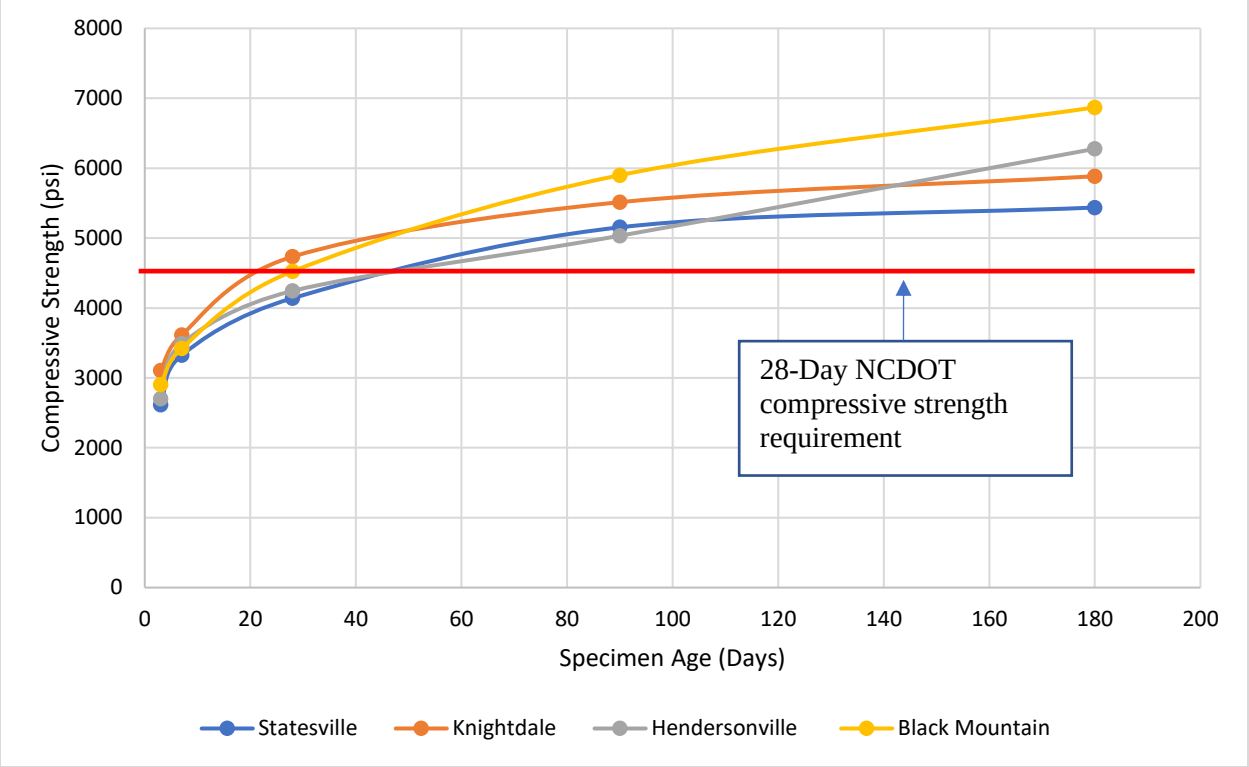

Figure B.6: Average compressive strength with mixtures grouped by coarse aggregate source

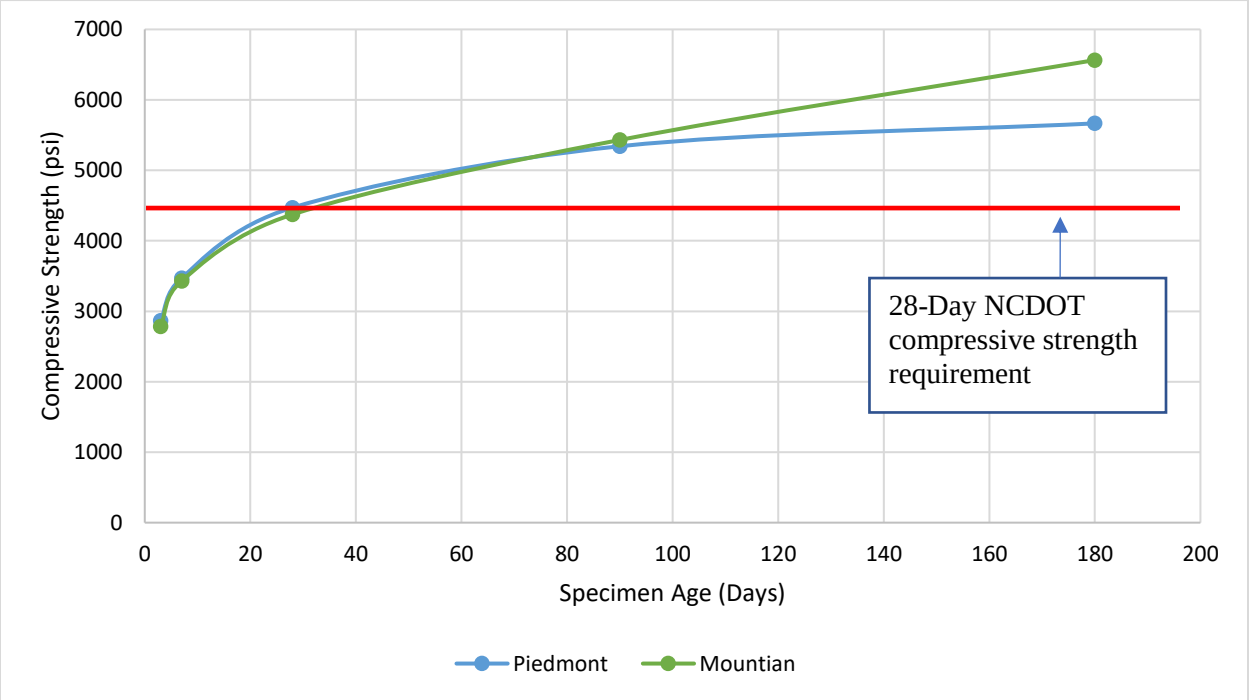

Figure B.7: Average compressive strength with mixtures grouped by region of North Carolina from which the coarse aggregate was sourced

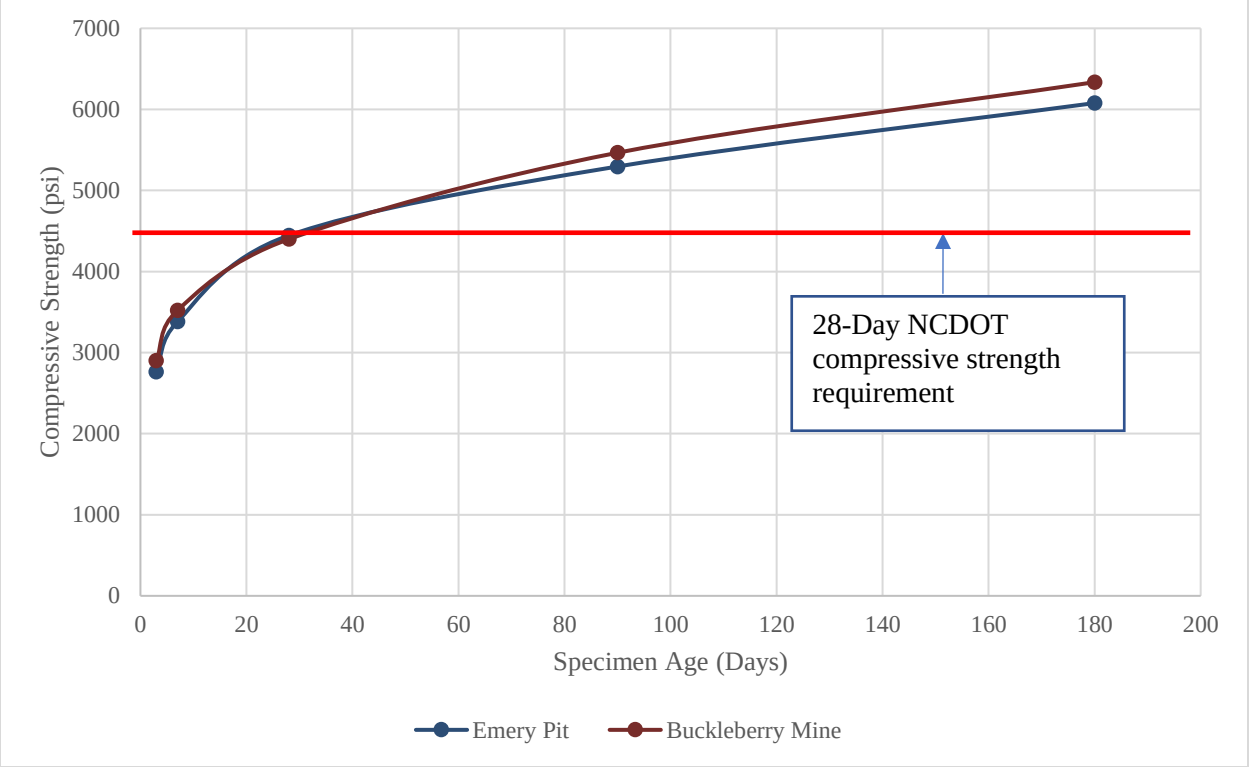

Figure B.8: Compressive strength with mixtures grouped by location from which the fine aggregate was sourced

Table B.6: Average MOE test results

Mixture ID	3-day average	7-day average	28-day average	90-day average	180-day average	270-day average	360-day average*
C1N1O	2,239,000	2,589,000	2,855,000	2,719,000	2,948,000	3,537,000	3,476,000
C1N1OF20	2,095,000	2,370,000	2,710,000	3,088,000	2,888,000	3,708,000	3,586,000
C1N1OF30	2,024000	2,082,000	2,445,000	2,651,000	2,440,000	3,393,000	3,399,000
C1N2O	2,488,000	2,510,000	2,718,000	2,943,000	3,162,000	3,669,000	3,595,000
C1N2OF2O	2,389,000	2,271,000	2,666,000	2,750,000	3,041,000	3,562,000	5,607,000 (595)
C1N2OF30	2,302,000	2,165,000	2,487,000	2,953,000	2,985,000	3,737,000	5,476,000 (595)
C2N1O	2,594,000	2,448,000	2,660,000	2,757,000	2,896,000	3,520,000	5,408,000 (579)
C2N1OF20	1,967,000	2,111,000	2,490,000	2,537,000	2,754,000	3,288,000	4,905,000 (572)
C2N1OF30	2,034,000	2,022,000	2,337,000	2,436,000	3,221,000	3,056.000	3,147,000
C2N2O	2,305,000	2,475,000	2,622,000	2,706,000	2,981,000	3,525,000	5,357,000 (588)
C2N2OF20	2,283,000	2,309,000	2,395,000	2,682,000	2,691,000	3,282,000	4,940,000 (588)
C2N2OF30	2,110,000	2,083,000	2,370,000	2,613,000	2,678,000	3,388,000	5,041,000 (579)
C3N1O	1,930,000	2,327,000	2,440,000	2,512,000	3,236,000	3,077,000	3,007,000
C3N1OF20	1,676,000	1,954,000	2,097,000	2,271,000	2,844,000	2,960,000	3,346,000
C3N1OF30	1,788,000	1,744,000	2,161,000	2,286,000	2,897,000	3,147,000	3,657.000
C3N2O	1,874,000	2,211,000	2,299,000	2,658,000	2,893,000	3,257,000	3,322,000
C3N2OF20	1,815,000	1,994,000	1,988,000	2,407,000	2,883,000	---	3,987,000
C3N2OF30	1,852,000	2,094,000	1,887,000	2,409,000	2,891,000	---	3,691,000
C4N1O	1,967,000	2,049,000	2,357,000	2,888,000	3,165,000	3,041,000	4,233,000
C4N1OF20	1,772,000	1,829,000	2,218,000	2,916,000	3,125,000	3,309,000	3,913,000
C4N1OF30	1,609,000	1,767,000	2,223,000	2,761,000	2,916,000	2,985,000	4,036,000
C4N2O	1,907,000	2,088,000	2,195,000	2,749,000	2,952,000	---	3,690,000
C4N2OF20	2,112,000	1,980,000	2,103,000	2,781,000	3,304,000	---	3,912,000
C4N2OF30	1,521,000	2,015,000	2,023,000	2,298,000	2,826,000	---	2,050,000

* due to an issue, several mixtures were tested for late age MOE at an age greater than 360 days. The age at which these tests were made is denoted in parentheses next to the average test result.

Table B.7: Average MOE summarized by aggregate and fly ash content

Material		Modulus of Elasticity (psi)	
		28 Day average	Standard deviation
Coarse Aggregate	Statesville	2,640,000	243,000
	Knightdale	2,480,000	200,000
	Hendersonville	2,150,000	209,000
	Black Mountain	2,180,000	175,000
	Piedmont	2,560,000	234,000
	Mountain	2,170,000	190,000
Fine Aggregate	Emery Pit	2,420,000	284,000
	Buckleberry Mine	2,310,000	286,000
Fly ash Content	100% OPC	2,510,000	277,000
	20% Fly ash replacement	2,350,000	298,000
	30% Fly ash replacement	2,240,000	233,000

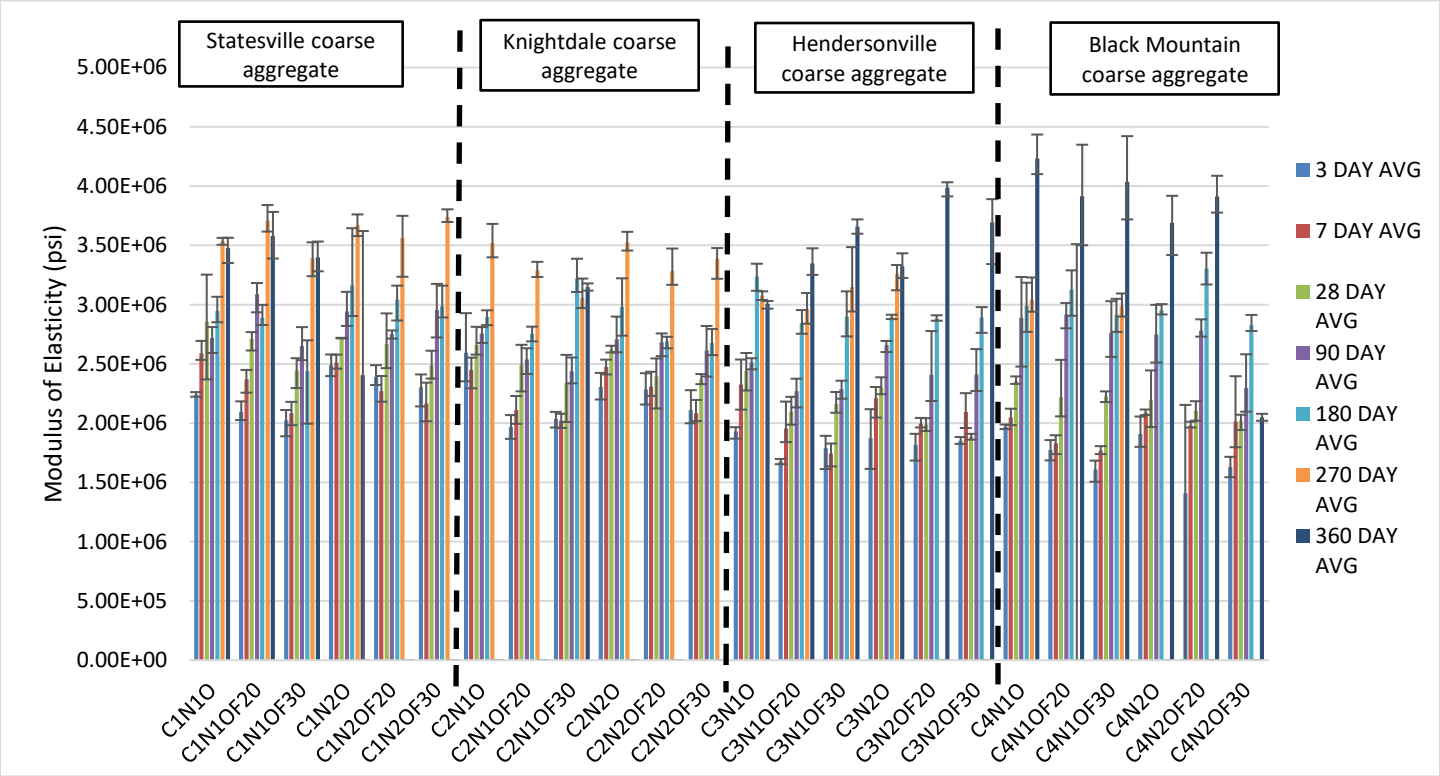

Figure B.9: Average MOE test results with mixtures grouped by coarse aggregate source

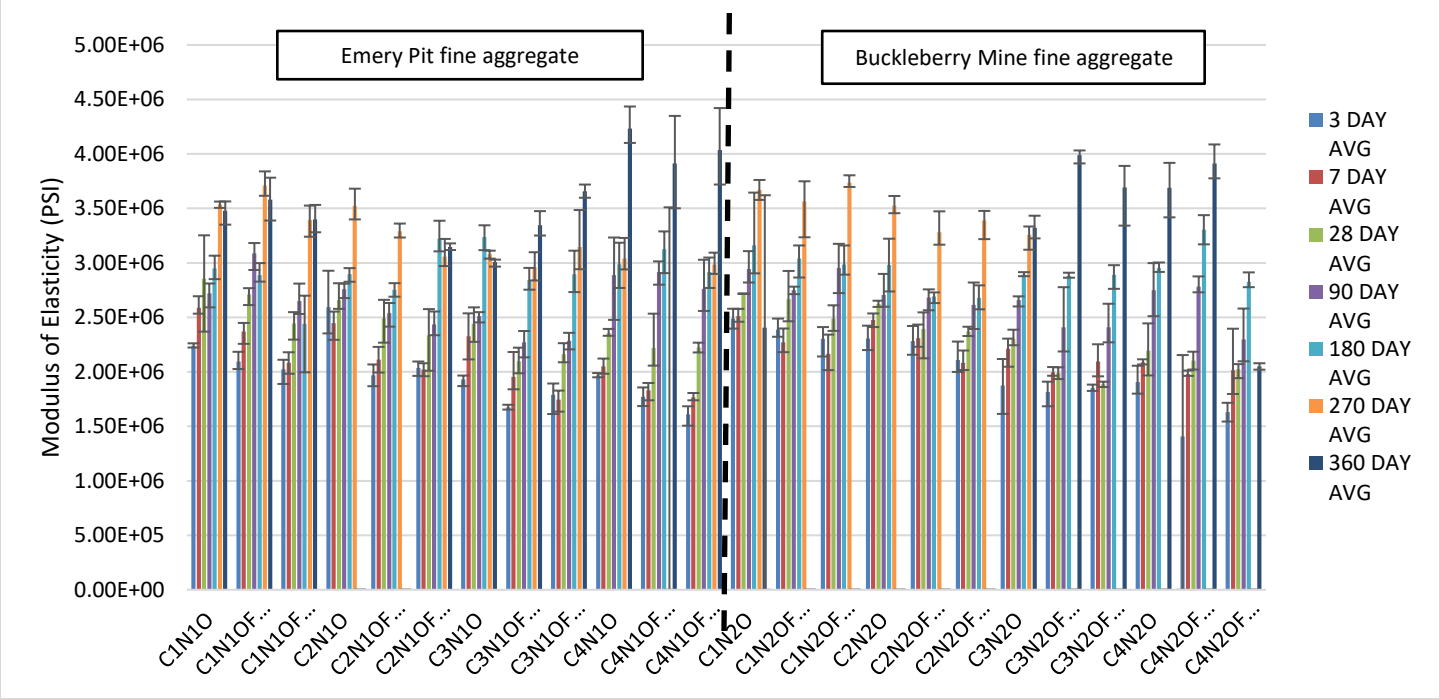

Figure B.10: Average MOE test results with mixtures grouped by fine aggregate source

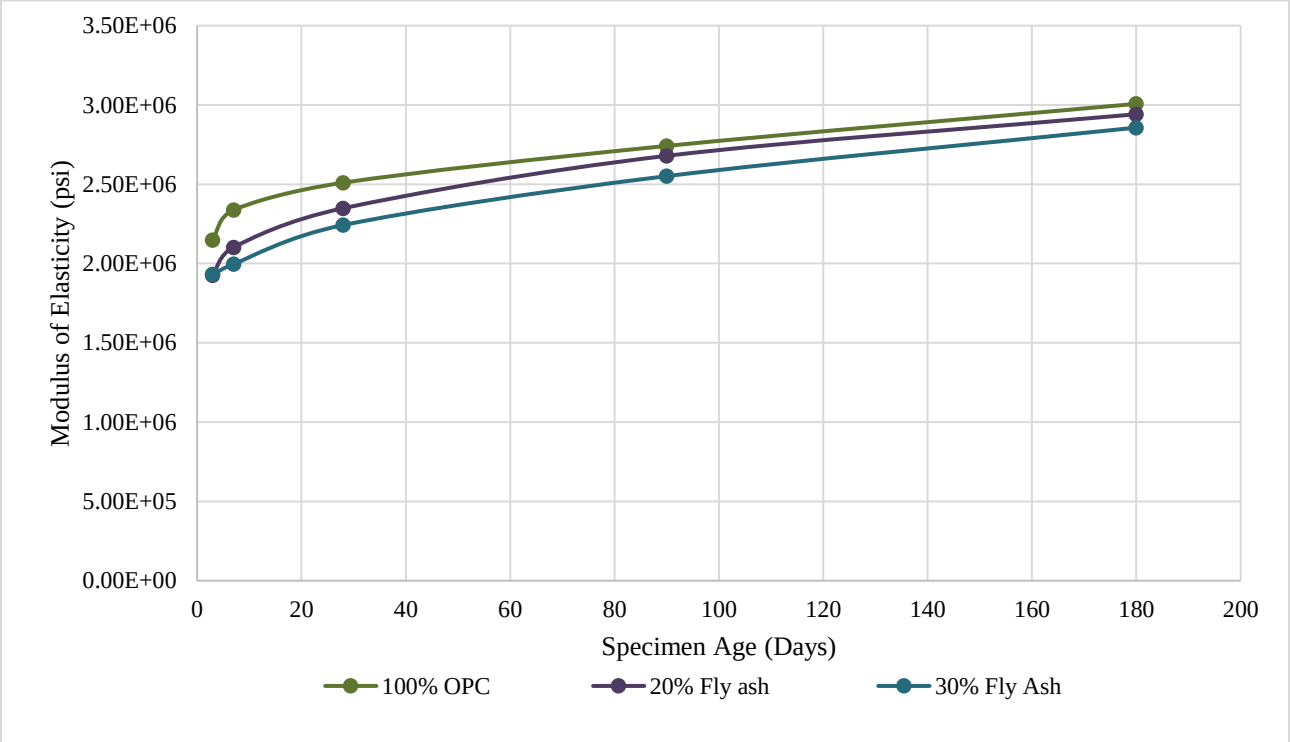

Figure B.11: Average MOE with mixtures grouped by fly ash content

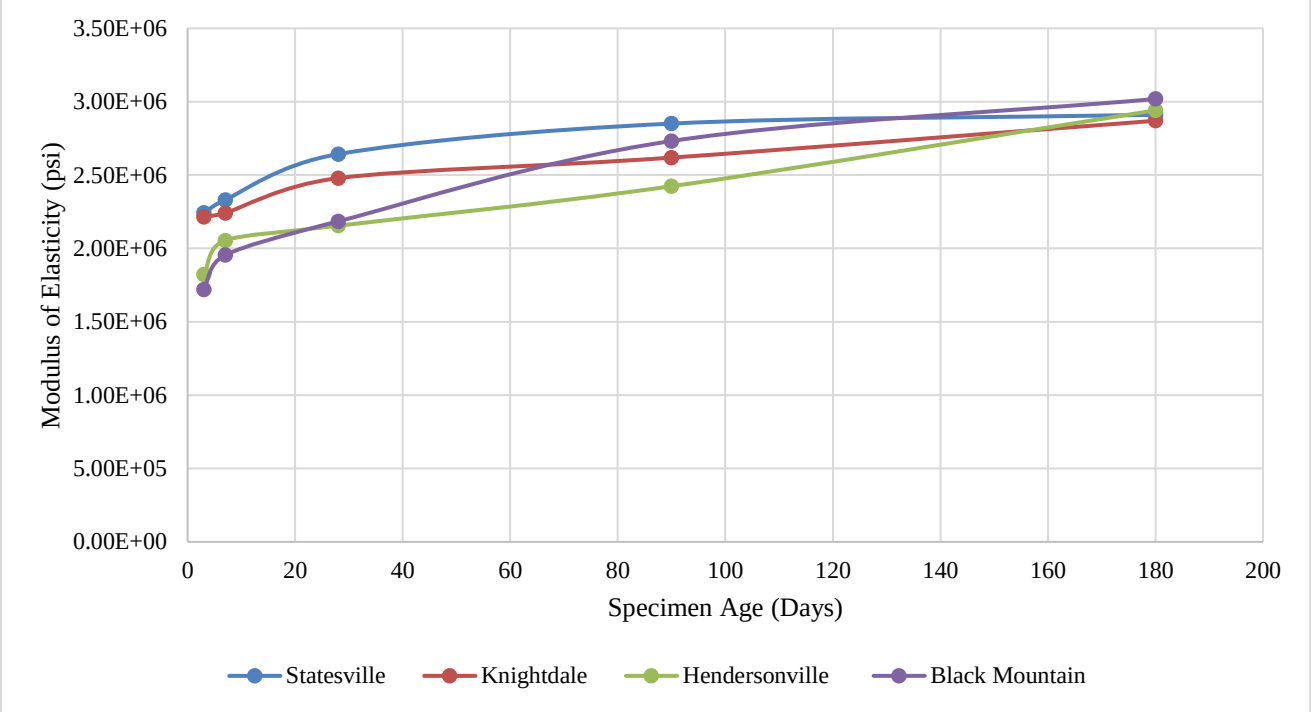

Figure B.12: Average MOE with mixtures grouped by coarse aggregate source

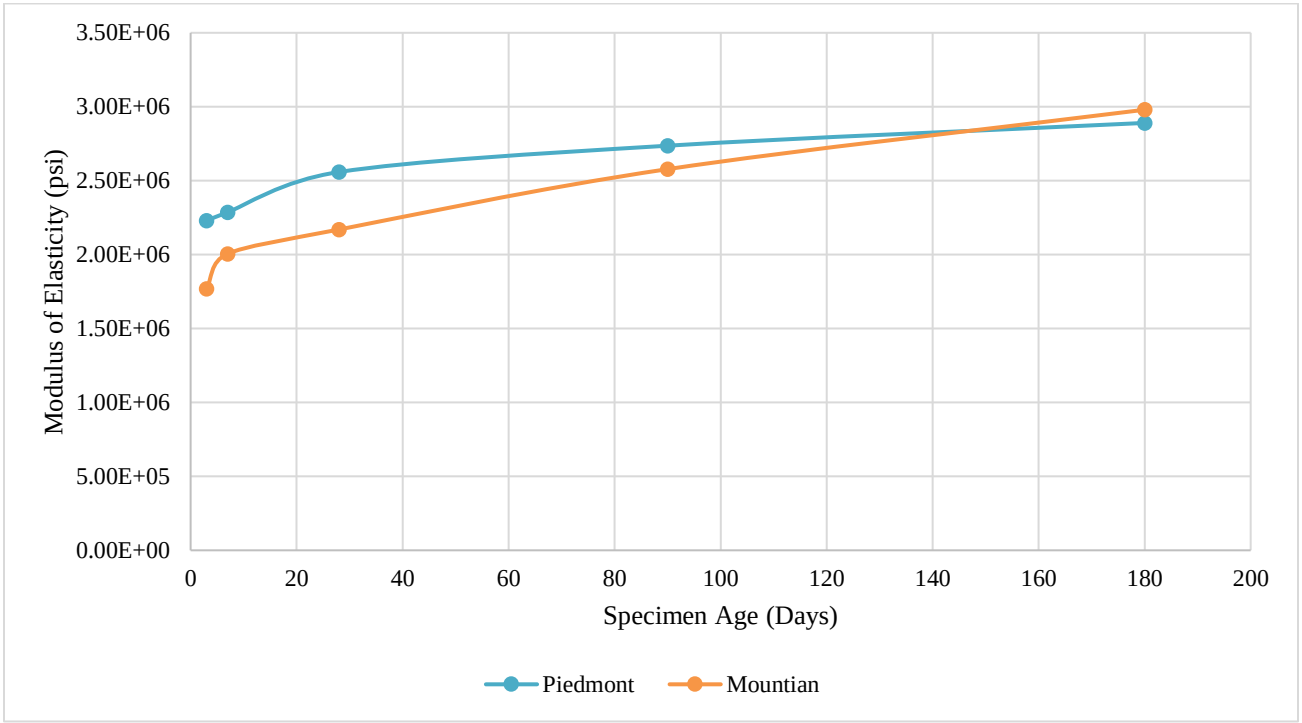

Figure B.13: Average MOE with mixtures grouped by region of North Carolina from which the coarse aggregate was sourced

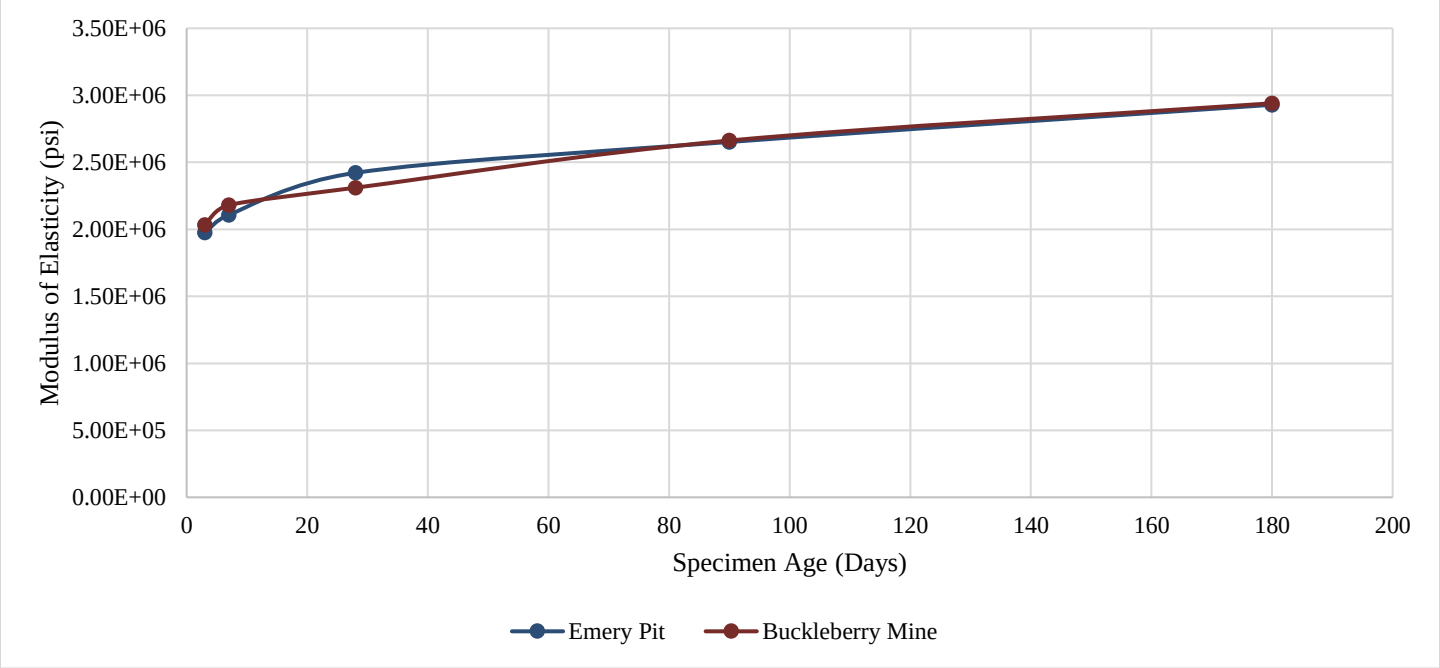

Figure B.14: Average MOE with mixtures grouped by location from which the fine aggregate was sourced

Table B.8: Average Poisson's ratio test results

Mixture ID	3-day average	7-day average	28-day average	90-day average	180-day average	270-day average	360-day average*
C1N1O	0.119	0.119	0.138	0.145	0.151	0.159	0.168
C1N1OF20	0.113	0.132	0.141	0.159	0.174	0.168	0.192
C1N1OF30	0.124	0.144	0.150	0.151	0.166	0.124	0.169
C1N2O	0.104	0.112	0.126	0.141	0.170	0.148	0.170
C1N2OF2O	0.131	0.128	0.151	0.168	0.165	0.150	0.268 (595)
C1N2OF30	0.122	0.126	0.133	0.169	0.157	0.157	0.269 (595)
C2N1O	0.126	0.135	0.135	0.142	0.143	0.169	0.273 (579)
C2N1OF20	0.128	0.124	0.132	0.138	0.148	0.170	0.256 (572)
C2N1OF30	0.115	0.125	0.134	0.167	0.166	0.169	0.165
C2N2O	0.149	0.141	0.139	0.144	0.167	0.171	0.303 (588)
C2N2OF20	0.136	0.129	0.146	0.130	0.141	0.171	0.263 (588)
C2N2OF30	0.120	0.130	0.146	0.171	0.147	0.178	0.287 (579)
C3N1O	0.121	0.127	0.127	0.147	0.146	0.162	0.146
C3N1OF20	0.125	0.109	0.108	0.147	0.155	0.178	0.175
C3N1OF30	0.124	0.111	0.124	0.154	0.165	0.188	0.150
C3N2O	0.105	0.128	0.118	0.148	0.144	0.156	0.181
C3N2OF20	0.114	0.118	0.123	0.161	0.168	---	0.161
C3N2OF30	0.103	0.123	0.126	0.154	0.179	---	0.130
C4N1O	0.115	0.140	0.129	0.127	0.156	0.171	0.178
C4N1OF20	0.125	0.119	0.132	0.161	0.175	0.182	0.128
C4N1OF30	0.102	0.095	0.127	0.144	0.169	0.172	0.155
C4N2O	0.109	0.122	0.150	0.135	0.150	---	0.143
C4N2OF20	0.104	0.116	0.143	0.171	0.164	---	0.185
C4N2OF30	0.081	0.120	0.155	0.131	0.150	---	0.178

* due to an issue, several mixtures were tested for late age Poisson's ratio at an age greater than 360 days. The age at which these tests were made is denoted in parentheses next to the average test result.

Table B.9: Average Poisson's ratio summarized by aggregate and fly ash content

Material		Poisson's ratio	
		28 Day average	Standard deviation
Coarse Aggregate	Statesville	0.14	0.02
	Knightdale	0.14	0.01
	Hendersonville	0.12	0.02
	Black Mountain	0.14	0.02
	Piedmont	0.14	0.01
	Mountain	0.13	0.02
Fine Aggregate	Emery Pit	0.13	0.02
	Buckleberry Mine	0.14	0.02
Fly ash Content	100% OPC	0.13	0.02
	20% Fly ash replacement	0.14	0.02
	30% Fly ash replacement	0.14	0.02

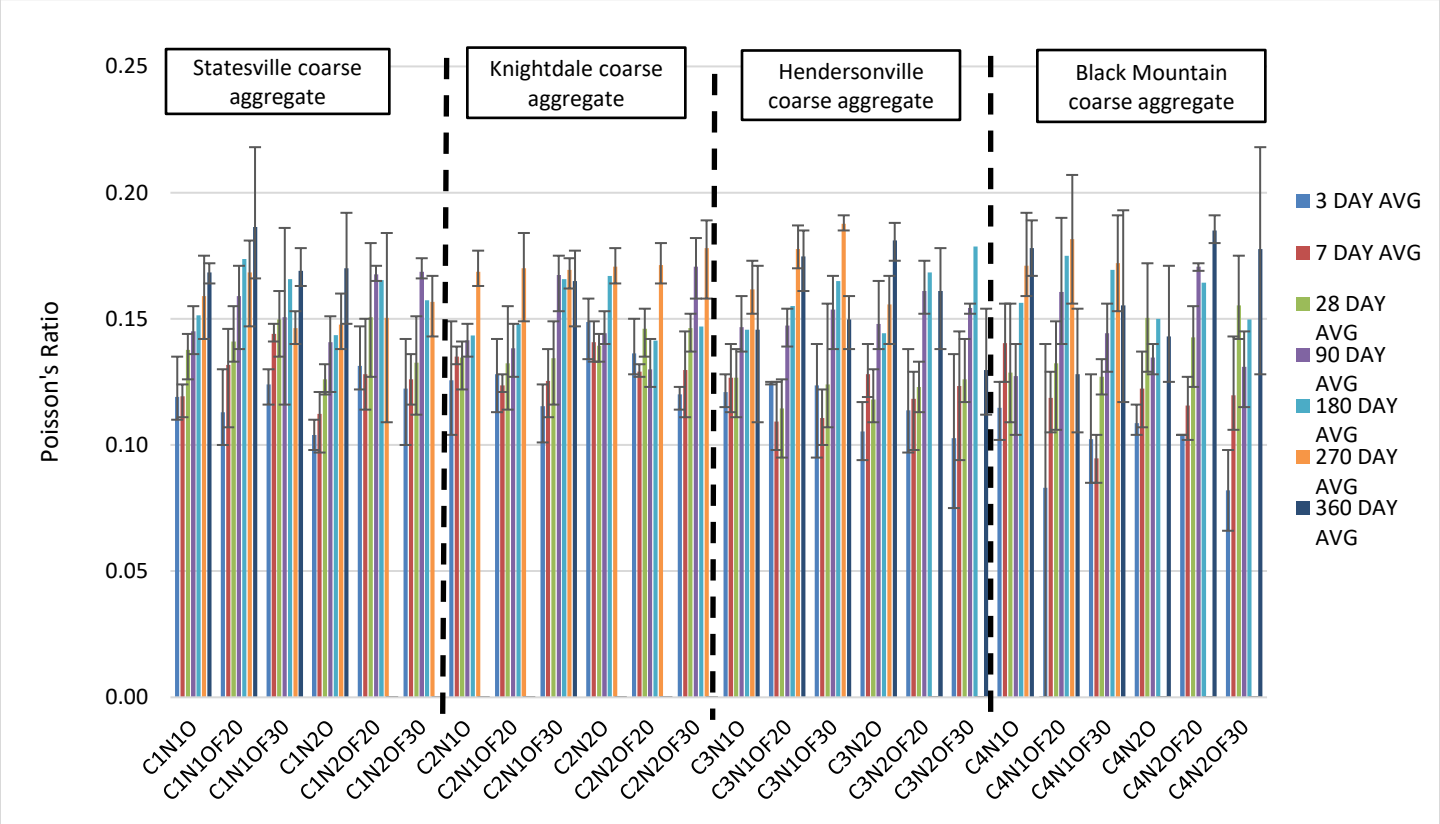

Figure B.9: Average Poisson's ratio test results with mixtures grouped by coarse aggregate source

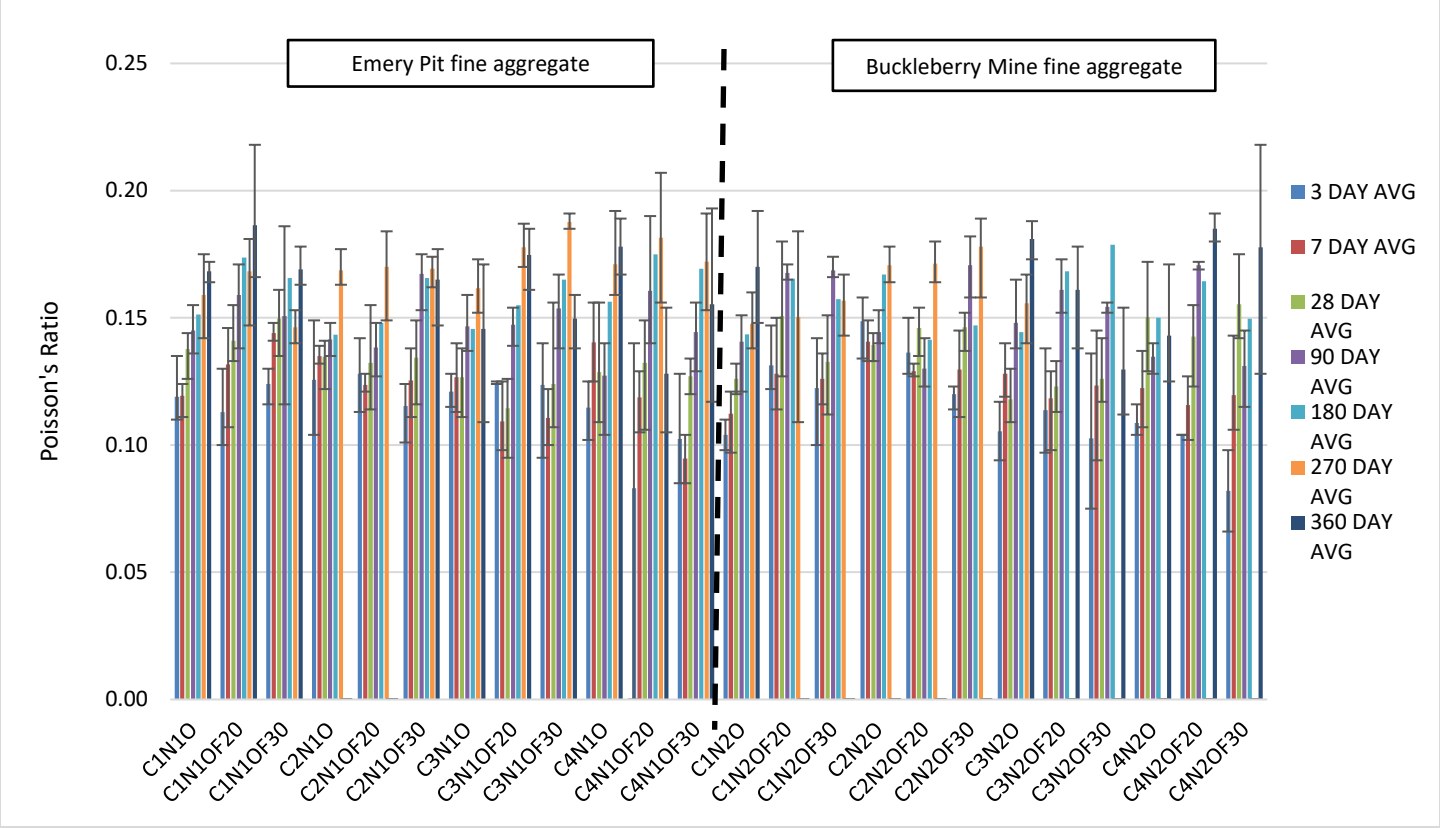

Figure B.10: Average Poisson's ratio test results with mixtures grouped by fine aggregate source

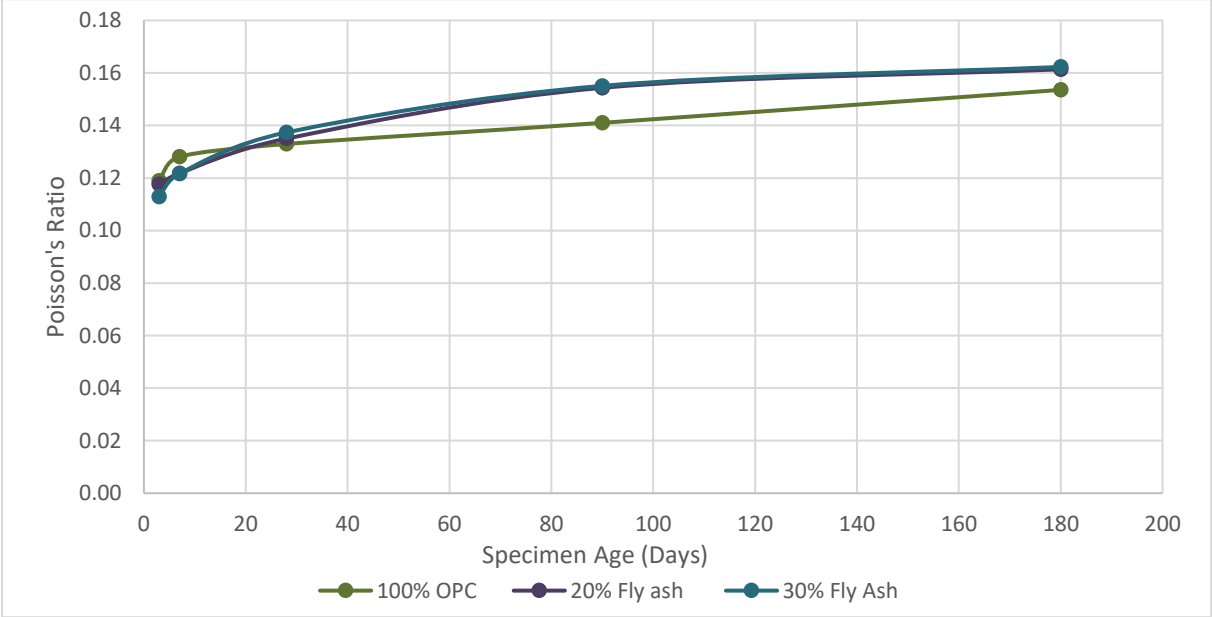

Figure B.11: Average Poisson's ratio with mixtures grouped by fly ash content

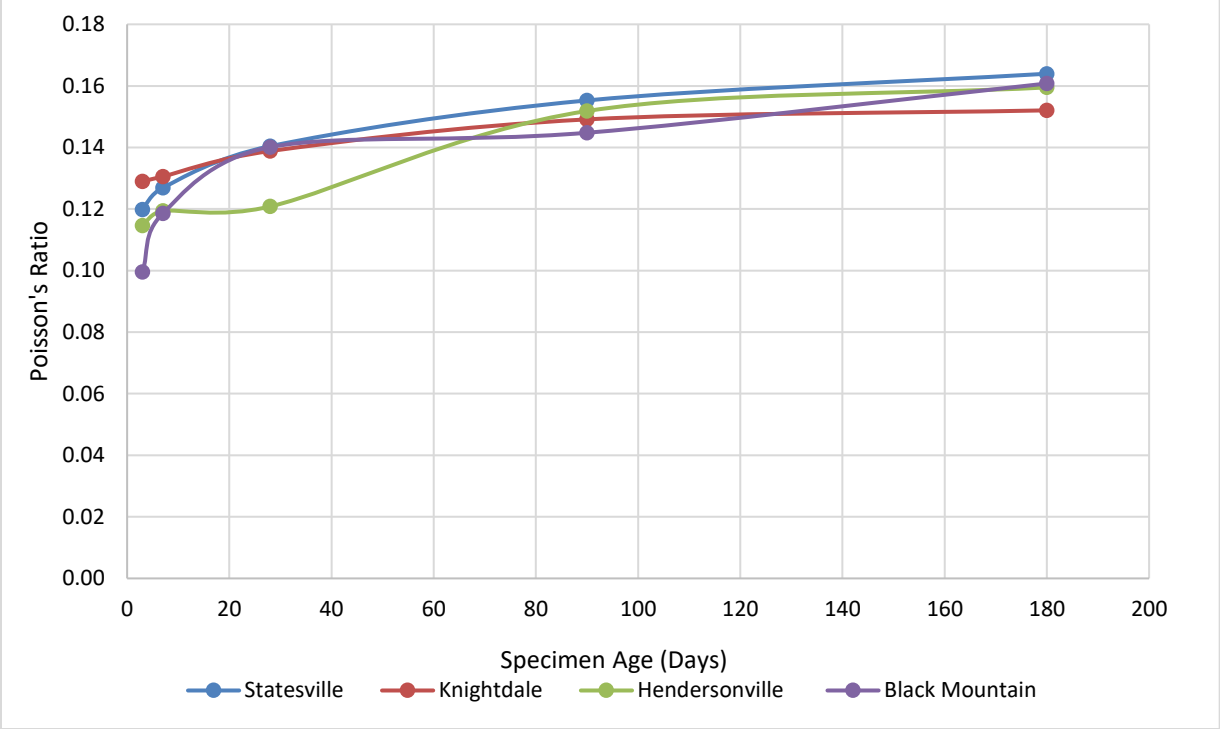

Figure B.12: Average Poisson's ratio with mixtures grouped by coarse aggregate source

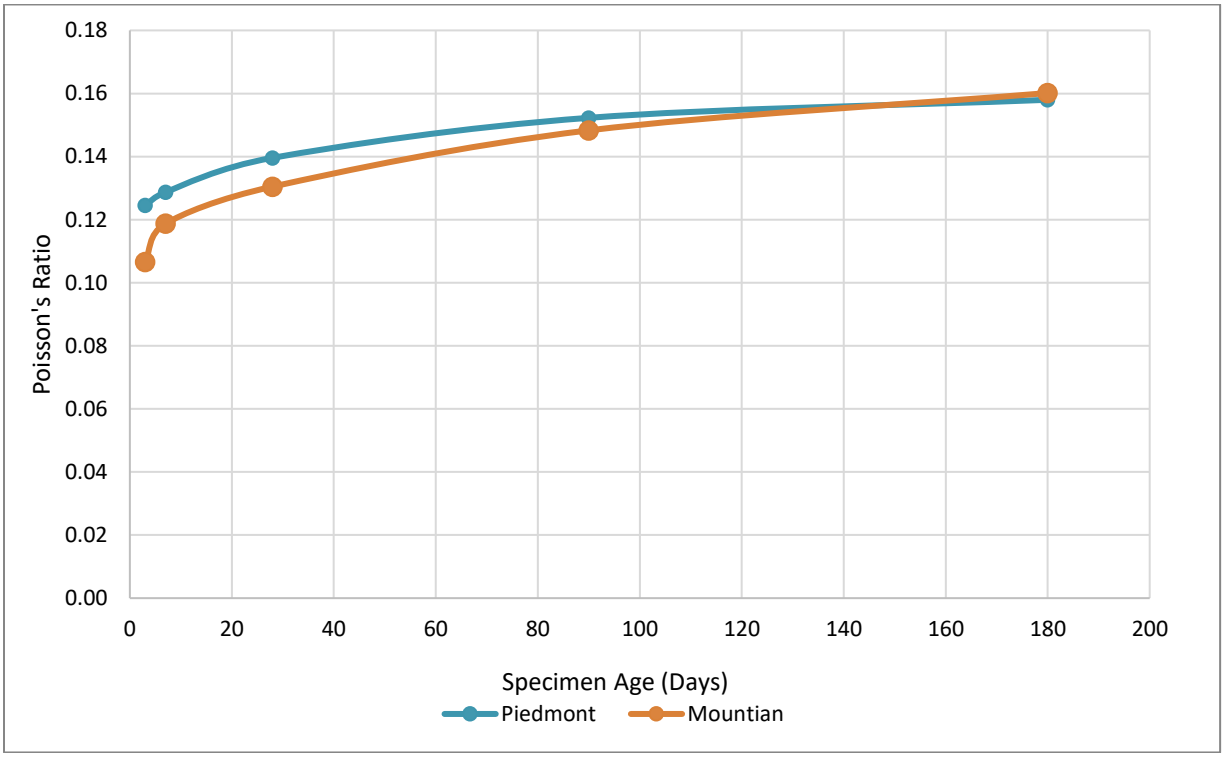

Figure B.13: Average Poisson's ratio with mixtures grouped by region of North Carolina from which the coarse aggregate was sourced

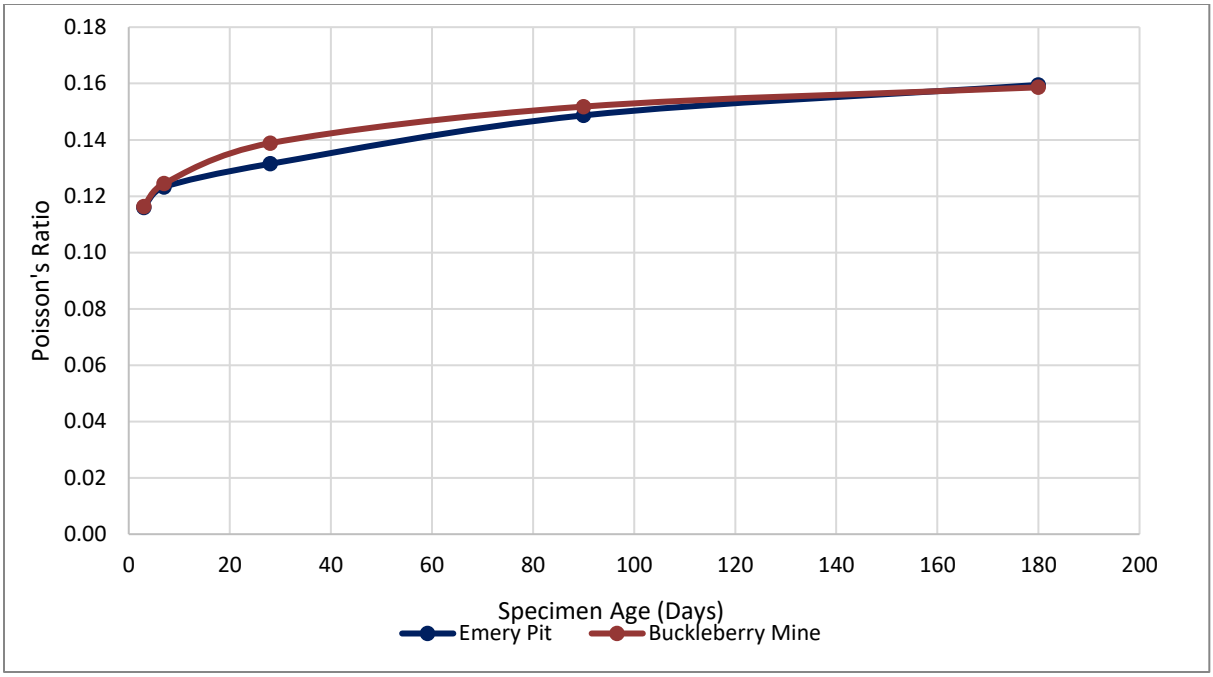

Figure B.14: Average Poisson's ratio with mixtures grouped by location from which the fine aggregate was sourced

Table B.10: MOR test results

Mixture ID	Specimen 1	Specimen 2	28-day average
C1N1O	715	674	695
C1N1OF20	591	639	615
C1N1OF30	508	591	550
C1N2O	688	658	673
C1N2OF20	584	640	612
C1N2OF30	553	556	554
C2N1O	688	658	673
C2N1OF20	547	574	561
C2N1OF30	491	539	515
C2N2O	602	626	614
C2N2OF20	587	500	543
C2N2OF30	501	517	509
C3N1O	673	699	686
C3N1OF20	616	597	607
C3N1OF30	525	532	528
C3N2O	622	644	633
C3N2OF20	601	604	603
C3N2OF30	527	555	541
C4N1O	709	698	704
C4N1OF20	630	624	627
C4N1OF30	594	619	607
C4N2O	637	605	621
C4N2OF20	662	673	668
C4N2OF30	630	599	614

Table B.11: Average 28-day MOR with mixtures grouped by aggregate source and fly ash content

Material		Modulus of Rupture (psi)	
		28 Day average	Standard deviation
Coarse Aggregate	Statesville	616	62
	Knightdale	569	65
	Hendersonville	600	57
	Black Mountain	640	38
	Piedmont	593	67
	Mountain	620	52
Fine Aggregate	Emery Pit	614	67
	Buckleberry Mine	599	54
Fly ash Content	100% OPC	662	37
	20% Fly ash replacement	604	43
	30% Fly ash replacement	552	43

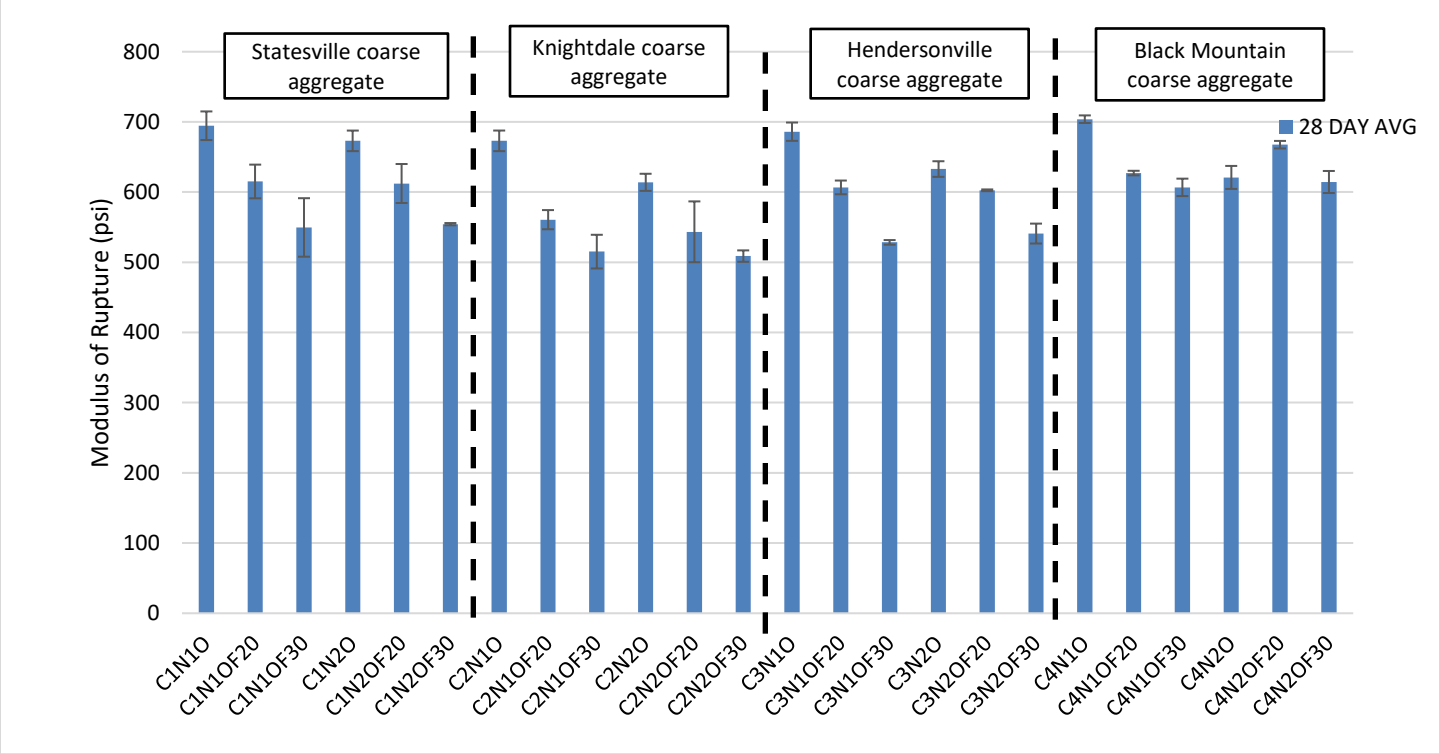

Figure B.21: 28-day MOR test results with mixtures grouped by coarse aggregate source

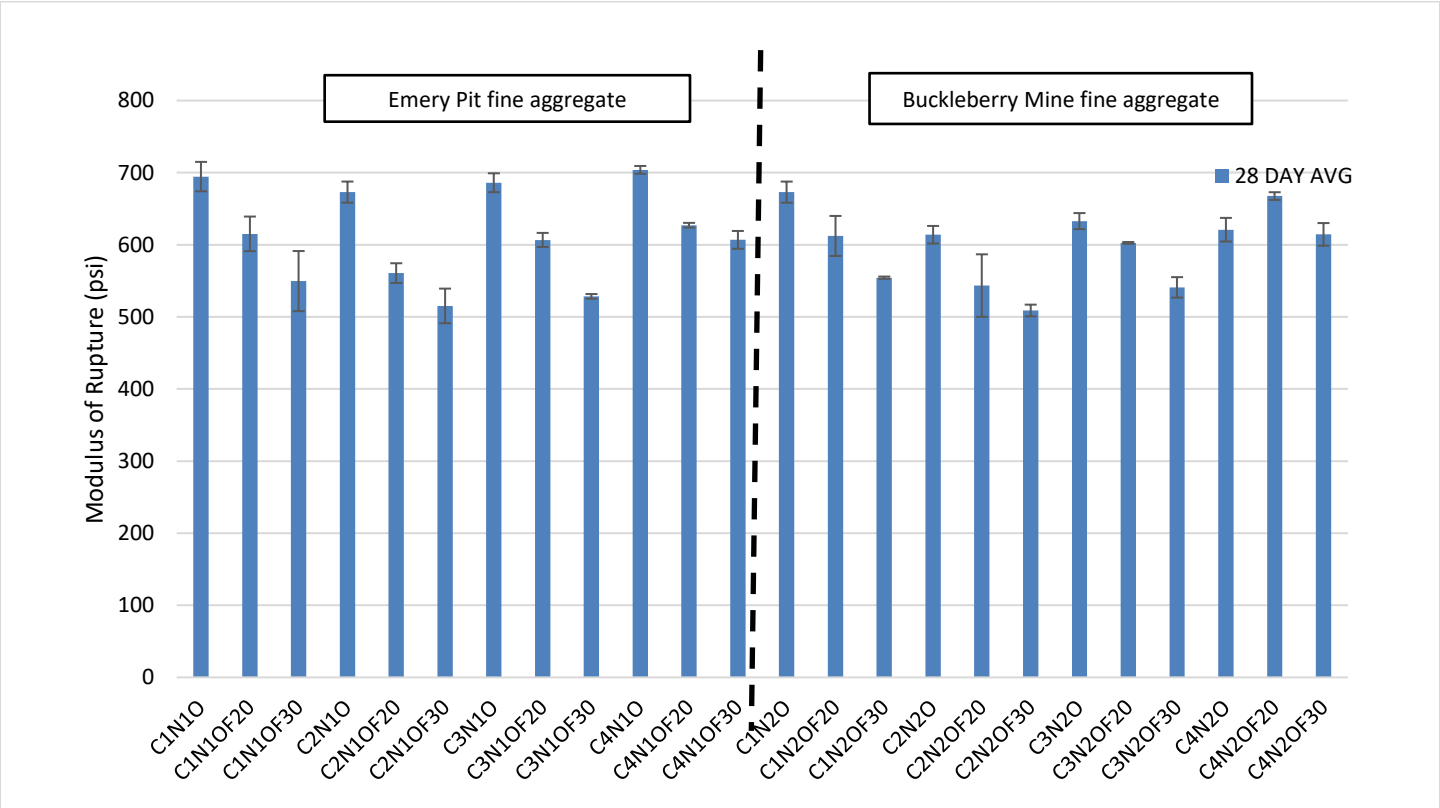

Figure B.22: 28-day MOR test results with mixtures grouped by fine aggregate source

Table B.12: Average CTE test results

Mixture ID	Coefficient of thermal expansion ($\times 10^{-6}$ inch per inch per degree Fahrenheit)				270-day average	360-day average*
	14-day average	28-day average	90-day average	180-day average		
C1N1O	5.595	5.666	5.477	5.400	5.338	5.49
C1N1OF20	5.461	5.433	5.390	5.310	5.419	5.52
C1N1OF30	5.356	5.325	5.251	5.151	5.270	5.33
C1N2O	5.397	5.358	5.313	5.191	5.362	5.37
C1N2OF20	5.218	5.195	5.142	5.127	5.352	5.41
C1N2OF30	5.289	5.164	5.172	5.153	5.296	5.35
C2N1O	5.293	5.227	5.183	5.128	5.193	5.18 (595)
C2N1OF20	5.152	5.124	5.112	5.162	5.193	5.29
C2N1OF30	5.028	5.049	5.098	4.997	5.025	5.27
C2N2O	5.053	5.073	5.014	4.886	4.980	5.06
C2N2OF20	5.032	5.003	4.956	4.953	5.081	5.03
C2N2OF30	4.853	4.771	4.807	4.739	4.957	4.94 (579)
C3N1O	5.126	5.040	5.029	5.071	5.131	5.14
C3N1OF20	4.944	4.987	4.827	5.022	5.065	5.07
C3N1OF30	4.918	4.881	4.861	4.983	5.014	5.08
C3N2O	5.013	4.923	4.815	4.951	4.960	5.00
C3N2OF20	4.737	4.739	4.839	4.856	4.993	4.94
C3N2OF30	4.685	4.675	4.583	4.720	4.862	4.81
C4N10	5.584	5.657	5.604	5.568	5.724	5.70 (453)
C4N1OF20	5.497	5.522	5.463	5.490	5.698	5.66 (454)
C4N1OF30	5.429	5.390	5.204	5.410	5.589	5.61 (449)
C4N2O	5.460	5.416	5.570	5.474	---	5.48
C4N2OF20	5.350	5.200	5.318	5.478	---	5.55 (475)
C4N2OF30	5.248	5.144	5.210	5.274	5.419	5.48 (469)

* due to an issue, several mixtures were tested for CTE at an age greater than 360 days. The age at which these tests were made is denoted in parentheses next to the average test result.

Table B.13 Average CTE test results grouped by aggregate source and fly ash content

Material		Coefficient of Thermal Expansion ($\times 10^{-6}$ inch per inch per degree Fahrenheit)			
		14-Day average	28-Day average	90-Day average	180-Day average
Coarse Aggregate	Statesville	5.39	5.35	5.29	5.22
	Knightdale	5.07	5.04	5.03	4.98
	Hendersonville	4.90	4.87	4.83	4.93
	Black Mountain	5.43	5.39	5.39	5.45
	Piedmont	5.23	5.20	5.16	5.10

	Mountain	5.17	5.13	5.11	5.19
Fine Aggregate	Emery Pit	5.28	5.28	5.21	5.22
	Buckleberry Mine	5.17	5.05	5.06	5.07
Fly ash Content	100% OPC	5.32	5.29	5.25	5.21
	20% Fly ash replacement	5.17	5.15	5.13	5.17
	30% Fly ash replacement	5.10	5.05	5.02	5.05

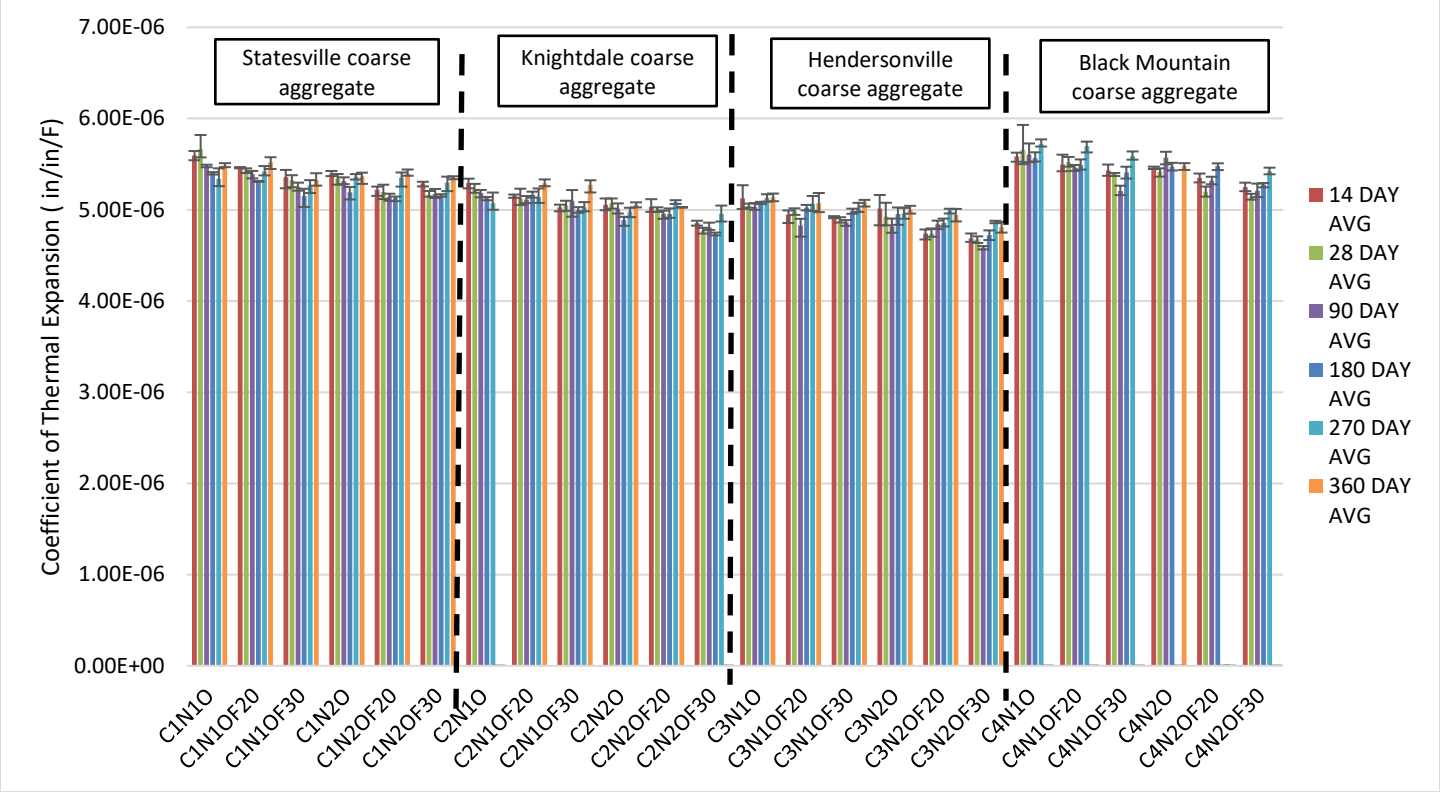

Figure B.23: Average CTE with mixtures grouped by coarse aggregate source

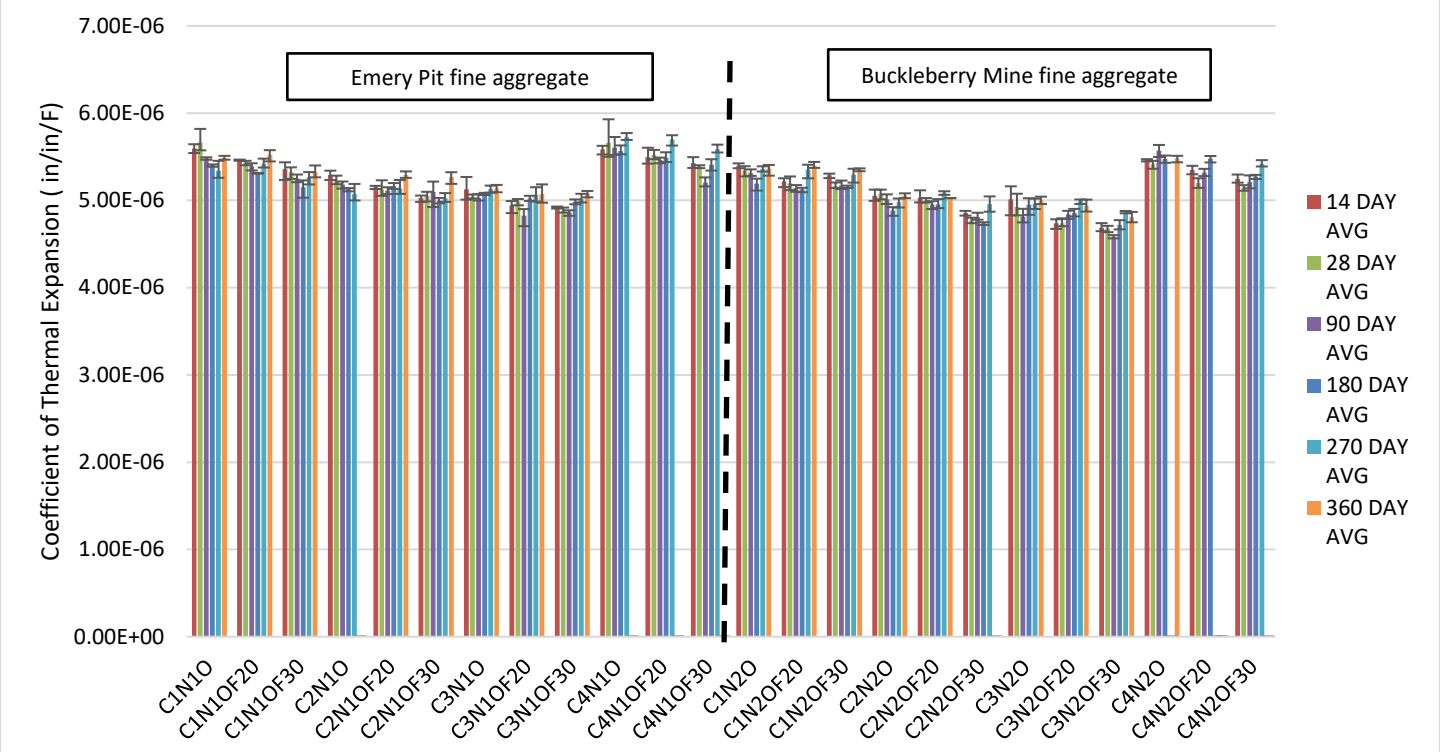

Figure B.24: Average CTE test results with mixtures grouped by fine aggregate source

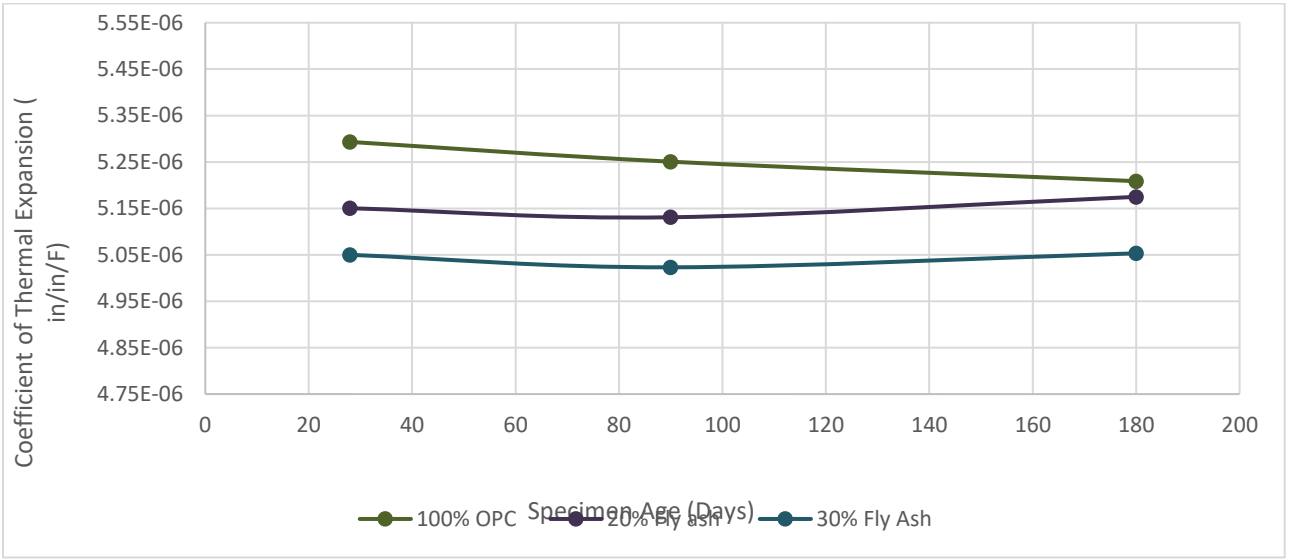

Figure B.25: Average CTE with mixtures grouped by fly ash content

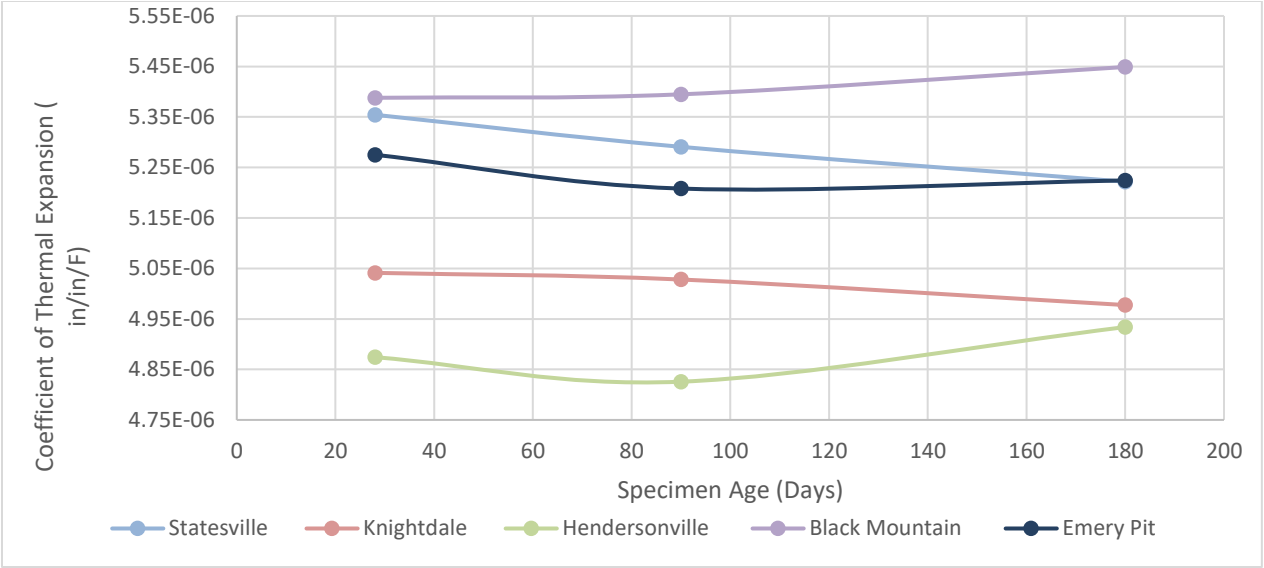

Figure B.26: Average CTE with mixtures grouped by coarse aggregate source

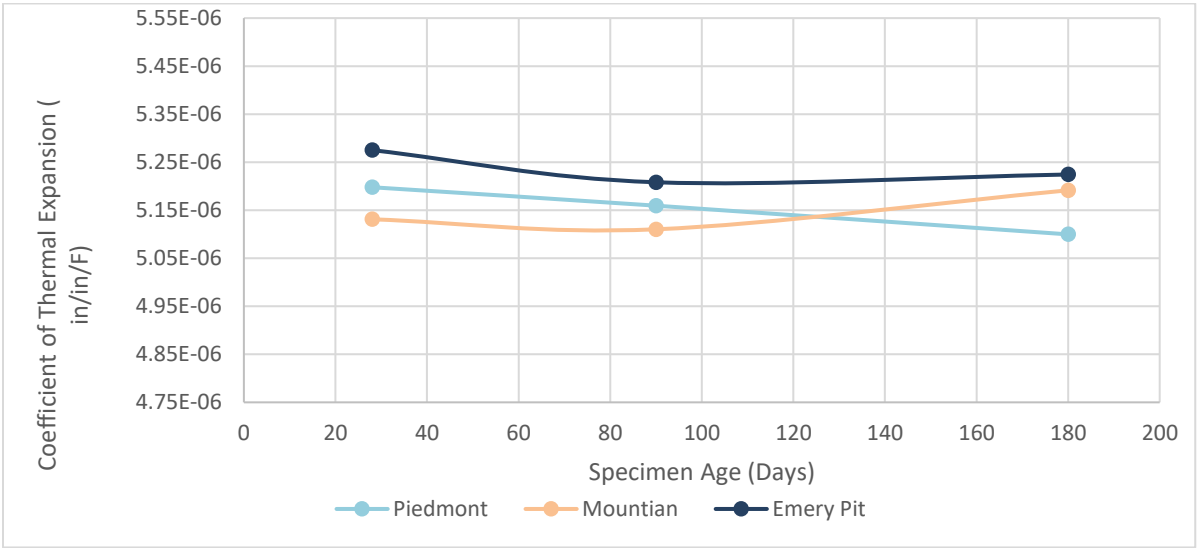

Figure B.27: Average CTE with mixtures grouped by region of North Carolina from which the coarse aggregate was sourced

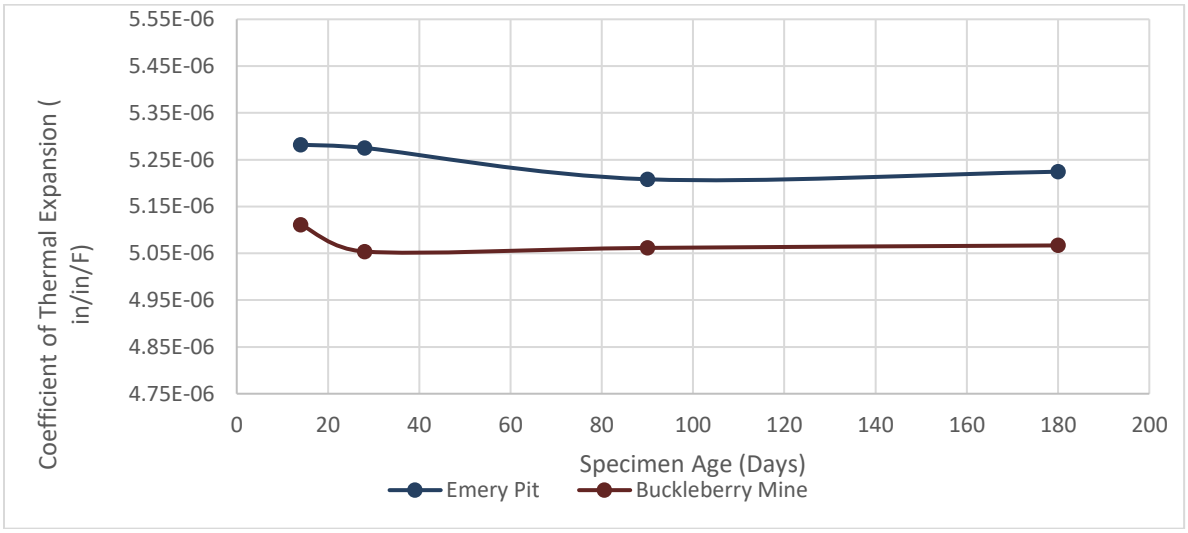

Figure B.28: Average CTE with mixtures grouped by location from which the fine aggregate was sourced

Table B.14: Average thermal conductivity test results

Mixture ID	Thermal conductivity (Btu/ (ft · hr · °F))	
	56-day average	90-day average
C1N1O	1.057	1.007
C1N1OF20	0.922	0.903
C1N1OF30	0.886	0.829
C1N2O	1.150	1.133
C1N2OF2O	0.930	0.914
C1N2OF30	0.871	0.875
C2N1O	1.040	1.037
C2N1OF20	0.793	0.732
C2N1OF30	0.959	0.906
C2N2O	0.926	0.882
C2N2OF20	0.834	0.785
C2N2OF30	0.834	0.755
C3N1O	0.996	0.961
C3N1OF20	0.837	0.863
C3N1OF30	0.877	0.859
C3N2O	1.017	0.951
C3N2OF20	0.938	0.889
C3N2OF30	0.929	0.914
C4N1O	0.964	0.951
C4N1OF20	1.077	1.032
C4N1OF30	1.032	0.902
C4N2O	0.972	0.929
C4N2OF20	0.982	0.961
C4N2OF30	0.930	0.896

Table B.15: Average thermal conductivity test results with concrete mixtures grouped by aggregate source and fly ash content

Material		Thermal Conductivity (Btu/ (ft · hr · °F))	
		56-day average	90-day average
Coarse Aggregate	Statesville	0.97	0.93
	Knightdale	0.90	0.85
	Hendersonville	0.93	0.91
	Black Mountain	0.99	0.95
	Piedmont	0.93	0.89
	Mountain	0.96	0.93
Fine Aggregate	Emery Pit	0.95	0.92
	Buckleberry Mine	0.94	0.90
Fly ash Content	100% OPC	1.02	0.97

	20% Fly ash replacement	0.91	0.88
	30% Fly ash replacement	0.91	0.87

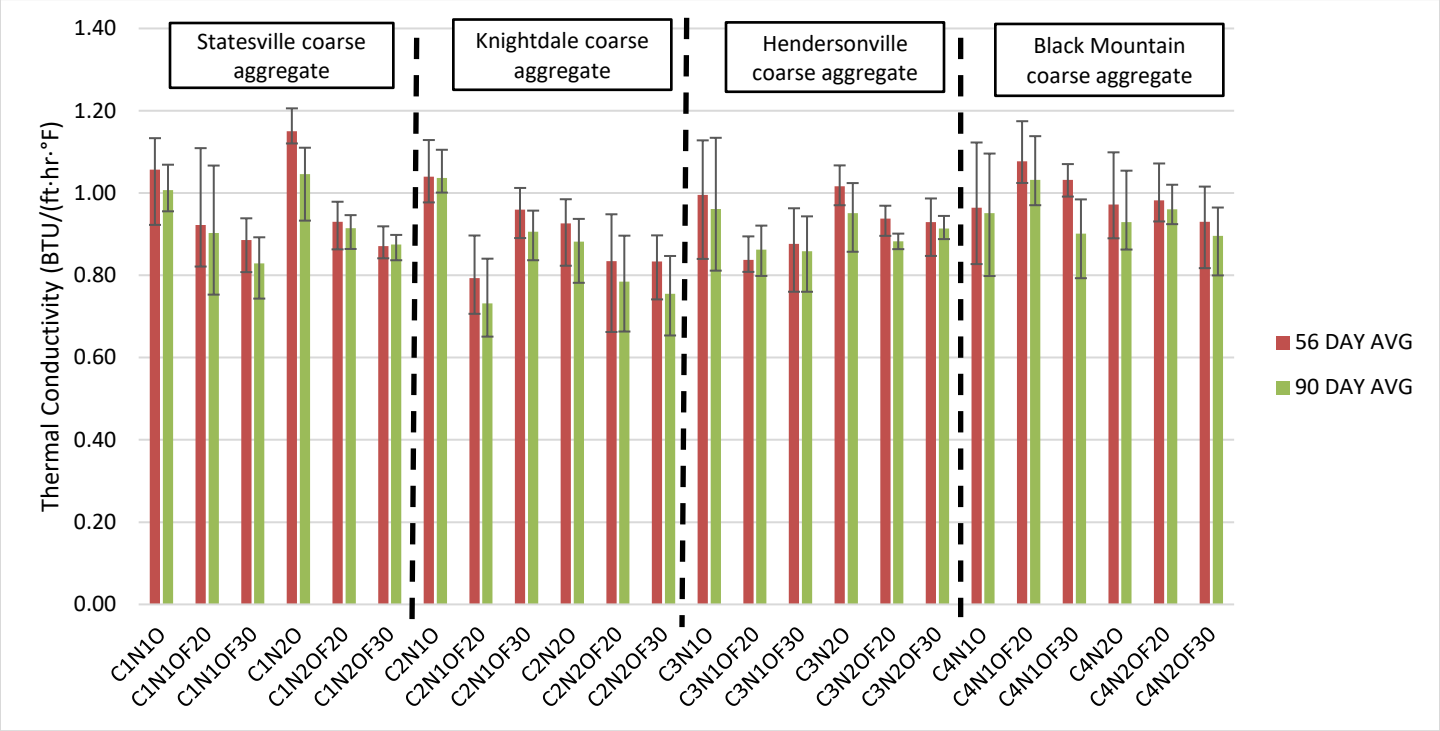

Figure B.29: Average thermal conductivity test results with mixtures grouped by coarse aggregate source

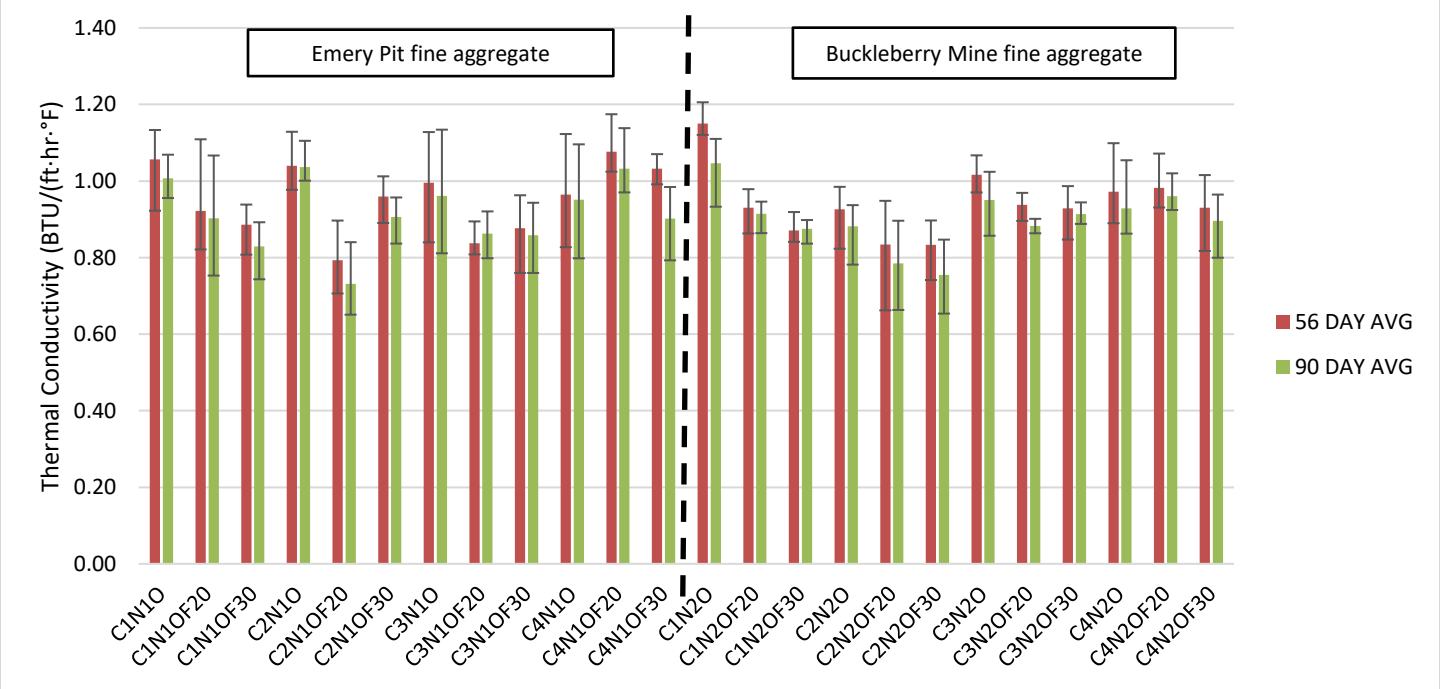

Figure B.30: Average thermal conductivity test results test results with mixtures grouped by fine aggregate source

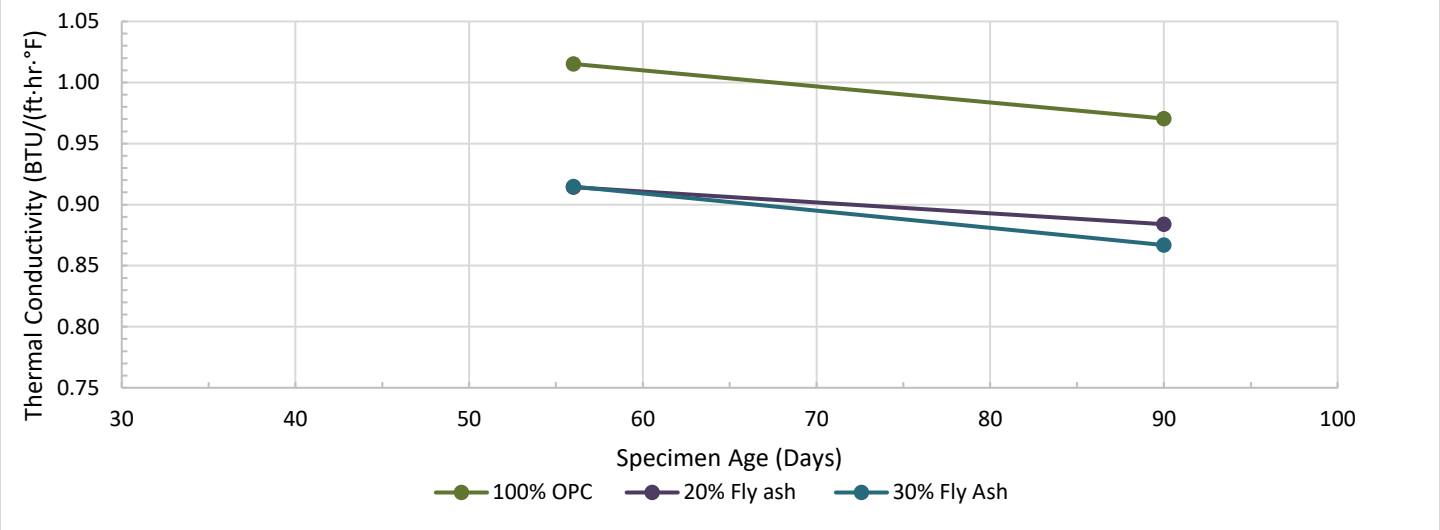

Figure B.31: Average thermal conductivity test results with mixtures grouped by fly ash content

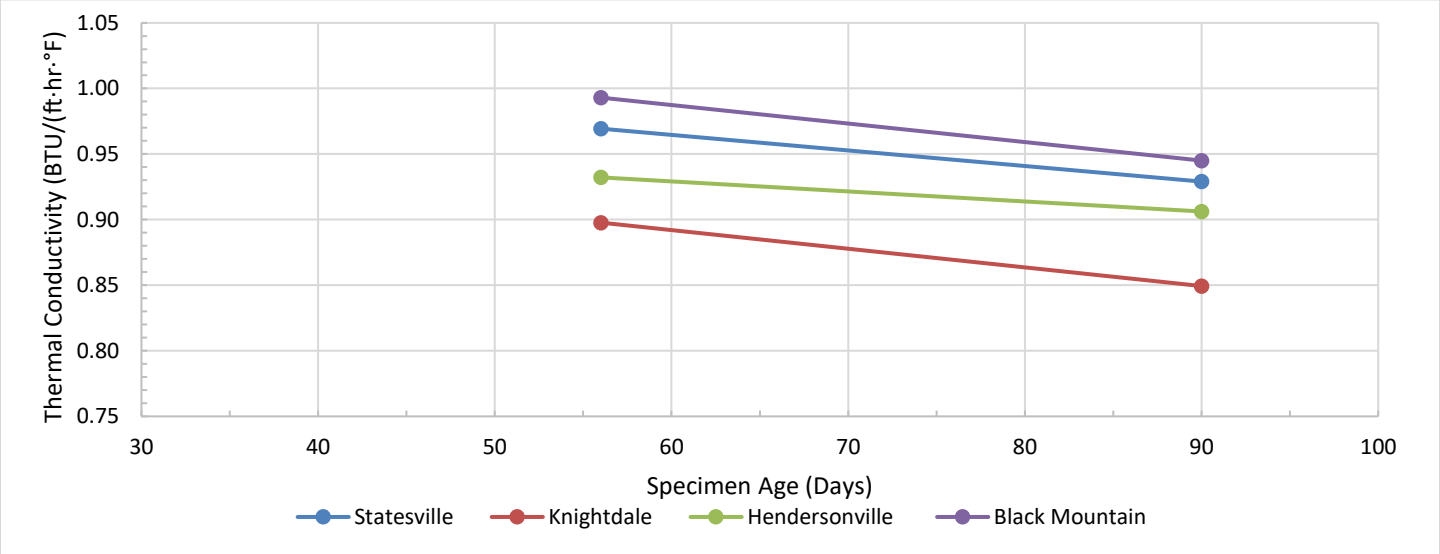

Figure B.32: Average thermal conductivity test results with mixtures grouped by coarse aggregate source

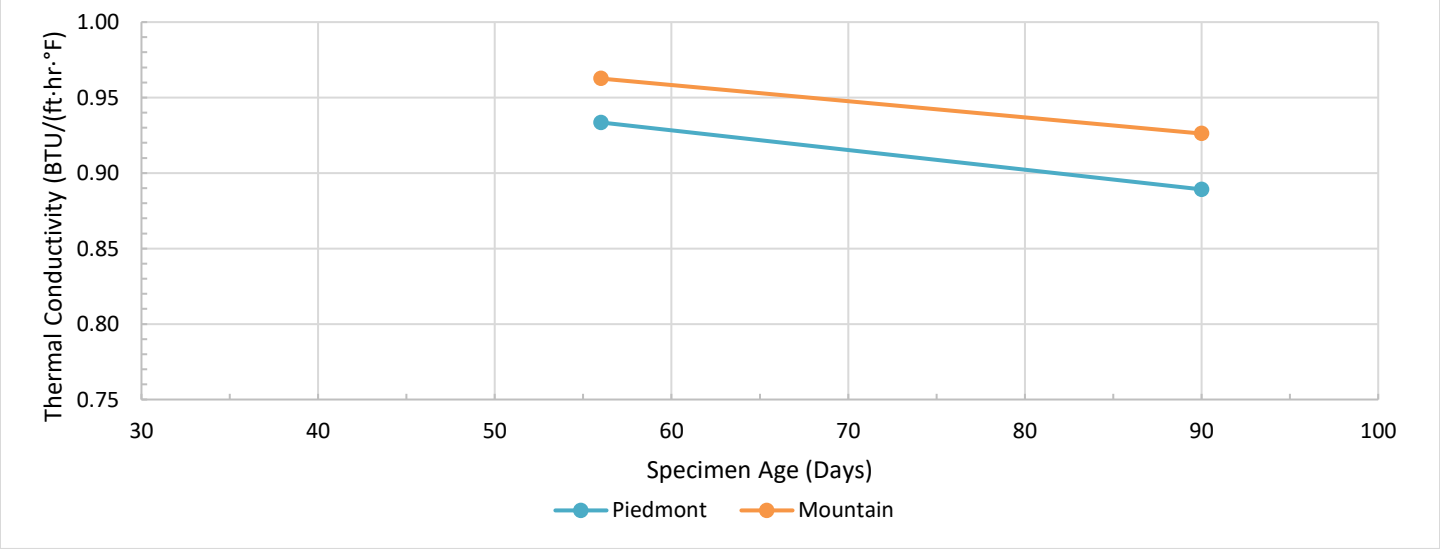

Figure B.33: Average thermal conductivity test results with mixtures grouped by region of North Carolina from which the coarse aggregate was sourced

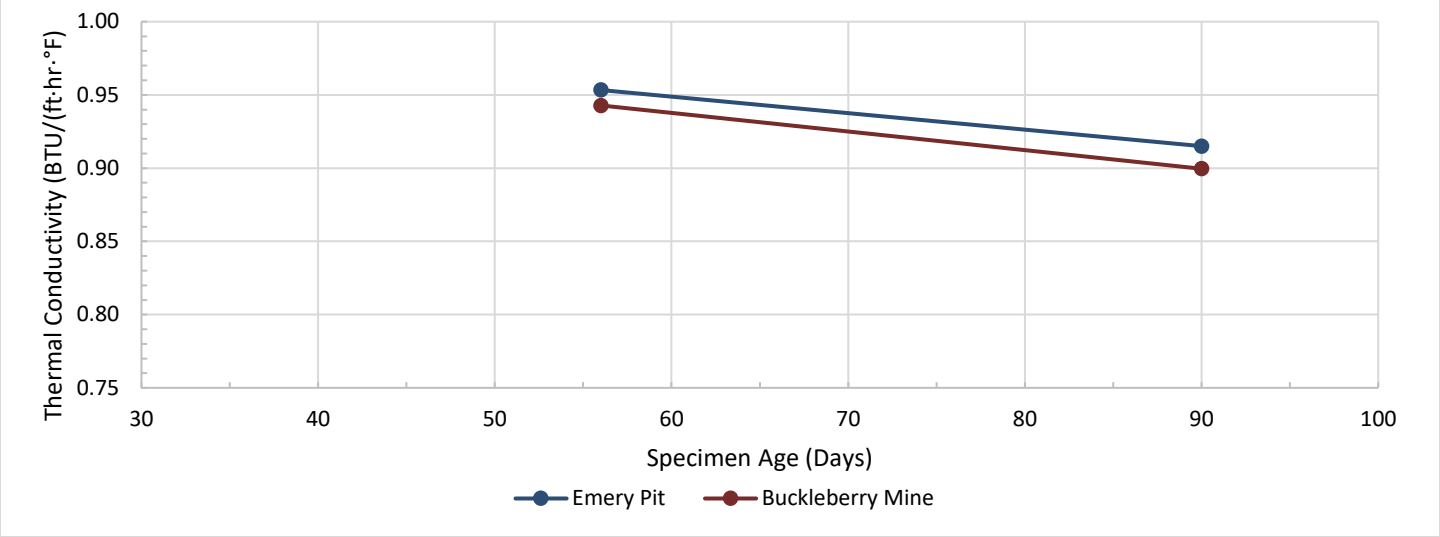

Figure B.34: Average thermal conductivity test results with mixtures grouped by location from which the fine aggregate was sourced

Table B.16: Average heat capacity test results

Mixture ID	Heat capacity (Btu/ (lb-°F))	
	56-day average	90-day average
C1N1O	0.194	0.189
C1N1OF20	0.186	0.174
C1N1OF30	0.178	0.170
C1N2O	0.183	0.177
C1N2OF2O	0.175	0.171
C1N2OF30	0.181	0.178
C2N1O	0.186	0.179
C2N1OF20	0.178	0.171
C2N1OF30	0.184	0.176
C2N2O	0.182	0.175
C2N2OF20	0.177	0.170
C2N2OF30	0.175	0.170
C3N1O	0.184	0.178
C3N1OF20	0.179	0.173
C3N1OF30	0.174	0.170
C3N2O	0.183	0.184
C3N2OF20	0.187	0.184
C3N2OF30	0.182	0.176
C4N1O	0.185	0.182
C4N1OF20	0.186	0.179
C4N1OF30	0.179	0.175
C4N2O	0.187	0.179
C4N2OF20	0.180	0.175
C4N2OF30	0.178	0.171

Table 4.16: Average heat capacity test results summarized by aggregate and fly ash content

Material		Heat Capacity (Btu/ (lb-°F))	
		56 Day average	90-day average
Coarse Aggregate	Statesville	0.183	0.176
	Knightdale	0.180	0.173
	Hendersonville	0.182	0.178
	Black Mountain	0.183	0.177
	Piedmont	0.182	0.175
	Mountain	0.182	0.177
Fine Aggregate	Emery Pit	0.183	0.173
	Buckleberry Mine	0.181	0.176
Fly ash Content	100% OPC	0.186	0.180
	20% Fly ash replacement	0.181	0.175
	30% Fly ash replacement	0.179	0.173

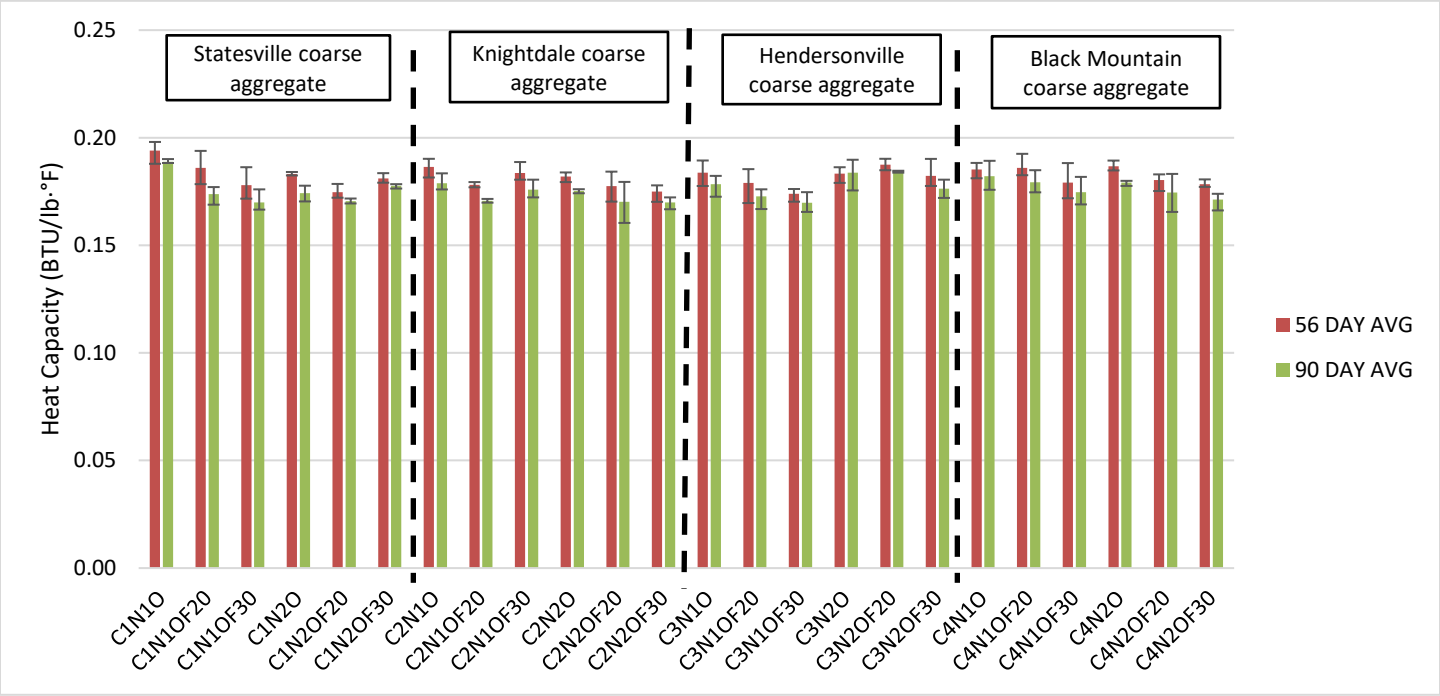

Figure B.35: Average heat capacity test results with mixtures grouped by coarse aggregate source

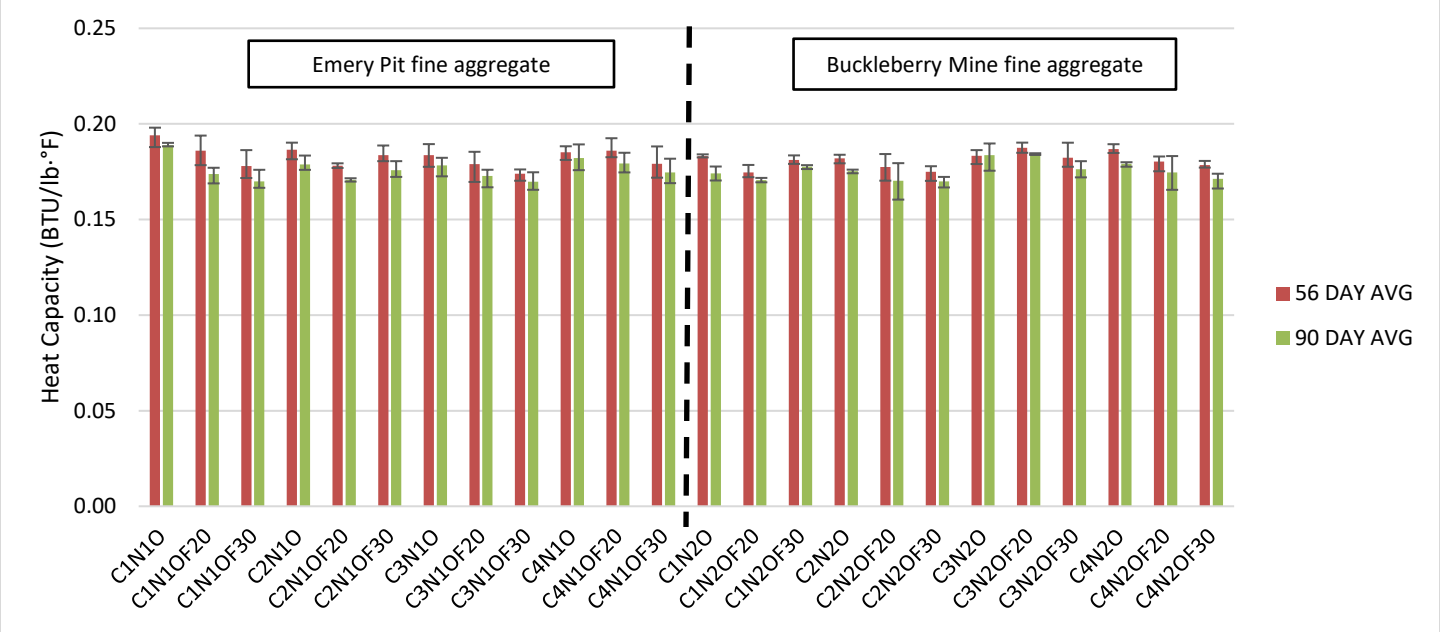

Figure B.36: Average heat capacity test results test results with mixtures grouped by fine aggregate source

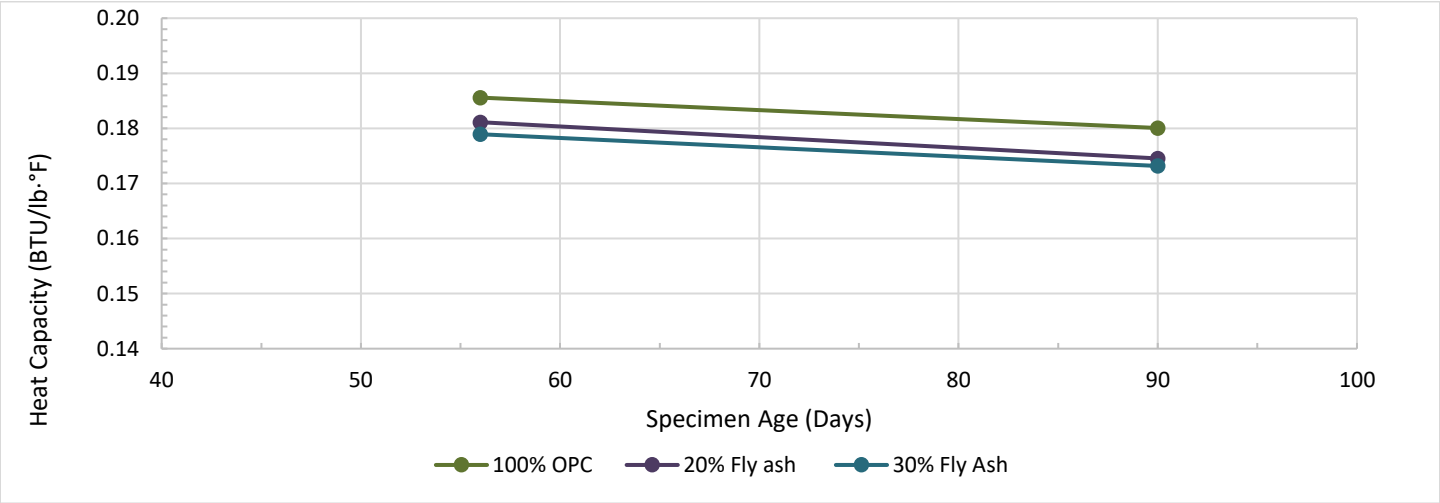

Figure B.37: Average heat capacity test results with mixtures grouped by fly ash content

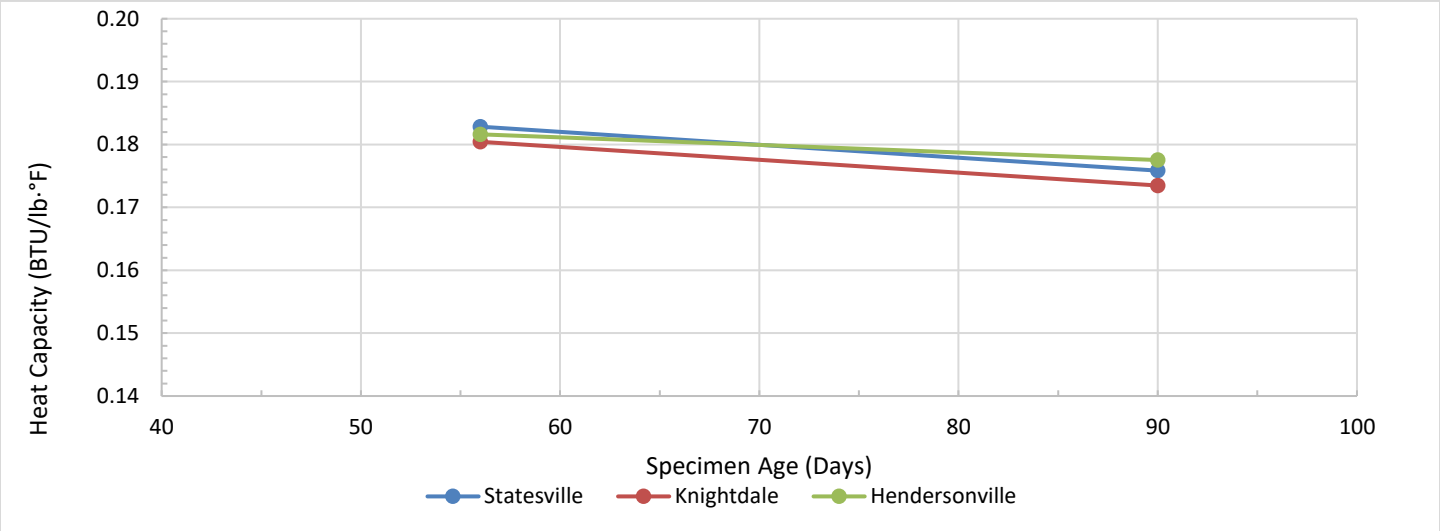

Figure B.38: Average heat capacity test results with mixtures grouped by coarse aggregate source

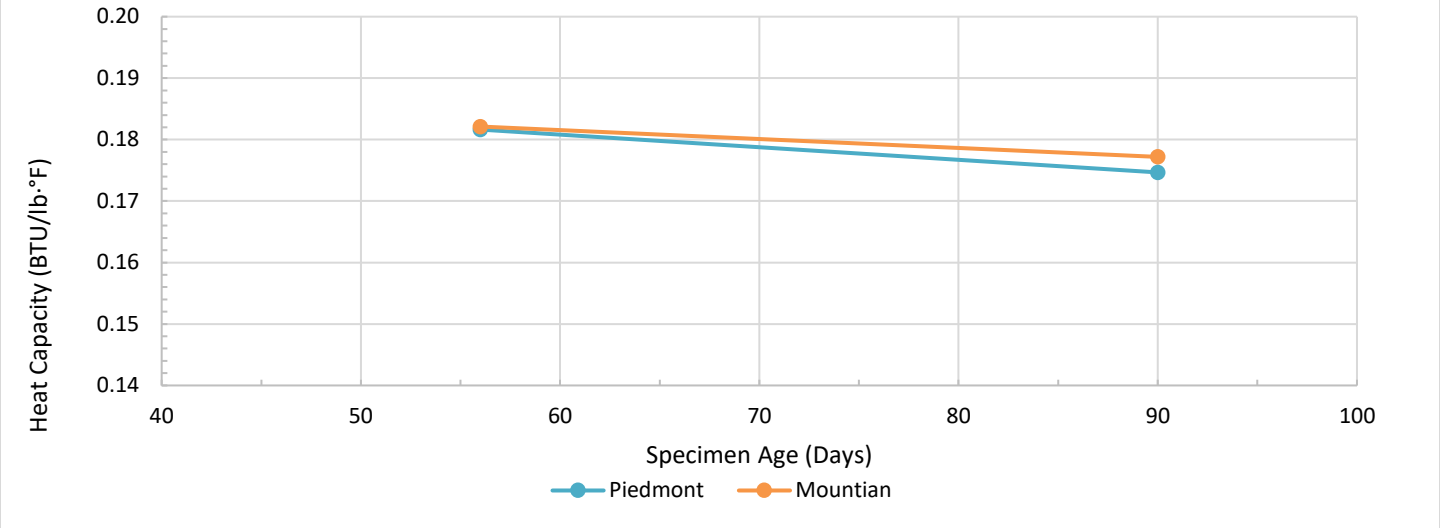

Figure B.39: Average heat capacity test results with mixtures grouped by region of North Carolina from which the coarse aggregate was sourced

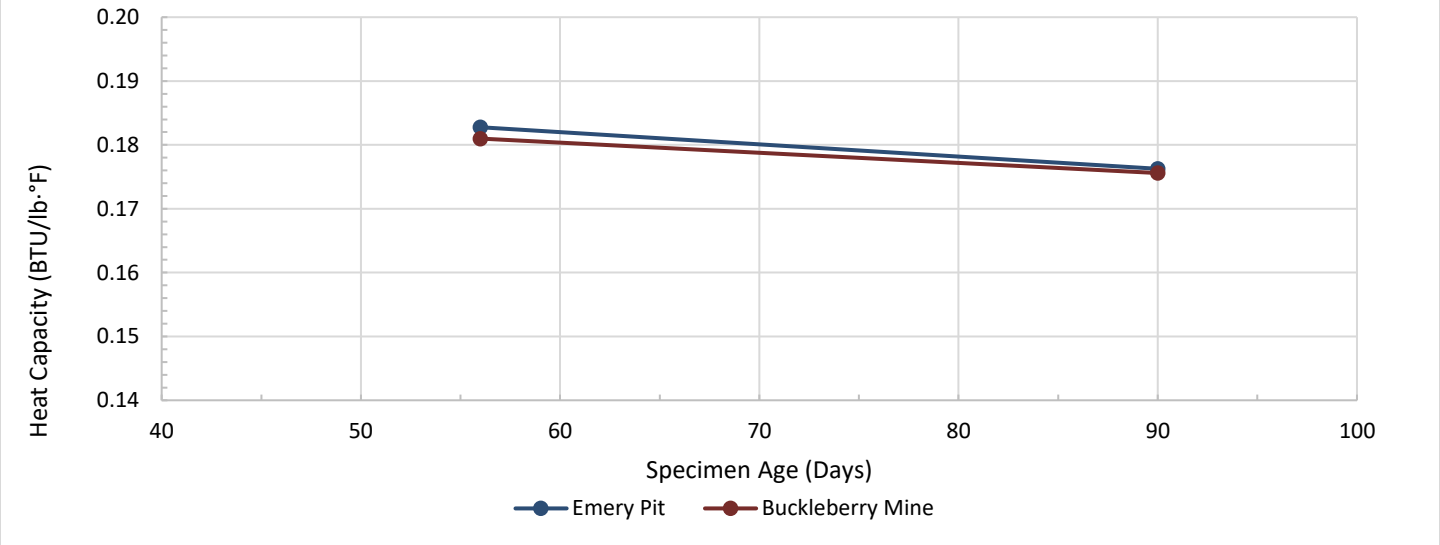

Figure B.40: Average heat capacity test results with mixtures grouped by location from which the fine aggregate was sourced

Table B.18: Average surface resisitivity test results

Mixture ID	Surface resistivity (KΩ-cm)						
	3-day average	7-day average	28-day average	90-day average	180-day average	270-day average	360-day average*
C1N1O	7.1	8.4	10.7	14.6	17.5	17.0	14.9
C1N1OF20	5.2	6.0	11.7	28.7	41.1	45.9	47.6
C1N1OF30	4.6	5.5	12.1	31.1	43.5	53.1	62.2
C1N2O	7.8	10.0	12.7	17.3	20.5	19.1	16.8
C1N2OF2O	6.2	7.0	12.7	31.5	44.7	50.8	90.9 (595)
C1N2OF30	5.2	6.1	14.8	35.2	53.2	64.4	131.7 (595)
C2N1O	8.3	8.6	11.6	15.3	16.5	15.9	18.0 (579)

C2N1OF20	5.5	6.5	13.1	29.6	36.3	41.5	71.3 (572)
C2N1OF30	4.5	5.5	10.0	22.4	30.7	37.8	58.6
C2N2O	8.3	10.1	12.2	17.0	18.7	15.9	19.8 (588)
C2N2OF20	5.9	6.8	11.3	29.6	36.4	42.9	73.4 (588)
C2N2OF30	5.5	6.4	13.9	33.3	47.2	59.8	75.3 (579)
C3N1O	6.4	8.1	11.7	16.2	15.0	14.7	15.0
C3N1OF20	4.9	6.1	10.2	19.0	30.1	37.1	48.3
C3N1OF30	4.8	5.5	10.1	23.6	30.9	52.9	94.4
C3N2O	7.0	8.7	12.1	16.0	16.8	15.9	18.3
C3N2OF20	5.7	7.4	11.7	20.9	34.7	---	75.8
C3N2OF30	5.0	6.0	9.4	21.6	28.3	---	80.4
C4N1O	6.2	8.3	11.1	15.4	14.8	15.0	18.3
C4N1OF20	5.4	5.9	8.2	15.0	22.6	49.6	52.1
C4N1OF30	4.6	6.2	9.4	22.0	38.3	74.7	125.1
C4N2O	7.9	10.1	14.3	19.3	18.7	---	23.5
C4N2OF20	5.5	6.9	10.6	20.0	32.7	---	75.6
C4N2OF30	5.5	6.5	10.4	23.8	40.1	---	89.3

* due to an issue, several mixtures were tested for surface resistivity at an age greater than 360 days. The age at which these tests were made is denoted in parentheses next to the average test result.

Table B.19: Average 28-Day surface resistivity results with concrete mixtures grouped by aggregate and fly ash content

Material		Surface Resistivity (KΩ-cm)	
		28-Day average	Standard deviation
Coarse Aggregate	Statesville	12.4	1.3
	Knightdale	12.0	1.3
	Hendersonville	10.9	1.1
	Black Mountain	10.7	2.0
	Piedmont	12.2	1.3
	Mountain	10.8	1.6
Fine Aggregate	Emery Pit	10.8	1.3
	Buckleberry Mine	12.2	1.6
Fly ash Content	100% OPC	12.0	1.1
	20% Fly ash replacement	11.2	1.5
	30% Fly ash replacement	11.2	2.0

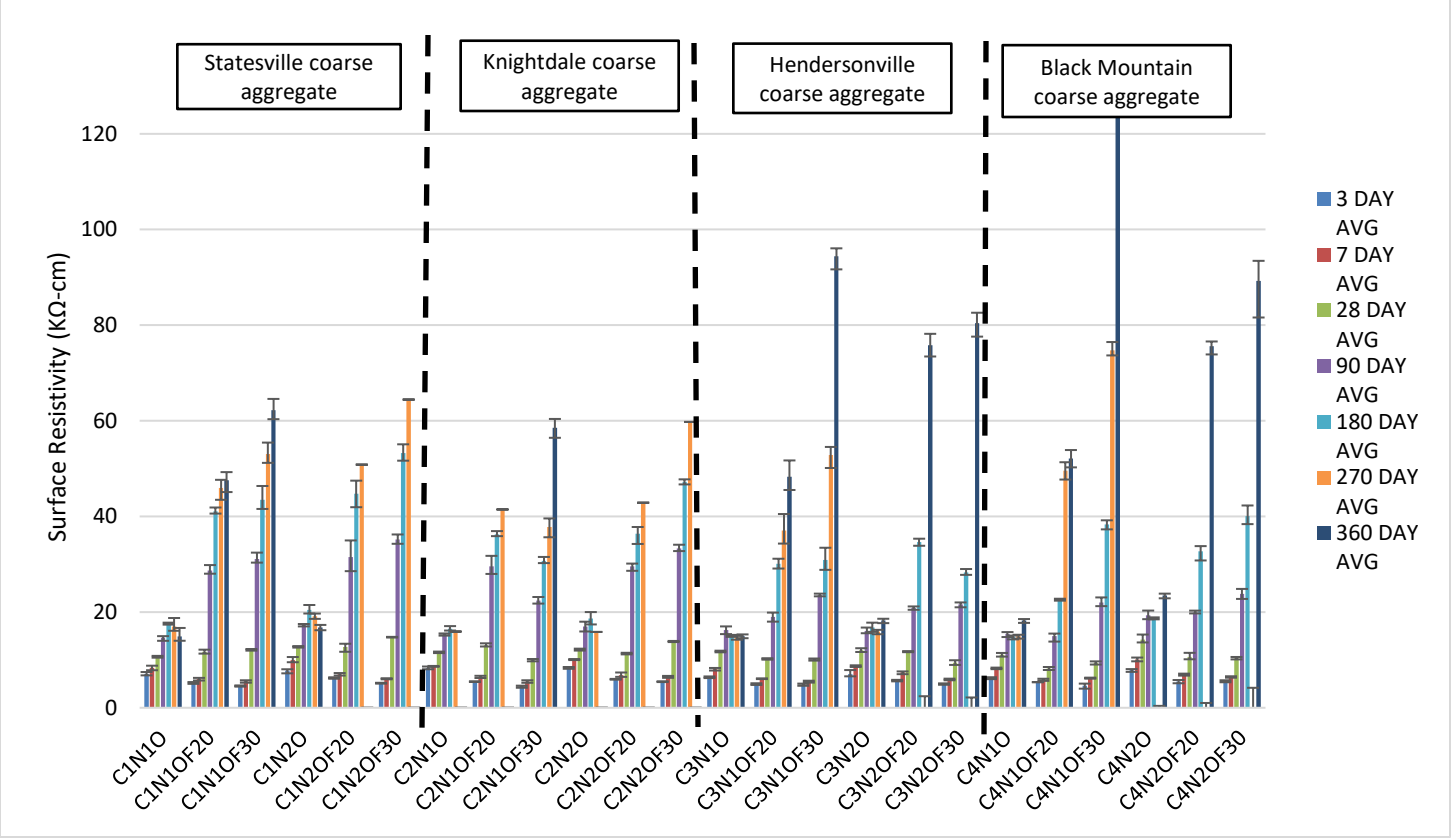

Figure B.41: Average surface resistivity test results with mixtures grouped by coarse aggregate source

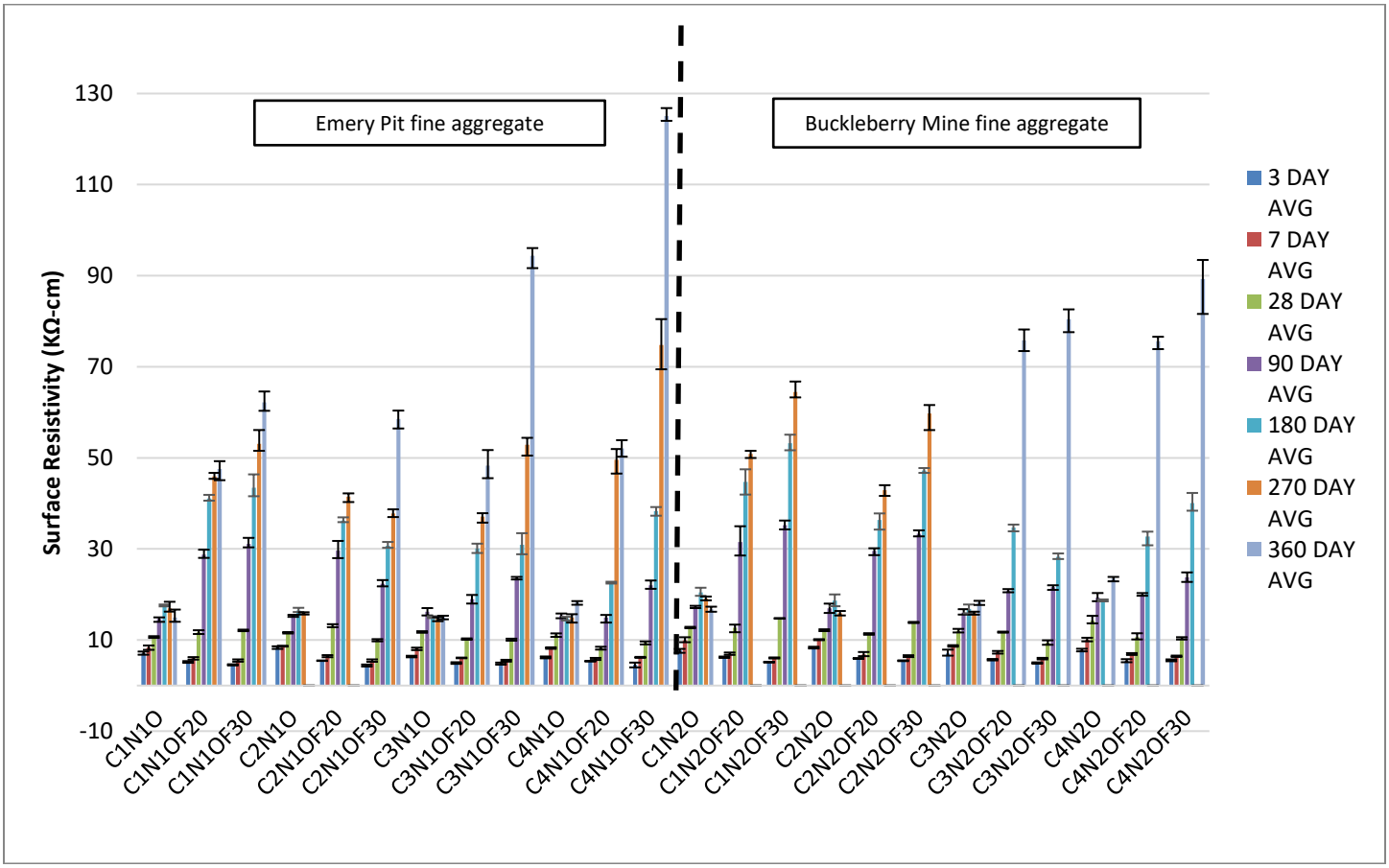

Figure B.42: Average surface resistivity test results test results with mixtures grouped by fine aggregate source

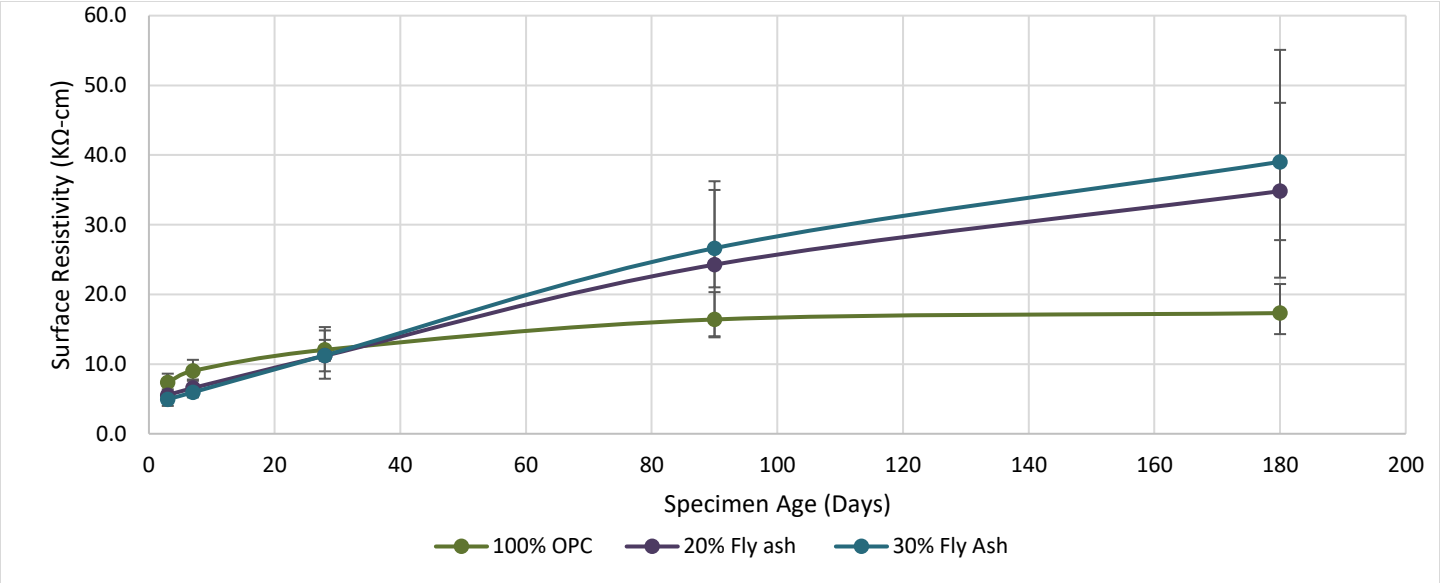

Figure B.43: Average surface resistivity test results with mixtures grouped by fly ash content

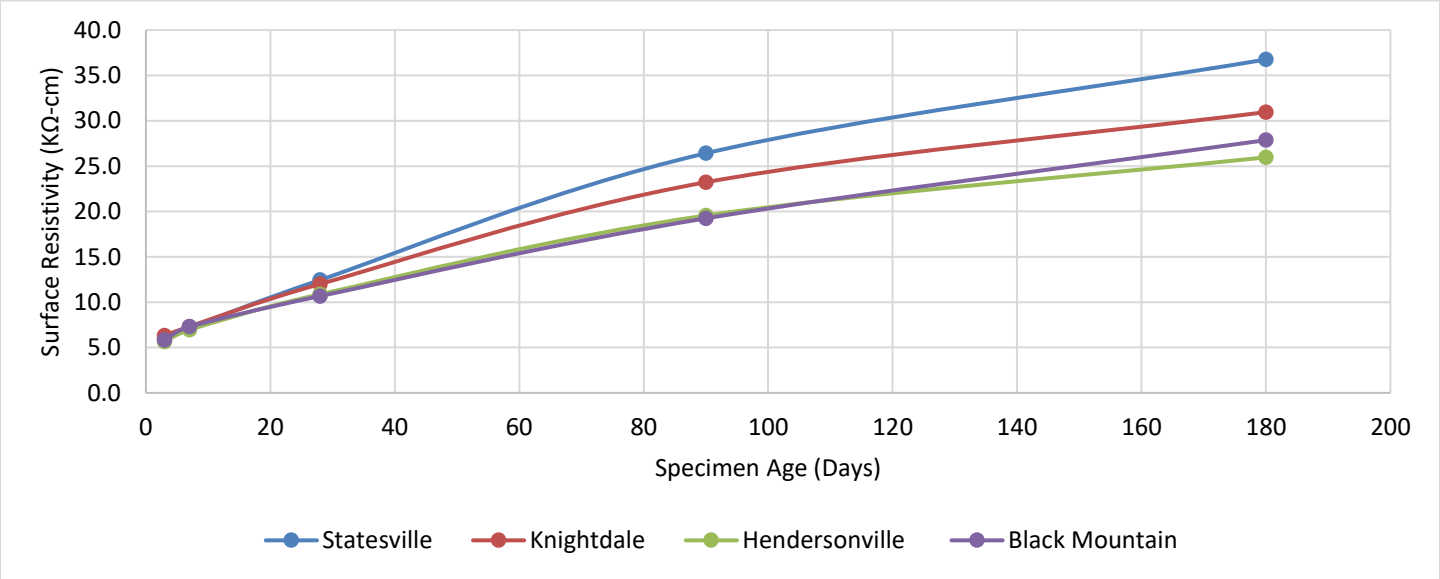

Figure B.44: Average surface resistivity test results with mixtures grouped by coarse aggregate source

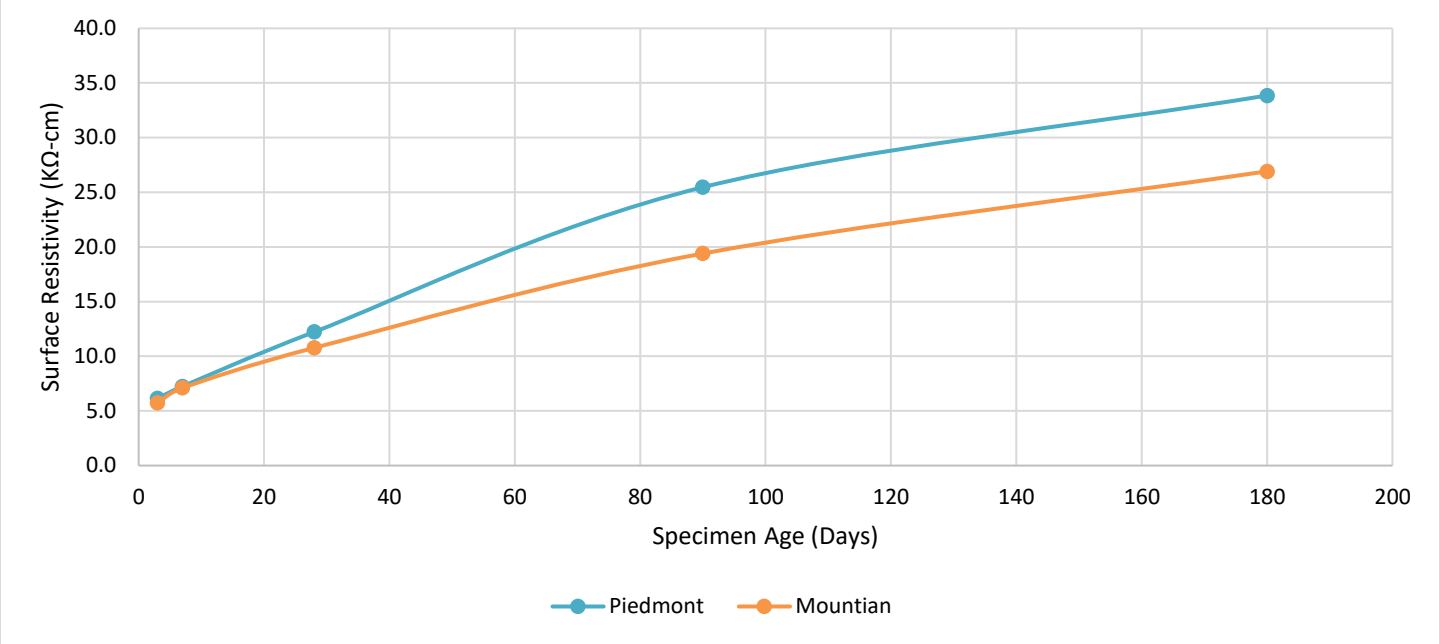

Figure B.45: Average surface resistivity test results with mixtures grouped by region of North Carolina from which the coarse aggregate was sourced

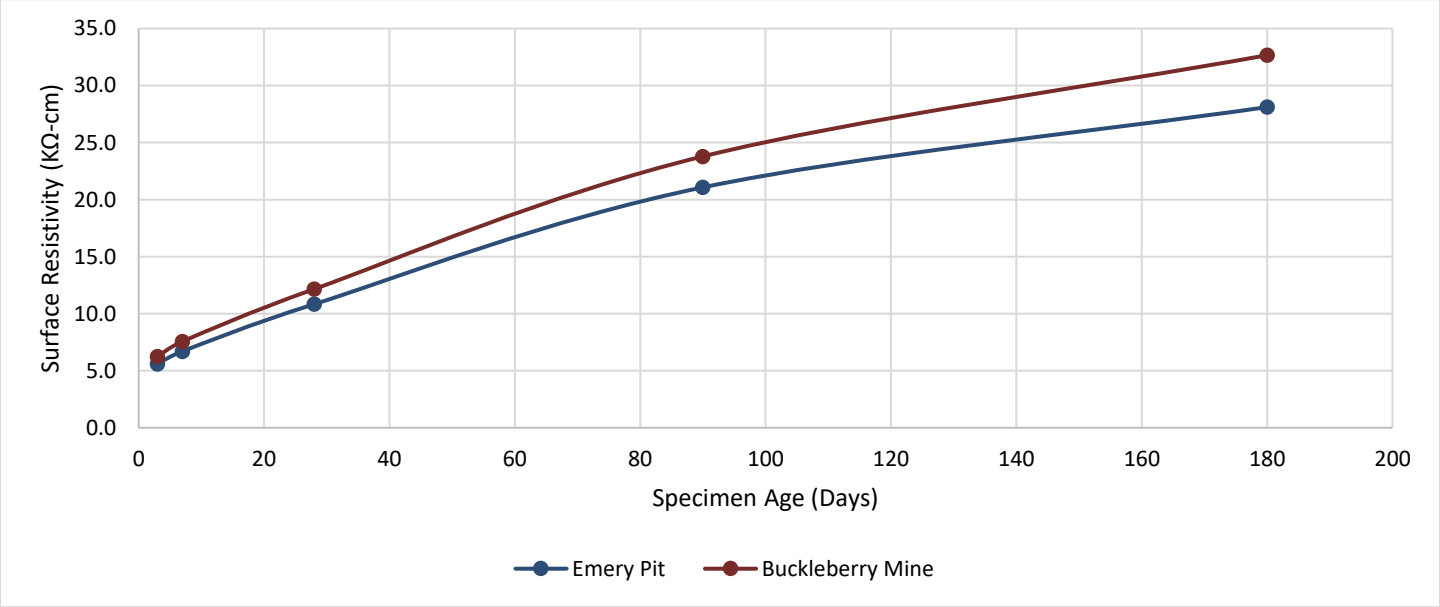

Figure B.46: Average surface resistivity test results with mixtures grouped by location from which the fine aggregate was sourced

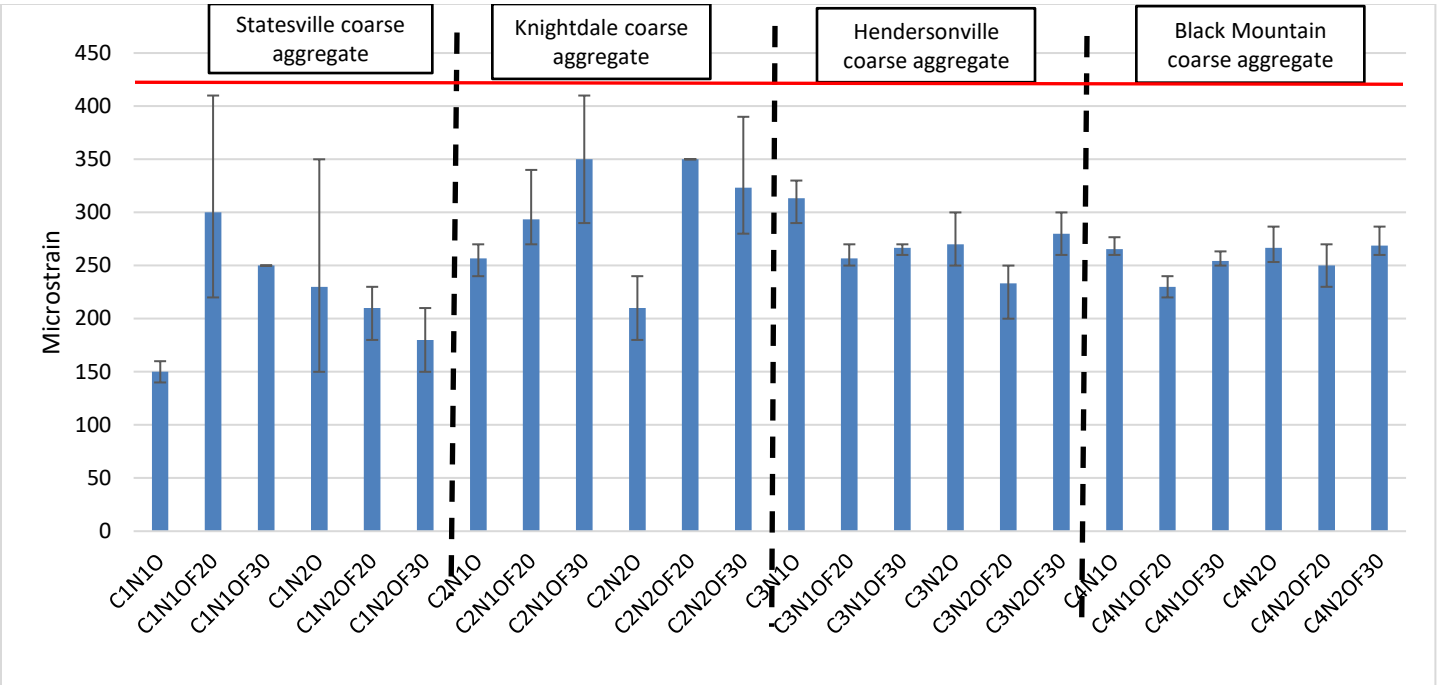

Figure B.47: Average 28-day volumetric shrinkage test results with mixtures grouped by coarse aggregate source

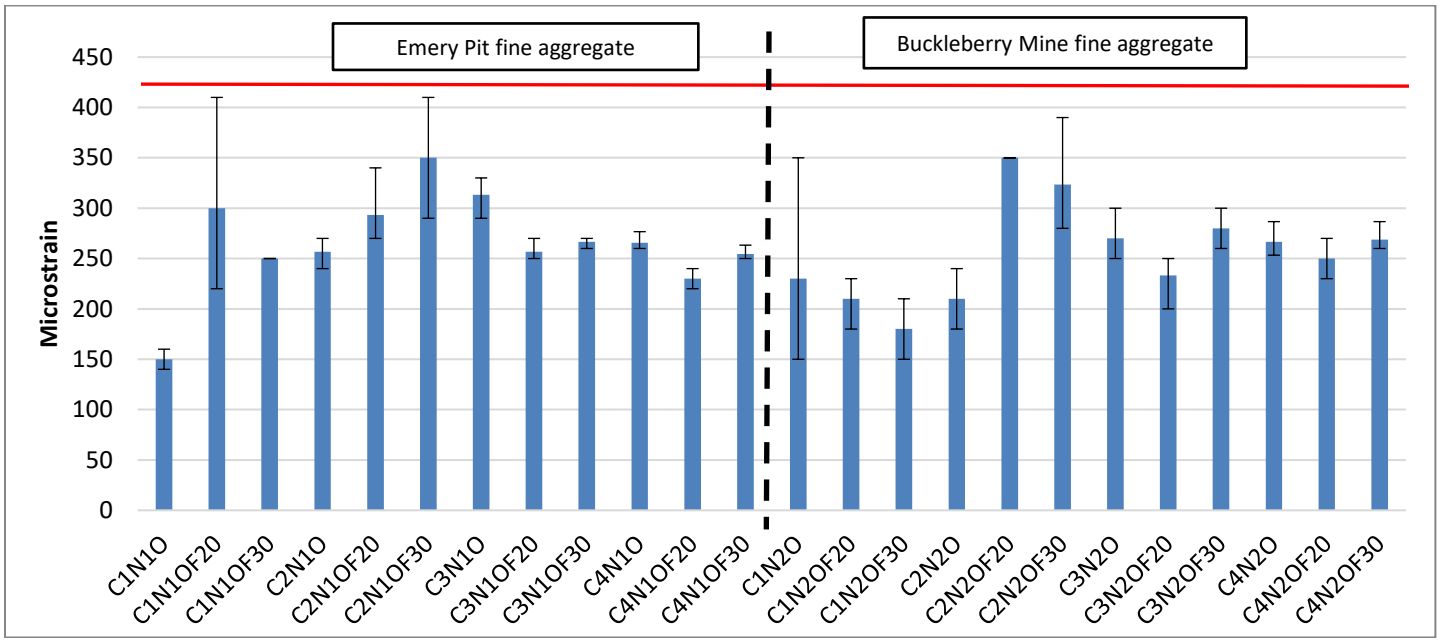

Figure B.48: Average 28-day volumetric shrinkage test results test results with mixtures grouped by fine aggregate source

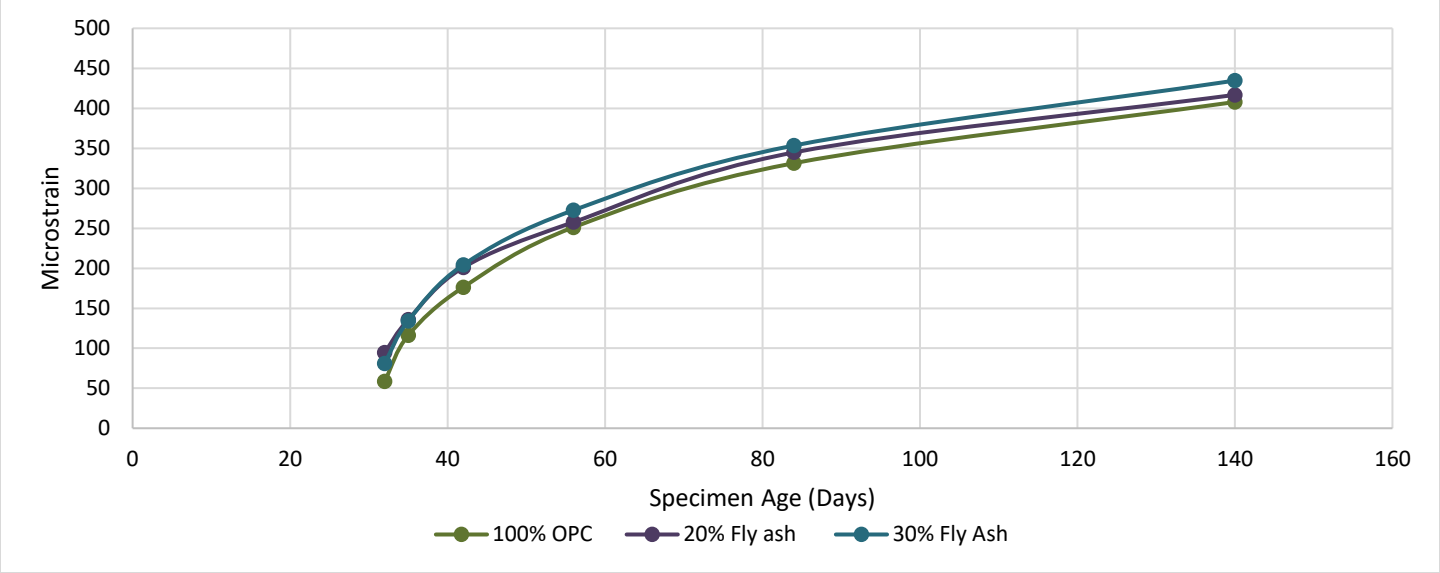

Figure B.49: Average volumetric shrinkage test results with mixtures grouped by fly ash content

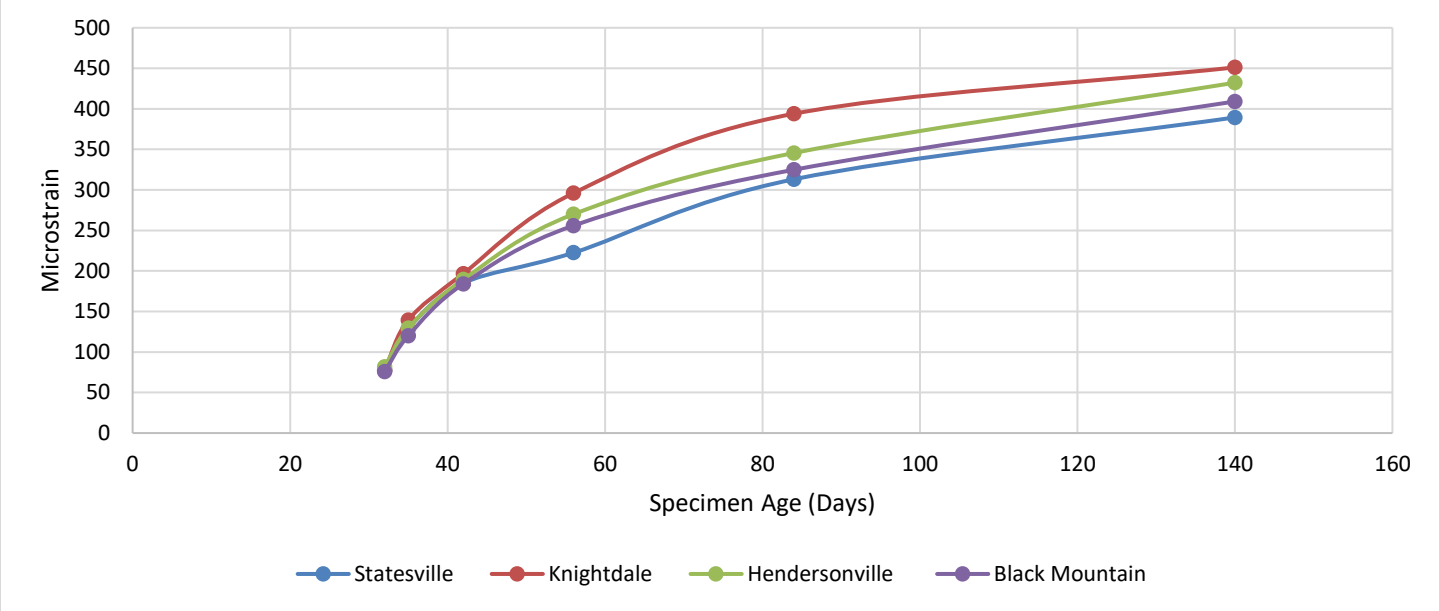

Figure B.50: Average volumetric shrinkage test results with mixtures grouped by coarse aggregate source

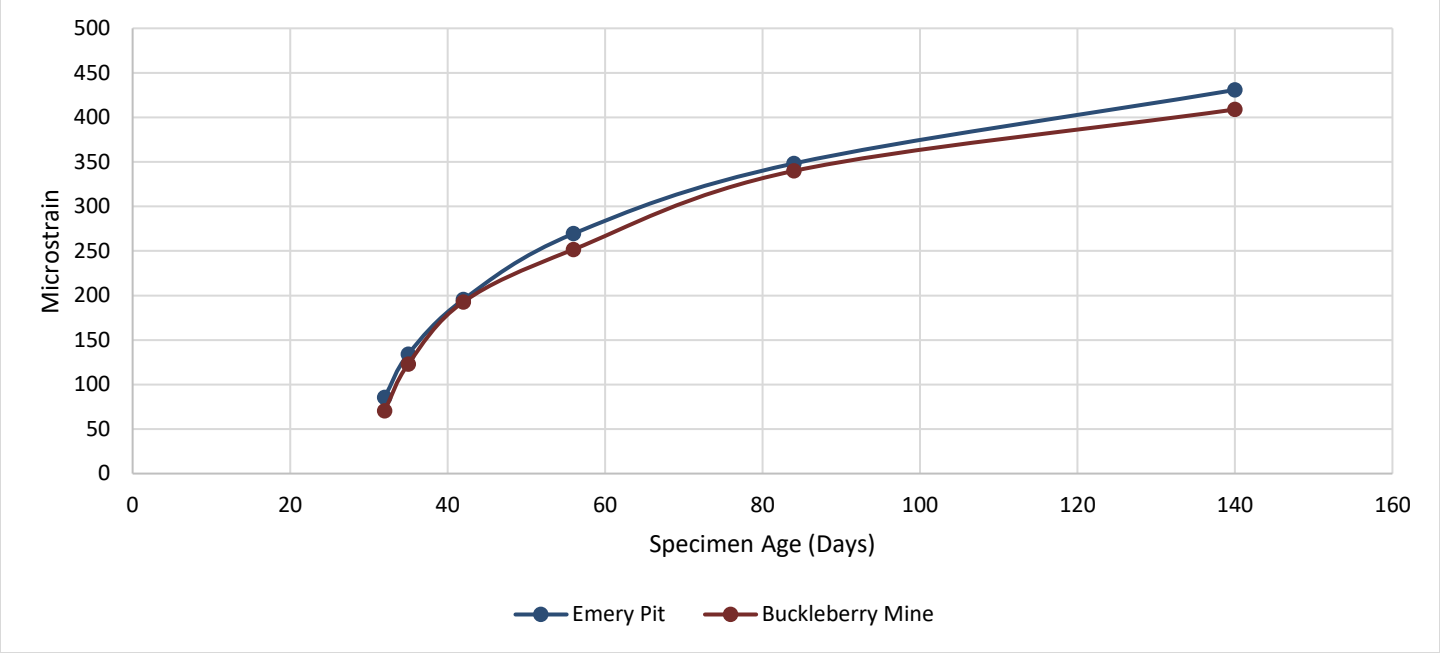

Figure B.51: Average volumetric shrinkage test results with mixtures grouped by region of North Carolina from which the coarse aggregate was sourced

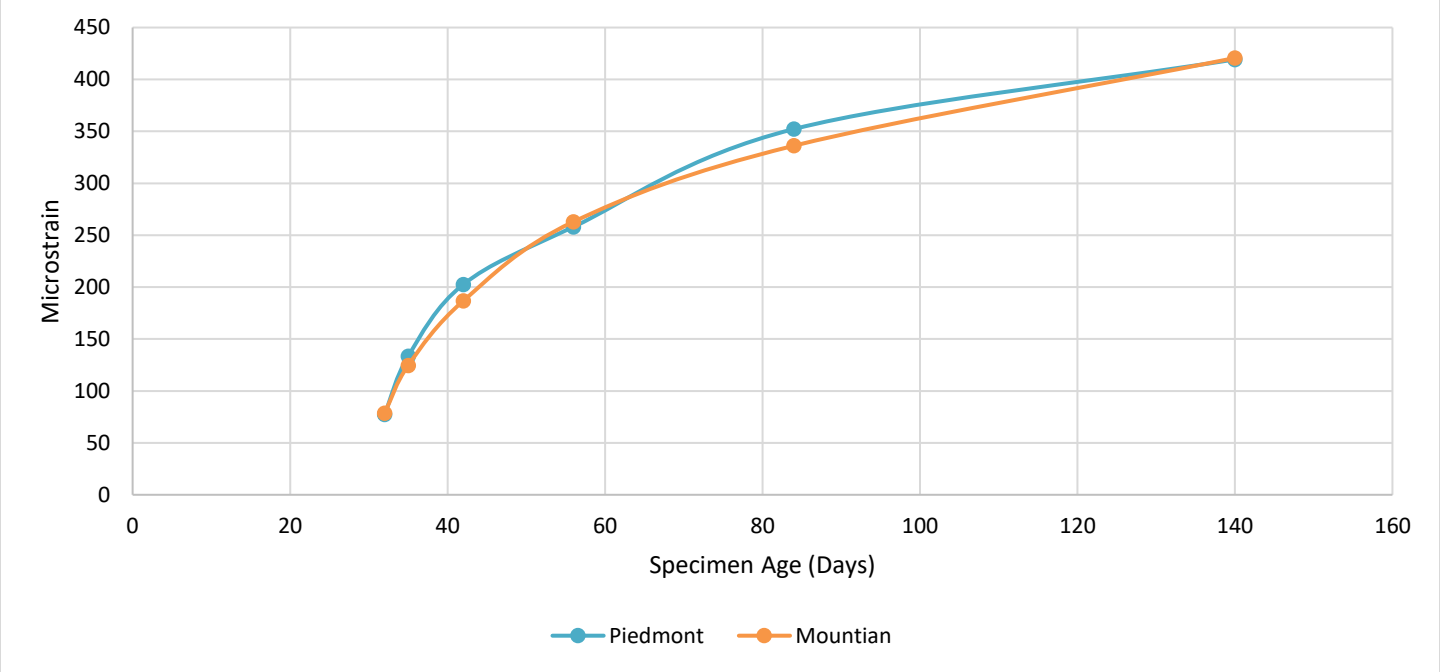

Figure B.52: Average volumetric shrinkage test results with mixtures grouped by location from which the fine aggregate was sourced

APPENDIX C – SUPPORTING MATERIAL FOR PAVEMENT DESIGN, PERFORMANCE, AND SLAB THICKNESS ANALYSIS USING PAVEMENT ME DESIGN SIMULATIONS

Table C.1: Default inputs**

	Input Parameter	Constant Value
Design Life		30 years
Performance Criteria	Initial IRI (in/mi)	63
	Terminal IRI (in/mi)	185
	Transverse Cracking (% of slabs cracked)	10
	Mean Joint Faulting (in)	0.12
Traffic Data for Analysis	Two-Way AADTT	6000
	Number of Lanes in Design Direction	2
	Percent of Trucks in Design Direction	50
	Percent of Trucks in Design Lane	90
	Operational Speed (mph)	65
	Average Axel Width (ft)	8.5
	Dual Tire Spacing (in)	12
	Tire Pressure (psi)	120
	Tandem Axel Spacing (in)	51.6
	Triden Axel Spacing (in)	49.2
	Quad Axel Spacing (in)	49.2
	Mean Wheel Location (in)	18
	Traffic Wander Standard Deviation (in)	10
	Design Lane Width (ft)	12
	Average Axel Spacing (short, medium, long) (ft)	12, 15, 18
	Percent of Trucks (short, medium, long) (%)	17, 22, 61
JPCP Design Properties	Permanent Curl/Wrap Effective Temperature Difference (°F)	-10
	Joint Spacing (ft)	15
	Sealant Type	Performed
	Dowel Diameter (in)	1.25
	Dowel Spacing (in)	12
	Widened Slab	Not Widened
JPCP Design Properties	Tied Shoulders	Tied
	Load Transfer Efficiency (%)	50
	Erodibility Index	Erosion Resistant (3)

	PCC-Base Contact Friction	Full Friction
	Friction Loss (months)	240
	Surface Shortwave Absorptivity	0.85
Layer 1: PCC	Cementitious Material Content (pcy)	550
	Water/Cement Ratio	0.48
	Ultimate Shrinkage (calculated)(micro-strain)	Computer Input Values
	Reversible Shrinkage (% of ultimate shrinkage)	50
	Time to Develop 50% of Ultimate Shrinkage (days)	35
	Curing Method	Curing Compound
Layer 2:	Layer 2:	Lime Stabilized
	Thickness (in)	8
	Unit Weight (pcf)	150
	Elastic/Resilient Modulus (psi)	450000
	Thermal Conductivity (BTU/hr-ft-°F)	1.25
	Heat Capacity (BTU/lb-°F)	0.28
Layer 3:	Layer 3:	Crushed Gravel (A-1-a)
	Thickness (in)	10
	Poisson's ratio	0.35
	Coefficient of Lateral Earth Pressure (k0)	0.5
	Elastic/Resilient Modulus (psi)	25000
Layer 4:	Layer 4:	A-6
	Thickness (in)	Semi-Infinite
	Coefficient of Lateral Earth Pressure (k0)	0.5
	Elastic/Resilient Modulus (psi)	14000

** Default inputs referencing NCDOT 2015-03 Report

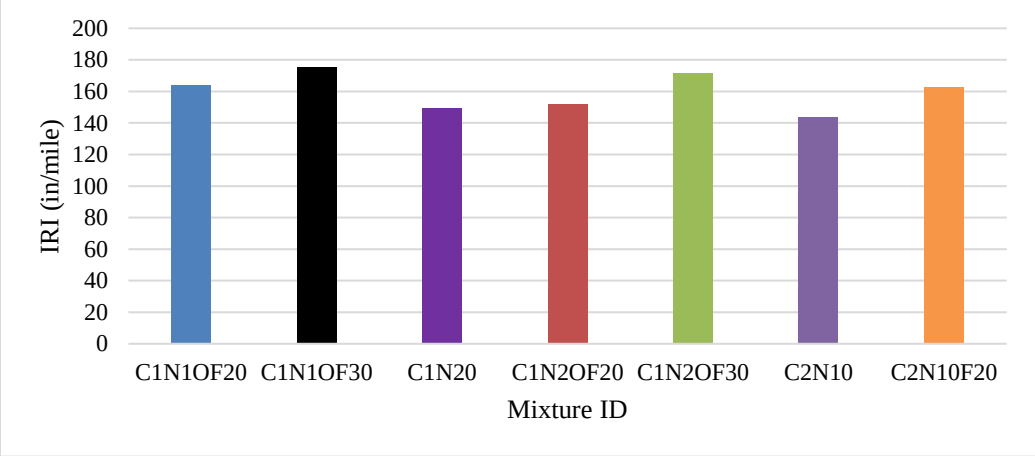

Figure C.1: Level 1 IRI performance indicator results

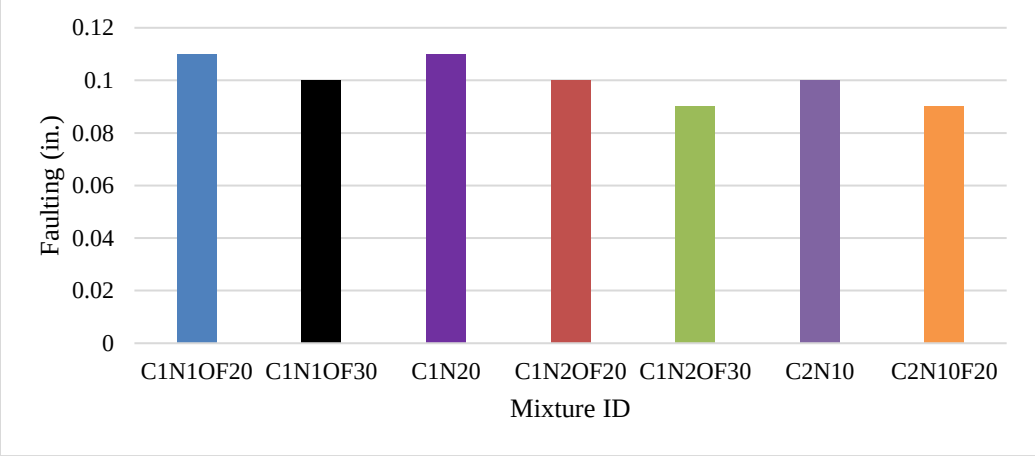

Figure C.2: Level 1 faulting indicator results

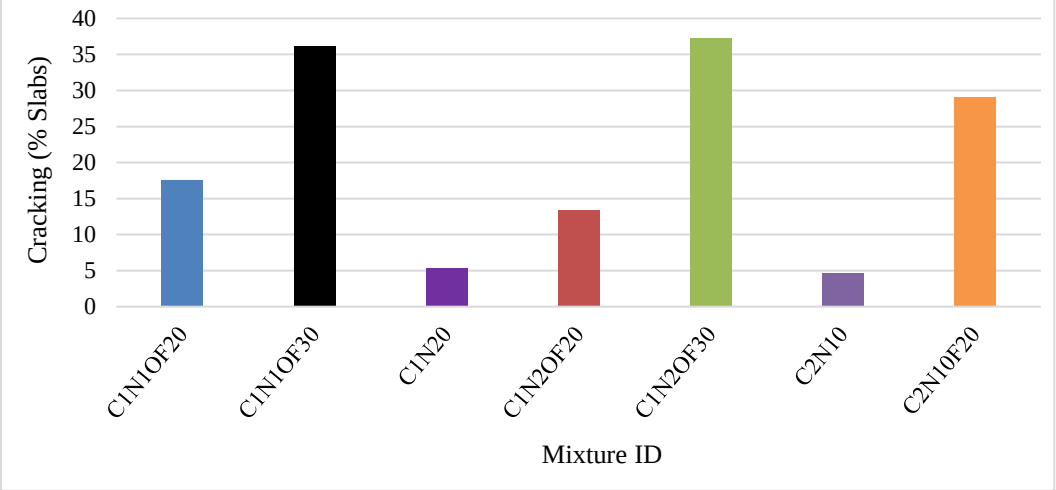

Figure C.3: Level 1 cracking indicator results

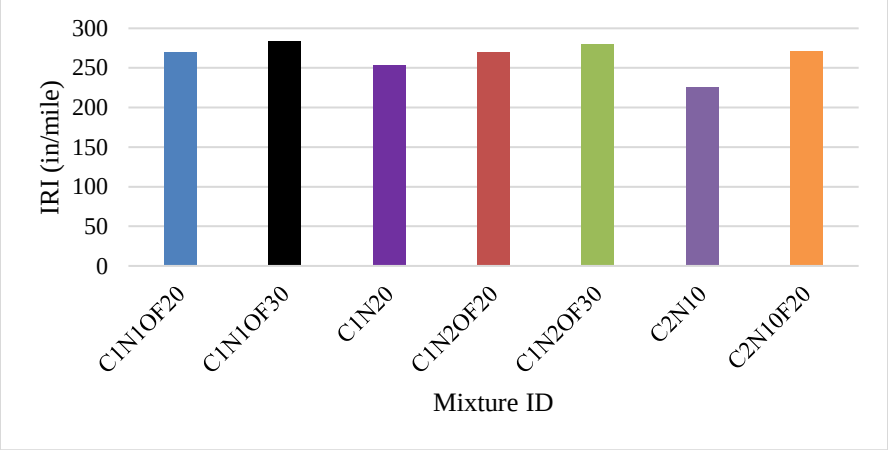

Figure C.4: Level 2 IRI indicator results

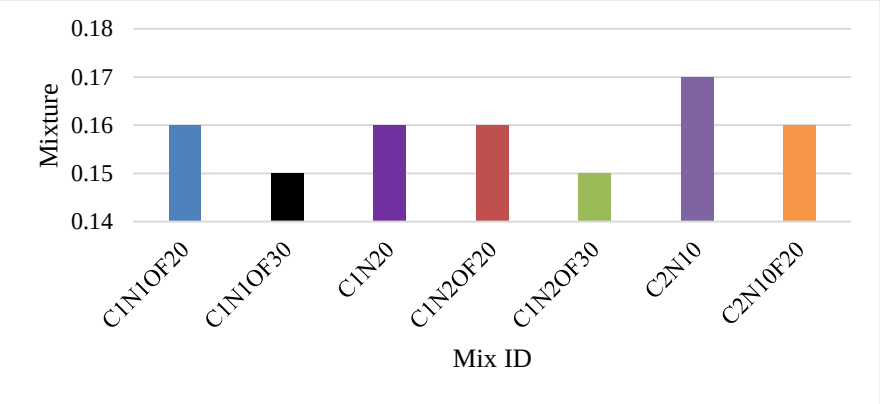

Figure C.5: Level 2 faulting indicator results

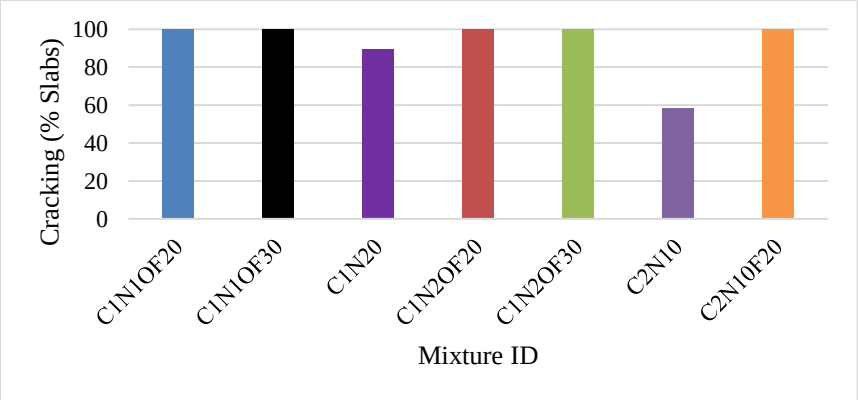

Figure C.6: Level 2 cracking indicator results

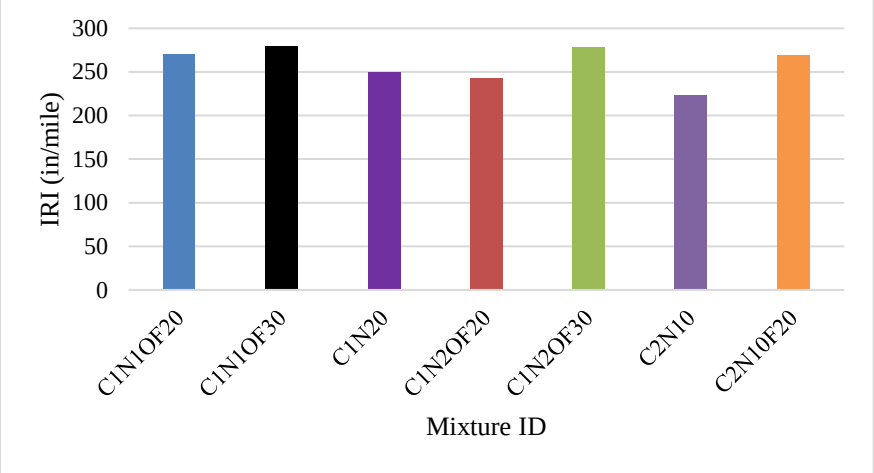

Figure C.7: Level 3 IRI indicator results

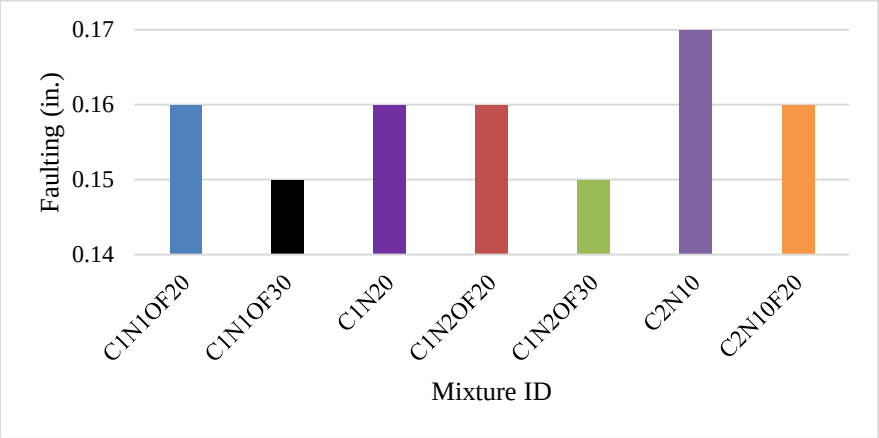

Figure C.8: Level 3 faulting indicator results

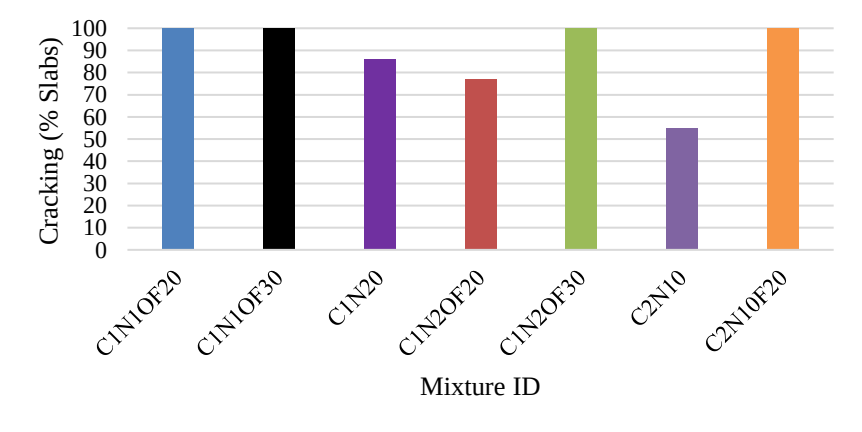

Figure C.9: Level 3 cracking indicator results

Table C.2: Baseline model

	Input Parameter	Constant Value
Design Life		30 years
Performance Criteria	Initial IRI (in/mi)	63
	Terminal IRI (in/mi)	185

	Transverse Cracking (% of slabs cracked)	10
	Mean Joint Faulting (in)	0.12
Traffic Data for Analysis	Two-Way AADTT	6000
	Number of Lanes in Design Direction	2
	Percent of Trucks In Design Direction	50
	Percent of Trucks In Design Lane	90
	Design Lane Width (ft)	12
	Average Axel Spacing (short, medium, long) (ft)	12, 15, 18
	Percent of Trucks (short, medium, long) (%)	17, 22, 61
JPCP Design Properties	Permanent Curl/Wrap Effective Temperature Difference (°F)	-10
	Joint Spacing (ft)	15
	Sealant Type	Performed
	Dowel Diameter (in)	1.25
	Dowel Spacing (in)	12
	Widened Slab	Not Widened
	Tied Shoulders	Tied
	Surface Shortwave Absorptivity	0.85

Table C.3: 28 Day CTE and compressive strength values

MIXTURE ID	28 Day CTE	28 Day Compressive Strength
C1N20	5.358	5051
C1N2OF20	5.195	4425
C1N2OF30	5.164	3610
C2N10	5.227	5829
C2N1OF20	5.124	4361
C2N1OF30	5.049	3897
C2N20	5.073	5676
C2N2OF20	5.003	4603
C2N2OF30	4.771	4037
C3N10	5.04	5375
C3N1OF20	4.987	4149
C3N1OF30	4.881	3592
C3N20	4.923	5293
C3N2OF20	4.739	4027
C3N2OF30	4.675	3287
C4N10	5.657	5509
C4N1OF20	5.522	4239
C4N1OF30	5.39	4147

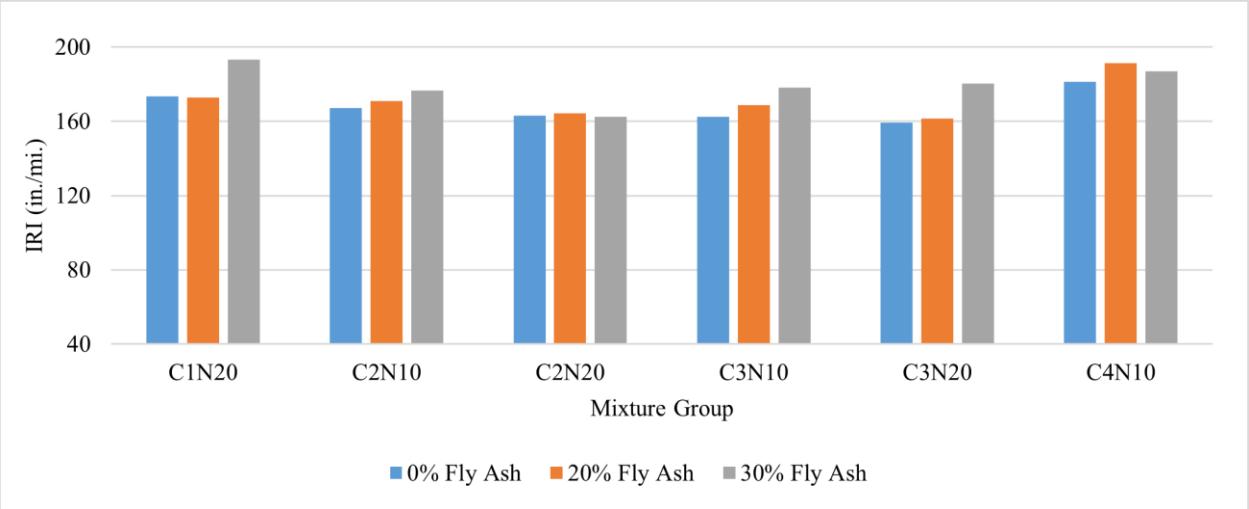

Figure C.10: IRI indicator comparison

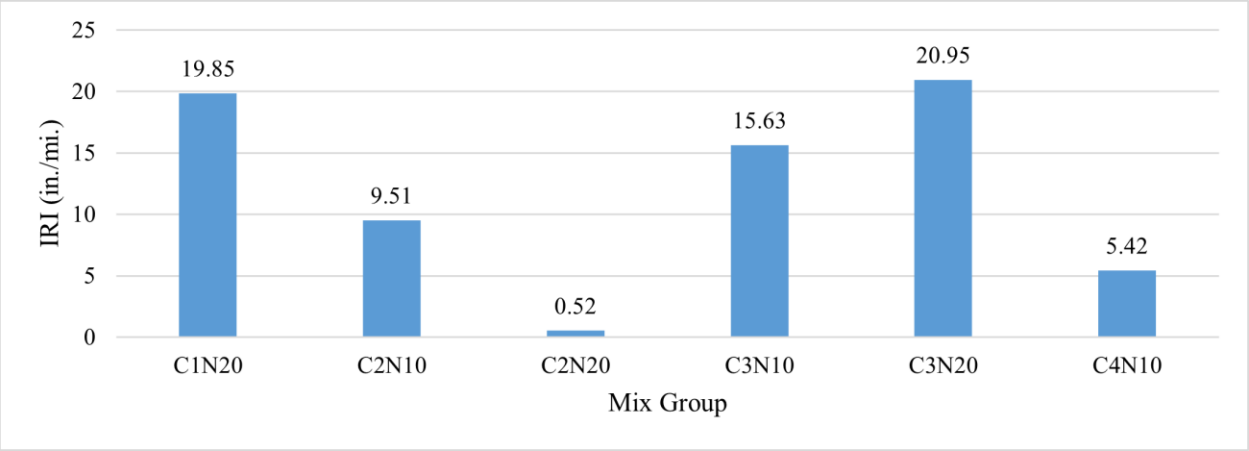

Figure C.11: Change in IRI indicator between 0% and 30% fly ash mixtures

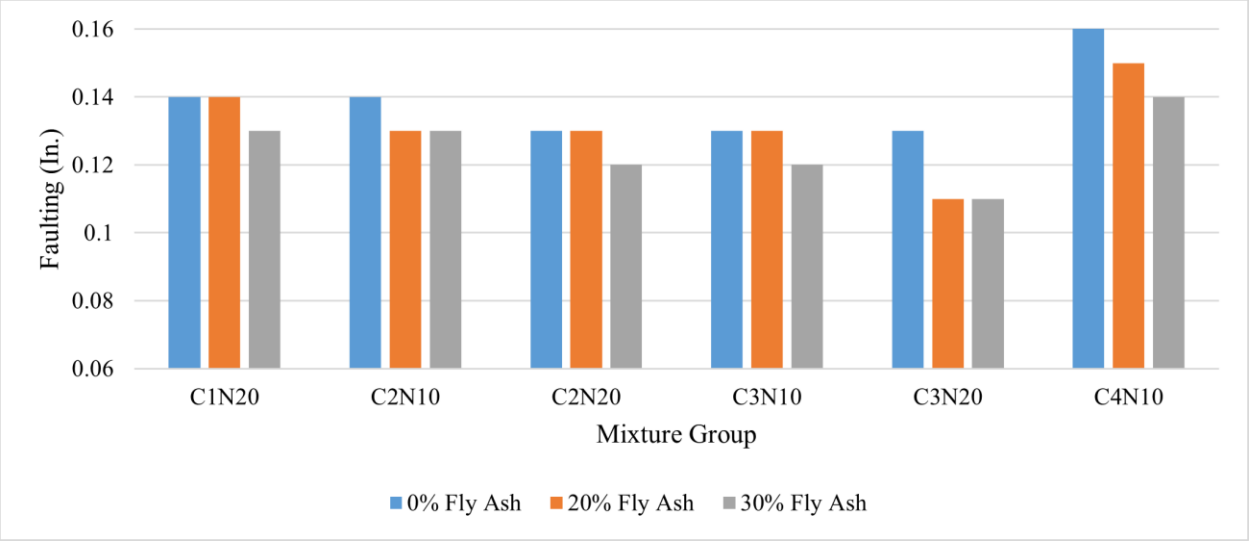

Figure C.12: Faulting indicator comparison

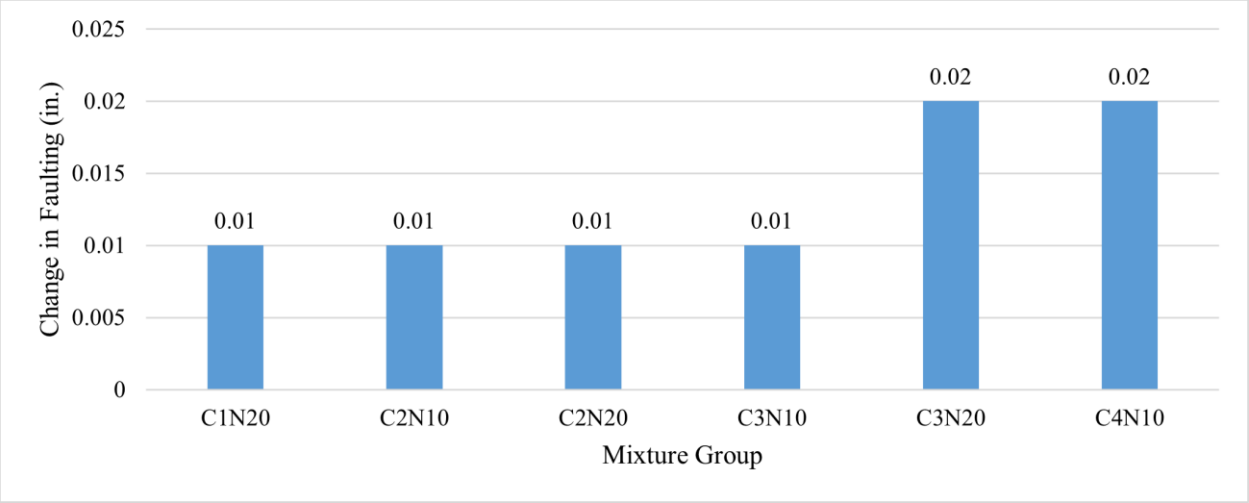

Figure C.13: Faulting indicator change between 0% and 30% fly ash mixtures

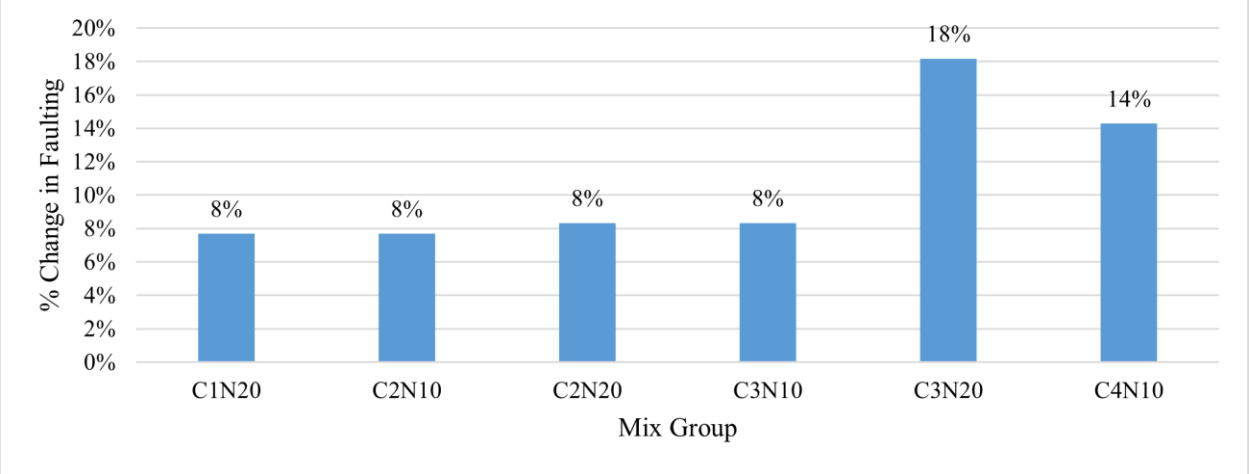

Figure C.14: % Decrease in faulting between 0% and 30% fly ash mixtures

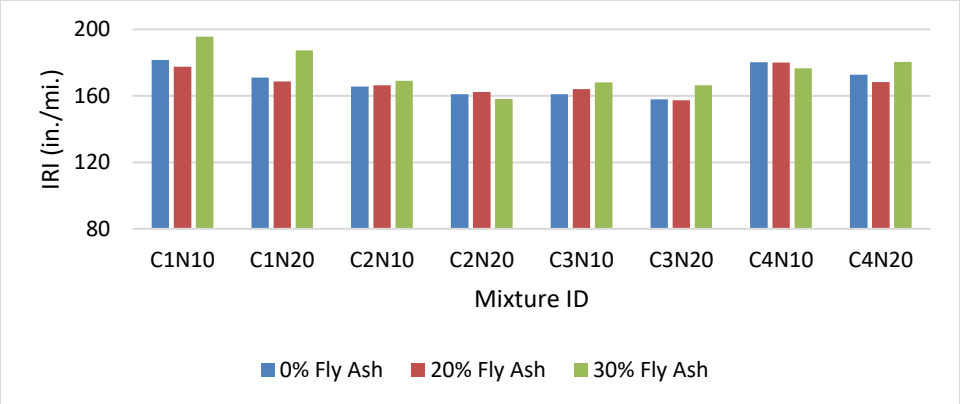

Figure C.15: Comparison of IRI simulation results (Level 1)

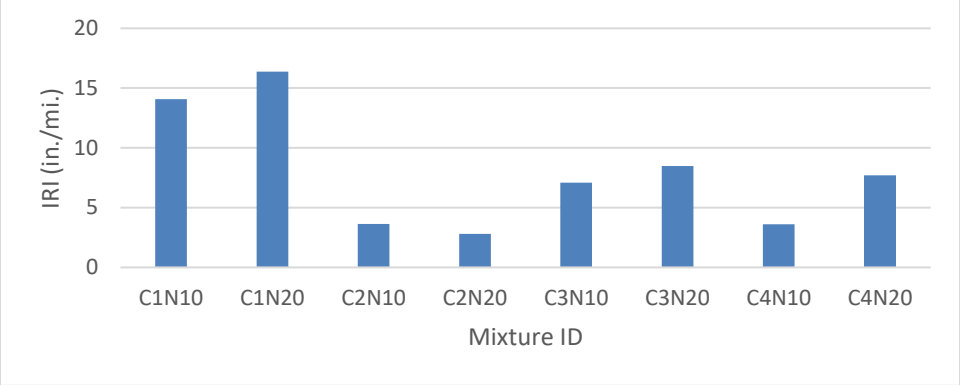

Figure C.16: Difference in IRI for 0% and 30% fly ash mixtures (Level 1)

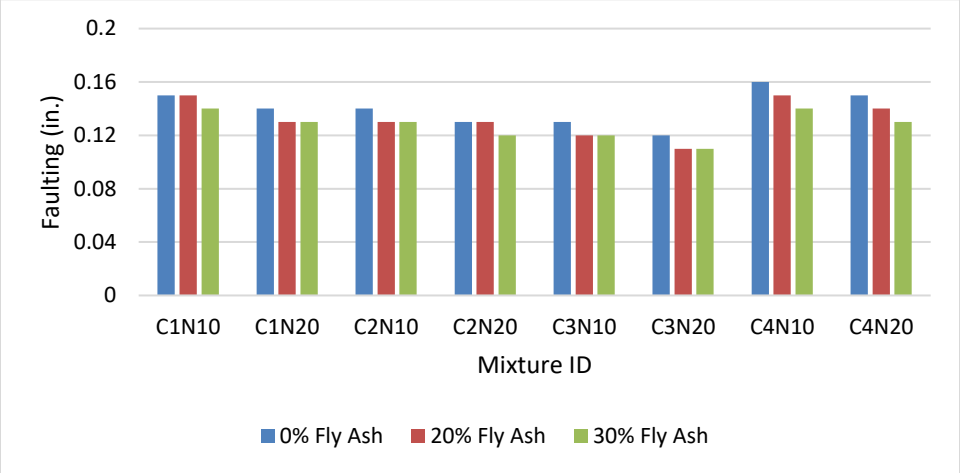

Figure C.17: Comparison of faulting simulation results (Level 1)

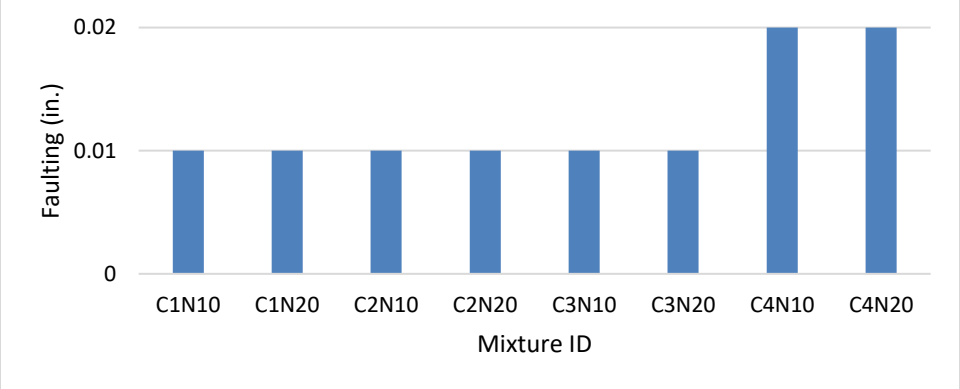

Figure C.18: Difference in faulting for 0% and 30% fly ash mixtures (Level 1)

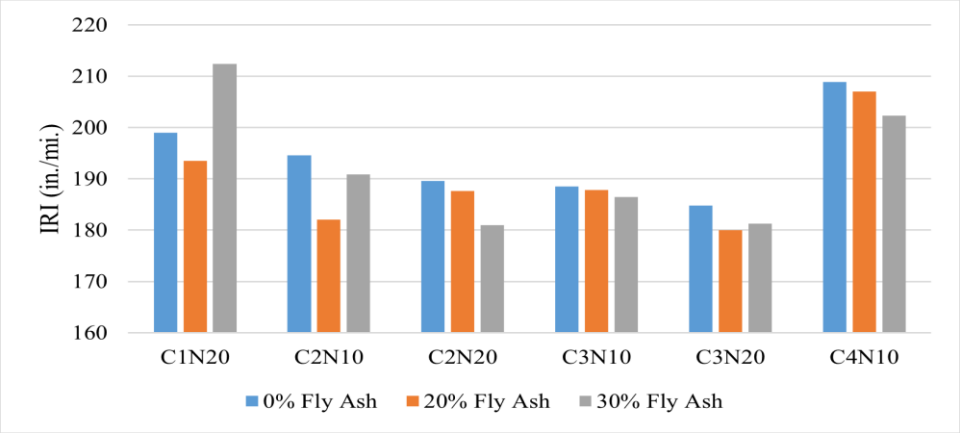

Figure C.19: IRI performance indicator comparison (Level 3)

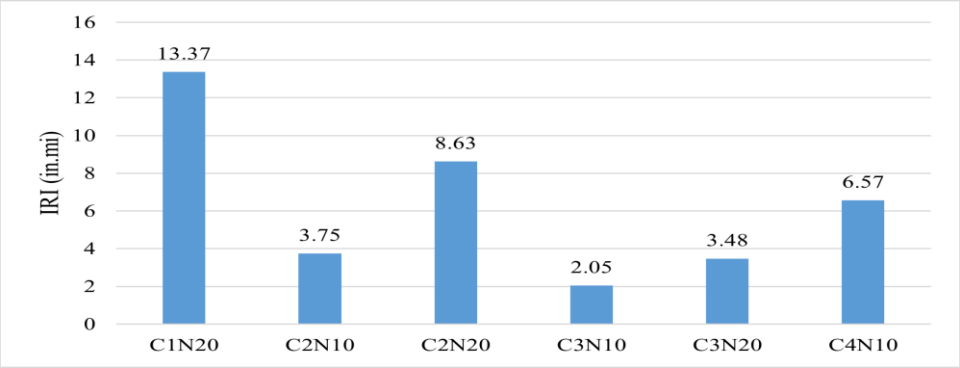

Figure C.20: Change in IRI performance indicator between 0% fly ash and 30% fly ash (Level 3)

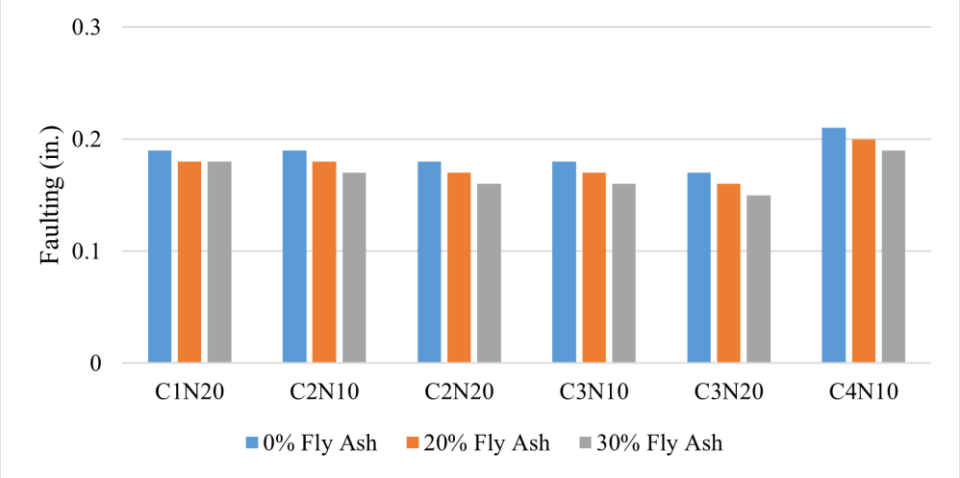

Figure C.21: Faulting indicator results (Level 3)

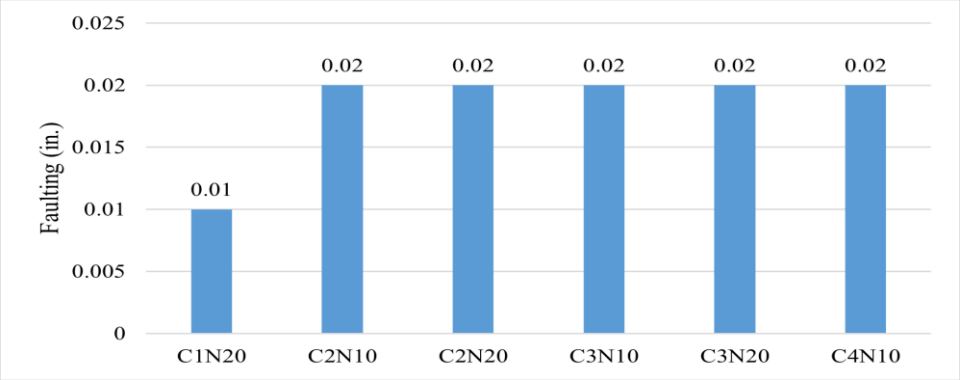

Figure C.22: Change in faulting indicator between 0% fly ash and 30% fly ash mixtures (Level 3)

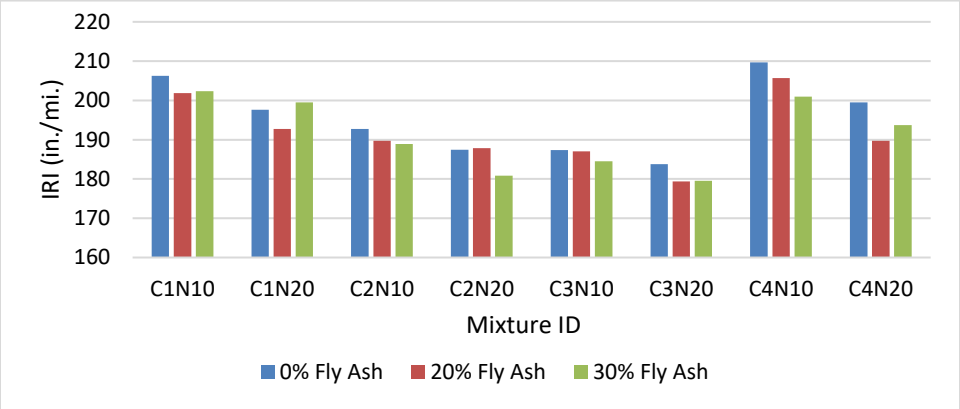

Figure C.23: IRI performance indicator comparison (Level 1)

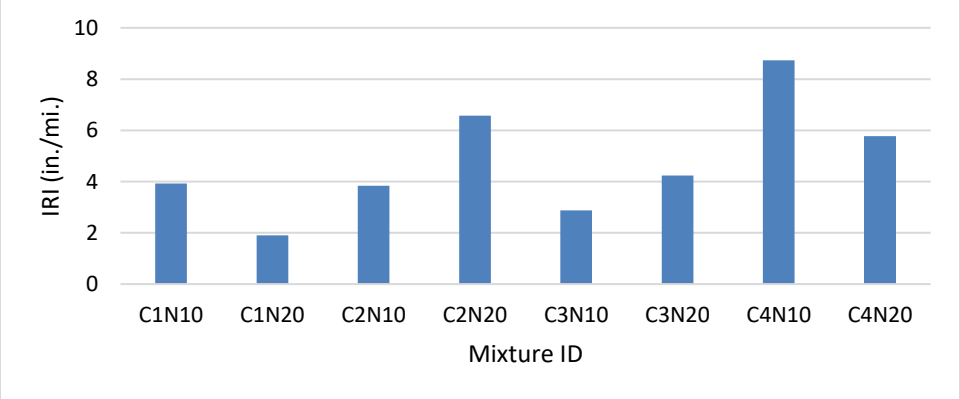

Figure C.24: Change in IRI performance indicator between 0% fly ash and 30% fly ash (Level 1)

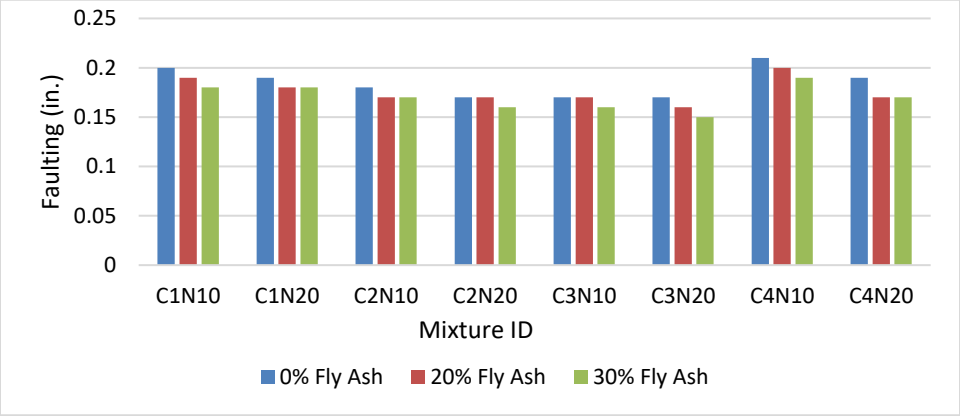

Figure C.25: Faulting performance indicator comparison (Level 1)

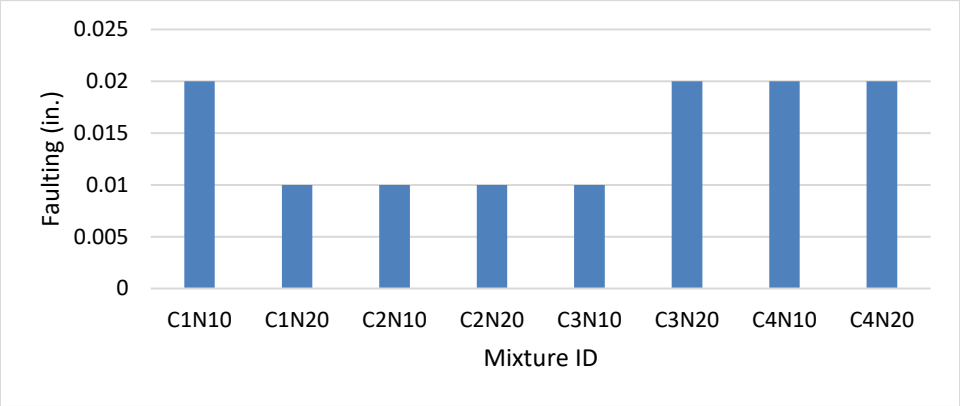

Figure C.26: Change in faulting performance indicator between 0% fly ash and 30% fly ash (Level 1)

Table C.4: Baseline model

	Input Parameter	Constant Value
Design Life		30 years
Performance Criteria	Initial IRI (in/mi)	63
	Terminal IRI (in/mi)	185
	Transverse Cracking (% of slabs cracked)	10
	Mean Joint Faulting (in)	0.12
Traffic Data for Analysis	Two-Way AADTT	6000
	Number of Lanes in Design Direction	2
	Design Lane Width (ft)	12
JPCP Design Properties	Joint Spacing (ft)	15
	Sealant Type	Performed
	Dowel Diameter (in)	1.25
	Dowel Spacing (in)	12
	Widened Slab	Not Widened
	Tied Shoulders	Tied

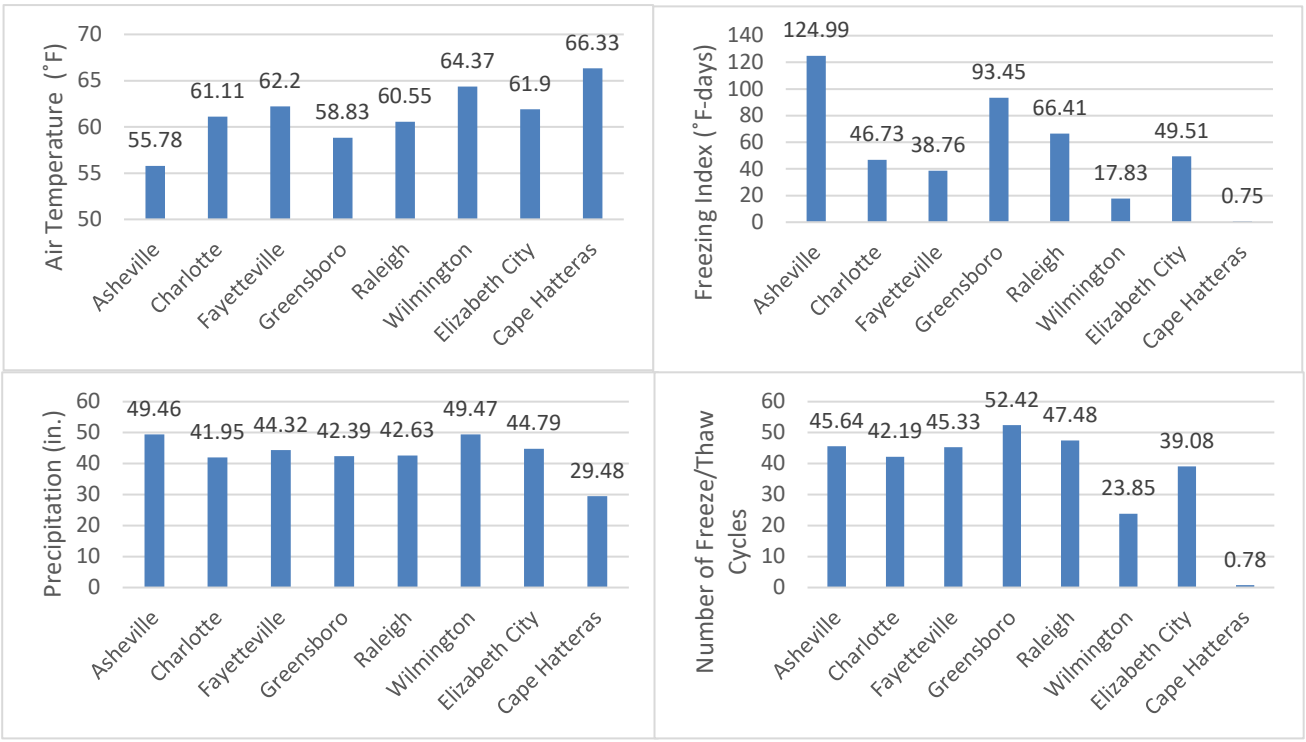

Figure C.27: Climate station data comparison

Table C.5: Mixture C1N20 Level 3 test data

Mixture C1N20	
Coefficient of Thermal Expansion (CTE)	5.358
28-Day Compressive Strength (CS)	5051

Table C.6: Baseline model

	Input Parameter	Constant Value
Design Life		30 years
Performance Criteria	Initial IRI (in/mi)	63
	Terminal IRI (in/mi)	185
	Transverse Cracking (% of slabs cracked)	10
	Mean Joint Faulting (in)	0.12
Traffic Data for Analysis	Two-Way AADTT	12000
	Number of Lanes in Design Direction	2
	Percent of Trucks In Design Direction	50
	Percent of Trucks In Design Lane	90
	Design Lane Width (ft)	12
	Average Axel Spacing (short, medium, long) (ft)	12, 15, 18
	Percent of Trucks (short, medium, long) (%)	17, 22, 61
JPCPDes	Permanent Curl/Wrap Effective Temperature Difference (°F)	-10

	Joint Spacing (ft)	15
	Sealant Type	Performed
	Dowel Diameter (in)	1.25
	Dowel Spacing (in)	12
	Widened Slab	Not Widened
	Tied Shoulders	Tied
	Surface Shortwave Absorptivity	0.85

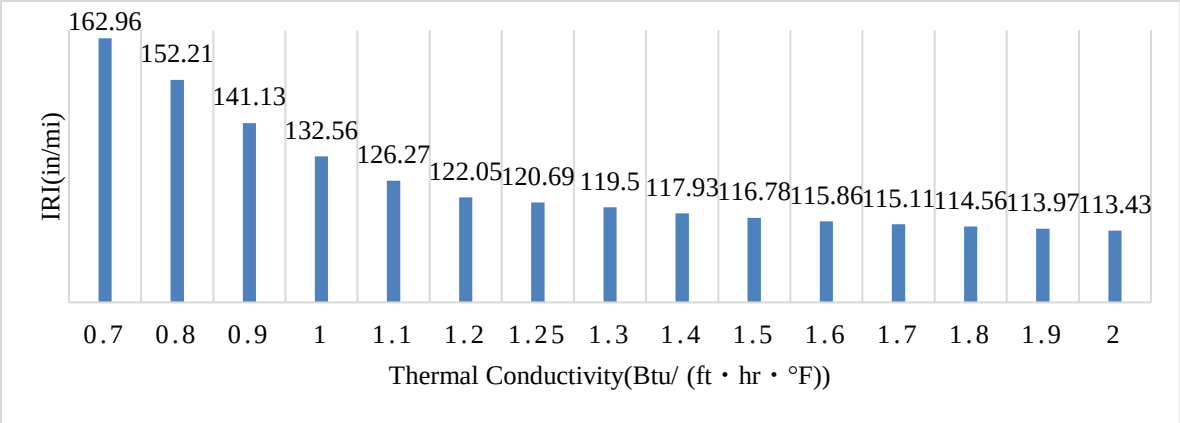

Figure C.28: Effects of thermal conductivity on IRI

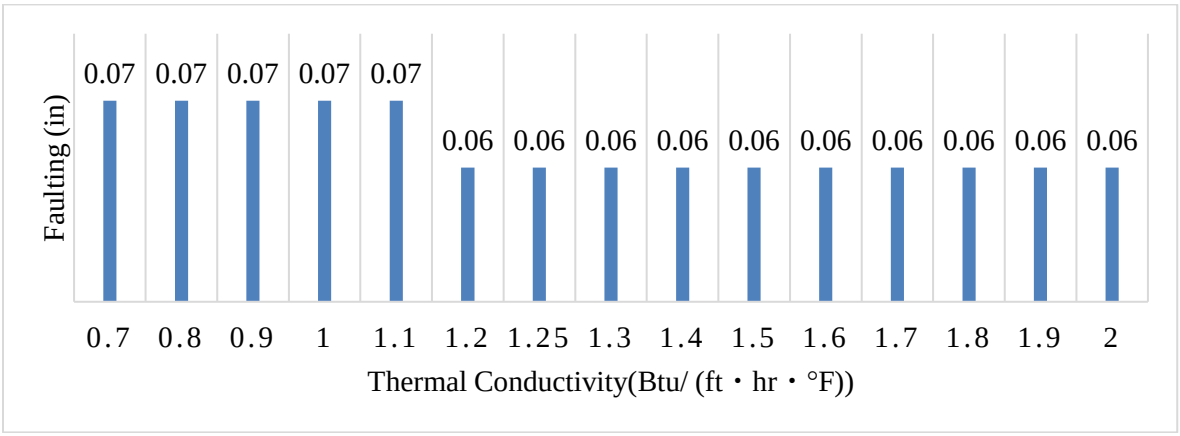

Figure C.29: Effects of thermal conductivity on faulting

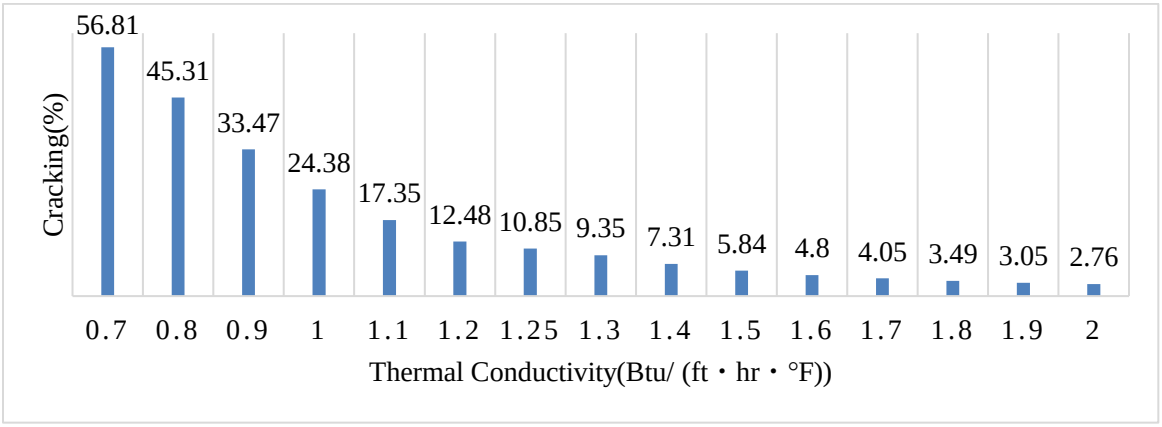

Figure C.30: Effects of thermal conductivity on cracking

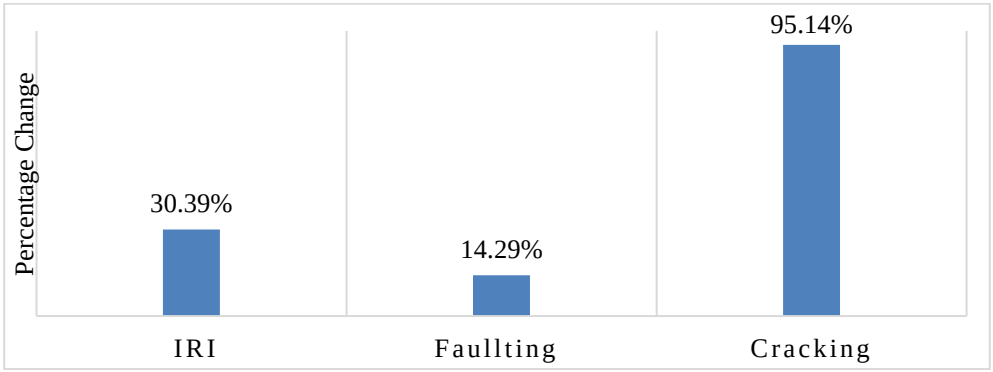

Figure C.31: Percentage change in baseline model

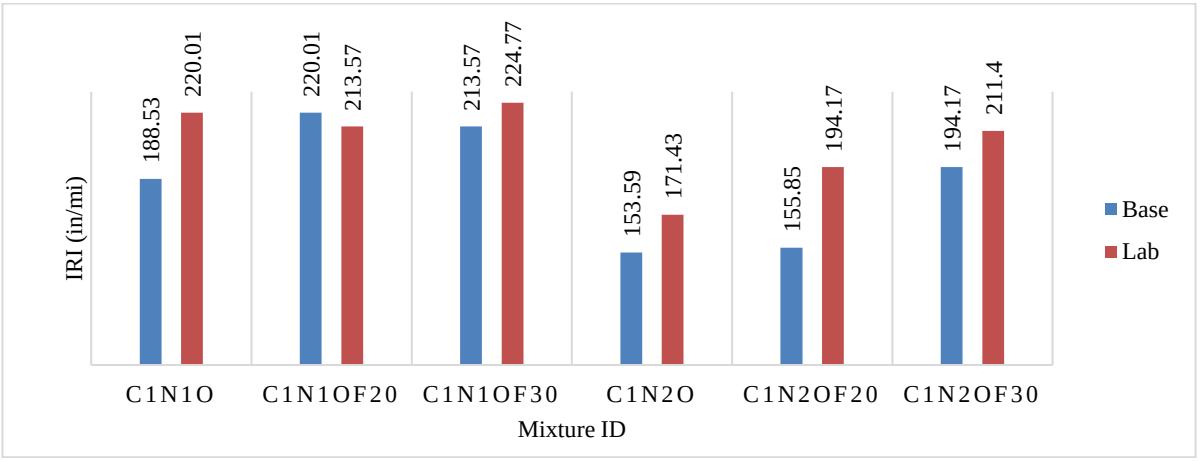

Figure C.32: Effects of laboratory obtained thermal conductivity on IRI

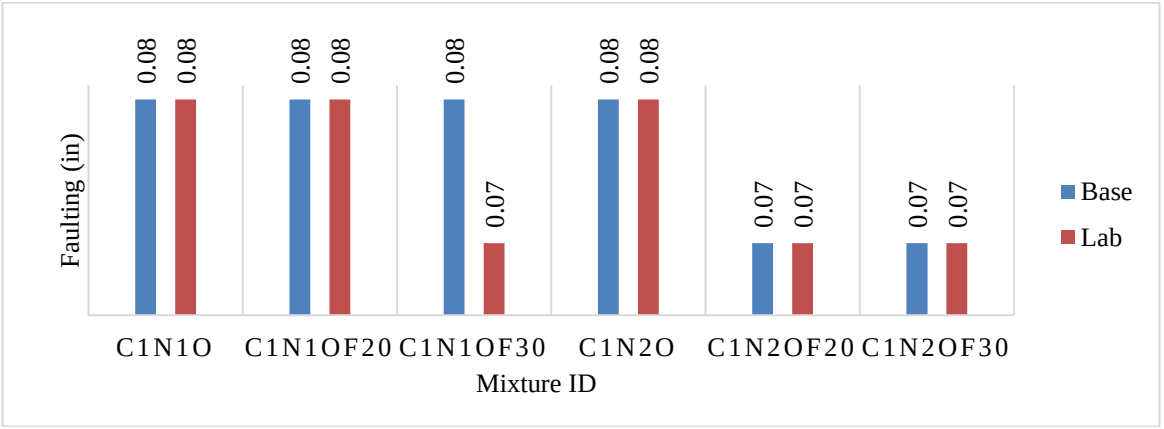

Figure C.33: Effects of laboratory obtained thermal conductivity on faulting

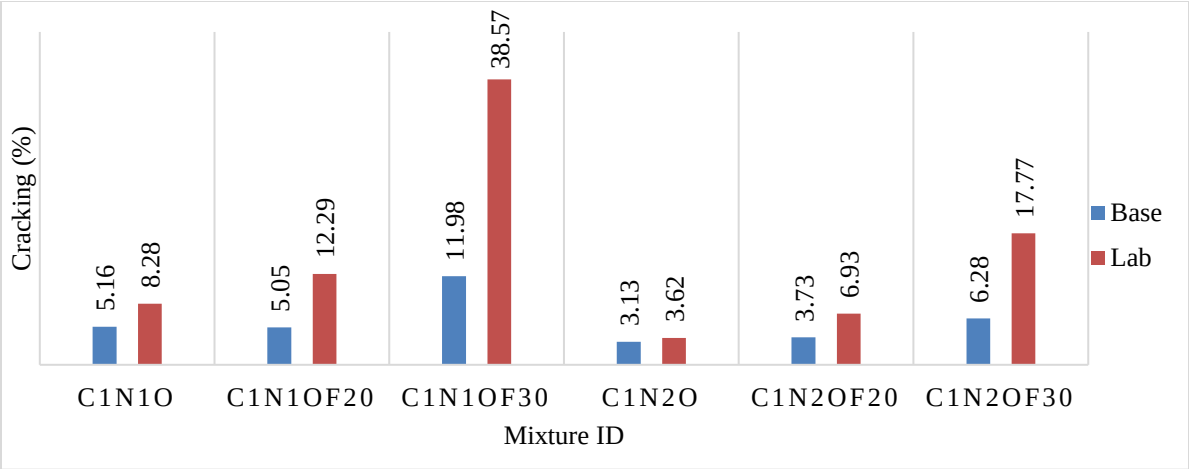

Figure C.34: Effects of laboratory obtained thermal conductivity on cracking